



universität
wien

MASTERARBEIT / MASTER'S THESIS

Titel der Masterarbeit / Title of the Master's Thesis

„Subtractions in QCD and SCET“

verfasst von / submitted by

Christoph Bartsch, BSc

angestrebter akademischer Grad / in partial fulfilment of the requirements for the degree of

Master of Science (MSc)

Wien, 2020 / Vienna, 2020

Studienkennzahl lt. Studienblatt /
degree programme code as it appears on
the student record sheet:

UA 066 876

Studienrichtung lt. Studienblatt /
degree programme as it appears on
the student record sheet:

Masterstudium Physik UG2002

Betreut von / Supervisor:

Univ.Prof. Dr. André H. Hoang

Abstract

This thesis is a case study for the process $e^+e^- \rightarrow \text{di-jets}$ with particular emphasis on the concept of subtractions arising in QCD and Soft-Collinear Effective Theory (SCET). Our discussion will focus on the event shape variable thrust τ . On the basis of this example we illustrate how established subtraction schemes, particularly the Catani-Seymour dipole subtraction, allow for a numerical calculation of differential cross sections, avoiding the problem of infrared (IR) divergences. In the dijet-region where $\tau \ll 1$ a hierarchy of disparate scales leads to the occurrence of large logarithms $\alpha_s \log(\tau) \simeq 1$ spoiling the fixed-order perturbative series. Effective Field Theory (EFT) methods are used to systematically resum these logarithms to all orders. This is achieved by formulating factorisation theorems that break up the cross section into a product of factorisation functions, each associated with a single dynamic scale and renormalisation group equation (RGE). In the factorised framework of SCET we focus on the collinear jet function which we show to contain divergences unlike those found in QCD, rendering the conventional approach to subtractions inapplicable. The main conceptual advancement put forward by this thesis is to rewrite the jet function in terms of a finite, numerically calculable quantity we call the subtracted jet function, which allows for the application of conventional subtraction schemes. We explicitly show the analytic cancellation of divergences in this object and demonstrate its numerical computability. To conclude we discuss the new, semi-analytic approach to performing resummed calculations enabled by the subtracted jet function.

Zusammenfassung

Diese Arbeit ist eine Fallstudie für den Prozess $e^+e^- \rightarrow 2\text{-Jets}$ mit besonderem Augenmerk auf Subtraktionen im Kontext der QCD und Soft-Collinear Effective Theory (SCET). Dabei steht die “event shape” Observable “thrust” τ im Mittelpunkt der Diskussion. Anhand letzterer wird gezeigt wie konventionelle Subtraktionsmethoden, insbesondere die Catani-Seymour Dipol-Subtraktion, die in Zwischenschritten auftretenden Infrarot-Singularitäten umgehen, und eine numerische Berechnung von differentiellen Wirkungsquerschnitten ermöglichen. Im 2-Jet-Limes $\tau \ll 1$ führt eine Reihe hierarchischer Skalen zu großen Logarithmen $\alpha_s \log(\tau) \simeq 1$, die ein Scheitern der Störungsreihe bei endlicher Ordnung zur Folge haben. Methoden der effektiven Feldtheorie (EFT) ermöglichen eine Resummation der Logarithmen zu allen Ordnungen. Dies wird durch die Formulierung von Faktorisierungstheoremen erreicht, die ein Aufspalten des Wirkungsquerschnitts in ein Produkt von Faktorisierungsfunktionen erlauben, wobei jeder eine einzige dynamische Skala und Renormierungsgruppengleichung (RGE) zugewiesen werden kann. Wir betrachten im Speziellen die in SCET auftretende kollineare Jet-Funktion und zeigen dass die darin auftretenden Divergenzen nicht mit den aus der QCD bekannten Strukturen übereinstimmen und eine Anwendung üblicher Subtraktionsmethoden invalidieren. Die in dieser Arbeit vorgestellte konzeptionelle Neuerung besteht in der Umformulierung der Jet-Funktion mithilfe einer endlichen, numerisch berechenbaren Größe, der sogenannten subtrahierten Jet-Funktion, die eine Anwendung konventioneller Subtraktionsmethoden erlaubt. Wir zeigen analytisch dass in diesem Objekt keine Divergenzen auftreten, demonstrieren numerische Berechenbarkeit, und schließen mit einer Diskussion des neuen, semi-analytischen Zugangs für resummierte Rechnungen, der durch die subtrahierte Jet-Funktion ermöglicht wird.

Contents

1	Introduction	1
2	Fixed order calculations in QCD	4
2.1	Prelude: infrared divergences in QCD	4
2.2	Born-level total cross section for $e^+e^- \rightarrow \gamma^* \rightarrow q\bar{q}$	5
2.3	Next-to-leading order matrix elements	6
2.4	Next-to-leading order total cross section	9
2.5	General structure of the cross-section for $e^+e^- \rightarrow \gamma^* \rightarrow q\bar{q} + X$	12
2.6	Thrust at next-to-leading order	13
2.7	Infrared safety and thrust	17
2.8	A naive numerical approach for thrust	18
3	Catani-Seymour dipole subtraction	20
3.1	The promise of the subtraction method	20
3.2	General construction of counter terms	23
3.3	Subtraction for $e^+e^- \rightarrow$ di-jets	26
3.4	Derivation of Catani-Seymour counter terms	26
3.5	Analytic subtraction for thrust	29
4	Numerical implementation, comparison to analytic results and experiment	31
4.1	Comments on numerical implementation using Monte Carlo	31
4.2	Comparison between analytic and numerical results and facing the experiment	34
5	Introduction to Soft-Collinear Effective Theory	38
5.1	Lightcone decomposition	38
5.2	Momentum regions for $e^+e^- \rightarrow$ di-jets	39
5.3	SCET Lagrangian for $e^+e^- \rightarrow$ di-jets	40
5.4	n -collinear quark Lagrangian	41
5.5	Collinear Wilson lines	45
5.6	Other sectors and final Lagrangian for $e^+e^- \rightarrow$ di-jets	50
5.7	Ultrasoft Wilson lines	51
6	SCET factorisation theorem for thrust	54
6.1	Factorisation of the total cross section in the di-jet limit	54
6.2	Hemisphere mass distribution and thrust	58
7	NLO ingredients for the factorisation theorem	62
7.1	Hard and hemisphere soft functions	62
7.2	Massive next-to-leading order SCET jet function	64
7.3	Evaluation of diagrams using cutting rules	65
7.4	Massive jet function and jet correlator results	75
7.5	Massless jet function and jet correlator results	75
7.6	Jet function renormalisation	76
7.7	Discussion of results and non-local singularity	77
7.8	Subtracted massive jet function: a first look	77

8	Integrand-level subtraction of real emission and virtual contributions	81
8.1	$J_{n,2}$ RR-subtraction	82
8.2	$J_{n,4}$ RR-subtraction	84
8.3	Subtracted real emission and virtual jet function (final results)	86
8.4	Subtracted jet function in the factorisation theorem	88
9	Conclusion and outlook	89
A	Phase space in d spacetime dimensions	90
B	Integral identities and conventions for Dimensional Regularisation	91
C	Ultraviolet divergences in the QCD virtual correction	92
D	Colour/Helicity space formulation of amplitudes	93
E	Dipole operator matrix elements in the soft and collinear limit	97
F	Dipole map and factorisation of dipole phase space	99
G	Alternative calculation of subtracted real emission thrust distribution	103
H	Feynman rules	105
I	Plus distribution miscellanies	106

1 Introduction

At modern day particle colliders, experimental data is acquired with progressively higher accuracy and exceedingly small uncertainties. This poses the challenge to theorists of providing increasingly precise predictions for the measured observables, allowing to put tight constraints on the underlying model. In turn, this requires an ever more accurate knowledge of the theoretical parameters used to arrive at the prediction. Since the Standard Model of Particle Physics (SM) is formulated within the framework of quantum field theory (QFT) these theoretical parameters usually come in the form of renormalised coupling constants, particle masses, mixing angles, etc.. The latter depend on the setup of the theory and as such also need to be extracted from experimental data.

Strongly coupled theories such as Quantum Chromodynamics (QCD) present an additional difficulty in making the connection between theory parameters, chief among them the strong coupling α_s [1] and the top mass m_t [2, 3], and measurement in that they exhibit confinement. This means that at low energies (compared to center of mass energies of modern colliders) on the order $\Lambda_{\text{QCD}} \simeq 200\text{MeV}$ the interaction between the fundamental quarks and gluons is so strong that they bind into composite hadrons. This leads to the situation that data at particle accelerators can only be obtained on hadronic final states whose precise relation to the underlying partonic degrees of freedom eludes current perturbative methods.

In the face of this challenge it is all the more important to develop a theoretical framework which separates a given prediction (i.e. observables like cross sections) into contributions that are amenable to a first-principles calculation while at the same time providing a means of consistently incorporating the strong coupling dynamics which is of an essentially non-perturbative nature. Traditionally this has been achieved through so-called factorisation theorems[4]. In this context Effective Field Theory (EFT) techniques[5] have proven especially useful in taking advantage of strong scale hierarchies present in certain classes of kinematic final state configurations. Amongst others, these final states are characterised by large energy deposits localised in narrow angular regions of the detector, corresponding to collimated sprays of particles known as jets[6]. The Soft-Collinear Effective Theory (SCET)[7–10] in particular has been successful in providing factorisation theorems in this kinematic region for various classes of observables.

In this work we will exclusively focus on the observable thrust τ for the process $e^+e^- \rightarrow q\bar{q} + X$. Thrust is a so-called event shape[11] and as such it quantifies the collective geometric appearance of all particles in a given event. If a such an event resembles two back-to-back jets (di-jets) it will be assigned a low value $\tau \simeq 0$, while events where particles are evenly distributed over all directions, or indeed consist of more than two jets, will correspond to higher values. When computing the thrust distribution (or any event shape) in the di-jet region the structure of perturbation theory dictates that the disparate scales present in this limit enter the prediction as logarithms of the large ratios of these scales. Thus, when the perturbative series is truncated at fixed order, infamous large logarithms remain that scale as $\alpha_s \log(\tau) \simeq 1$ even though $\alpha_s \ll 1$. With higher-order corrections the same size as the leading-order result this leads to a breakdown of naive perturbation theory.

The factorisation theorem formulated within SCET[12, 13] overcomes this problem by factoring the observable into a product of so-called factorisation functions, each of which is associated with only a single physical scale as well as the renormalisation scale μ through the presence of ultraviolet (UV) divergences. The thus implied renormalisation group equations (RGEs) for each factorisation function allow for a systematic all-orders resummation of the logarithmically enhanced terms in the observable to regain control over the perturbative result.

However, even at the fixed-order level a further complication arises when observables are computed in a theory with massless particles such as QCD. In addition to UV divergences, known to be treatable

through the process of renormalisation, these theories also allow for infrared (IR) divergences to occur in intermediate steps of the calculation. The latter are essentially due to degeneracies in the final state kinematics and although the divergences cancel (for so-called IR safe quantities) in the final result, their occurrence presents a significant obstacle to anyone looking for a numerical implementation. Since regularisation is not available in a numerical approach, a diverse set of techniques, collectively referred to as subtraction methods, have been devised which treat these divergences such as to make finite numerical computations possible. Representing this broad class of prescriptions, the dipole subtraction method[14] will be considered in more detail in this thesis.

Owing to the divergent nature of the factorisation functions discussed above, calculations in the factorised EFT framework have conventionally been carried out fully analytically. In this thesis we intend to take a first step towards combining the notions of factorisation and subtraction and propose a new, semi-analytic approach to performing resummed calculations. Concretely, this will entail a reformulation of the SCET collinear jet function that will allow to retain analytic control over the UV divergent behaviour that is essential to the RG running, while separating off information that is more demanding to obtain analytically, such as quark mass effects, into a finite, in principle numerically calculable part. We provide an explicit proof-of-concept of numerical computability of the subtracted jet function in certain kinematic regions. This improves on the current fully analytic approach in that having performed the resummation in a minimal setting by conventional means, the additional information can be incorporated purely numerically without any need for further analytic calculation. Further work may build upon this thesis to include decay information (e.g. for top-quarks) which is currently not available analytically.

This thesis is organised as follows:

- Chapter 1 consists of this introduction and outline.
- In Chapter 2 we compute the fixed order amplitudes for $e^+e^- \rightarrow q\bar{q} + X$ in full QCD up to next-to-leading order (NLO) in α_s , assuming all final state partons as massless. Thereby we investigate the structure of IR divergences in real emission and virtual contributions occurring at various stages of the calculation. We compute the total cross section and thrust distribution touching on the concept of IR safety crucial to attaining finite perturbative results.
- The introduction to the concept of subtraction will be the aim of Chapter 3. Focusing on the so-called dipole subtraction method we first discuss the general ideas and concepts in order to then apply it to the previously obtained thrust distribution. Again, particular emphasis will be placed on the analytic structure of the subtraction procedure.
- Chapter 4 briefly ties up some loose ends and sets up the premise of the remaining thesis. We first discuss some details of the numerical implementation of the subtraction method providing an explicit example for the equivalence of the numerical and analytic approaches. We then proceed to compare the fixed-order result to actual experimental data encountering the aforementioned problem of large logarithms in the di-jet region.
- This serves as motivation for introducing SCET in Chapter 5. We discuss methods common to most EFTs such as power counting and integrating out degrees of freedom to explicitly construct the collinear quark effective Lagrangian. The occurrence of new operators called Wilson lines in the effective theory is physically motivated and their algebraic properties highlighted to be used in later calculations.

- In Chapter 6 we go through the main steps necessary to establish a factorisation theorem for thrust within the SCET framework. The collinear jet function will naturally emerge as the time-ordered product of appropriate effective theory operators. We briefly comment on the physical significance of the remaining shape functions and the factorisation theorem in general.
- Chapter 7 deals with the explicit computation of the jet function for massive primary quarks using the Cutkosky cutting rules. By performing the calculation in this way the effective theory calculation is set up analogously to the full QCD case, exhibiting real emission and virtual parts. However, in the EFT context a new, non-local divergent structure arises that cannot be treated with the subtraction methods discussed in chapter two.
- This prompts the introduction of the subtracted massive jet function in Chapter 8. In this object the non-local divergence, together with additional ambiguities related to zero-bin subtractions of the conventional jet function can be removed. All the remaining divergences are manifestly IR and can in principle be dealt with by appropriate subtraction schemes known from QCD. We conclude the chapter by introducing the subtracted jet function into the factorisation theorem and outlining the potential calculational advantages of the semi-analytic approach thus implied.
- The final Chapter 9 summarises the findings of this thesis and points to potential further work building upon the formalism that was previously developed.

It should be noted that throughout the thesis we have at various stages provided information at a level of detail that goes beyond what would strictly be necessary to achieve the main purpose outlined above. We hope that discussing these details, which are often not explicitly addressed in the literature, in a pedagogic way will provide some value to future students seeking to take up the subject, without presenting a noticeable distraction to the more advanced reader.

2 Fixed order calculations in QCD

In this section we collect results pertaining to the parton level matrix elements for the process $e^+e^- \rightarrow$ hadrons which we will use throughout the thesis. At leading order (LO) we consider diagrams contributing to $e^+e^- \rightarrow q\bar{q}$ and $e^+e^- \rightarrow q\bar{q} + g$ at next-to-leading order (NLO) in α_s . We also give explicit expressions for the gauge-invariant part of the squared matrix elements (i.e. the partonic tensor). Since we are considering true S -matrix elements all external particles, assumed massless, are on their respective mass shell. In this section, and throughout the thesis, we will adopt Feynman gauge, i.e. $\xi = 1$ in Eqs.(H.2) and (H.3), in all our calculations.

When computing the total cross section and thrust distribution at NLO particular emphasis will be placed on the local structure of IR divergences present in the individual real emission and virtual contributions.

However, before we proceed to practical calculations we provide a quick reminder on how IR divergences arise in the context of QCD.

2.1 Prelude: infrared divergences in QCD

When performing calculations in a theory with massless particles such as QCD, in addition to the known high-energy UV divergences new kinds of divergences associated with low-energy, or long-range dynamics appear. These infrared (IR) divergences already manifest at tree-level as a singular dependence of the amplitude on final state particle momenta, as is illustrated¹ in Fig. 2.1.

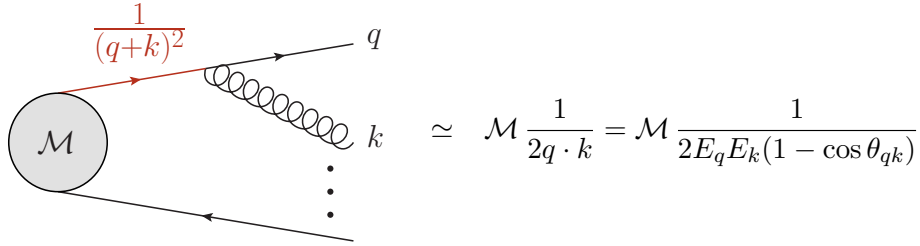


Fig. (2.1): Massless quark q emanating from some amplitude \mathcal{M} and emitting a gluon k . The propagator associated with the internal line goes on-shell in the limit when final state particles become soft or collinear, which corresponds to a large distance traveled by the intermediary quark. It is for this reason that IR divergences are identified with long-range phenomena.

Using the parametrisation $q^\mu = (E_q, \mathbf{q})^\mu$, $k^\mu = (E_k, \mathbf{k})^\mu$, we see that the propagator associated with the internal quark line goes on-shell in one of three scenarios,

$$\frac{1}{(q+k)^2} = \frac{1}{2E_q E_k (1 - \cos \theta_{qk})} \rightarrow \infty \quad \leftrightarrow \quad \begin{cases} E_q \rightarrow 0, & \text{soft,} \\ E_k \rightarrow 0, & \text{soft,} \\ \theta_{qk} \rightarrow 0, & \text{collinear.} \end{cases} \quad (2.2)$$

Notice that all of the above limits correspond to kinematic situations in which the final state including the additionally soft or collinearly emitted gluon is degenerate with the original final state made up of only the quark. While these divergences are visible at the amplitude level through a singular dependence on kinematic final state variables, when performing phase space integrals over such amplitudes in dimensional regularisation ($d = 4 - 2\epsilon$) they manifest as ϵ -poles in the associated cross section.

Let us now turn to analyse virtual contributions involving loops with massless gluons. There the loop integrals themselves, in addition to the ubiquitous UV divergences may produce additional

¹All Feynman diagrams appearing in this thesis were drawn using the software **JaxoDraw**[15].

ϵ -poles associated with internal propagators going on-shell. Schematically such an amplitude is shown in Fig. 2.3.

$$\int d^4k \mathcal{M} \simeq \mathcal{M} \left[\frac{c_1}{\epsilon_{\text{IR}}^2} + \frac{c_2}{\epsilon_{\text{IR}}} + \frac{c_3}{\epsilon_{\text{UV}}} + \dots \right].$$

Fig. (2.3): Infrared divergences appear as additional poles in the parameter ϵ of dimensional regularisation.

For virtual contributions the divergences are thus already explicitly visible in terms of poles at the amplitude level. Since the limits in Eq.(2.2) can overlap, e.g. the gluon can become soft while aligned with the quark, higher order ϵ_{IR} -poles can occur even at one loop. A general theory around IR divergences has been developed in the form of the Landau equations[16] and the Coleman-Norton theorem[17], which we will not explore here.

We have seen that both real emission and virtual contributions separately exhibit IR divergent behaviour when massless particles are present in the amplitude. The crucial observation to make is that in a real world experiment any detector has finite energy (angular) resolution below which it cannot discern soft (or two collinear) particles in the final state. Therefore, in this limit it cannot distinguish whether the final state measured corresponded to a real emission below the sensitivity threshold or a virtual contribution. Consequently quantum mechanics prompts us to coherently add the amplitudes before squaring them to obtain the desired cross section. Since this cross section is always measured to be finite, and we can imagine a detector of finite, but in principle arbitrarily high resolution we begin to suspect that some non-trivial cancellations must be occurring between real emission and virtual contributions.

That these cancellations do indeed take place and that this happens order-by-order in perturbation theory is guaranteed by the celebrated KLN theorem[18]. The remaining section is now dedicated to showing how such cancellations take place in practical calculations yielding finite theoretical predictions.

2.2 Born-level total cross section for $e^+e^- \rightarrow \gamma^* \rightarrow q\bar{q}$

At leading order $\mathcal{O}(\alpha_s^0)$ in the strong coupling only the diagram in Eq.(2.4) contributes,

$$= i\mathcal{M}_2^{\text{LO}}. \quad (2.4)$$

Adopting the above momentum convention, and using the Feynman rules in App. H, the leading-order (LO) matrix element is given by

$$i\mathcal{M}_2^{\text{LO}} = i\tilde{\mu}^{2\epsilon} e^2 e_q \bar{u}(q) \gamma_\mu v(\bar{q}) \frac{1}{s} \bar{v}(e_+) \gamma^\mu u(e_-), \quad (2.5)$$

where $s = Q^2 = (e_+ + e_-)^2 = (q + \bar{q})^2$ is the invariant momentum transfer and e_q the quark electric charge. The parameter $\tilde{\mu}$ introduced by dimensional regularisation² is defined in Eq.(B.4).

²General conventions and notations adopted for dimensional regularisation are outlined in App. B.

Squaring the amplitude in Eq.(2.5), performing the sum over spins and colours in the final state, and averaging over the spin of the incoming leptons gives

$$|\mathcal{M}_2^{\text{LO}}|^2 \equiv \frac{1}{4} \sum_{\text{spins, cols.}} |\mathcal{M}_2^{\text{LO}}|^2 = \frac{1}{4} \tilde{\mu}^{4\epsilon} e^4 e_q^2 N_C \text{Tr}[\gamma_\mu \not{\epsilon}_+ \gamma_\nu \not{\epsilon}_-] \frac{1}{s^2} \text{Tr}[\gamma^\mu \not{q} \gamma^\nu \not{\bar{q}}] \quad (2.6)$$

$$= \left\{ e^2 \tilde{\mu}^{2\epsilon} \left[e_+^\mu e_-^\nu + e_-^\mu e_+^\nu - \frac{s}{2} g^{\mu\nu} \right] \right\} \frac{1}{s^2} \left\{ 4e^2 e_q^2 \tilde{\mu}^{2\epsilon} N_C \left[q_\mu \bar{q}_\nu + \bar{q}_\mu q_\nu - \frac{s}{2} g_{\mu\nu} \right] \right\} \equiv L^{\mu\nu} \frac{1}{s^2} H_{2\mu\nu}^{\text{LO}},$$

where we introduced the gauge-invariant, symmetric leptonic tensor $L_{\mu\nu}(e_+, e_-)$ and the leading order partonic tensor $H_{2\mu\nu}^{\text{LO}}(q, \bar{q})$, which satisfy $Q^\mu L_{\mu\nu} = Q^\mu H_{2\mu\nu}^{\text{LO}} = 0$ due to the Ward identity.

The amplitude in Eq.(2.6) still contains information about the spatial direction along which the final state quarks recoil. If we do not care about this information we can replace the leptonic tensor by its d -dimensional, orientation-averaged analogue

$$\langle L_{\mu\nu} \rangle = \frac{e^2 \tilde{\mu}^{2\epsilon} (1 - \epsilon)}{3 - 2\epsilon} (-s g_{\mu\nu} + Q_\mu Q_\nu), \quad (2.7)$$

which still satisfies the Ward identity and $L^\mu_\mu = \langle L^\mu_\mu \rangle|_{\epsilon=0}$. We note also the factor $\frac{1-\epsilon}{3-2\epsilon}$ that generalises the orientation-averaged sum over the $d - 2 = 2(1 - \epsilon)$ photon polarisations.

To compute the total cross section we therefore have to integrate the quantity

$$d\sigma_2^{\text{LO}} = \frac{1}{2s} \langle L^{\mu\nu} \rangle \frac{1}{s^2} H_{2\mu\nu}^{\text{LO}} d\Phi_2, \quad (2.8)$$

over the final state two-particle phase space whose measure we denote by $d\Phi_2$ (see Eq.(A.3)). In Eq.(2.8) the decomposition of the squared amplitude into a leptonic and partonic part with the photon propagator tying the two together is manifest. As long as we turn off QED interactions after the initial photon production, that is, the leptonic part remains at $\mathcal{O}(\alpha_{\text{em}})$, this form of the amplitude remains valid to all orders in α_s for the partonic part. Exploiting the Ward identity it suffices to contract the partonic tensor only with the part of $\langle L_{\mu\nu} \rangle$ proportional to $g_{\mu\nu}$, yielding the amplitude

$$|\mathcal{M}_2^{\text{LO}}|^2 = \langle L^{\mu\nu} \rangle \frac{1}{s^2} H_{2\mu\nu}^{\text{LO}} = 4e^4 e_q^2 \tilde{\mu}^{4\epsilon} N_C \frac{(1 - \epsilon)^2}{3 - 2\epsilon}. \quad (2.9)$$

Since the matrix element in Eq.(2.9) no longer depends on any final state momenta the integral over phase space in Eq.(2.8) becomes a simple multiplication and the total leading-order cross section reads

$$\sigma_2^{\text{LO}} = 4\pi \tilde{\mu}^{2\epsilon} \alpha_{\text{em}}^2 e_q^2 N_C \frac{e^{\gamma_E \epsilon} \mu^{2\epsilon}}{s^{1+\epsilon}} \frac{(1 - \epsilon)^2}{(3 - 2\epsilon)} \frac{\Gamma(1 - \epsilon)}{\Gamma(2 - 2\epsilon)} \equiv \hat{\sigma}(\epsilon) \frac{e^{\gamma_E \epsilon} \mu^{2\epsilon}}{s^{1+\epsilon}} = \hat{\sigma}(\epsilon) \frac{\mu^{2\epsilon}}{s^{1+\epsilon}} \left\{ 1 + \mathcal{O}(\epsilon) \right\}, \quad (2.10)$$

where the (trivial) expansion in ϵ on the rightmost side was performed to be able to compare to later results more easily. In addition, we will take Eq.(2.10) to be the definition of the universal prefactor

$$\hat{\sigma}(\epsilon) = 4\pi \tilde{\mu}^{2\epsilon} \alpha_{\text{em}}^2 e_q^2 N_C \frac{(1 - \epsilon)^2}{(3 - 2\epsilon)} \frac{\Gamma(1 - \epsilon)}{\Gamma(2 - 2\epsilon)}, \quad (2.11)$$

which will also appear in next-to-leading order calculations in the following sections.

2.3 Next-to-leading order matrix elements

At next-to-leading order $\mathcal{O}(\alpha_s)$ we have to treat the real emission and virtual diagrams shown in Eq.(2.12). Since the leptonic tensor will not be modified compared to tree level, it suffices to write

down the partonic part of the amplitude for each diagram which we will denote by $i\mathcal{H}$,

$$\begin{aligned}
& \text{Diagram 1: } i\mathcal{H}_{3\mu,A}^{r,1} \\
& \text{Diagram 2: } i\mathcal{H}_{3\mu,A}^{r,2} \\
& \text{Diagram 3: } i\mathcal{H}_{2\mu}^v \\
& \text{Diagram 4: } i\mathcal{H}_{2\mu}^{LO}
\end{aligned} \tag{2.12}$$

Starting with the real emission amplitude for the gluon being emitted from the quark,

$$\begin{aligned}
i\mathcal{H}_{3\mu,A}^{r,1} &= \bar{u}_i(q)(ig_s T_{ij}^A \tilde{\mu}^\epsilon \gamma_\sigma) \frac{i(\not{q} + \not{k})}{(q+k)^2} (ie e_q \tilde{\mu}^\epsilon \gamma_\mu) v_j(\bar{q})(\epsilon^*)^\sigma(k) \\
&= -ie e_q g_s \tilde{\mu}^{2\epsilon} T_{ij}^A \bar{u}_i(q) \frac{\gamma_\sigma (\not{q} + \not{k}) \gamma_\mu}{(q+k)^2} v_j(\bar{q})(\epsilon^*)^\sigma(k) \\
&\equiv i\mathcal{H}_{3\sigma\mu,A}^{r,1} (\epsilon^*)^\sigma(k),
\end{aligned} \tag{2.13}$$

where we have explicitly pulled out the polarisation degrees of freedom of the gluon (ϵ^*) for later convenience. We see that since we are only considering the partonic “half” of the diagram, the real emission amplitude carries an open Lorentz index μ for the photon and an open colour index A for the emitted gluon. In complete analogy we find the amplitude where the gluon is emitted from the anti-quark,

$$i\mathcal{H}_{3\mu,A}^{r,2} = i\mathcal{H}_{3\sigma\mu,A}^{r,2} (\epsilon^*)^\sigma(k) = ie e_q g_s \tilde{\mu}^{2\epsilon} T_{ij}^A \bar{u}_i(q) \frac{\gamma_\mu (\not{q} + \not{k}) \gamma_\sigma}{(\bar{q}+k)^2} v_j(\bar{q})(\epsilon^*)^\sigma(k). \tag{2.14}$$

The virtual contribution seen in the second line of Eq.(2.12) takes the form

$$\begin{aligned}
i\mathcal{H}_{2\mu}^v &= \bar{u}_i(q)(ig_s \tilde{\mu}^\epsilon T_{ij}^B \gamma_\rho) \int \bar{d}k \frac{-ig^{\rho\sigma} \delta^{AB}}{k^2 + i0} \frac{i(\not{q} + \not{k})}{(q+k)^2 + i0} (ie e_q \tilde{\mu}^\epsilon \gamma_\mu) \frac{-i(\not{\bar{q}} - \not{k})}{(\bar{q}-k)^2 + i0} (ig_s \tilde{\mu}^\epsilon T_{jk}^A \gamma^\sigma) v_k(\bar{q}) \\
&= -e e_q g_s^2 \tilde{\mu}^{3\epsilon} (T^A T^A)_{ik} \bar{u}_i(q) \int \bar{d}k \frac{\gamma^\rho (\not{q} + \not{k}) \gamma_\mu (\not{\bar{q}} - \not{k}) \gamma_\rho}{[k^2 + i0][(q+k)^2 + i0][(\bar{q}-k)^2 + i0]} v_k(\bar{q}).
\end{aligned} \tag{2.15}$$

For completeness we also give the expression for the partonic part of the leading order amplitude

$$i\mathcal{H}_{2\mu}^{LO} = ie e_q \tilde{\mu}^\epsilon \bar{u}_i(q) \gamma_\mu v_i(\bar{q}). \tag{2.16}$$

To obtain the partonic tensor $H_{\mu\nu}$ we have to appropriately square the above matrix elements. Depending on the number of partons in the final state we have to calculate the interference diagrams

shown in Eq.(2.17) at $\mathcal{O}(\alpha_s)$,

$$H_{3\mu\nu}^{\mathbf{r}} = \left| \text{diagram 1} + \text{diagram 2} \right|^2, \quad H_{2\mu\nu}^{\mathbf{v}} = \left| \text{diagram 3} + \text{diagram 4} \right|^2, \quad (2.17)$$

where we implicitly assume a sum over final state quantum numbers. Writing out the contributions resulting from the squares in Eq.(2.17) to each partonic tensor explicitly gives us

$$\begin{aligned} H_{3\mu\nu}^{\mathbf{r}} &= H_{3\mu\nu}^{\mathbf{r},11} + H_{3\mu\nu}^{\mathbf{r},22} + H_{3\mu\nu}^{\mathbf{r},12} + H_{3\mu\nu}^{\mathbf{r},21}, \\ H_{2\mu\nu}^{\mathbf{v}} &= H_{2\mu\nu}^{\mathbf{v},\mathbf{LO}} + H_{2\mu\nu}^{\mathbf{LO},\mathbf{v}}. \end{aligned} \quad (2.18)$$

Let us begin with the real emission contributions, in particular the square of Eq.(2.13) is computed as

$$H_{3\mu\nu}^{\mathbf{r},11} = \sum_{\text{pols., spins, cols.}} \mathcal{H}_{3\mu\sigma,A}^{\mathbf{r},1} (\mathcal{H}_{3\nu\tau,A}^{\mathbf{r},1})^\dagger (\epsilon^*)^\sigma(k) \epsilon^\tau(k). \quad (2.19)$$

To carry out the summation over final state quantum numbers in Eq.(2.19) we use the gluon polarisation sum

$$\sum_{\text{pols.}} (\epsilon^*)^\mu(k) \epsilon^\nu(k) = -g^{\mu\nu} + \frac{k^\mu \bar{k}^\nu + \bar{k}^\mu k^\nu}{k \cdot \bar{k}}, \quad (2.20)$$

where for a given gluon momentum $k^\mu = (k^0, \mathbf{k})^\mu$ we have $\bar{k}^\mu = (k^0, -\mathbf{k})^\mu$. At this point we could go ahead and just substitute Eq.(2.20) into Eq.(2.19) obtaining terms multiplying $g_{\mu\nu}$ and $k_\mu \bar{k}_\nu$. However, we know that by the Ward identity the terms involving k_μ vanish in the gauge-invariant sum

$$k^\mu [\mathcal{H}_{3\mu,A}^{\mathbf{r},1} + \mathcal{H}_{3\mu,A}^{\mathbf{r},2}] = 0. \quad (2.21)$$

Thus when squaring the amplitude we choose to neglect these terms in intermediate steps on the grounds that they will cancel once we add up all contributions to Eq.(2.18). It therefore suffices to consider only those terms of the partonic tensor that are obtained by contracting with the first term in Eq.(2.20), i.e. we define

$$H_{3,\mathbf{gi}\mu\nu}^{\mathbf{r},11} \equiv \sum_{\text{spins, cols.}} \mathcal{H}_{3\mu\sigma,A}^{\mathbf{r},1} (\mathcal{H}_{3\nu\tau,A}^{\mathbf{r},1})^\dagger (-g^{\sigma\tau}) = -e^2 e_q^2 g_s^2 \tilde{\mu}^{4\epsilon} C_F N_C \frac{\Delta_{\mu\nu}^{\mathbf{r},11}(k, q, \bar{q})}{(2q \cdot k)^2}, \quad (2.22)$$

where $\Delta_{\mu\nu}^{\mathbf{r},11}(k, q, \bar{q}) = \text{Tr}[\gamma^\sigma (\not{q} + \not{k}) \gamma_\mu \not{q} \gamma_\nu (\not{q} + \not{k}) \gamma_\sigma] = -16(1 - \epsilon)(k \cdot q) [\bar{q}_\mu k_\nu + k_\mu \bar{q}_\nu - g_{\mu\nu}(k \cdot \bar{q})]$. Note that we have $H_{3,\mathbf{gi}\mu\nu}^{\mathbf{r},11} \neq H_{3\mu\nu}^{\mathbf{r},11}$, but in the gauge-invariant (\mathbf{gi}) sum of all these contributions we recover Eq.(2.18).

The squared amplitude for the emission of the gluon from the anti-quark can be obtained from Eq.(2.22) by exchanging $q \leftrightarrow \bar{q}$ and therefore reads

$$H_{3,\mathbf{gi}\mu\nu}^{\mathbf{r},22} = -e^2 e_q^2 g_s^2 \tilde{\mu}^{4\epsilon} C_F N_C \frac{\Delta_{\mu\nu}^{\mathbf{r},22}(k, q, \bar{q})}{(2\bar{q} \cdot k)^2}, \quad (2.23)$$

where $\Delta_{\mu\nu}^{\mathbf{r},22}(k, q, \bar{q}) = \Delta_{\mu\nu}^{\mathbf{r},11}(k, \bar{q}, q)$ by symmetry. We now turn to computing the real emission interference terms which exhibit a similar structure,

$$H_{3,\mathbf{gi}\mu\nu}^{\mathbf{r},12} = \sum_{\text{spins, cols.}} \mathcal{H}_{3\mu\sigma,A}^{\mathbf{r},1} (\mathcal{H}_{3\nu\tau,A}^{\mathbf{r},2})^\dagger (-g^{\sigma\tau}) = e^2 e_q^2 g_s^2 \tilde{\mu}^{4\epsilon} C_F N_C \frac{\Delta_{\mu\nu}^{\mathbf{r},12}(k, q, \bar{q})}{(2q \cdot k)(2\bar{q} \cdot k)}. \quad (2.24)$$

This time however, the tensor $\Delta_{\mu\nu}^{\mathbf{r},12}(k, q, \bar{q}) = \text{Tr}[\gamma^\sigma(\not{q} + \not{k})\gamma_\mu \not{q} \gamma_\sigma(\not{q} + \not{k})\gamma_\nu \not{q}]$ representing the Dirac trace takes a substantially more complicated form in d -dimensions which is why we will not explicitly state it here. In fact, it will turn out that for our purposes knowing the tensor in its full generality will not be necessary anyway (see Eq.(2.32)). The second interference diagram is again related by exchanging $q \leftrightarrow \bar{q}$ and yields

$$H_{\mathbf{3},\mathbf{gi}}^{\mathbf{r},21}_{\mu\nu} = e^2 e_q^2 g_s^2 \tilde{\mu}^{4\epsilon} C_F N_C \frac{\Delta_{\mu\nu}^{\mathbf{r},21}(k, q, \bar{q})}{(2\bar{q} \cdot k)(2q \cdot k)}, \quad (2.25)$$

where $\Delta_{\mu\nu}^{\mathbf{r},21}(k, q, \bar{q}) = \Delta_{\nu\mu}^{\mathbf{r},12}(k, \bar{q}, q)$, which are equal modulo contraction with a symmetric quantity.

The final term we are missing at $\mathcal{O}(\alpha_s)$ is the interference between the one-loop vertex correction Eq.(2.15) and the tree-level matrix element Eq.(2.16),

$$H_{\mathbf{2}\mu\nu}^{\mathbf{v},\mathbf{LO}} = \sum_{\text{spins}} \mathcal{H}_{\mathbf{2}\mu}^{\mathbf{v}} (\mathcal{H}_{\mathbf{2}\nu}^{\mathbf{LO}})^\dagger = ie^2 e_q^2 g_s^2 \tilde{\mu}^{2\epsilon} C_F N_C I_{\mathbf{2}\mu\nu}^{\mathbf{v},\mathbf{LO}}, \quad (2.26)$$

with the one-loop integral over the virtual gluon momentum given by

$$I_{\mathbf{2}\mu\nu}^{\mathbf{v},\mathbf{LO}} = \tilde{\mu}^{2\epsilon} \int d^d k \frac{\text{Tr}[\not{q} \gamma^\rho (\not{q} + \not{k}) \gamma_\mu (\not{q} - \not{k}) \gamma_\rho \not{q} \gamma_\nu]}{[k^2 + i0] [(q+k)^2 + i0] [(\bar{q}-k)^2 + i0]}. \quad (2.27)$$

Just as we remarked below Eq.(2.24), we do not need to evaluate the full trace in Eq.(2.27). Since at next-to-leading order the partonic tensor still satisfies $Q^\mu H_{\mathbf{2}\mu\nu}^{\mathbf{v}} = 0$, when we later contract with the leptonic tensor it will suffice to consider the integral

$$\begin{aligned} I_{\mathbf{2}}^{\mathbf{v},\mathbf{LO}} &= g^{\mu\nu} I_{\mathbf{2}\mu\nu}^{\mathbf{v},\mathbf{LO}} = -\tilde{\mu}^{2\epsilon} \int d^d k \frac{8(1-\epsilon) [s^2 - 4(q \cdot k)(\bar{q} \cdot k) - 2sk \cdot (q - \bar{q}) + \epsilon sk^2]}{[k^2 + i0] [(q+k)^2 + i0] [(\bar{q}-k)^2 + i0]} \\ &= 8(1-\epsilon) \frac{(-i)}{16\pi^2} \left(\frac{4\pi\tilde{\mu}^2}{-s-i0} \right)^\epsilon \frac{s \Gamma(1+\epsilon) \Gamma(1-\epsilon)^2}{\Gamma(1-2\epsilon)} \left[\frac{2}{\epsilon^2} + \frac{3}{\epsilon} + \frac{8}{1-2\epsilon} \right]. \end{aligned} \quad (2.28)$$

Now that all contributions to the partonic tensor are known we can proceed to compute the total cross section and more differential observables.

2.4 Next-to-leading order total cross section

For the real emission diagrams we consider the three-particle final state analogue to Eq.(2.8) which we write as

$$d\sigma_{\mathbf{3}}^{\mathbf{r}} = \frac{1}{2s} \langle L^{\mu\nu} \rangle \frac{1}{s^2} H_{\mathbf{3}\mu\nu}^{\mathbf{r}} d\Phi_{\mathbf{3}}. \quad (2.29)$$

where the final state dependence of the invariant momentum transfer is now given by $s = Q^2 = (q + \bar{q} + k)^2$. The spin- and orientation-averaged leptonic tensor is still given as in Eq.(2.7), and the real emission part of the partonic tensor can be obtained as

$$H_{\mathbf{3}\mu\nu}^{\mathbf{r}} = H_{\mathbf{3},\mathbf{gi}}^{\mathbf{r},11}_{\mu\nu} + H_{\mathbf{3},\mathbf{gi}}^{\mathbf{r},22}_{\mu\nu} + H_{\mathbf{3},\mathbf{gi}}^{\mathbf{r},12}_{\mu\nu} + H_{\mathbf{3},\mathbf{gi}}^{\mathbf{r},21}_{\mu\nu}. \quad (2.30)$$

Since $Q^\mu H_{\mathbf{3}\mu\nu}^{\mathbf{r}} = 0$, we are again justified in contracting the partonic tensor only with the part of $\langle L_{\mu\nu} \rangle$ proportional to $g_{\mu\nu}$ to get the full amplitude squared. With this in mind we can safely write Eq.(2.29) as

$$d\sigma_{\mathbf{3}}^{\mathbf{r}} = \frac{1}{2s} \left[|\mathcal{M}_{\mathbf{3},\mathbf{gi}}^{\mathbf{r},11}|^2 + |\mathcal{M}_{\mathbf{3},\mathbf{gi}}^{\mathbf{r},22}|^2 + \mathcal{M}_{\mathbf{3},\mathbf{gi}}^{\mathbf{r},12} + \mathcal{M}_{\mathbf{3},\mathbf{gi}}^{\mathbf{r},21} \right] d\Phi_{\mathbf{3}}, \quad (2.31)$$

where the squared matrix elements are now obtained by only contracting (c.f. Eq.(2.7))

$$|\mathcal{M}_{3,\text{gi}}^{\text{r},\text{ij}}|^2 = \frac{1}{s} \frac{e^2(1-\epsilon)}{3-2\epsilon} \left(-g^{\mu\nu} H_{3\mu\nu}^{\text{r},\text{ij}} \right), \quad \mathbf{i}, \mathbf{j} \in \{1, 2\}. \quad (2.32)$$

We now state the results for all the amplitudes shown in Eq.(2.31) as manifest functions of the final state parton momenta,

$$\begin{aligned} |\mathcal{M}_{3,\text{gi}}^{\text{r},11}|^2 &= \hat{\mathcal{M}} \frac{\tilde{\mu}^{4\epsilon}}{s} \frac{(1-\epsilon)^3}{3-2\epsilon} \frac{\bar{q} \cdot k}{q \cdot k} = \hat{\mathcal{M}} \frac{\tilde{\mu}^{4\epsilon}}{s} \frac{(1-\epsilon)^3}{3-2\epsilon} \frac{1-x_q}{1-x_{\bar{q}}}, \\ |\mathcal{M}_{3,\text{gi}}^{\text{r},22}|^2 &= \hat{\mathcal{M}} \frac{\tilde{\mu}^{4\epsilon}}{s} \frac{(1-\epsilon)^3}{3-2\epsilon} \frac{q \cdot k}{\bar{q} \cdot k} = \hat{\mathcal{M}} \frac{\tilde{\mu}^{4\epsilon}}{s} \frac{(1-\epsilon)^3}{3-2\epsilon} \frac{1-x_{\bar{q}}}{1-x_q}, \\ \mathcal{M}_{3,\text{gi}}^{\text{r},12} = \mathcal{M}_{3,\text{gi}}^{\text{r},21} &= -\frac{\hat{\mathcal{M}}}{(q \cdot k)(\bar{q} \cdot k)} \frac{\tilde{\mu}^{4\epsilon}}{s} \frac{(1-\epsilon)^2}{3-2\epsilon} \left[\epsilon(q \cdot k)(\bar{q} \cdot k) - \frac{1}{2}(q \cdot \bar{q}) s \right] \\ &= \hat{\mathcal{M}} \frac{\tilde{\mu}^{4\epsilon}}{s} \frac{(1-\epsilon)^2}{3-2\epsilon} \left[\frac{1-x_k}{(1-x_q)(1-x_{\bar{q}})} - \epsilon \right], \end{aligned} \quad (2.33)$$

where we separated off the common amplitude-level prefactor

$$\hat{\mathcal{M}} = 8e^4 e_q^2 g_s^2 \tilde{\mu}^{2\epsilon} C_F N_C, \quad (2.34)$$

that will frequently reappear in later calculations. On the right-most side of Eq.(2.33) we have rewritten the matrix elements in terms of the momentum fractions

$$x_p = 2 \frac{p \cdot Q}{s}, \quad p \in \{q, \bar{q}, k\}, \quad (2.35)$$

which satisfy $0 \leq x_p \leq 1$ and are normalised to $x_q + x_{\bar{q}} + x_k = 2$ and will turn out to be particularly convenient variables for the integration over the final particle phase space $d\Phi_3$ (see Eq.(A.4)). Since all particles are assumed to be massless we also have $s = 2(\bar{q} \cdot q + q \cdot k + \bar{q} \cdot k)$. Adding all the contributions from Eq.(2.33) leads to a particularly simple form of the total squared real emission amplitude,

$$|\mathcal{M}_3^{\text{r}}|^2 = |\mathcal{M}_{3,\text{gi}}^{\text{r},11}|^2 + |\mathcal{M}_{3,\text{gi}}^{\text{r},22}|^2 + \mathcal{M}_{3,\text{gi}}^{\text{r},12} + \mathcal{M}_{3,\text{gi}}^{\text{r},21} = \hat{\mathcal{M}} \frac{\tilde{\mu}^{4\epsilon}}{s} \frac{(1-\epsilon)^2}{3-2\epsilon} \left[\frac{x_q^2 + x_{\bar{q}}^2 - \epsilon x_k^2}{(1-x_q)(1-x_{\bar{q}})} \right]. \quad (2.36)$$

In the above amplitude we can transparently see the potential sources of IR-divergent behaviour. Exploiting the kinematic properties of the final state particles we can write

$$1 - x_q = \frac{E_{\bar{q}} E_k}{s} (1 - \cos \theta_{\bar{q}k}), \quad 1 - x_{\bar{q}} = \frac{E_q E_k}{s} (1 - \cos \theta_{qk}), \quad (2.37)$$

identifying the collinear limits where the gluon is aligned with the quark ($\theta_{qk} \rightarrow 0 \Rightarrow x_{\bar{q}} \rightarrow 1$) or the anti-quark ($\theta_{\bar{q}k} \rightarrow 0 \Rightarrow x_q \rightarrow 1$) corresponding to single poles in the amplitude. The soft limit ($E_k \rightarrow 0 \Rightarrow x_k \rightarrow 0$) together with momentum conservation imply that $x_q, x_{\bar{q}} \rightarrow 1$ simultaneously leading to a quadratic divergence in Eq.(2.36).

Instead of directly integrating Eq.(2.36) we proceed to calculate the total cross section according to the contributions coming from the individual amplitudes in Eq.(2.33) such that

$$\sigma_3^{\text{r}} = \sigma_3^{\text{r},11} + \sigma_3^{\text{r},22} + \sigma_3^{\text{r},12} + \sigma_3^{\text{r},21}, \quad (2.38)$$

where the terms on the left-hand side are found by integrating separately each term in Eq.(2.31). This gives us the ability to better track the origin of any infrared divergences arising. Performing the

phase space integrals we find

$$\begin{aligned}
\sigma_{\mathbf{3}}^{\mathbf{r},11} &= \sigma_{\mathbf{3}}^{\mathbf{r},22} = \hat{\sigma}(\epsilon) \frac{\alpha_s C_F}{2\pi} \frac{e^{\gamma_E \epsilon} \mu^{4\epsilon}}{s^{1+2\epsilon}} (1-\epsilon) \frac{\Gamma(2-\epsilon)\Gamma(-\epsilon)}{\Gamma(3-3\epsilon)} \\
&= \hat{\sigma}(\epsilon) \frac{\alpha_s C_F}{2\pi} \frac{\mu^{4\epsilon}}{s^{1+2\epsilon}} \left\{ -\frac{1}{2\epsilon} - \frac{5}{4} + \mathcal{O}(\epsilon) \right\}, \\
\sigma_{\mathbf{3}}^{\mathbf{r},12} &= \sigma_{\mathbf{3}}^{\mathbf{r},21} = \hat{\sigma}(\epsilon) \frac{\alpha_s C_F}{2\pi} \frac{e^{\gamma_E \epsilon} \mu^{4\epsilon}}{s^{1+2\epsilon}} \left[\frac{(1-\epsilon)\Gamma(-\epsilon)^2}{\Gamma(2-3\epsilon)} - \epsilon \frac{\Gamma(1-\epsilon)^2}{\Gamma(3-3\epsilon)} \right] \\
&= \hat{\sigma}(\epsilon) \frac{\alpha_s C_F}{2\pi} \frac{\mu^{4\epsilon}}{s^{1+2\epsilon}} \left\{ \frac{1}{\epsilon^2} + \frac{2}{\epsilon} + 6 - \frac{7\pi^2}{12} + \mathcal{O}(\epsilon) \right\},
\end{aligned} \tag{2.39}$$

with the prefactor $\hat{\sigma}(\epsilon)$ given as in Eq.(2.11). Expanding in ϵ we can see that only the interference terms $\sigma_{\mathbf{3}}^{\mathbf{r},12}, \sigma_{\mathbf{3}}^{\mathbf{r},21}$ contribute to the soft divergence associated with the quadratic pole. Combining these results the real emission contribution to the total cross section can thus be written as

$$\sigma_{\mathbf{3}}^{\mathbf{r}} = \hat{\sigma}(\epsilon) \frac{\alpha_s C_F}{2\pi} \frac{\mu^{4\epsilon}}{s^{1+2\epsilon}} \left\{ \frac{2}{\epsilon^2} + \frac{3}{\epsilon} + \frac{19}{2} - \frac{7\pi^2}{6} + \mathcal{O}(\epsilon) \right\}, \tag{2.40}$$

which could have also been obtained by directly integrating Eq.(2.36).

Let us now turn to computing the total cross section for the virtual contributions coming from the one-loop interference diagrams shown in the second line of Eq.(2.12). Schematically we write

$$d\sigma_{\mathbf{2}}^{\mathbf{v}} = \frac{1}{2s} \langle L^{\mu\nu} \rangle \frac{1}{s^2} H_{\mathbf{2}\mu\nu}^{\mathbf{v}} d\Phi_{\mathbf{2}}, \tag{2.41}$$

where the partonic tensor for the virtual-tree interference is given by the gauge-invariant sum

$$H_{\mathbf{2}\mu\nu}^{\mathbf{v}} = H_{\mathbf{2},\mathbf{gi}\mu\nu}^{\mathbf{v},\mathbf{LO}} + H_{\mathbf{2},\mathbf{gi}\mu\nu}^{\mathbf{LO},\mathbf{v}} = H_{\mathbf{2},\mathbf{gi}\mu\nu}^{\mathbf{v},\mathbf{LO}} + (H_{\mathbf{2},\mathbf{gi}\mu\nu}^{\mathbf{v},\mathbf{LO}})^* = 2\text{Re}\{H_{\mathbf{2},\mathbf{gi}\mu\nu}^{\mathbf{v},\mathbf{LO}}\}, \tag{2.42}$$

Again, we will only need to contract with the part of $\langle L_{\mu\nu} \rangle$ proportional to $g_{\mu\nu}$ to obtain the desired amplitude, while the terms involving $Q_\mu Q_\nu$ cancel in the sum Eq.(2.42). In accord with Eq.(2.32) we thus compute

$$\begin{aligned}
\mathcal{M}_{\mathbf{2},\mathbf{gi}}^{\mathbf{v},\mathbf{LO}} &= \frac{1}{s} \frac{e^2(1-\epsilon)}{3-2\epsilon} (-g^{\mu\nu} H_{\mathbf{2}\mu\nu}^{\mathbf{v},\mathbf{LO}}) \\
&= -\frac{\hat{\mathcal{M}}}{2(4\pi)^2} \tilde{\mu}^{2\epsilon} \left(\frac{4\pi\tilde{\mu}^2}{-s-i0} \right)^\epsilon \frac{\Gamma(1+\epsilon)\Gamma(1-\epsilon)^2(1-\epsilon)^2}{\Gamma(1-2\epsilon)} \frac{1}{3-2\epsilon} \left[\frac{2}{\epsilon^2} + \frac{3}{\epsilon} + \frac{8}{1-2\epsilon} \right],
\end{aligned} \tag{2.43}$$

where we have used Eqs.(2.26) and (2.28), and we still have to take the real part to obtain the partonic tensor. The only factor in Eq.(2.43) that is not already manifestly real and we therefore have to worry about is

$$\text{Re} \left\{ \left(\frac{4\pi\tilde{\mu}^2}{-s-i0} \right)^\epsilon \right\} = \left(\frac{4\pi\tilde{\mu}^2}{s} \right)^\epsilon \text{Re} \{ (-1-i0)^{-\epsilon} \} = \left(\frac{4\pi\tilde{\mu}^2}{s} \right)^\epsilon \text{Re} \{ e^{i\pi\epsilon} \} = \left(\frac{4\pi\tilde{\mu}^2}{s} \right)^\epsilon \cos(\pi\epsilon). \tag{2.44}$$

The cross section in Eq.(2.41) can now be written in terms of Eq.(2.43) as

$$d\sigma_{\mathbf{2}}^{\mathbf{v}} = \frac{1}{2s} |\mathcal{M}_{\mathbf{2}}^{\mathbf{v}}|^2 d\Phi_{\mathbf{2}}, \quad \text{and} \quad |\mathcal{M}_{\mathbf{2}}^{\mathbf{v}}|^2 = 2\text{Re} \left\{ \mathcal{M}_{\mathbf{2},\mathbf{gi}}^{\mathbf{v},\mathbf{LO}} \right\}, \tag{2.45}$$

where the phase space integrand is given explicitly by

$$2\text{Re} \left\{ \mathcal{M}_{\mathbf{2},\mathbf{gi}}^{\mathbf{v},\mathbf{LO}} \right\} = -\frac{\hat{\mathcal{M}}}{(4\pi)^2} \tilde{\mu}^{2\epsilon} \left(\frac{4\pi\tilde{\mu}^2}{s} \right)^\epsilon \cos(\pi\epsilon) \frac{\Gamma(1+\epsilon)\Gamma(1-\epsilon)^2(1-\epsilon)^2}{\Gamma(1-2\epsilon)} \frac{1}{3-2\epsilon} \left[\frac{2}{\epsilon^2} + \frac{3}{\epsilon} + \frac{8}{1-2\epsilon} \right]. \tag{2.46}$$

Notice that just as we found at leading order, the amplitude Eq.(2.46) is a function of the momentum transfer s and no longer depends on any individual final state momenta. The integration over the final particle phase space in Eq.(2.45) can again be facilitated by the use of Eq.(A.3). The total cross section coming from the virtual-tree interference diagrams thus reads

$$\begin{aligned}\sigma_2^{\mathbf{Y}} &= -\hat{\sigma}(\epsilon) \frac{\alpha_s C_F}{2\pi} \frac{e^{\gamma_E \epsilon} \mu^{4\epsilon}}{s^{1+2\epsilon}} \cos(\pi\epsilon) \frac{\Gamma(1+\epsilon)\Gamma(1-\epsilon)^2}{\Gamma(1-2\epsilon)} \left[\frac{2}{\epsilon^2} + \frac{3}{\epsilon} + \frac{8}{1-2\epsilon} \right] \\ &= -\hat{\sigma}(\epsilon) \frac{\alpha_s C_F}{2\pi} \frac{\mu^{4\epsilon}}{s^{1+2\epsilon}} \left\{ \frac{2}{\epsilon^2} + \frac{3}{\epsilon} + 8 - \frac{7\pi^2}{6} + \mathcal{O}(\epsilon) \right\}.\end{aligned}\quad (2.47)$$

Comparing with the real emission contribution Eq.(2.40), we see that the divergences cancel³ in the sum and we are left with a finite total cross section

$$\sigma_{2/3}^{\mathbf{NLO}} = \sigma_3^{\mathbf{r}} + \sigma_2^{\mathbf{Y}} = \hat{\sigma}(\epsilon) \frac{\alpha_s C_F}{2\pi} \frac{\mu^{4\epsilon}}{s^{1+2\epsilon}} \frac{3}{2} + \mathcal{O}(\epsilon). \quad (2.48)$$

Together with the leading order result Eq.(2.10) this gives

$$\sigma = \sigma_2^{\mathbf{LO}} + \sigma_{2/3}^{\mathbf{NLO}} = \hat{\sigma}(\epsilon) \left\{ \frac{\mu^{2\epsilon}}{s^{1+\epsilon}} + \frac{\alpha_s C_F}{2\pi} \frac{\mu^{4\epsilon}}{s^{1+2\epsilon}} \frac{3}{2} + \mathcal{O}(\epsilon) \right\} = \sigma_2^{\mathbf{LO}} \left\{ 1 + \frac{\alpha_s C_F}{\pi} \frac{3}{4} + \mathcal{O}(\epsilon) \right\}, \quad (2.49)$$

where we have brought the result into a form that is more recognisable from the literature[19].

2.5 General structure of the cross-section for $e^+e^- \rightarrow \gamma^* \rightarrow q\bar{q} + X$

As we have seen explicitly for the LO and NLO calculations in the previous section (e.g. Eq.(2.9)), the squared amplitude decomposes into a leptonic and partonic part for the processes $e^+e^- \rightarrow \gamma^* \rightarrow q\bar{q}(+g)$ at $\mathcal{O}(\alpha_{\text{em}})$. If we now allow for the final state to contain any number of final state partons \tilde{X} radiated from the primary $q\bar{q}$ -pair, we can write the amplitude abstractly as

$$i\mathcal{M}(e^+e^- \rightarrow \gamma^* \rightarrow q\bar{q} + \tilde{X}) = i \left[\tilde{\mu}^\epsilon e_q \langle \tilde{X}, q\bar{q} | \mathcal{J}_v^\mu(0) | 0 \rangle \right] \frac{1}{s} \left[\tilde{\mu}^\epsilon e^2 \bar{v}(e^+) \gamma_\mu u(e^-) \right], \quad (2.50)$$

with the vector production current $\mathcal{J}_v^\mu(x) = \bar{\Psi}(x) \gamma^\mu \Psi(x)$ ensuring that only final states compatible with virtual photon decay into a primary $q\bar{q}$ -pair contribute. At leading order where $|\tilde{X}\rangle = |0\rangle$ we simply have

$$\langle q\bar{q} | \mathcal{J}_v^\mu(0) | 0 \rangle = \bar{u}(q) \gamma^\mu v(\bar{q}), \quad (2.51)$$

in accordance with what we found in Eq.(2.5). The fact that we evaluate the current at $x = 0$ can be justified with an appropriate choice of final state momenta \tilde{X}, q, \bar{q} , which need to satisfy $e^+ + e^- = q + \bar{q} + \tilde{X}$, and the translational invariance of the theory. We reiterate that the manifest form of Eq.(2.50) holds only when QED interactions are turned off after the initial photon production. At higher orders in α_{em} , effects like initial state radiation of photons would not be described by an amplitude of this structure. However, the partonic matrix element $\langle \tilde{X}, q\bar{q} | \mathcal{J}_v^\mu(0) | 0 \rangle$ may be evaluated to any order in α_s without breaking the factorised form.

So far we have been explicit about the intermediate state being an off-shell photon γ^* . In a realistic setting, at center of mass energies of $s \sim 50\text{GeV}$ and higher we would have to additionally consider mediation by an off-shell Z^* Boson, which for the purposes of this thesis will not be necessary. The structure of the amplitude in this more general case can be found in [20].

³See App. C on why we are allowed to cancel the divergences without having to worry about the distinction between UV and IR.

Squaring the amplitude Eq.(2.50) and summing over spins thus yields

$$\frac{1}{4} \sum_{\text{spins}} |\mathcal{M}(e^+e^- \rightarrow q\bar{q} + \tilde{X})|^2 = L_{\mu\nu} \frac{1}{s^2} \left[\tilde{\mu}^{2\epsilon} e^2 e_q^2 \langle 0 | \mathcal{J}_v^\dagger{}^\mu(0) | \tilde{X}, q\bar{q} \rangle \langle \tilde{X}, q\bar{q} | \mathcal{J}_v^\nu(0) | 0 \rangle \right], \quad (2.52)$$

with the leptonic tensor given as in Eq.(2.6) and the partonic tensor $H_{\tilde{X}, q\bar{q}}^{\mu\nu}$ associated with the production of the final state $\tilde{X}, q\bar{q}$ identified by the square brackets on the right-hand side.

The total cross section is now obtained by summing over all allowed final states $X = q\bar{q} + \tilde{X}$ as

$$\begin{aligned} \sigma &= \frac{1}{2s} \sum_X \int d\Pi_X (2\pi)^d \delta^{(d)}(Q - \sum_{i \in X} p_i) \langle L_{\mu\nu} \rangle \frac{1}{s^2} \left[\tilde{\mu}^{2\epsilon} e^2 e_q^2 \langle 0 | \mathcal{J}_v^\dagger{}^\mu(0) | X \rangle \langle X | \mathcal{J}_v^\nu(0) | 0 \rangle \right] \\ &= \frac{1}{2s} \sum_X \int d\Phi_X \langle L_{\mu\nu} \rangle \frac{1}{s^2} H_X^{\mu\nu}, \end{aligned} \quad (2.53)$$

where we have replaced the leptonic tensor by its orientation-averaged counterpart Eq.(2.7) and have absorbed the overall momentum conserving delta function into the phase space measure $d\Phi_X$ to be notationally consistent with the definitions for the two- and three-particle cases found in Eqs.(A.3) and (A.4).

This particular form of the cross section will prove useful in Sec. 6 when we wish to derive a factorisation theorem within the effective theory (EFT) framework of Soft-Collinear effective theory (SCET) in the limit where all final state partons are either soft or collinear.

2.6 Thrust at next-to-leading order

This section concerns itself with computing the differential cross section for the event shape variable thrust[11]

$$T = \max_{\mathbf{n}} \frac{\sum_{\mathbf{p}_i} |\mathbf{p}_i \cdot \mathbf{n}|}{\sum_{\mathbf{p}_i} |\mathbf{p}_i|}, \quad (2.54)$$

where the maximum is taken with respect to all spatial unit vectors \mathbf{n} , and which one can show to approach unity when the event under consideration becomes a perfect di-jet event as seen in the center of mass frame. The vector \mathbf{n}_T at which the maximum is attained is conventionally called the thrust axis. As a simple example let us consider thrust for a two-particle final state, which by momentum conservation must be perfectly di-jet like in the center of mass frame, and hence have $T = 1$. Indeed, using $\mathbf{p}_1 = -\mathbf{p}_2$ for the final state momenta we find

$$T = \max_{\mathbf{n}} \frac{|\mathbf{p}_1 \cdot \mathbf{n}| + |\mathbf{p}_2 \cdot \mathbf{n}|}{|\mathbf{p}_1| + |\mathbf{p}_2|} = \max_{\mathbf{n}} \frac{2|\mathbf{p}_1||\mathbf{n}| \cos \theta_{p_1 n}}{2|\mathbf{p}_1|} = 1, \quad (2.55)$$

where the maximum is reached when the angle between \mathbf{p}_1 and \mathbf{n} vanishes and so the thrust axis \mathbf{n}_T is (anti-)aligned with one (or the other) parton momentum.

We will define the computationally more convenient quantity $\tau = 1 - T$, which, for the next-to-leading order process $e^+e^- \rightarrow q\bar{q} + g$ considered earlier can be written in terms of the momentum fractions Eq.(2.35) as

$$\tau(x_q, x_{\bar{q}}, x_k) = \min(1 - x_q, 1 - x_{\bar{q}}, 1 - x_k) = \min(1 - x_q, 1 - x_{\bar{q}}, x_q + x_{\bar{q}} - 1) \equiv \tau(x_q, x_{\bar{q}}), \quad (2.56)$$

where the normalisation $x_q + x_{\bar{q}} + x_k = 2$ was used to eliminate the dependence on the gluon momentum fraction. This can be seen from simple geometric insights, which we want to facilitate with Fig. 2.57 and the following comment.

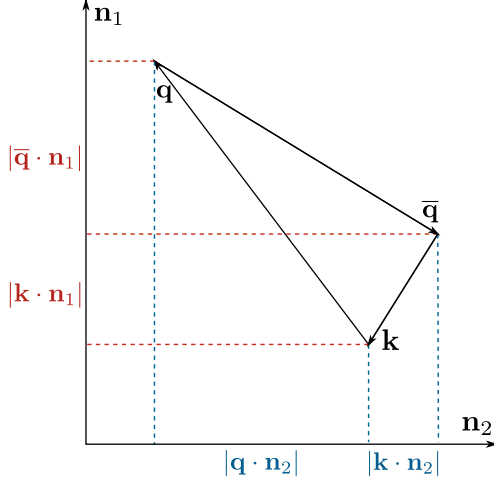


Fig.(2.57): Momentum conservation implies that the spacial final state momenta $\mathbf{q}, \bar{\mathbf{q}}, \mathbf{k}$, lie in a plane. Depending on the choice of reference vector $\mathbf{n}_{1,2}$ within that plane, we can see that the sum of the absolute values of the two smaller projections onto the given vector is always equal to the absolute value of largest projection. Concretely we can read off that $|\bar{\mathbf{q}} \cdot \mathbf{n}_1| + |\mathbf{k} \cdot \mathbf{n}_1| = |\mathbf{q} \cdot \mathbf{n}_1|$ while $|\mathbf{q} \cdot \mathbf{n}_2| + |\mathbf{k} \cdot \mathbf{n}_2| = |\bar{\mathbf{q}} \cdot \mathbf{n}_2|$, and similar for any other choice of \mathbf{n} in between.

From the considerations of figure Fig. 2.57 we see that for any \mathbf{n} ,

$$|\mathbf{q} \cdot \mathbf{n}| + |\bar{\mathbf{q}} \cdot \mathbf{n}| + |\mathbf{k} \cdot \mathbf{n}| = 2 \max\{|\mathbf{q} \cdot \mathbf{n}|, |\bar{\mathbf{q}} \cdot \mathbf{n}|, |\mathbf{k} \cdot \mathbf{n}|\}. \quad (2.58)$$

Next we note that thrust is defined in the center of mass frame and thus for massless, on-shell particles we have

$$Q^\mu = (Q, \mathbf{0})^\mu \quad \Rightarrow \quad |\mathbf{q}| + |\bar{\mathbf{q}}| + |\mathbf{k}| = Q, \quad x_q = \frac{2q^0}{Q}, \quad (2.59)$$

with the momentum fractions for \bar{q}, k given analogously. With this we can write the momentum projections $|\mathbf{q} \cdot \mathbf{n}| = \frac{Q}{2} x_q |\cos \theta_q|$, where θ_i , $i = q, \bar{q}, k$, denotes the angle between the respective final state momentum and the reference vector \mathbf{n} . Plugging Eq.(2.58) and Eq.(2.59) into the definition of thrust at NLO we obtain

$$T = \max_{\mathbf{n}} \frac{|\mathbf{q} \cdot \mathbf{n}| + |\bar{\mathbf{q}} \cdot \mathbf{n}| + |\mathbf{k} \cdot \mathbf{n}|}{|\mathbf{q}| + |\bar{\mathbf{q}}| + |\mathbf{k}|} = \max_{\mathbf{n}} \left(\max\{x_q |\cos \theta_q|, x_{\bar{q}} |\cos \theta_{\bar{q}}|, x_k |\cos \theta_k|\} \right) \quad (2.60)$$

$$= \max\{x_q, x_{\bar{q}}, x_k\},$$

from which Eq.(2.56) readily follows. The form Eq.(2.60) allows us to quickly verify that for a perfect di-jet event, where one of the $x_i = 0$, we still have $T = 1$ as before, while for a perfectly spherical tri-jet event where $x_q = x_{\bar{q}} = x_k = 2/3$ we correspondingly have $T = 2/3$, from which follows that $\tau = 1 - T \in [0, 1/3]$ for any event at the given order.

The differential thrust distribution we would like to compute is thus given by Eq.(2.31) with the additional constraint

$$\begin{aligned} \delta(\tau - \tau(x_q, x_{\bar{q}})) &= \delta(x_q + x_{\bar{q}} - \tau - 1) \theta(2 - 2x_{\bar{q}} - x_q) \theta(2 - 2x_q - x_{\bar{q}}) \\ &\quad + \delta(1 - \tau - x_{\bar{q}}) \theta(2x_{\bar{q}} + x_q - 2) \theta(x_{\bar{q}} - x_q) \\ &\quad + \delta(1 - \tau - x_q) \theta(2x_q + x_{\bar{q}} - 2) \theta(x_q - x_{\bar{q}}) \\ &\equiv \delta_{\text{i}}(x_q, x_{\bar{q}}, \tau) + \delta_{\text{ii}}(x_q, x_{\bar{q}}, \tau) + \delta_{\text{iii}}(x_q, x_{\bar{q}}, \tau), \end{aligned} \quad (2.61)$$

which restricts the physical phase space to slices of constant τ , i.e.,

$$\frac{d\sigma_{\mathbf{3}}^{\mathbf{r}}}{d\tau} = \frac{1}{2s} \int \left[|\mathcal{M}_{\mathbf{3},\mathbf{gi}}^{\mathbf{r},11}|^2 + |\mathcal{M}_{\mathbf{3},\mathbf{gi}}^{\mathbf{r},22}|^2 + \mathcal{M}_{\mathbf{3},\mathbf{gi}}^{\mathbf{r},12} + \mathcal{M}_{\mathbf{3},\mathbf{gi}}^{\mathbf{r},21} \right] \delta(\tau - \tau(x_q, x_{\bar{q}})) d\Phi_{\mathbf{3}}. \quad (2.62)$$

Since the phase space we are considering is just two-dimensional we can draw the regions in $(x_q, x_{\bar{q}})$ -space defined by the observable Eq.(2.61) in a Dalitz plot shown in Fig. 2.63.

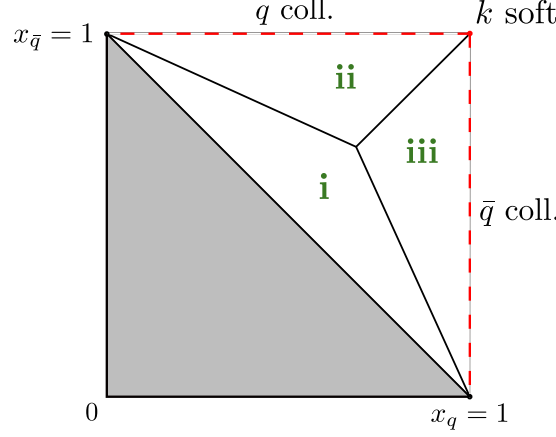


Fig. (2.63): Dalitz plot showing the phase space regions defined by the observable Eq.(2.61). The shaded region is forbidden by momentum conservation. The dashed, red lines indicate the q -collinear ($\theta_{qk} \rightarrow 0 \Leftrightarrow x_{\bar{q}} \rightarrow 1$) and the \bar{q} -collinear singularity ($\theta_{\bar{q}k} \rightarrow 0 \Leftrightarrow x_q \rightarrow 1$) respectively. The soft singularity ($x_k \rightarrow 0$) corresponds to the top-right corner of the diagram where $x_q, x_{\bar{q}} \rightarrow 1$ simultaneously.

Just as before, we will proceed by evaluating Eq.(2.62) term-by-term, further splitting each contribution with respect to the individual terms occurring in the thrust observable Eq.(2.61). To facilitate this, we establish the notation

$$\frac{d\sigma_{\mathbf{3},\mathbf{i}}^{\mathbf{r},11}}{d\tau} \equiv \frac{1}{2s} \int |\mathcal{M}_{\mathbf{3},\mathbf{gi}}^{\mathbf{r},11}|^2 \delta_{\mathbf{i}}(x_q, x_{\bar{q}}, \tau) d\Phi_{\mathbf{3}}, \quad (2.64)$$

and similar for other contributions pertaining to the various amplitudes ($\mathbf{ij} = \mathbf{11}, \mathbf{22}, \mathbf{12}, \mathbf{21}$) and phase space regions ($\mathbf{x} = \mathbf{i}, \mathbf{ii}, \mathbf{iii}$).

For the matrix elements Eq.(2.33) and the thrust observable Eq.(2.61) at hand we therefore obtain

$$\begin{aligned} \frac{d\sigma_{\mathbf{3},\mathbf{i}}^{\mathbf{r},11}}{d\tau} &= \frac{\hat{\sigma}(\epsilon)(1-\epsilon)}{\Gamma(1-\epsilon)} \frac{\alpha_s C_F}{2\pi} \frac{e^{\gamma_E \epsilon} \mu^{4\epsilon}}{s^{1+2\epsilon}} \frac{\theta(\tau)}{\tau^\epsilon} \int_{2\tau}^{1-\tau} dx_q \frac{(1-x_q)^{1-\epsilon}}{(x_q - \tau)^{1+\epsilon}} \\ &= \hat{\sigma}(\epsilon) \frac{\alpha_s C_F}{2\pi} \frac{\mu^{4\epsilon}}{s^{1+2\epsilon}} \left\{ \left[-1 + 3\tau + (1-\tau)\log(1-2\tau) - (1-\tau)\log(\tau) \right] \theta(\tau) + \mathcal{O}(\epsilon) \right\}, \\ \frac{d\sigma_{\mathbf{3},\mathbf{i}}^{\mathbf{r},12}}{d\tau} &= \frac{\hat{\sigma}(\epsilon)}{\Gamma(1-\epsilon)} \frac{\alpha_s C_F}{2\pi} \frac{e^{\gamma_E \epsilon} \mu^{4\epsilon}}{s^{1+2\epsilon}} \left\{ \theta(\tau) \tau^{1-\epsilon} \int_{2\tau}^{1-\tau} dx_q \frac{1}{[(1-x_q)(x_q - \tau)]^{1+\epsilon}} \right. \\ &\quad \left. - \frac{\theta(\tau)}{\tau^\epsilon} \int_{2\tau}^{1-\tau} dx_q \frac{\epsilon}{[(1-x_q)(x_q - \tau)]^\epsilon} \right\} \\ &= \hat{\sigma}(\epsilon) \frac{\alpha_s C_F}{2\pi} \frac{\mu^{4\epsilon}}{s^{1+2\epsilon}} \left\{ \frac{2\tau}{1-\tau} \left[\log(1-2\tau) - \log(\tau) \right] \theta(\tau) + \mathcal{O}(\epsilon) \right\}, \end{aligned} \quad (2.65)$$

for all the independent terms where the observable restricts us to the phase space region (i) in Eq.(2.61). In the regions (ii) and (iii) we further need to calculate

$$\begin{aligned}
\frac{d\sigma_{\mathbf{3},\mathbf{ii}}^{\mathbf{r},11}}{d\tau} &= \frac{\hat{\sigma}(\epsilon)(1-\epsilon)}{\Gamma(1-\epsilon)} \frac{\alpha_s C_F}{2\pi} \frac{e^{\gamma_E \epsilon} \mu^{4\epsilon}}{s^{1+2\epsilon}} \frac{\theta(\tau)}{\tau^{1+\epsilon}} \int_{2\tau}^{1-\tau} dx_q \frac{(1-x_q)^{1-\epsilon}}{(x_q-\tau)^\epsilon}, \\
&= \hat{\sigma}(\epsilon) \frac{\alpha_s C_F}{2\pi} \frac{\mu^{4\epsilon}}{s^{1+2\epsilon}} \left\{ -\frac{1}{2} \left[\frac{1}{\epsilon} + 1 \right] \delta(\tau) + \frac{1}{2} \left[\frac{\theta(\tau)}{\tau} \right]_+ + \frac{1}{2} [3\tau - 4] \theta(\tau) + \mathcal{O}(\epsilon) \right\}, \\
\frac{d\sigma_{\mathbf{3},\mathbf{ii}}^{\mathbf{r},22}}{d\tau} &= \frac{\hat{\sigma}(\epsilon)(1-\epsilon)}{\Gamma(1-\epsilon)} \frac{\alpha_s C_F}{2\pi} \frac{e^{\gamma_E \epsilon} \mu^{4\epsilon}}{s^{1+2\epsilon}} \theta(\tau) \tau^{1-\epsilon} \int_{2\tau}^{1-\tau} dx_q \frac{1}{(1-x_q)^{1+\epsilon} (x_q-\tau)^\epsilon} \\
&= \hat{\sigma}(\epsilon) \frac{\alpha_s C_F}{2\pi} \frac{\mu^{4\epsilon}}{s^{1+2\epsilon}} \left\{ \tau \left[\log(1-2\tau) - \log(\tau) \right] \theta(\tau) + \mathcal{O}(\epsilon) \right\}, \\
\frac{d\sigma_{\mathbf{3},\mathbf{ii}}^{\mathbf{r},12}}{d\tau} &= \frac{\hat{\sigma}(\epsilon)}{\Gamma(1-\epsilon)} \frac{\alpha_s C_F}{2\pi} \frac{e^{\gamma_E \epsilon} \mu^{4\epsilon}}{s^{1+2\epsilon}} \left\{ \frac{\theta(\tau)}{\tau^{1+\epsilon}} \int_{2\tau}^{1-\tau} dx_q \frac{(x_q-\tau)^{1-\epsilon}}{(1-x_q)^{1+\epsilon}} - \frac{\theta(\tau)}{\tau^\epsilon} \int_{2\tau}^{1-\tau} dx_q \frac{\epsilon}{[(1-x_q)(x_q-\tau)]^\epsilon} \right\} \\
&= \hat{\sigma}(\epsilon) \frac{\alpha_s C_F}{2\pi} \frac{\mu^{4\epsilon}}{s^{1+2\epsilon}} \left\{ \frac{1}{2} \left[\frac{1}{\epsilon^2} + \frac{3}{\epsilon} + 7 - \frac{5\pi^2}{12} \right] \delta(\tau) - \left[\frac{\theta(\tau)}{\tau} \right]_+ - \left[\frac{\theta(\tau) \log(\tau)}{\tau} \right]_+ \right. \\
&\quad \left. + \left[3 + \frac{1-\tau}{\tau} \log(1-2\tau) + \log(\tau) \right] \theta(\tau) + \mathcal{O}(\epsilon) \right\}.
\end{aligned} \tag{2.66}$$

To obtain the above results extensive use of **Mathematica**[21] and the package **HypExp**[22] was made. Since the squared matrix elements in Eq.(2.33), and the last two terms in Eq.(2.61) exhibit a symmetry under the exchange $q^\mu \leftrightarrow \bar{q}^\mu$, we can determine all other contributions from what we have calculated so far, in particular,

$$\begin{aligned}
\frac{d\sigma_{\mathbf{3},\mathbf{i}}^{\mathbf{r},11}}{d\tau} &= \frac{d\sigma_{\mathbf{3},\mathbf{i}}^{\mathbf{r},22}}{d\tau}, & \frac{d\sigma_{\mathbf{3},\mathbf{iii}}^{\mathbf{r},11}}{d\tau} &= \frac{d\sigma_{\mathbf{3},\mathbf{ii}}^{\mathbf{r},22}}{d\tau}, & \frac{d\sigma_{\mathbf{3},\mathbf{iii}}^{\mathbf{r},22}}{d\tau} &= \frac{d\sigma_{\mathbf{3},\mathbf{ii}}^{\mathbf{r},11}}{d\tau}, \\
\frac{d\sigma_{\mathbf{3},\mathbf{i}}^{\mathbf{r},21}}{d\tau} &= \frac{d\sigma_{\mathbf{3},\mathbf{i}}^{\mathbf{r},12}}{d\tau}, & \frac{d\sigma_{\mathbf{3},\mathbf{ii}}^{\mathbf{r},12}}{d\tau} &= \frac{d\sigma_{\mathbf{3},\mathbf{iii}}^{\mathbf{r},12}}{d\tau} = \frac{d\sigma_{\mathbf{3},\mathbf{ii}}^{\mathbf{r},21}}{d\tau} = \frac{d\sigma_{\mathbf{3},\mathbf{iii}}^{\mathbf{r},21}}{d\tau},
\end{aligned} \tag{2.67}$$

where each of the integrals for a contribution from the region (iii) would naturally occur as in Eq.(2.66) but in terms of $x_{\bar{q}}$ rather than x_q .

Note that the only two contributions that produce singular behaviour in the limit $\tau \rightarrow 0$ (i.e. they contain delta functions and plus distributions⁴) are shown in the first and third line of Eq.(2.66) respectively. In practice this means that all other integrals can be calculated in $d = 4$ dimensions without any need for regularisation, further simplifying the computation.

The complete real emission contribution to the thrust distribution can now be determined entirely by the results found in Eq.(2.65) and Eq.(2.66) and reads

$$\begin{aligned}
\frac{d\sigma_{\mathbf{3}}^{\mathbf{r}}}{d\tau} &= \sum_{\mathbf{x}=\mathbf{i}}^{\mathbf{iii}} \left\{ \frac{d\sigma_{\mathbf{3},\mathbf{x}}^{\mathbf{r},11}}{d\tau} + \frac{d\sigma_{\mathbf{3},\mathbf{x}}^{\mathbf{r},22}}{d\tau} + \frac{d\sigma_{\mathbf{3},\mathbf{x}}^{\mathbf{r},12}}{d\tau} + \frac{d\sigma_{\mathbf{3},\mathbf{x}}^{\mathbf{r},21}}{d\tau} \right\} = \hat{\sigma}(\epsilon) \frac{\alpha_s C_F}{\pi} \frac{\mu^{4\epsilon}}{s^{1+2\epsilon}} \left\{ \left[\frac{1}{\epsilon^2} + \frac{3}{2} \frac{1}{\epsilon} + \frac{7}{2} - \frac{5\pi^2}{12} \right] \delta(\tau) \right. \\
&\quad \left. - \frac{3}{2} \left[\frac{\theta(\tau)}{\tau} \right]_+ - 2 \left[\frac{\theta(\tau) \log(\tau)}{\tau} \right]_+ + \left[3 + \frac{9}{2} \tau + \left(\frac{2}{\tau(1-\tau)} - 3 \right) \log(1-2\tau) + \frac{1-3\tau}{1-\tau} \log(\tau) \right] \theta(\tau) \right\}.
\end{aligned} \tag{2.68}$$

Interpreting the finite terms as distributions and expanding in the ratio $\left(\frac{\mu^2}{s}\right)^\epsilon$ gives the real emission

⁴See App. I for the definition and properties of plus distributions.

contribution in a form more familiar from the literature,

$$\begin{aligned} \frac{d\sigma_3^{\mathbf{r}}}{d\tau} = \frac{\hat{\sigma}(\epsilon)}{s} \frac{\alpha_s C_F}{\pi} \left\{ \left[\frac{1}{\epsilon^2} + \frac{3}{2} \frac{1}{\epsilon} + \frac{2}{\epsilon} \log\left(\frac{\mu^2}{s}\right) + \frac{7}{2} - \frac{5\pi^2}{12} + 3\log\left(\frac{\mu^2}{s}\right) + 2\log^2\left(\frac{\mu^2}{s}\right) \right] \delta(\tau) \right. \\ \left. + \left[-\frac{3}{2} + 3\tau + \frac{9}{2}\tau^2 + \frac{2-3\tau(1-\tau)}{1-\tau} \log(1-2\tau) \right] \left[\frac{\theta(\tau)}{\tau} \right]_+ + \left[3\tau - \frac{2}{1-\tau} \right] \left[\frac{\theta(\tau)\log(\tau)}{\tau} \right]_+ \right\}. \end{aligned} \quad (2.69)$$

The virtual contribution to the thrust distribution is much easier to obtain since the only kinematically allowed configuration of the final state quark pair, as was shown in Eq.(2.55), is exactly back to back ($\tau = 0$) and hence

$$\frac{d\sigma_2^{\mathbf{v}}}{d\tau} = \sigma_2^{\mathbf{v}} \delta(\tau) = -\frac{\hat{\sigma}(\epsilon)}{s} \frac{\alpha_s C_F}{\pi} \left[\frac{1}{\epsilon^2} + \frac{3}{2} \frac{1}{\epsilon} + \frac{2}{\epsilon} \log\left(\frac{\mu^2}{s}\right) + 4 - \frac{7\pi^2}{12} + 3\log\left(\frac{\mu^2}{s}\right) + 2\log^2\left(\frac{\mu^2}{s}\right) \right] \delta(\tau), \quad (2.70)$$

with the total virtual cross section $\sigma_2^{\mathbf{v}}$ as in Eq.(2.47). Combining the results from Eq.(2.69) and Eq.(2.70), this leaves us with the finite next-to-leading order thrust distribution

$$\begin{aligned} \frac{d\sigma_{2/3}^{\text{NLO}}}{d\tau} = \frac{d\sigma_3^{\mathbf{r}}}{d\tau} + \frac{d\sigma_2^{\mathbf{v}}}{d\tau} = \frac{\hat{\sigma}(\epsilon)}{s} \frac{\alpha_s C_F}{\pi} \left\{ \left[\frac{\pi^2}{6} - \frac{1}{2} \right] \delta(\tau) \right. \\ \left. + \left[-\frac{3}{2} + 3\tau + \frac{9}{2}\tau^2 + \frac{2-3\tau(1-\tau)}{1-\tau} \log(1-2\tau) \right] \left[\frac{\theta(\tau)}{\tau} \right]_+ + \left[3\tau - \frac{2}{1-\tau} \right] \left[\frac{\theta(\tau)\log(\tau)}{\tau} \right]_+ \right\}, \end{aligned} \quad (2.71)$$

which agrees with the usual result found in the literature[23]. Together with the leading order result $\frac{d\sigma_2^{\text{LO}}}{d\tau} = \sigma_2^{\text{LO}} \delta(\tau)$ the above thrust distribution gives the total cross section of Eq.(2.49) when integrated over all allowed values of τ ,

$$\int_0^{\frac{1}{3}} d\tau \left[\frac{d\sigma_2^{\text{LO}}}{d\tau} + \frac{d\sigma_{2/3}^{\text{NLO}}}{d\tau} \right] = \sigma, \quad (2.72)$$

which provides an important consistency check. In arriving at Eq.(2.72) we have crucially made use of the fact that the plus distributions are integrable in the di-jet limit $\tau = 0$ as per Eq.(1.3). Note that since Eq.(2.71) is an experimentally accessible quantity, the dependence on the renormalisation scale μ has dropped out.

2.7 Infrared safety and thrust

A crucial theoretical concept in perturbative QCD calculations is that of infrared safe observables. In essence, IR-safety states that the measurement we are making (the observable we are computing) is insensitive to final state particles becoming soft or collinear. In practice this means that IR-divergences cancel between real emission and virtual corrections at any given order, just as they did for thrust in Eq.(2.71).

Let us consider the general case where an observable O is specified by the measurement functions $O_{\mathbf{m}}(p_1, \dots, p_m)$ depending on m final state parton momenta. Note that at a given order in perturbation theory, say $\mathcal{O}(\alpha_s^k)$, we have to consider these measurement functions for all final state particle numbers up to some maximum n , that is, the cross section we are computing is schematically given by the perturbative expansion

$$\begin{aligned} \frac{d\sigma}{dO} \simeq \int d\Phi_2 |\mathcal{M}_2|^2(p_1, p_2) \delta(O - O_2(p_1, p_2)) + \int d\Phi_3 |\mathcal{M}_3|^2(p_1, p_2, p_3) \delta(O - O_3(p_1, p_2, p_3)) \\ + \dots + \int d\Phi_n |\mathcal{M}_n|^2(p_1, \dots, p_n) \delta(O - O_n(p_1, \dots, p_n)) + \mathcal{O}(\alpha_s^{k+1}), \end{aligned} \quad (2.73)$$

where for concreteness we have assumed a leading order process with two final state partons. Each of the amplitudes $|\mathcal{M}_{\mathbf{m}}|^2$, $m = 2, \dots, n$ is evaluated up to $\mathcal{O}(\alpha_s^k)$ and we have $|\mathcal{M}_{\mathbf{n+1}}|^2 = 0 + \mathcal{O}(\alpha_s^{k+1})$ by definition.

Now a cancellation of IR-divergences between the individual contributions of Eq.(2.73) can be guaranteed if for $m = 2, \dots, n - 1$ the formal requirements

$$\begin{aligned} O_{\mathbf{m+1}}(p_1, \dots, (1-z)p_m, zp_m) &= O_{\mathbf{m}}(p_1, \dots, p_m) && \text{(collinear safety),} \\ O_{\mathbf{m+1}}(p_1, \dots, p_m, 0) &= O_{\mathbf{m}}(p_1, \dots, p_m) && \text{(soft safety),} \end{aligned} \quad (2.74)$$

are met. To ensure IR-safety, analogous relations also have to hold for all other (pairs of) momenta in the above measurement functions that lead to singular behaviour of the amplitude in the respective soft-collinear limits. We say that in the first line of Eq.(2.74) the parton $(m+1)$ has gone collinear to the parton (m) with momentum fraction $0 < z < 1$, while in the second line the parton $(m+1)$ has gone soft. This is illustrated in Fig. 2.75.

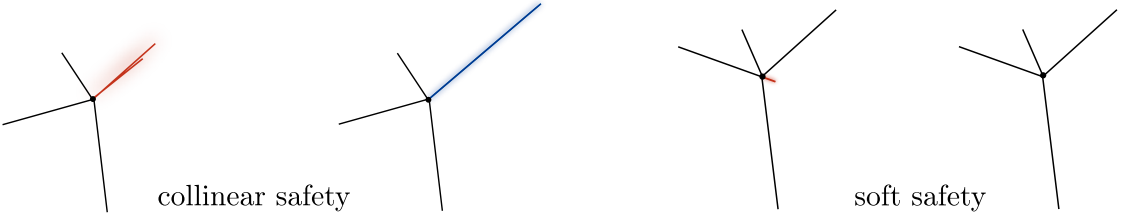
$$O_{\mathbf{m+1}}(p_1, \dots, (1-z)p_m, zp_m) = O_{\mathbf{m}}(p_1, \dots, p_m) \quad O_{\mathbf{m+1}}(p_1, \dots, p_m, 0) = O_{\mathbf{m}}(p_1, \dots, p_m)$$


Fig. (2.75): Geometric representation of soft-collinear safety. We see that an IR-safe observable is not sensitive to the presence of collinear and soft radiation in the final state.

Let us now briefly check that thrust is indeed IR-safe and that the cancellation of IR-singularities in Eq.(2.71) was therefore not just a lucky coincidence. Writing $T_{\mathbf{m+1}}(p_1, \dots, p_{m+1})$ for the thrust observable Eq.(2.54) where the sum runs over $(m+1)$ final state parton momenta, we first explicitly check collinear safety,

$$\begin{aligned} T_{\mathbf{m+1}}(p_1, \dots, (1-z)p_m, zp_m) &= \max_{\mathbf{n}} \left[\frac{\sum_i^{m-1} |\mathbf{p}_i \cdot \mathbf{n}| + |(1-z)\mathbf{p}_m \cdot \mathbf{n}| + |z\mathbf{p}_m \cdot \mathbf{n}|}{\sum_i^{m-1} |\mathbf{p}_i| + |(1-z)\mathbf{p}_m \cdot \mathbf{n}| + |z\mathbf{p}_m \cdot \mathbf{n}|} \right] \\ &= \max_{\mathbf{n}} \frac{\sum_i^m |\mathbf{p}_i \cdot \mathbf{n}|}{\sum_i^m |\mathbf{p}_i|} = T_{\mathbf{m}}(p_1, \dots, p_m), \end{aligned} \quad (2.76)$$

with soft safety being trivially satisfied. The fact that thrust is IR-safe will also become important in subsequent sections when we discuss the dipole subtraction procedure.

2.8 A naive numerical approach for thrust

To set up the premise for the introduction of the dipole subtraction method in the coming sections, we want to first show how not to compute observables numerically. Highlighting the shortcomings of the naive approach will help us to appreciate the necessity for subtractions and what practical purpose they serve.

Returning to the thrust distribution of Sec. 2.6 we notice that the phase space integrals Eqs.(2.65) and (2.66) for the real emission contributions can be carried out in $d=4$ once we strictly require $\tau > 0$ in the measurement function. Since this means that we exclude the perfect di-jet limit, the singular boundaries of phase space in Fig. 2.63 are not integrated over. Thus, evaluating all contributions

assuming $\tau > 0$ and $\epsilon = 0$ we obtain the real emission contribution

$$\left. \frac{d\sigma_{\mathbf{3}}^{\mathbf{r}}}{d\tau} \right|_{\epsilon=0}^{\tau>0} = \frac{\hat{\sigma}(0)}{s} \frac{\alpha_s C_F}{\pi} \theta(\tau) \left\{ -\frac{3}{2} \frac{1}{\tau} - 2 \frac{\log(\tau)}{\tau} + 3 + \frac{9}{2} \tau + \left(\frac{2}{\tau(1-\tau)} - 3 \right) \log(1-2\tau) + \frac{1-3\tau}{1-\tau} \log(\tau) \right\}, \quad (2.77)$$

which in principle could also be obtained numerically. Since we are avoiding the strict di-jet limit the leading order and virtual contribution are simply

$$\left. \frac{d\sigma_{\mathbf{2}}^{\mathbf{v}}}{d\tau} \right|_{\epsilon=0}^{\tau>0} = \left. \frac{d\sigma_{\mathbf{2}}^{\mathbf{LO}}}{d\tau} \right|_{\epsilon=0}^{\tau>0} = 0. \quad (2.78)$$

Comparing the first two terms in Eq.(2.77) to the previous result in Eq.(2.68) we see that the singular behaviour in the limit $\tau \rightarrow 0$ is correctly reproduced and the remaining finite terms agree as well. However, we are missing the singular and (crucially) finite contributions from $\tau = 0$ in both real emission and virtual parts. Additionally, the proper regularisation of singular contributions in terms of plus distributions is absent in the real emission contribution. The latter is particularly troubling since the thus calculated thrust distribution is not integrable. Indeed, unlike Eq.(2.72), we find

$$\int_0^{\frac{1}{3}} d\tau \left. \frac{d\sigma_{\mathbf{3}}^{\mathbf{r}}}{d\tau} \right|_{\epsilon=0}^{\tau>0} = \infty \neq \sigma, \quad (2.79)$$

which is obviously inconsistent with the finite total cross section we obtained in Eq.(2.49). We conclude that we have to augment the naive approach discussed here with a prescription that allows us to extend the numerical integration into the strict di-jet limit $\tau = 0$ to provide for a proper, controlled cancellation of IR divergences as well as incorporating the finite contributions proportional to $\delta(\tau)$ that were missing in Eqs.(2.77) and (2.78). The prescription used in this thesis will come in the form of the dipole subtraction method which is the subject of the coming sections.

3 Catani-Seymour dipole subtraction

In this section we will discuss the motivation and general idea behind the dipole subtraction method first proposed in [14].

We have already seen how to calculate the total cross section Eq.(2.48) and thrust distribution Eq.(2.71) for the process $e^+e^- \rightarrow$ di-jets at NLO. This required computing real emission and virtual corrections in dimensional regularisation, both of which contained IR-divergences. The fact that these divergences canceled to yield a finite result was attributed to the observables satisfying the IR-safety properties of Eq.(2.74).

Note that the success of calculating observables in this way was crucially dependent on the respective phase space integrations to be analytically solvable, so that the cancellation of poles in ϵ could be explicitly performed. While we showed that this was possible for a special case, this may not be feasible for more general amplitudes and observables. When analytic integration becomes too cumbersome, or indeed impossible, we usually resort to approximate, numerical procedures. However, in the present case we are confronted with a particularly non-trivial task since a numerical routine cannot implement dimensional regularisation and the phase space integrals we are considering are in general hopelessly divergent in four spacetime dimensions.

This is the exact problem the subtraction method was designed to solve. Roughly speaking, the idea is to rearrange the divergences between real emission and virtual contributions in such a way that all major phase space integrations can be carried out manifestly in four dimensions, yielding finite cross sections. Structurally this may thus be interpreted as taking

$$\frac{d\sigma_{\mathbf{m}/\mathbf{m}+1}^{\text{NLO}}}{dO} = \frac{d\sigma_{\mathbf{m}+1}^{\mathbf{r}}}{dO} + \frac{d\sigma_{\mathbf{m}}^{\mathbf{v}}}{dO} = \left[\frac{d\sigma_{\mathbf{m}+1}^{\mathbf{r}}}{dO} - \frac{d\sigma^{\mathbf{c}}}{dO} \right]_{\epsilon=0} + \left[\frac{d\sigma_{\mathbf{m}}^{\mathbf{v}}}{dO} + \frac{d\sigma^{\mathbf{c}}}{dO} \right]_{\epsilon=0} \equiv \frac{d\sigma_{\mathbf{m}+1}^{\mathbf{r}}_{\text{sub}}}{dO} + \frac{d\sigma_{\mathbf{m}}^{\mathbf{v}}_{\text{sub}}}{dO}, \quad (3.1)$$

where we have chosen to consider a process with m final state partons at LO, so that the NLO real emission contribution will produce a $(m+1)$ -parton state. The counter term $\frac{d\sigma^{\mathbf{c}}}{dO}$ is particular to the chosen subtraction prescription. All brackets in 3.1 can ultimately be finitely evaluated in $d=4$ dimensions, provided a minimum number of simplified (compared to the full calculation) integrals can be computed analytically to facilitate the cancellation of divergences. Let us now be more specific about the structure of the counter term in the Catani-Seymour prescription.

3.1 The promise of the subtraction method

We will now give an outline of the general structure for the evaluation of arbitrary observables at next-to-leading order using the subtraction method. Schematically we write the next-to-leading order cross section for an observable O (c.f. Eq.(2.73) for notation) as

$$\begin{aligned} \frac{d\sigma_{\mathbf{m}/\mathbf{m}+1}^{\text{NLO}}}{dO} &= \frac{d\sigma_{\mathbf{m}+1}^{\mathbf{r}}}{dO} + \frac{d\sigma_{\mathbf{m}}^{\mathbf{v}}}{dO} \\ &= \int d\Phi_{\mathbf{m}+1} |\mathcal{M}_{\mathbf{m}+1}^{\mathbf{r}}|^2 \delta O_{\mathbf{m}+1}(p_1, \dots, p_{m+1}) + \int d\Phi_{\mathbf{m}} |\mathcal{M}_{\mathbf{m}}^{\mathbf{v}}|^2 \delta O_{\mathbf{m}}(p_1, \dots, p_m), \end{aligned} \quad (3.2)$$

in which both terms are separately divergent in four dimensions. To avoid notational clutter we have introduced the short hand

$$\delta(O - O_{\mathbf{m}}(p_1, \dots, p_m)) \equiv \delta O_{\mathbf{m}}(p_1, \dots, p_m), \quad (3.3)$$

for the restriction on m -parton phase space imposed by the measurement function $O_{\mathbf{m}}$ which we will use from now on. For simplicity let us consider the concrete case where the additionally emitted

parton with momentum p_{m+1} is exclusively due to a splitting of the m -th parton in the leading order amplitude, as pictured in Fig. 3.4.

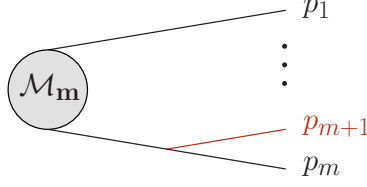


Fig. (3.4): For the present discussion we assume the parton that is additionally emitted at NLO to originate from a single splitting of the m -th parton in the leading order amplitude. In the general case multiple such splittings will occur between any number of partons, see Sec. 3.2.

To facilitate a subtraction for this process we require two ingredients. The first is a dummy amplitude $|\mathcal{M}_{\mathbf{m}+1}^c|^2$, defined on $(m+1)$ -parton phase space, that reproduces the singular behaviour of the real emission amplitude $|\mathcal{M}_{\mathbf{m}+1}^r|^2$ in d dimensions, thus acting as a local counter term. The second is a momentum map

$$f(p_1, \dots, p_m, p_{m+1}) = (q_1, \dots, q_m), \quad (3.5)$$

that projects the $(m+1)$ -parton configuration $\{p_1, \dots, p_m, p_{m+1}\}$ to a suitable m -parton configuration $\{q_1, \dots, q_m\}$. Here the projected momenta are functions $q_i = q_i(p_1, \dots, p_m, p_{m+1})$. The momentum map is set up in such a way that the subtracted real emission cross section, defined as

$$\frac{d\sigma_{\mathbf{m}+1}^{\text{r sub}}}{dO} = \int d\Phi_{\mathbf{m}+1} \left[|\mathcal{M}_{\mathbf{m}+1}^r|^2 \Big|_{\epsilon=0} \delta O_{\mathbf{m}+1}(p_1, \dots, p_{m+1}) - |\mathcal{M}_{\mathbf{m}+1}^c|^2 \Big|_{\epsilon=0} \delta O_{\mathbf{m}}(f(p_1, \dots, p_{m+1})) \right], \quad (3.6)$$

is a finite quantity that can be (numerically) integrated in four dimensions. For this to work the projected momenta q_i need to correctly reproduce the m -parton configuration obtained from the $(m+1)$ -parton configuration in the respective soft-collinear limits of p_{m+1} . The map f we will construct indeed meets this criterion by giving

$$q_m = p_m + p_{m+1}, \quad \text{and} \quad q_i = p_i, \quad \text{for } i = 1, \dots, m-1, \quad (3.7)$$

in the strict singular limits. This provides for the fact that in these limits the $(m+1)$ -parton final state reduces to the original m -parton configuration, concretely

$$\begin{array}{lll} p_{m+1} \text{ collinear to } p_m: & p_{m+1} \rightarrow zp_m, p_m \rightarrow (1-z)p_m & \Rightarrow \quad q_m = (1-z)p_m + zp_m = p_m, \\ p_{m+1} \text{ soft:} & p_{m+1} \rightarrow 0 & \Rightarrow \quad q_m = p_m + 0 = p_m. \end{array} \quad (3.8)$$

For an IR safe observable in the sense of Eq.(2.74) this implies

$$\begin{array}{lll} p_{m+1} \text{ collinear to } p_m: & O_{\mathbf{m}+1}(p_1, \dots, (1-z)p_m, zp_m) = O_{\mathbf{m}}(p_1, \dots, p_m) \\ & = O_{\mathbf{m}}(p_1, \dots, zp_m + (1-z)p_m) \\ & = O_{\mathbf{m}}(q_1, \dots, q_m), \\ p_{m+1} \text{ soft:} & O_{\mathbf{m}+1}(p_1, \dots, p_m, 0) = O_{\mathbf{m}}(p_1, \dots, p_m) \\ & = O_{\mathbf{m}}(p_1, \dots, p_m + 0) \\ & = O_{\mathbf{m}}(q_1, \dots, q_m), \end{array} \quad (3.9)$$

where in both cases the first equality is due to IR safety and the remaining equalities follow from the properties Eq.(3.8) of the momentum map. Note that Eq.(3.9) is crucial in ensuring that the cancellation of divergences between real emission amplitude and the counter term in Eq.(3.6) can actually occur.

Another convenient property the momentum projection f satisfies is momentum conservation,

$$\sum_i^m q_i = \sum_i^{m+1} p_i, \quad \text{and} \quad q_i^2 = 0, \quad \text{for } i = 1, \dots, m, \quad (3.10)$$

over the entire phase space. This will become relevant presently when we want to interpret the projected momenta q_i as pertaining to the final state of a leading order matrix element.

Since we have subtracted the dummy amplitude from the real emission contribution, according to Eq.(3.6) we need to add it back to the virtual correction to leave the cross section Eq.(3.2) unchanged. However, we immediately run into the problem that $|\mathcal{M}_{\mathbf{m}+1}^c|^2$ is defined on an $(m+1)$ -parton phase space, while $|\mathcal{M}_{\mathbf{m}}^v|^2$ depends only on the m parton momenta of the leading-order process, thus rendering a direct recombination of the amplitudes under a common phase space integral difficult.

Here the proposed dipole subtraction shows another one of its strengths. The claim is that the counter term factorises into a m -parton, leading order amplitude $|\mathcal{M}_{\mathbf{LO}}^c|^2$ times a factor V explicitly depending on the additional parton momentum and encapsulating the singular behaviour of the $(m+1)$ -parton amplitude, such that

$$|\mathcal{M}_{\mathbf{m}+1}^c|^2(p_1, \dots, p_m, \mathbf{p}_{m+1}) = |\mathcal{M}_{\mathbf{LO}}^c|^2(q_1, \dots, q_m) \times V(\mathbf{p}_{m+1}, q_1, \dots, q_m). \quad (3.11)$$

In addition the momentum mapping Eq.(3.5) allows for a factorisation of the $(m+1)$ -parton phase space into the m -parton phase space of the virtual amplitude times an integration over the single particle phase space pertaining to \mathbf{p}_{m+1} . Schematically we can therefore write the counter term as⁵

$$\begin{aligned} & \int d\Phi_{\mathbf{m}+1} |\mathcal{M}_{\mathbf{m}+1}^c|^2(p_1, \dots, p_m, \mathbf{p}_{m+1}) \delta O_{\mathbf{m}}(q_1, \dots, q_m) \\ &= \int d\Phi_{\mathbf{m}}(q_1, \dots, q_m) |\mathcal{M}_{\mathbf{LO}}^c|^2(q_1, \dots, q_m) \delta O_{\mathbf{m}}(q_1, \dots, q_m) \int d\mathbf{p}_{m+1}(q_1, \dots, q_m) V(\mathbf{p}_{m+1}, q_1, \dots, q_m), \end{aligned} \quad (3.12)$$

where the dependence of the measure $d\mathbf{p}_{m+1}(q_1, \dots, q_m)$ on the projected momenta comes from a Jacobian factor induced by the momentum map which we study in detail in App.F. The promise is that if the integral over the single particle phase space can be carried out analytically in d dimensions, we can recombine the result with the virtual amplitude, ensuring an exact cancellation of IR-divergences, provided that the observable under consideration is IR-safe. This then allows the limit $\epsilon \rightarrow 0$ to be taken, leaving the remaining m -parton phase space integral to be (numerically) evaluated in $d=4$ dimensions. This prompts the definition of the subtracted virtual contribution to the cross section Eq.(3.2) as

$$\frac{d\sigma_{\mathbf{m} \text{ sub}}^v}{dO} = \int d\Phi_{\mathbf{m}} \left[|\mathcal{M}_{\mathbf{m}}^v|^2 \delta O_{\mathbf{m}}(p_1, \dots, p_m) + |\mathcal{M}_{\mathbf{m}}^c|^2 O_{\mathbf{m}}(q_1, \dots, q_m) \int d\mathbf{p}_{m+1} V(\mathbf{p}_{m+1}) \right] \Big|_{\epsilon=0}, \quad (3.13)$$

where we have suppressed the dependence of $V(\mathbf{p}_{m+1})$ on the projected momenta q_1, \dots, q_m for notational brevity.

Thus to perform a numerical calculation of an observable as in Eq.(3.1), we need to know the real emission amplitude in $d=4$ dimensions only, while the virtual correction, as well as the dummy amplitude will in principle need to be evaluated in arbitrary dimension d . However, we will see (c.f.

⁵See App.F for a more detailed discussion and proof of the phase space factorisation property Eq.(3.12).

Apps. D and E) that the counter terms are constructed using the universal soft-collinear limit of tree-level QCD amplitudes. This implies that the dummy amplitude can be constructed in a process- and observable-independent manner. In particular the single particle phase space integrals in Eq.(3.12) can be universally computed and then applied to any process and observable.

3.2 General construction of counter terms

Recall that up to now we have restricted our analysis to a single splitting between the momenta p_m, p_{m+1} at NLO. In the more realistic setting we will discuss now we have to take into account all allowed splittings from other final state partons in order to reproduce the divergent behaviour of the real emission matrix element.

For simplicity let us specify to processes without initial-state radiation, that is, at NLO the additional parton is emitted only from final state particles. This restricted case will still apply in the context of $e^+e^- \rightarrow$ di-jets, which we are ultimately interested in, and simplify the definition of the counter terms. We will also restrict our discussion to the subtraction of appropriately spin/colour-summed matrix elements and do not consider subtractions for amplitudes of fixed helicity.

Our starting point for the explicit construction of the dummy amplitude is that the singular part of a given (colour/spin-summed) $(m+1)$ -parton final state real emission matrix element in the soft-collinear limit can be written as⁶

$$\text{sing}_{\text{soft/coll.}} \left\{ |\mathcal{M}_{\mathbf{m}+1}^r|^2 \equiv {}_{\mathbf{m}+1} \langle 1, \dots, m+1 | 1, \dots, m+1 \rangle_{\mathbf{m}+1} \right\} \subseteq \sum_{k \neq (i \neq j)} \mathcal{D}_{ij,k}(p_1, \dots, p_{m+1}) \quad (3.14)$$

$$\equiv |\mathcal{M}_{\mathbf{m}+1}^c|^2,$$

where the sum runs over all distinct tuples $\{(i, j), k\}$ of final state partons called dipoles. In particular we will refer to the particles (i, j) as emitter(s) and to k as spectator. The symbol \subseteq denotes the fact that the sum over the dipole contributions $\mathcal{D}_{ij,k}$ reproduces all singular terms of the amplitude plus possible additional terms that are soft-collinear-finite.

To make the summation over dipoles in Eq.(3.14) clear, we give an example. The dipoles $\{(1, 2), 3\}$ and $\{(1, 3), 2\}$ are distinct and have to be taken into account separately, while the dipoles $\{(1, 2), 3\}$ and $\{(2, 1), 3\}$ are identical and thus only counted once.

That we talk about dipoles in this context derives from the fact that a given contribution $\mathcal{D}_{ij,k}$ on the left-hand side of Eq.(3.14) is (roughly) associated with the divergences occurring in the interference diagrams

$$|\mathcal{M}_{\mathbf{m}+1}^r|^2 \supseteq \mathcal{M}_{\mathbf{m}+1}^r \mathcal{M}_{\mathbf{m}+1}^{r\dagger} + \mathcal{M}_{\mathbf{m}+1}^{r\dagger} \mathcal{M}_{\mathbf{m}+1}^r, \quad (3.15)$$

contributing to the squared real emission matrix element. Note, however, that there is generally no one-to-one correspondence of divergences appearing in individual dipole contributions and real emission interference diagrams. The singularity structure only matches up between the two once all dipoles $\{(i, j), k\}$ are summed up, as are all interference diagrams. This is essentially due to the soft

⁶Check App. D for an introduction to the Colour/Helicity space formulation of amplitudes.

limit of the real emission amplitude being sensitive to contributions from all other final state particles (c.f. Eq.(D.12)).

The dipole factors $\mathcal{D}_{ij,k}$ can be obtained as the matrix elements of the corresponding colour/helicity-space dipole operator⁷ $\mathbf{D}_{ij,k}$,

$$\mathcal{D}_{ij,k} = {}_{\mathbf{m}}\langle 1, \dots, \underline{i}, \underline{j}, \underline{k}, \dots, m+1 | \mathbf{D}_{ij,k} | 1, \dots, \underline{i}, \underline{j}, \underline{k}, \dots, m+1 \rangle_{\mathbf{m}}, \quad (3.16)$$

which is defined in terms of colour charge operators \mathbf{T}_i^a and helicity operators $\mathbf{V}_{ij,k}(y_{ij,k}, z_i)$, the latter also containing kinematic information about the partons constituting the dipole, and reads

$$\mathbf{D}_{ij,k} = -\frac{1}{2(i \cdot j)} \frac{\mathbf{T}_k \cdot \mathbf{T}_{ij}}{\mathbf{T}_{ij}^2} \mathbf{V}_{ij,k}(y_{ij,k}, z_i). \quad (3.17)$$

The kinematic dependence of the dipole operator can be expressed entirely in terms of the momentum invariants

$$y_{ij,k} = \frac{i \cdot j}{i \cdot j + i \cdot k + j \cdot k}, \quad z_i = \frac{i \cdot k}{k \cdot (i + j)}. \quad (3.18)$$

The reduced m -parton amplitude in Eq.(3.16) is obtained from the amplitude with $m+1$ partons featuring on the left-hand side of Eq.(3.14) by replacing the three particles $\{(i, j), k\}$ pertaining to the given dipole with the two particles $\{\underline{i}, \underline{j}, \underline{k}\}$. The corresponding three-to-two momentum projection is given by

$$\underline{i} \underline{j}^\mu = i^\mu + j^\mu - \frac{y_{ij,k}}{1 - y_{ij,k}} k^\mu, \quad \underline{k}^\mu = \frac{1}{1 - y_{ij,k}} k^\mu, \quad (3.19)$$

which exactly implements momentum conservation $\underline{i} \underline{j}^\mu + \underline{k}^\mu = i^\mu + j^\mu + k^\mu$ as we anticipated in Eq.(3.10). The projected momenta are on-shell $\underline{i} \underline{j}^2 = \underline{k}^2 = 0$ and in the soft-collinear limit defined by $i \cdot j \rightarrow 0$ (implying $y_{ij,k} \rightarrow 0$) they reduce to $\underline{i} \underline{j}^\mu \rightarrow i^\mu + j^\mu$ and $\underline{k}^\mu \rightarrow k^\mu$. As we alluded to in the preceding section, we thus do not have a single momentum map f as in Eq.(3.5) from $(m+1)$ -parton phase space $\{p_1, \dots, p_{m+1}\}$ to that for m partons $\{q_1, \dots, q_m\}$, but one for each dipole contribution, $f_{ij,k}$, which only acts on the three momenta $\{(i, j), k\}$ of the given dipole, leaving the other $m-2$ momenta untouched, that is

$$f_{ij,k}(1, \dots, i, \dots, \underline{j}, \dots, \underline{k}, \dots, m+1) = (1, \dots, \underline{i}, \underline{j}, \dots, m+1), \quad (3.20)$$

with the m projected momenta $\{1, \dots, \underline{i}, \underline{j}, \dots, m+1\}$ and identifying the momentum \underline{j} as pertaining to the parton additionally emitted at NLO.

Aside from the kinematics, the two-particle configuration $\{\underline{i}, \underline{j}, \underline{k}\}$ we are mapping to corresponds to different particle types depending on the particles $\{(i, j), k\}$ that were present before the reduction. The quantum numbers of the emitter are determined according to the recipe

$$\begin{aligned} (i, j) &= (q, g) \mapsto \underline{i} \underline{j} = q, \\ (i, j) &= (\bar{q}, g) \mapsto \underline{i} \underline{j} = \bar{q}, \\ (i, j) &= (g, g) \mapsto \underline{i} \underline{j} = g, \\ (i, j) &= (q, \bar{q}) \mapsto \underline{i} \underline{j} = g, \end{aligned} \quad (3.21)$$

which can be inferred by thinking about which exchanges are allowed by QCD in the diagram Eq.(3.15) for a given dipole $\{(i, j), k\}$. The spectator \underline{k} always corresponds to the same particle type as k .

⁷See App. D for a more thorough definition and discussion of the individual operators in Eq.(3.17) and why we can expect the dipole operator to generate counter terms with the correct singular limit.

Diagrammatically we may think of a particular dipole mapping specified by Eqs.(3.19) and (3.21) as reducing the NLO diagram to a LO diagram according to the prescription

$$(3.22)$$

In terms of Colour/Helicity space amplitudes we may think of the above as taking

$$\begin{aligned} & \mathbf{m+1} \langle 1, \dots, (i, j), \dots, k, \dots, m+1 | 1, \dots, (i, j), \dots, k, \dots, m+1 \rangle_{\mathbf{m+1}} \\ & \longmapsto \mathcal{D}_{ij,k} = \mathbf{m} \langle 1, \dots, \underline{i}, \underline{j}, \underline{k}, \dots, m+1 | \mathbf{D}_{ij,k} | 1, \dots, \underline{i}, \underline{j}, \underline{k}, \dots, m+1 \rangle_{\mathbf{m}}. \end{aligned} \quad (3.23)$$

Having established the momentum mapping, we show in App. F that it facilitates the phase space factorisation

$$d\Phi_3(i, j, k) = d\Phi_2(\underline{i}, \underline{j}, \underline{k}) dj(\underline{i}, \underline{j}, \underline{k}), \quad (3.24)$$

where the single particle phase space pertaining to the additional parton emission (j) can be written in terms of the momentum invariants Eq.(3.18) as⁸

$$dj(\underline{i}, \underline{j}, \underline{k}) = \frac{dz_i dy_{ij,k} d^{d-3}\Omega}{(2\pi)^{1-2\epsilon}} \frac{(2 \underline{i} \cdot \underline{k})^{1-\epsilon}}{16\pi^2} \frac{(1 - y_{ij,k})^{1-2\epsilon}}{(z_i(1 - z_i)y_{ij,k})^\epsilon} \Theta(z_i(1 - z_i)) \Theta(y_{ij,k}(1 - y_{ij,k})), \quad (3.25)$$

where $d^{d-3}\Omega$ is the angular measure associated with the $(d-2)$ -dimensional space perpendicular to \underline{i} and \underline{k} . In addition the now refined version of the counter term factorisation Eq.(3.11) reads

$$\mathcal{D}_{ij,k}(1, \dots, m+1) = |\mathcal{M}_{\text{LO}}^{c,ij,k}|^2(1, \dots, \underline{i}, \underline{j}, \underline{k}, \dots, m+1) \times V_{ij,k}(\underline{j}, 1, \dots, \underline{i}, \underline{j}, \underline{k}, \dots, m+1), \quad (3.26)$$

for each dipole contribution. We should note that the factorisation into the m parton amplitude $|\mathcal{M}_{\text{LO}}^{c,ij,k}|^2$ and the singular factor $V_{ij,k}$ still involves implicit sums over helicities and is thus not exact at this point. Additionally both factors in Eq.(3.26) still depend on the projected momenta q_1, \dots, q_m . However, both of these interdependencies go away once the integral over the phase space Eq.(3.25) is carried out analytically[14], allowing for a cancellation of divergences with the virtual matrix element according to Eq.(3.13).

With all the details now in place we can give explicit expressions for the subtracted real emission Eq.(3.6) and virtual correction Eq.(3.13) contributions to the cross section. Starting with the subtracted real emission part we obtain

$$\begin{aligned} \frac{d\sigma_{\mathbf{m+1} \text{ sub}}^{\text{r}}}{d\mathcal{O}} &= \int d\Phi_{\mathbf{m+1}}(1, \dots, m+1) \left\{ |\mathcal{M}_{\mathbf{m+1}}^{\text{r}}|^2(1, \dots, m+1) \delta\mathcal{O}_{\mathbf{m+1}}(1, \dots, m+1) \right. \\ &\quad \left. - \sum_{i \neq (j \neq k)} \mathcal{D}_{ij,k}(1, \dots, m+1) \delta\mathcal{O}_{\mathbf{m}}(f_{ij,k}(1, \dots, m+1)) \right\}, \end{aligned} \quad (3.27)$$

⁸For a detailed derivation of the single particle measure see the discussion starting with Eq.(F.10).

The factorisation properties Eqs.(3.24) and (3.26) allow us to write the virtual part as

$$\begin{aligned} \frac{d\sigma_{\mathbf{m}\text{sub}}^{\mathbf{v}}}{dO} &= \int d\Phi_{\mathbf{m}}(1, \dots, m) \left\{ |\mathcal{M}_{\mathbf{m}}^{\mathbf{v}}|^2(1, \dots, m) \delta O_{\mathbf{m}}(1, \dots, m) \right. \\ &\quad + \sum_{i \neq (j \neq k)} |\mathcal{M}_{\mathbf{m}}^{\mathbf{c}ij,k}|^2(f_{ij,k}(1, \dots, m+1)) \delta O_{\mathbf{m}}(f_{ij,k}(1, \dots, m+1)) \\ &\quad \left. \times \int d\mathbf{j}(\underline{i}\mathbf{j}, \underline{k}) V_{ij,k}(\mathbf{j}, f_{ij,k}(1, \dots, m+1)) \right\}. \end{aligned} \quad (3.28)$$

Note that we have denoted the momentum configuration of the virtual correction by $\{1, \dots, m\}$, while the momenta for a given dipole contribution are labelled as $\{1, \dots, \underline{i}\mathbf{j}, \underline{k}, \dots, m+1\}$. By virtue of Eq.(3.21) we can uniquely identify the projected momenta of each dipole with the leading-order configuration such that ultimately each term in Eq.(3.28) is integrated over phase space in terms of the momenta $\{1, \dots, m\}$.

For completeness we want to mention that generalisations of Eqs.(3.27) and (3.28) for the treatment of initial-state radiation and identified partons in the final state exist, but will not be considered in this thesis. The formalism developed so far suffices for an application to the process $e^+e^- \rightarrow \text{di-jets}$ we were considering earlier, which will be the concern of the upcoming sections.

3.3 Subtraction for $e^+e^- \rightarrow \text{di-jets}$

We consider the full real emission matrix element Eq.(2.36) in more detail by rewriting

$$\begin{aligned} |\mathcal{M}_3^{\mathbf{r}}|^2 &\propto \frac{x_q^2 + x_{\bar{q}}^2}{(1-x_q)(1-x_{\bar{q}})} - \epsilon \frac{(2-x_q-x_{\bar{q}})^2}{(1-x_q)(1-x_{\bar{q}})} \\ &= \left\{ \frac{1}{1-x_{\bar{q}}} \left[\frac{2}{2-x_q-x_{\bar{q}}} - (1+x_q) \right] - \epsilon \frac{1-x_q}{1-x_{\bar{q}}} \right\} + \left\{ x_q \leftrightarrow x_{\bar{q}} \right\} - 2\epsilon. \end{aligned} \quad (3.29)$$

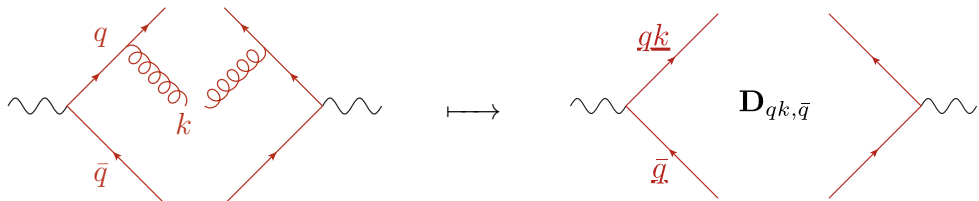
Applying the procedure outlined in the previous section for the $q\bar{q} + g$ final state under consideration leads to the d -dimensional Catani-Seymour counter terms

$$\begin{aligned} \mathcal{D}_{qk,\bar{q}}(x_q, x_{\bar{q}}, \epsilon) &= \hat{\mathcal{M}} \frac{\tilde{\mu}^{4\epsilon}}{Q^2} \frac{(1-\epsilon)^2}{3-2\epsilon} \left\{ \frac{1}{1-x_{\bar{q}}} \left[\frac{2}{2-x_q-x_{\bar{q}}} - (1+x_q) \right] + \frac{1-x_q}{x_{\bar{q}}} - \epsilon \frac{1}{x_{\bar{q}}} \frac{1-x_q}{1-x_{\bar{q}}} \right\}, \\ \mathcal{D}_{\bar{q}k,q}(x_q, x_{\bar{q}}, \epsilon) &= \mathcal{D}_{qk,\bar{q}}(x_{\bar{q}}, x_q, \epsilon), \end{aligned} \quad (3.30)$$

where $\hat{\mathcal{M}}$ is defined as in Eq.(2.34). In Eq.(3.30) the dipole contribution $\mathcal{D}_{qk,\bar{q}}$ will take care of the q -collinear ($x_{\bar{q}} \rightarrow 1$) and the soft singularity in Eq.(3.29) when it is approached from the q -collinear direction (c.f. Fig. 2.63). $\mathcal{D}_{\bar{q}k,q}$ acts analogously for the case $q \leftrightarrow \bar{q}$.

3.4 Derivation of Catani-Seymour counter terms

In this section we want to derive the dipole contributions Eq.(3.30) using the general formalism outlined in Sec. 3.2. According to Eq.(3.14) we need to consider two dipoles for the process $e^+e^- \rightarrow q\bar{q} + g$ at NLO. Focusing on the contribution $\mathcal{D}_{qk,\bar{q}}$ from the dipole $\{(q, k), \bar{q}\}$ we can diagrammatically understand the dipole reduction in the sense of Eqs.(3.22) and (3.23) as mapping



$$\mathbf{3}\langle (q, k), \bar{q} | (q, k), \bar{q} \rangle \mathbf{3} \quad \longmapsto \quad \mathbf{2}\langle q\bar{k}, \bar{q} | \mathbf{D}_{qk,\bar{q}} | q\bar{k}, \bar{q} \rangle \mathbf{2}, \quad (3.31)$$

with the dipole momentum map giving $f_{qk,\bar{q}}(q, \bar{q}, k) = (q\underline{k}, \bar{q})$, and we have a similar contribution for $\mathcal{D}_{\bar{q}k,q}$. The full counter term to the real emission matrix element Eq.(2.36) is then obtained according to Eq.(3.14) as the sum

$$|\mathcal{M}_3^c|^2 = \mathcal{D}_{qk,\bar{q}} + \mathcal{D}_{\bar{q}k,q}. \quad (3.32)$$

We will work out the dipole contribution $\mathcal{D}_{qk,\bar{q}}$ coming from the dipole $\{(q, k), \bar{q}\}$ in detail. Due to charge conjugation, the other dipole contribution from $\{(\bar{q}, k), q\}$ can then be obtained from $\mathcal{D}_{qk,\bar{q}}$ by exchanging $q \leftrightarrow \bar{q}$. Starting with the kinematics for the quark ($q\underline{k}$) and the anti-quark \bar{q} we have

$$q\underline{k}^\mu = q^\mu + k^\mu - \frac{y_{qk,\bar{q}}}{1 - y_{qk,\bar{q}}} \bar{q}^\mu, \quad \bar{q}^\mu = \frac{1}{1 - y_{qk,\bar{q}}} \bar{q}^\mu, \quad y_{qk,\bar{q}} = \frac{q \cdot k}{q \cdot \bar{q} + q \cdot k + \bar{q} \cdot k} = 1 - x_{\bar{q}}, \quad (3.33)$$

where we have expressed the kinematic invariant $y_{qk,\bar{q}}$ in terms of the momentum fractions defined in Eq.(2.35) for later convenience. To evaluate the counter term we have to compute the matrix element of the dipole operator $\mathbf{D}_{qk,\bar{q}}$ with respect to the reduced two particle amplitude $|q\underline{k}, \bar{q}\rangle_2$, that is

$$\mathcal{D}_{qk,\bar{q}} = -\frac{1}{2(q \cdot k)} \mathbf{2}\langle q\underline{k}, \bar{q} | \frac{\mathbf{T}_{\bar{q}} \cdot \mathbf{T}_{qk}}{\mathbf{T}_{qk}^2} \mathbf{V}_{qk,\bar{q}}(y_{qk,\bar{q}}, z_q) | q\underline{k}, \bar{q} \rangle_2. \quad (3.34)$$

We commence by noting that the state described by the amplitude is a colour singlet and hence colour conservation Eq.(D.16) applied to the case at hand reads

$$[\mathbf{T}_{qk}^a + \mathbf{T}_{\bar{q}}^a] |q\underline{k}, \bar{q}\rangle_2 = 0, \quad (3.35)$$

for any colour a of the emitted gluon. The factor of the dipole operator Eq.(3.34) pertaining to the colour degrees of freedom of both the emitter pair and the spectator can then be simplified using the colour charge operator algebra

$$\frac{\mathbf{T}_{\bar{q}} \cdot \mathbf{T}_{qk}}{\mathbf{T}_{qk}^2} |q\underline{k}, \bar{q}\rangle_2 = -\frac{\mathbf{T}_{qk}^2}{\mathbf{T}_{qk}^2} |q\underline{k}, \bar{q}\rangle_2 = -|q\underline{k}, \bar{q}\rangle_2, \quad (3.36)$$

leaving only the helicity and kinematic dependence to be determined. Making the sum over helicities explicit we can use Eq.(D.25) to determine the dipole contribution

$$\begin{aligned} \mathcal{D}_{qk,\bar{q}} &= \sum_{s_1, s_2, s'_1, s'_2} \frac{1}{2(q \cdot k)} \mathbf{2}\langle q\underline{k}, \bar{q} | s_1, s_2 \rangle \langle s_1 | \otimes \langle s_2 | (\mathbf{V}_{qk,\bar{q}} \otimes \mathbf{1}) (|s'_1\rangle \otimes |s'_2\rangle) \langle s'_1, s'_2 | q\underline{k}, \bar{q} \rangle_2 \\ &= \frac{8\pi\tilde{\mu}^{2\epsilon}\alpha_s C_F}{2(q \cdot k)} \left[\frac{2}{1 - z_q(1 - y_{qk,\bar{q}})} - (1 + z_q) - \epsilon(1 - z_q) \right] \mathbf{2}\langle q\underline{k}, \bar{q} | q\underline{k}, \bar{q} \rangle_2, \end{aligned} \quad (3.37)$$

where $y_{qk,\bar{q}}$ and z_q are defined as in Eq.(3.18) and we have emphasised the fact that the spin dependence of $\mathbf{V}_{qk,\bar{q}}$ is entirely determined by the emitter (c.f. Eq.(D.23)). The kinematic invariants appearing in Eq.(3.37) can again be written in terms of momentum fractions where they take the form

$$\begin{aligned} z_q &= \frac{q \cdot \bar{q}}{\bar{q} \cdot (q + k)} & 1 + z_q &= 1 + x_q - \frac{(1 - x_q)(1 - x_{\bar{q}})}{x_{\bar{q}}} & 1 - z_q &= \frac{\bar{q} \cdot k}{\bar{q} \cdot (q + k)} = \frac{1 - x_q}{x_{\bar{q}}} \\ & & \frac{1}{1 - z_q(1 - y_{qk,\bar{q}})} &= \frac{q \cdot \bar{q} + q \cdot k + \bar{q} \cdot k}{k \cdot (q + \bar{q})} = \frac{Q^2}{2(k \cdot Q)} = \frac{1}{2 - x_q - x_{\bar{q}}}, \end{aligned} \quad (3.38)$$

recalling that $Q^2 = 2(q \cdot \bar{q} + q \cdot k + \bar{q} \cdot k)$ when all final state particles are massless. By Eq.(D.4) we have $\mathbf{2}\langle q\underline{k}, \bar{q} | q\underline{k}, \bar{q} \rangle_2 = |\mathcal{M}_2^{\text{LO}}|^2(q\underline{k}, \bar{q})$, i.e. the (colour/helicity-averaged) leading-order matrix

element we computed in Eq.(2.9) in terms of the projected momenta $\{q\underline{k}, \bar{q}\}$. Note that to combine this contribution with the virtual correction as in Eq.(3.28) we have to assign the projected momenta to the leading-order configuration $\{q, \bar{q}\}$ according to Eq.(3.21), that is $\{q\underline{k}, \bar{q}\} \equiv \{q, \bar{q}\}$. For the other dipole configuration $\mathcal{D}_{\bar{q}k,q}$ the identification correspondingly reads $\{\bar{q}\underline{k}, q\} \equiv \{\bar{q}, q\}$.

While in the generic case the different assignments of projected momenta onto the leading-order configuration for each dipole are important to keep track of for the remaining phase space integration, in the particular case we are considering we recall from Eq.(2.9) that $|\mathcal{M}_2^{\text{LO}}|^2(q\underline{k}, \bar{q}) = |\mathcal{M}_2^{\text{LO}}|^2(q, \bar{q}) = |\mathcal{M}_2^{\text{LO}}|^2$ has no kinematic dependence.

Combining results we obtain the final expression for the counter terms coming from the dipole $\{(q, k), \bar{q}\}$,

$$\mathcal{D}_{qk,\bar{q}}(q, \bar{q}, k) = |\mathcal{M}_2^{\text{LO}}|^2 \frac{8\pi\tilde{\mu}^{2\epsilon}\alpha_s C_F}{2(q \cdot k)} \left[\frac{Q^2}{k \cdot (q + \bar{q})} - 1 - \frac{q \cdot \bar{q}}{\bar{q} \cdot (q + k)} - \epsilon \frac{\bar{q} \cdot k}{\bar{q} \cdot (q + k)} \right], \quad (3.39)$$

which, upon substitution of Eq.(3.33) and Eq.(3.38), can be brought to the form shown in Eq.(3.30). Here we recognise the general factorised form of the dipole contribution that was claimed in Eq.(3.26), where now

$$\mathcal{D}_{qk,\bar{q}} = |\mathcal{M}_{\text{LO}}^{\text{c},qk,\bar{q}}|^2 \times V_{qk,\bar{q}}(k, q, \bar{q}) \quad (3.40)$$

with the leading order matrix element and the singular factor identified by

$$|\mathcal{M}_{\text{LO}}^{\text{c},qk,\bar{q}}|^2 = |\mathcal{M}_2^{\text{LO}}|^2, \quad V_{qk,\bar{q}}(k, q, \bar{q}) = \frac{8\pi\tilde{\mu}^{2\epsilon}\alpha_s C_F}{2(q \cdot k)} \left[\frac{Q^2}{k \cdot (q + \bar{q})} - 1 - \frac{q \cdot \bar{q}}{\bar{q} \cdot (q + k)} - \epsilon \frac{\bar{q} \cdot k}{\bar{q} \cdot (q + k)} \right]. \quad (3.41)$$

The form Eq.(3.39) is convenient to subtract from the real emission matrix element Eq.(2.36) since it is given in terms of the physical parton momenta (q, \bar{q}, k) . However, according to Eq.(3.28), to add the counter term back to the virtual correction we still need to analytically integrate over the single particle phase space leading to the soft-collinear singularities. We employ the dipole phase space factorisation Eq.(3.24), which for the dipole under consideration reads

$$d\Phi_3(q, \bar{q}, k) = d\Phi_2(q\underline{k}, \bar{q}) dk(q\underline{k}, \bar{q}). \quad (3.42)$$

Proceeding to compute the integral over the factorised single parton phase space $dk(q\underline{k}, \bar{q})$ (c.f. Eq.(3.25)), we introduce the notation

$$\begin{aligned} \int_k \mathcal{D}_{qk,\bar{q}} &\equiv \int dk(q\underline{k}, \bar{q}) \mathcal{D}_{qk,\bar{q}} = |\mathcal{M}_2^{\text{c},qk,\bar{q}}|^2 \int dk(q\underline{k}, \bar{q}) V_{qk,\bar{q}}(k, q, \bar{q}) = |\mathcal{M}_2^{\text{LO}}|^2 \frac{\alpha_s C_F}{4\pi} \left(\frac{4\pi\tilde{\mu}^2}{Q^2} \right)^\epsilon \\ &\times \frac{1}{\Gamma(1-\epsilon)} \int_0^1 dz dy \frac{(1-y)^{1-2\epsilon}}{y^{1+\epsilon}(z(1-z))^\epsilon} \left[\frac{2}{1-z(1-y)} - (1+z) - \epsilon(1-z) \right], \\ &= \frac{\hat{\mathcal{M}}}{16\pi^2} \tilde{\mu}^{2\epsilon} \left(\frac{4\pi\tilde{\mu}^2}{Q^2} \right)^\epsilon \frac{(1-\epsilon)^2}{3-2\epsilon} \frac{\Gamma(1-\epsilon)^2}{\Gamma(1-3\epsilon)} \left[\frac{1}{\epsilon^2} + \frac{3}{2\epsilon} + \frac{5}{1-3\epsilon} \right], \end{aligned} \quad (3.43)$$

where we have brought the result into a form that is more readily comparable to the virtual amplitude Eq.(2.46). In the calculation of Eq.(3.43) we have set $y_{qk,\bar{q}} \equiv y$ and $z_q \equiv z$ for readability and have used $2q \cdot k = yQ^2$, $2q\underline{k} \cdot \bar{q} = Q^2$, to rewrite the inner products appearing in the single-particle phase space measure and the dipole factor. It is straightforward to check that for the other dipole in Eq.(3.31) we have

$$\int_k \mathcal{D}_{\bar{q}k,q} = \int dk(\bar{q}\underline{k}, q) \mathcal{D}_{\bar{q}k,q} = \int_k \mathcal{D}_{qk,\bar{q}}. \quad (3.44)$$

3.5 Analytic subtraction for thrust

For the process $e^+e^- \rightarrow \text{di-jets}$ under consideration the general structure of the subtraction procedure in Eq.(3.27) and Eq.(3.28) entails the following form of the subtracted real emission and virtual thrust distribution contributions,

$$\begin{aligned}\frac{d\sigma_{\mathbf{3}\text{sub}}^{\mathbf{r}}}{d\tau} &= \frac{1}{2s} \int d\Phi_{\mathbf{3}}(q, \bar{q}, k) \left[|\mathcal{M}_{\mathbf{3}}^{\mathbf{r}}|^2 \Big|_{\epsilon=0} \delta(\tau - \tau(q, \bar{q}, k)) - [\mathcal{D}_{qk, \bar{q}} + \mathcal{D}_{\bar{q}k, q}] \Big|_{\epsilon=0} \delta(\tau) \right], \\ \frac{d\sigma_{\mathbf{2}\text{sub}}^{\mathbf{v}}}{d\tau} &= \frac{1}{2s} \int d\Phi_{\mathbf{2}}(q, \bar{q}) \left[|\mathcal{M}_{\mathbf{2}}^{\mathbf{v}}|^2 + \int_k \mathcal{D}_{qk, \bar{q}} + \int_k \mathcal{D}_{\bar{q}k, q} \right] \Big|_{\epsilon=0} \delta(\tau),\end{aligned}\quad (3.45)$$

where the real emission and virtual amplitudes are given in Eqs.(2.36) and (2.46) respectively.

Starting out with the subtracted real emission contribution to the thrust distribution we can use the explicit form of the real emission amplitude Eq.(3.29) and the counter terms Eq.(3.30) in terms of the momentum fractions Eq.(2.35) to write

$$\frac{d\sigma_{\mathbf{3}\text{sub}}^{\mathbf{r}}}{d\tau} = \frac{1}{2s} \int d\Phi_{\mathbf{3}}(x_q, x_{\bar{q}}) \left[|\mathcal{M}_{\mathbf{3}}^{\mathbf{r}}|^2 \Big|_{\epsilon=0} [\delta(\tau - \tau(x_q, x_{\bar{q}})) - \delta(\tau)] + \frac{\hat{\mathcal{M}}}{3s} \left(\frac{1-x_q}{x_{\bar{q}}} + \frac{1-x_{\bar{q}}}{x_q} \right) \delta(\tau) \right], \quad (3.46)$$

which is a manifestly four dimensional quantity. If we wanted to analytically evaluate the terms involving delta functions we would run into two problems. For one, there cannot feasibly occur any cancellation in the term proportional to $[\delta(\tau - \tau(x_q, x_{\bar{q}})) - \delta(\tau)]$ at the level of the integrand, since the first term needs to have $\tau > 0$ for the phase space integral to be sufficiently regularised as we have seen in Eq.(3.46), while the second term only contributes at $\tau = 0$. The second problem we have to deal with is that the term proportional to $|\mathcal{M}_{\mathbf{3}}^{\mathbf{r}}|^2|_{\epsilon=0} \delta(\tau)$ prompts us to compute the total real emission cross-section in $d=4$ dimensions, which we know to be a divergent quantity. Therefore we cannot naively make sense of the ill-defined expression in Eq.(3.46).

However, both of these problems only arise in the analytic calculation of the thrust distribution. In a numerical setting the exact distributional form of Eq.(3.46) cannot be determined and we will resort to the computation of another observable, the so-called cumulant (see Eq.(4.1)) representing the contribution to the total cross section coming from a certain interval (bin) $\tau \in [\tau_-, \tau_+]$ of thrust. The analogue of Eq.(3.46) for the thrust cumulant will in fact allow for a cancellation of divergences (c.f. discussion below Eq.(4.6)).

One way to evaluate the real emission subtracted thrust distribution analytically is to first evaluate the phase space integrals for both the amplitude and counter terms in d dimensions so that everything is sufficiently regularised, perform the subtraction, and only then take the limit $\epsilon \rightarrow 0$, i.e. we redefine

$$\begin{aligned}\frac{d\sigma_{\mathbf{3}\text{sub}}^{\mathbf{r}}}{d\tau} &= \frac{1}{2s} \left[\int d\Phi_{\mathbf{3}}(q, \bar{q}, k) |\mathcal{M}_{\mathbf{3}}^{\mathbf{r}}|^2 \delta(\tau - \tau(q, \bar{q}, k)) - [\mathcal{D}_{qk, \bar{q}} + \mathcal{D}_{\bar{q}k, q}] \delta(\tau) \right] \Big|_{\epsilon=0} \\ &= \left[\frac{d\sigma_{\mathbf{3}}^{\mathbf{r}}}{d\tau} - \frac{1}{2s} \int d\Phi_{\mathbf{3}}(q, \bar{q}, k) [\mathcal{D}_{qk, \bar{q}} + \mathcal{D}_{\bar{q}k, q}] \delta(\tau) \right] \Big|_{\epsilon=0}.\end{aligned}\quad (3.47)$$

The phase space integral over the counter terms can be easily performed by noting that due to the dipole phase space factorisation property and Eq.(3.44) we have

$$\begin{aligned}\frac{1}{s} \int d\Phi_{\mathbf{2}} \int_k \mathcal{D}_{qk, \bar{q}} \delta(\tau) &= \frac{1}{2s} \int d\Phi_{\mathbf{3}}(q, \bar{q}, k) [\mathcal{D}_{qk, \bar{q}} + \mathcal{D}_{\bar{q}k, q}] \delta(\tau) \\ &= \hat{\sigma}(\epsilon) \frac{\alpha_s C_F}{\pi} \frac{e^{\gamma_E \epsilon} \mu^{4\epsilon}}{s^{1+2\epsilon}} \frac{\Gamma(1-\epsilon)^2}{\Gamma(1-3\epsilon)} \left[\frac{1}{\epsilon^2} + \frac{3}{2\epsilon} + \frac{5}{1-3\epsilon} \right] \delta(\tau) \\ &= \hat{\sigma}(\epsilon) \frac{\alpha_s C_F}{\pi} \frac{\mu^{4\epsilon}}{s^{1+2\epsilon}} \left\{ \frac{1}{\epsilon^2} + \frac{3}{2\epsilon} + 5 - \frac{7\pi^2}{12} + \mathcal{O}(\epsilon) \right\} \delta(\tau)\end{aligned}\quad (3.48)$$

which conveniently allowed us to reuse the result already derived in Eq.(3.43). Combining Eq.(3.48) with Eq.(2.69) as described in Eq.(3.47) we arrive at the subtracted real emission thrust distribution

$$\begin{aligned} \frac{d\sigma_{\mathbf{3}\text{sub}}^{\mathbf{r}}}{d\tau} &= \frac{\hat{\sigma}(\epsilon=0)}{s} \frac{\alpha_s C_F}{\pi} \left\{ \left[-\frac{3}{2} + \frac{\pi^2}{6} \right] \delta(\tau) + \left[-\frac{3}{2} + 3\tau + \frac{9}{2}\tau^2 + \frac{2-3\tau(1-\tau)}{1-\tau} \log(1-2\tau) \right] \left[\frac{\theta(\tau)}{\tau} \right]_+ \right. \\ &\quad \left. + \left[3\tau - \frac{2}{1-\tau} \right] \left[\frac{\theta(\tau)\log(\tau)}{\tau} \right]_+ \right\}. \end{aligned} \quad (3.49)$$

Note that in arriving at the above result we have given away one of the major advantages of the subtraction method, namely the ability to compute the cross section directly in $d = 4$ dimensions, without having to know the details of the amplitude in d dimensions. In App. G we propose another method to analytically calculate Eq.(3.49) manifestly in $d=4$ dimensions, employing a different kind of regularisation.

We now turn to the subtracted virtual contribution in Eq.(3.45) which is again simpler to treat than the real emission case. Here we have to combine the d -dimensional results for the original amplitude Eq.(2.46) and the integrated counter terms Eq.(3.43) before taking the limit $\epsilon \rightarrow 0$. Exploiting Eq.(3.44) we can write

$$\begin{aligned} \frac{d\sigma_{\mathbf{2}\text{sub}}^{\mathbf{v}}}{d\tau} &= \frac{1}{2s} \int d\Phi_{\mathbf{2}} \left[\frac{\hat{\mathcal{M}}}{16\pi^2} \tilde{\mu}^{2\epsilon} \left(\frac{4\pi\tilde{\mu}^2}{Q^2} \right)^\epsilon \frac{(1-\epsilon)^2}{3-2\epsilon} \Gamma(1-\epsilon)^2 \right] \Big|_{\epsilon=0} \\ &\quad \times \left\{ \left[\frac{2}{\epsilon^2} + \frac{3}{\epsilon} \right] \left[-\frac{\cos(\pi\epsilon)\Gamma(1+\epsilon)}{\Gamma(1-2\epsilon)} + \frac{1}{\Gamma(1-3\epsilon)} \right] - \frac{8}{1-2\epsilon} \frac{\cos(\pi\epsilon)\Gamma(1+\epsilon)}{\Gamma(1-2\epsilon)} \right. \\ &\quad \left. + \frac{10}{1-3\epsilon} \frac{1}{\Gamma(1-3\epsilon)} \right\} \Big|_{\epsilon=0} \delta(\tau) = \frac{\hat{\sigma}(\epsilon=0)}{s} \frac{\alpha_s C_F}{\pi} \delta(\tau), \end{aligned} \quad (3.50)$$

where the first term in the second line, containing the factor with poles in ϵ , vanishes in the limit $\epsilon \rightarrow 0$, thus facilitating the subtraction.

Finally combining the results Eq.(3.49) and Eq.(3.50) for the subtracted real emission and virtual thrust distribution contributions and comparing with Eq.(2.71) establishes

$$\frac{d\sigma_{\mathbf{3}\text{sub}}^{\mathbf{r}}}{d\tau} + \frac{d\sigma_{\mathbf{2}\text{sub}}^{\mathbf{v}}}{d\tau} = \frac{d\sigma_{\mathbf{2}/\mathbf{3}}^{\text{NLO}}}{d\tau} \Big|_{\epsilon=0}, \quad (3.51)$$

confirming that Eq.(3.1) in fact holds true for thrust in $e^+e^- \rightarrow q\bar{q} + g$.

In having computed the counter term Eq.(3.48) analytically we can see another crucial property of the subtraction procedure. The counter term is proportional to $\delta(\tau)$ and as such it can only act locally in the kinematic variable we are considering. This makes sense since the original divergences occurring in the real emission and virtual contributions Eqs.(2.69) and (2.70) were also only local in thrust, i.e. they were of the form

$$\frac{d\sigma_{\mathbf{3}}^{\mathbf{r}}}{d\tau}, \frac{d\sigma_{\mathbf{2}}^{\mathbf{v}}}{d\tau} \stackrel{\text{sing. } \epsilon \rightarrow 0}{\simeq} \left\{ \frac{c_1}{\epsilon^2} + \frac{c_2}{\epsilon} \right\} \delta(\tau). \quad (3.52)$$

This should be kept in mind in the subsequent discussion of thrust in the context of SCET, where the structure of divergences is going to be more complicated.

4 Numerical implementation, comparison to analytic results and experiment

This section aims at tying together the analytic and numerical approach to computing observables in QCD. By providing some details on the implementation of the subtraction procedure using Monte Carlo methods and numerically carrying out the subtraction for the thrust distribution discussed in previous chapters we demonstrate equivalence to the conventional analytic methods.

We proceed to compare the obtained distributions to experimental data encountering a vast discrepancy to the theoretical result which we will attribute to the infamous problem of large logarithms. The concept of resummation, used to regain control of the perturbative prediction, as well as non-perturbative effects are briefly discussed and provide the conceptual setup for the later introduction of SCET.

4.1 Comments on numerical implementation using Monte Carlo

Here we want to briefly discuss some aspects regarding the adaptation of the dipole subtraction method, introduced in an analytic context in the previous sections, to allow for its implementation using numerical procedures such as Monte Carlo integration. Additionally we want to highlight some of the practical advantages of the latter technique, such as parallelisation, albeit without any reference to a specific implementation (i.e. computer code).

For concreteness let us first discuss the thrust distribution Eq.(2.71), which in the analytic calculation came out to be a (mathematical) distribution. In a numerical procedure we cannot actually determine the distributional structure itself but have to contend ourselves with computing cumulants of the cross section

$$\Sigma_{2/3}^{\text{NLO}}(\tau^-, \tau^+) \equiv \int_{\tau^-}^{\tau^+} d\tau \frac{d\sigma_{2/3}^{\text{NLO}}}{d\tau}, \quad (4.1)$$

which in the case at hand represents the NLO contribution of the differential cross section to the total cross section from some interval (also called bin) of thrust $[\tau^-, \tau^+]$. Recall that at NLO the thrust variable $\tau \in [0, \tau_{\text{max}}]$, where $\tau_{\text{max}} = 1/3$. In the following we will use the short-hand $\Sigma_{2/3}^{\text{NLO}}(\tau^+) = \Sigma_{2/3}^{\text{NLO}}(0, \tau^+)$ for the cumulant including the di-jet contribution from $\tau = 0$, which we will also refer to as the zero-bin.

To compute the cumulant in Eq.(4.1) directly from the matrix elements Eqs.(2.33) and (2.46) we have to specify the corresponding two- and three-particle measurement functions on phase space,

$$\begin{aligned} O_3(q, \bar{q}, k) &= \chi(\tau(q, \bar{q}, k) \in [\tau^-, \tau^+]), \\ O_2(q, \bar{q}) &= \begin{cases} 1, & \text{if } 0 \in [\tau^-, \tau^+] \\ 0, & \text{else,} \end{cases} \end{aligned} \quad (4.2)$$

where $\chi(x \in [a, b])$ denotes the characteristic function of the interval $[a, b]$. Using the thus defined observables we partition the allowed range of the thrust parameter $[0, \tau_{\text{max}}]$ into B small bins $[\tau_i^-, \tau_i^+]$, $i = 1, \dots, B$, $\tau_1^- = 0, \tau_B^+ = \tau_{\text{max}}$. The bins do not overlap and for simplicity we assume that all bins are of equal size, such that the NLO contribution to the total cross section Eq.(2.48) is recovered in the sum

$$\sum_{i=1}^B \Sigma_{2/3}^{\text{NLO}}(\tau_i^-, \tau_i^+) = \sigma_{2/3}^{\text{NLO}}. \quad (4.3)$$

As we decrease the bin size the individual cumulants provide a progressively closer approximation to the differential cross section which, adopting the notation Eq.(3.3), we recall was defined through the

measurement functions

$$\begin{aligned}\delta O_3(q, \bar{q}, k) &= \delta(\tau - \tau(q, \bar{q}, k)), \\ \delta O_2(q, \bar{q}) &= \delta(\tau).\end{aligned}\tag{4.4}$$

The fact that the measurement functions Eq.(4.2) provide a good approximation to the original thrust distribution obtained through the measurement functions Eq.(4.4) can be seen by noting that for the three-particle cumulant of a small bin $[\tau - \delta_\tau, \tau + \delta_\tau]$ of size $2\delta_\tau$ around a given value of τ we have

$$\frac{1}{2\delta_\tau} \int d\tau' \frac{d\sigma_3^{\mathbf{r}}}{d\tau'} \chi(\tau' \in [\tau - \delta_\tau, \tau + \delta_\tau]) \xrightarrow{\delta_\tau \rightarrow 0} \int d\tau' \frac{d\sigma_3^{\mathbf{r}}}{d\tau'} \delta(\tau' - \tau) = \frac{d\sigma_3^{\mathbf{r}}}{d\tau}(\tau).\tag{4.5}$$

Correspondingly we can consider the two-particle final state contribution to the cumulant from the zero-bin $[0, \delta_\tau]$ which in the limit $\delta_\tau \rightarrow 0$ coincides with the strict di-jet region contribution to the thrust distribution from terms proportional to $\delta(\tau)$.

Coming back to the numerical computation of the cross section using the subtraction method we see that the analogue of Eq.(3.45) for the thrust cumulant reads

$$\begin{aligned}\Sigma_{2/3}^{\text{NLO}}(\tau^+) &= \frac{1}{2s} \int d\Phi_3(q, \bar{q}, k) \left[|\mathcal{M}_3^{\mathbf{r}}|^2 \Big|_{\epsilon=0} \chi(\tau(q, \bar{q}, k) \in [0, \tau^+]) - [\mathcal{D}_{qk, \bar{q}} + \mathcal{D}_{\bar{q}k, q}] \Big|_{\epsilon=0} \right] \\ &+ \frac{1}{2s} \int d\Phi_2(q, \bar{q}) \left[|\mathcal{M}_2^{\mathbf{y}}|^2 + \int_k \mathcal{D}_{qk, \bar{q}} + \int_k \mathcal{D}_{\bar{q}k, q} \right] \Big|_{\epsilon=0},\end{aligned}\tag{4.6}$$

whenever we are considering a zero-bin contribution from an interval of the form $[0, \tau^+]$. When the cumulant is calculated over a bin $[\tau^-, \tau^+]$ with $\tau^- > 0$ then the corresponding expression simply reads

$$\Sigma_{2/3}^{\text{NLO}}(\tau^-, \tau^+) = \frac{1}{2s} \int d\Phi_3(q, \bar{q}, k) |\mathcal{M}_3^{\mathbf{r}}|^2 \Big|_{\epsilon=0} \chi(\tau(q, \bar{q}, k) \in [\tau^-, \tau^+]),\tag{4.7}$$

where the subtraction terms do not need to be taken into account. Note that in the zero-bin contribution Eq.(4.6) the cancellation of divergences between real emission amplitude and counter terms near $\tau = 0$ can take place at the level of the integrand, since $\chi(\tau(q, \bar{q}, k) \in [0, \tau^+]) = 1$ there. We recall that this was not the case for the analytic calculation of the thrust distribution using Eq.(3.46). With this problem out of the way, the above integrals are now perfectly suited to be directly evaluated by a numerical routine.

Having established the notation and conventions for a numerical implementation of the subtraction procedure, we would now like to explore the freedom we have in choosing counter terms. So far we have only talked about the dipole counter terms defined by Eq.(3.16) which correctly reproduce the singular limits of the real emission amplitude, but in practice nothing prevents us from changing the structure of the soft-collinear finite terms included in the sum Eq.(3.14). In particular we consider the extreme case where the counter terms in Eq.(4.6) are chosen to precisely equal the real emission amplitude. Note that this essentially amounts to setting to zero the finite terms proportional to $\hat{\mathcal{M}}$ in Eq.(3.46). For this particular choice of counter term the zero-bin contribution to the thrust cumulant reads

$$\begin{aligned}\Sigma_{2/3}^{\text{NLO}}(\tau^+) &= \frac{1}{2s} \int d\Phi_3(q, \bar{q}, k) |\mathcal{M}_3^{\mathbf{r}}|^2 \Big|_{\epsilon=0} [\chi(\tau(q, \bar{q}, k) \in [0, \tau^+]) - 1] \\ &+ \frac{1}{2s} \int d\Phi_2(q, \bar{q}) \left[|\mathcal{M}_2^{\mathbf{y}}|^2 + \int_k |\mathcal{M}_3^{\mathbf{r}}|^2 \right] \Big|_{\epsilon=0}.\end{aligned}\tag{4.8}$$

Note that this would in practice not be a particularly wise choice of counter term, since we would have given away the advantage of not having to know $|\mathcal{M}_3^{\mathbf{r}}|^2$ analytically in d dimensions. However,

our choice serves an illustrative purpose and allows us to further connect the numerical and analytical calculations. We can recognise the second term in Eq.(4.8) as the total cross section as given in Eq.(2.48), while in the first term we can use

$$\chi(\tau(q, \bar{q}, k) \in [0, \tau^+]) - 1 = \chi(\tau(q, \bar{q}, k) \notin [0, \tau^+]) = \chi(\tau(q, \bar{q}, k) \in (\tau^+, \tau_{\max}]), \quad (4.9)$$

to identify it as the cumulant contribution from the interval $(\tau^+, \tau_{\max}]$ lying outside the zero-bin, i.e. we have

$$\Sigma_{2/3}^{\text{NLO}}(\tau^+) = \sigma_{2/3}^{\text{NLO}} - \Sigma_{2/3}^{\text{NLO}}(\tau^+, \tau_{\max}), \quad (4.10)$$

In this sense when we are computing (numerically or analytically) a cumulant of a differential cross section using a subtraction procedure, we always implicitly compute the total cross section as well. While in the case we just studied this becomes particularly apparent, the generic case where the finite terms of the counter term and the real emission amplitude do not match exactly (as in the dipole subtraction), just corresponds to swapping contributions between the two terms on the right-hand side of Eq.(4.10).

Up to this point we solely focused on the thrust distribution for $e^+e^- \rightarrow q\bar{q} + g$. Let us now consider the general case where we are interested in computing N differential cross sections in the (IR-safe) quantities O_n , $n = 1, \dots, N$ for a process with $m + 1$ partons at NLO. Using the notation established in Eq.(3.6) and Eq.(3.13) for the subtracted cross section contributions, and naturally generalising the measurement functions Eq.(4.2) to arbitrary observables, we can compute the N different cumulants

$$\Sigma_{\mathbf{m}/\mathbf{m}+1}^{\text{NLO}}(O_n^-, O_n^+) \equiv \Sigma_{\mathbf{m}+1, \text{sub}}^{\text{NLO}, \mathbf{r}}(O_n^-, O_n^+) + \Sigma_{\mathbf{m}, \text{sub}}^{\text{NLO}, \mathbf{v}}(O_n^-, O_n^+), \quad (4.11)$$

where, using the momentum map given in Eq.(3.5), the subtracted quantities read

$$\begin{aligned} \Sigma_{\mathbf{m}+1, \text{sub}}^{\text{NLO}, \mathbf{r}}(O_n^-, O_n^+) &= \int d\Phi_{\mathbf{m}+1}(p_1, \dots, \mathbf{p}_{m+1}) \left[|\mathcal{M}_{\mathbf{m}+1}^{\mathbf{r}}|^2 \Big|_{\epsilon=0} \chi(O_{n, \mathbf{m}+1}(p_1, \dots, \mathbf{p}_{m+1}) \in [O_n^-, O_n^+]) \right. \\ &\quad \left. - |\mathcal{M}_{\mathbf{m}+1}^{\mathbf{c}}|^2 \Big|_{\epsilon=0} \chi(O_{n, \mathbf{m}}(f(p_1, \dots, \mathbf{p}_{m+1})) \in [O_n^-, O_n^+]) \right], \\ \Sigma_{\mathbf{m}, \text{sub}}^{\text{NLO}, \mathbf{v}}(O_n^-, O_n^+) &= \int d\Phi_{\mathbf{m}}(q_1, \dots, q_m) \left[|\mathcal{M}_{\mathbf{m}}^{\mathbf{v}}|^2 \chi(O_{n, \mathbf{m}}(q_1, \dots, q_m) \in [O_n^-, O_n^+]) \right. \\ &\quad \left. + |\mathcal{M}_{\mathbf{LO}}^{\mathbf{c}}|^2 \chi(O_{n, \mathbf{m}}(q_1, \dots, q_m) \in [O_n^-, O_n^+]) \int d\mathbf{p}_{m+1} V(\mathbf{p}_{m+1}) \right] \Big|_{\epsilon=0}. \end{aligned} \quad (4.12)$$

The adaptation of the rough definitions Eq.(4.12) to the specifics of the Catani-Seymour subtraction involving sums over dipoles (c.f. Eqs.(3.27) and (3.28)) should pose no difficulty following our previous discussion.

It is with the above expressions that the Monte Carlo approach can really show its strength because it allows us to compute all N cumulants for the observables O_n in parallel. Since the method essentially relies on repeatedly evaluating the integrand at different points in its domain to estimate the value of the integral, it exhibits a number of properties that cannot be reproduced with analytic integration.

Let us consider for instance N products of functions (for simplicity we assume their domain to be one dimensional)

$$f(x)g_n(x), \quad n = 1, \dots, N. \quad (4.13)$$

A (very simple) Monte Carlo program will estimate their integral over a certain region I in their domain by randomly sampling M points $\{x_i\} \subset I$ and computing

$$\int_I dx f(x) g_n(x) \simeq \frac{\text{Vol}(I)}{M} \sum_{x_i \in I}^M f(x_i) g_n(x_i). \quad (4.14)$$

In an analytical calculation we would have to compute the N integrals represented by the left-hand side of Eq.(4.14) from scratch. When using Monte Carlo integration we can be more efficient and recycle some computations by splitting the integrand into pieces that occur in multiple integrals (such as $f(x)$) and pieces that are unique to each integral (such as $g_n(x)$). Schematically, the recurring piece can be evaluated once and for all right at the start of an integration routine:

- Randomly sample M points $\{x_i\} \subset I$.
- Evaluate $f(x_i)$ for all x_i .

We can then attach to the recurring pieces the remainder which is unique to each integral:

- In a loop $n = 1, \dots, N$ {
- Evaluate $g_n(x_i)$ for all x_i .
 - Compute $\frac{\text{Vol}(I)}{M} \sum_{x_i \in I}^M f(x_i) g_n(x_i)$
- }

Coming back to the original problem of calculating the N observables in Eq.(4.11), we see that each phase space integral Eq.(4.12) is roughly of the form shown in Eq.(4.14). Therefore we can make use of the Monte Carlo integration property just discussed by identifying the recurring and unique pieces therein.

Among the recurring pieces we find the squared amplitudes $|\mathcal{M}_{\mathbf{m}+1}^{\mathbf{r}}|^2$, $|\mathcal{M}_{\mathbf{m}}^{\mathbf{v}}|^2$, and the counter terms $|\mathcal{M}_{\mathbf{m}+1}^{\mathbf{c}}|^2$. The pieces that are unique to each cumulant are then just the measurement functions $\chi(O_{n,\mathbf{m}+1}(p_1, \dots, p_{m+1}) \in [O_n^-, O_n^+])$, etc., pertaining to the respective amplitudes. Implementing the algorithm outlined above we can thus numerically compute the N observables in an efficient, parallelised, manner.

4.2 Comparison between analytic and numerical results and facing the experiment

Combining the next-to-leading order thrust distribution in Eq.(2.71) with the leading order result which is just given by $\frac{d\sigma_2^{\text{LO}}}{d\tau} = \sigma_2^{\text{LO}} \delta(\tau)$, we can analytically compute the cumulant

$$\begin{aligned} \Sigma_\tau(\tau^+) &\equiv \frac{1}{\sigma_2^{\text{LO}}} \int_0^{\tau^+} d\tau \left[\frac{d\sigma_2^{\text{LO}}}{d\tau} + \frac{d\sigma_{2/3}^{\text{NLO}}}{d\tau} \right] \\ &= 1 + \frac{\alpha_s C_F}{\pi} \left\{ \frac{\pi^2}{6} - \frac{1}{2} - \frac{3}{2} \log(\tau^+) - 2 \log^2(\tau^+) \right\} + \Sigma_\tau^0(\tau^+, \alpha_s), \end{aligned} \quad (4.15)$$

which we have normalised by the leading order total cross section. To arrive at this result it is convenient to use the expressions Eq.(2.68) and Eq.(2.70) where a clean separation between singular contributions (plus distributions) and finite parts is manifest and use the relations in Eq.(I.3) to integrate. The function $\Sigma_\tau^0(\tau^+, \alpha_s)$ at NLO can be shown to read

$$\begin{aligned} \Sigma_\tau^0(\tau^+, \alpha_s) &= \frac{\alpha_s C_F}{\pi} \left\{ \frac{\pi^2}{6} + 3\tau^+ + \frac{9}{4}(\tau^+)^2 + \left[\frac{3}{2} - 3\tau^+ - \log(2 - 2\tau^+) \right] \log(1 - 2\tau^+) \right. \\ &\quad \left. + 3\tau^+ \log(\tau^+) - 2 \left[\text{Li}_2(1 - \tau^+) + \text{Li}_2\left(\frac{1}{2 - 2\tau^+}\right) + \text{Li}_2(2\tau^+) \right] \right\}, \end{aligned} \quad (4.16)$$

satisfying $\Sigma_\tau^0(\tau^+) \rightarrow 0$ as $\tau^+ \rightarrow 0$. While the function is negligible in the peak region, it becomes comparable to the singular terms for larger values of $\tau \sim 1/3$.

Computing the cumulant also numerically using the subtraction method and Monte Carlo integration we can compare to the analytic result by plotting it in the kinematically allowed range $0 < \tau_+ < 1/3$, which results in the diagrams shown in Fig. 4.17.

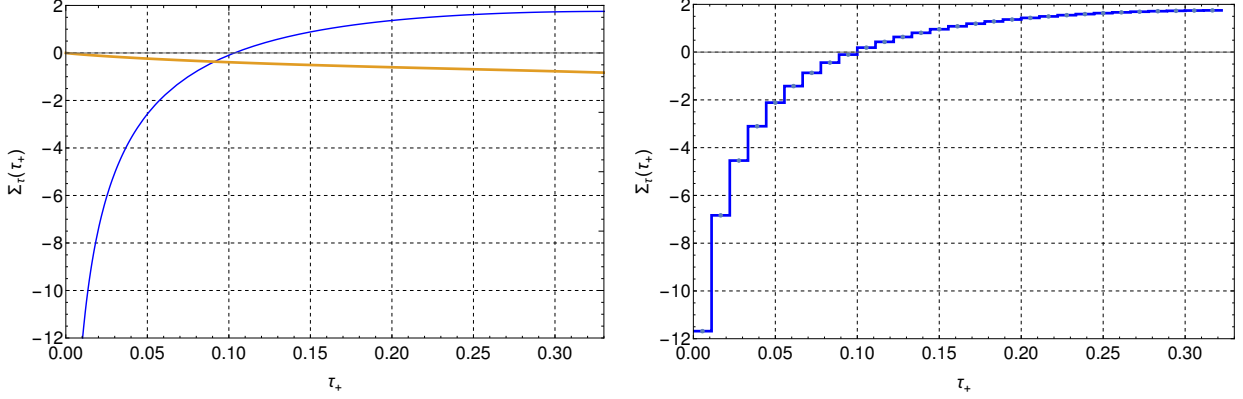


Fig. (4.17): Comparison of analytic (le.) and numerical (ri.) result for thrust distribution cumulant Eq.(4.15) in blue. The finite part contribution Σ_τ^0 is shown in orange for the analytic result. The numerical result was obtained by splitting the interval into 30 bins and performing the phase space integrals for the subtracted quantities Eq.(4.6) and Eq.(4.7) as outlined in Eqs.(4.11) and (4.12). For convenience we have set $\alpha_s C_F/\pi \equiv 1$, so that when $\tau^+ \rightarrow 1/3$ both cumulants approach the total cross section Eq.(2.49) which in this case is given by $\sigma/\sigma_2^{\text{LO}} = 1.75$.

The numerical result was obtained by evaluating the cumulants for each bin as described by Eq.(4.6) and Eq.(4.7) starting with the zero-bin and then cumulatively adding the results of all previous bins to the subsequent one.

From Eq.(4.15) and Fig. 4.17 we can clearly see that the thrust cumulant diverges logarithmically as we move into the di-jet region $\tau^+ \rightarrow 0$, also often called the peak region. To see why this is an appropriate name of this particular kinematic region let us plot the thrust distribution itself and compare it with data obtained from the LEP/OPAL experiment [24] in Fig. 4.18.

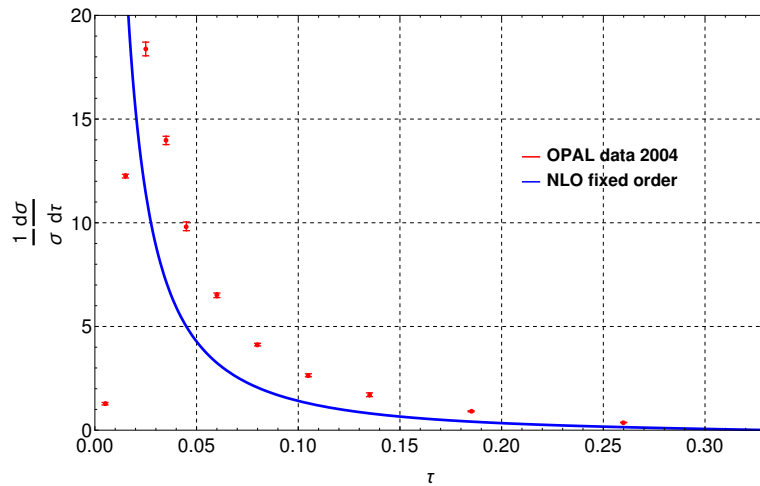


Fig. (4.18): The fixed order calculation ($\alpha_s(M_Z) = 0.1168$) is compared to measurements from the LEP/OPAL experiment [24] at $Q = 91\text{GeV}$. Note how the experimentally obtained quantity exhibits a peak near $\tau \simeq 0.025$ while the thrust distribution obtained from the fixed-order pQCD calculation diverges. Effective field theory methods will allow us to reproduce this peak.

In the tail region (large τ) the experimental data is qualitatively reproduced by the perturbative calculation. Here the disagreement mostly stems from the fact that we neglected Z^* boson exchange and quark masses in our calculation, as alluded to earlier.

In the peak region we run into trouble when $\alpha_s \log(\tau_+) \gtrsim 1$ in Eq.(4.15) becomes parametrically large, such that the perturbative expansion cannot represent a good approximation to the observable. This is what is known in the literature as the problem of large logarithms. Their origin lies in the fact that in a di-jet event we are dealing with a hierarchy of disparate scales. We will discuss the kinematics of the di-jet limit soon (c.f. Sec. 5.2) but for now we note that there are three main scales involved. The hard scale $\mu_h \sim Q$ is associated with the energy of the initial interaction, the jet scale $\mu_j \sim \sqrt{\tau}Q$ can be thought of as the invariant mass of the collimated spray of collinear particles, and $\mu_s \sim \tau Q$ represents the energy of soft (very low energy) radiation mediated between the jets. It is the ratios between these scales that appear in the logarithms in the cumulant Eq.(4.15) and the thrust distribution Eq.(2.71) that lead to large contributions when $\tau \rightarrow 0$.

To remedy this problem, let us consider the general structure of a perturbative expansion of the thrust cumulant to arbitrary order, which can be shown to be the form[25]

$$\begin{aligned} \Sigma_\tau(\tau^+) &= \sum_{n=0}^{\infty} \sum_{m=0}^{2n} \Sigma_{nm} \left(\frac{\alpha_s}{\pi} \right)^n L_{\tau^+}^m + \Sigma^0(\tau^+, \alpha_s) \\ &= 1 + \frac{\alpha_s}{\pi} [\Sigma_{12} L_{\tau^+}^2 + \Sigma_{11} L_{\tau^+} + \Sigma_{10}] \\ &\quad + \left(\frac{\alpha_s}{\pi} \right)^2 [\Sigma_{24} L_{\tau^+}^4 + \Sigma_{23} L_{\tau^+}^3 + \Sigma_{22} L_{\tau^+}^2 + \Sigma_{21} L_{\tau^+} + \Sigma_{20}] \\ &\quad + \dots + \Sigma_\tau^0(\tau^+, \alpha_s), \end{aligned} \tag{4.19}$$

where $\Sigma_\tau^0(\tau^+) \rightarrow 0$ for $\tau^+ \rightarrow 0$ is now itself an expansion starting at $\mathcal{O}(\alpha_s)$ and we have abbreviated $L_{\tau^+}^m \equiv \log^m(\tau^+)$. This can be immediately recognised as the generalisation of our result Eq.(4.15) at NLO by looking at the second line in Eq.(4.19). Notice the grid structure of the cumulant in terms of powers of α_s and L_{τ^+} . Standard fixed order perturbation theory evaluates the cumulant line by line and order by order in Σ_τ^0 which we have seen to lead to an inefficient approximation. An alternative way to systematically compute the terms of the above quantity that do not vanish in the limit $\tau \rightarrow 0$ can be found by considering the logarithm

$$\log(\Sigma_\tau - \Sigma_\tau^0)(\tau^+) = \log(C(\alpha_s)) + \log(S(\tau^+, \alpha_s)), \tag{4.20}$$

which can be split into a constant $C(\alpha_s)$ and singular $S(\tau^+, \alpha_s)$ part given respectively by the expansions

$$\log(C(\alpha_s)) = \sum_{n=1}^{\infty} \left(\frac{\alpha_s}{\pi} \right)^n C_n, \quad \log(S(\tau^+, \alpha_s)) = \sum_{n=1}^{\infty} \sum_{m=1}^{n+1} S_{nm} \left(\frac{\alpha_s}{\pi} \right)^n L_{\tau^+}^m. \tag{4.21}$$

Here the original coefficients Σ_{nm} can be found to be polynomials in the coefficients C_n and S_{nm} [25]. The crucial shift in perspective is to consider the singular part in Eq.(4.21) not as a series in α_s but rather in $\alpha_s L_{\tau^+} \sim 1$. We can then write equivalently

$$\begin{aligned} \log(S(\tau^+, \alpha_s)) &= \frac{\alpha_s}{\pi} [S_{12} L_{\tau^+}^2 + S_{11} L_{\tau^+}] \\ &\quad + \left(\frac{\alpha_s}{\pi} \right)^2 [S_{21} L_{\tau^+}^3 + S_{22} L_{\tau^+}^2 + S_{21} L_{\tau^+}] \\ &\quad + \left(\frac{\alpha_s}{\pi} \right)^3 [S_{34} L_{\tau^+}^4 + S_{33} L_{\tau^+}^3 + S_{32} L_{\tau^+}^2 + S_{31} L_{\tau^+}] + \dots, \end{aligned} \tag{4.22}$$

which essentially sums the logarithmically singular terms of the perturbation series top to bottom, column by column. If we evaluate the singular part of the cumulant up to the k^{th} column in Eq.(4.22), each representing an infinite stack of logarithms, we say that we are working in the $N^{k-1}\text{LL}$ approximation. For example, keeping only the first column is called the leading-log, or $\text{LL} = N^0\text{LL}$ approximation, keeping the first two terms next-to-leading log, NLL , then on to $N^2\text{LL}$ and so forth.

The effective field theory (EFT) framework of Soft-Collinear Effective Theory (SCET) [8–10] and in particular the factorisation theorem ([12, 13] and Sec. 6) for thrust allow to systematically evaluate these infinite stacks of logarithms using renormalisation group (RG) techniques. Resumming terms to all orders in perturbation theory enables us to reproduce the characteristic peak in Fig. 4.18 and thus gain qualitative agreement with experiment in the di-jet region. The resummed singular part from the EFT calculation is further matched onto the fixed order result (by adding back Σ_τ^0 , which the EFT does not correctly reproduce) leading to an overall theoretical prediction that resembles the measured distribution to good accuracy as shown in Fig. 4.23.

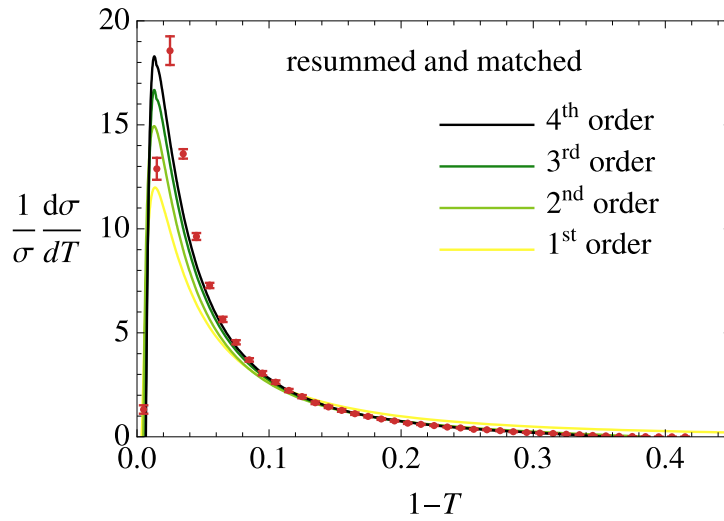


Fig. (4.23): Resummed thrust distribution ($\alpha_s(M_Z) = 0.1168$) taken from [26] and compared against data from the LEP/ALEPH experiment (red) [27] at $Q = 91\text{GeV}$. The different orders shown in the plot correspond to (1st) NLL resummation, no fixed order matching, (2nd) NNLL resummation, LO matching, (3rd) $N^3\text{LO}$ resummation, NLO matching, (4th) $N^3\text{LO}$ resummation, NNLO matching.

However, even when the cumulant is resummed at high logarithmic accuracy using EFT methods, we see that the agreement with experiment is more qualitative than quantitative. The reason is that the pQCD fixed order and SCET resummed computation both rely on partonic final states consisting of quarks and gluons, which, due to confinement and hadronisation, are not what is actually measured by an experiment which only ever detects colour neutral hadrons. These non-perturbative effects that bind the partons into hadrons cannot be accounted for by perturbation theory since they occur at the typical scale $\Lambda_{\text{QCD}} \simeq 200\text{MeV}$ where $\alpha_s(\Lambda_{\text{QCD}}) \gg 1$.

Although resummation is one of the main motivations to study EFTs we will not consider the technical ingredients required to perform such a calculation in this thesis. Instead we refer the reader to the detailed accounts in [28, 29]. The other reason why effective field theories like SCET have been so successful is the ability to transparently untangle degrees of freedom that are relevant to a given problem from those that are not. This is usually achieved using factorisation theorems. In the coming sections will therefore build a basic understanding of the SCET formalism and use it to derive a factorisation theorem for thrust.

5 Introduction to Soft-Collinear Effective Theory

This section aims at giving a brief, but self-contained introduction to the formalism of the Soft-Collinear effective theory (SCET)[7–10]. The ultimate goal is the construction of the effective theory Lagrangian applicable to the process $e^+e^- \rightarrow$ di-jets we have been considering so far. Along the way we will learn about the dominant momentum regions involved and their effective theory power counting. We will then conclude with a discussion of Wilson lines and soft-collinear factorisation at the operator level.

5.1 Lightcone decomposition

The canonical formulation of SCET relies heavily on the decomposition of momenta with respect to lightlike reference vectors, usually denoted n^μ and \bar{n}^μ such that $n^2 = \bar{n}^2 = 0$, plus a spacelike remainder p_\perp^μ that satisfies $n \cdot p_\perp = \bar{n} \cdot p_\perp = 0$. In terms of these variables a given momentum p^μ may be uniquely decomposed as:

$$p^\mu = \frac{n \cdot p}{n \cdot \bar{n}} \bar{n}^\mu + \frac{\bar{n} \cdot p}{n \cdot \bar{n}} n^\mu + p_\perp^\mu \equiv p_+^\mu + p_-^\mu + p_\perp^\mu, \quad (5.1)$$

where we can think of p_\perp^μ as being defined by this equation. For applications in SCET the frame is usually chosen such that n, \bar{n} are (anti-)parallel to the z -axis⁹,

$$n^\mu = (1, 0, 0, 1)^\mu, \quad \bar{n}^\mu = (1, 0, 0, -1)^\mu, \quad (5.2)$$

which we will conveniently associate with the directions of the two back-to-back jets we wish to study. Since the choice Eq.(5.2) implies the normalisation $n \cdot \bar{n} = 2$ we can also write Eq.(5.1) in terms of the n -collinear component $p^- = \bar{n} \cdot p$, the \bar{n} -collinear component $p^+ = n \cdot p$ and the transverse part, denoted p_\perp , as

$$p^\mu = p^+ \frac{\bar{n}^\mu}{2} + p^- \frac{n^\mu}{2} + p_\perp^\mu \equiv (p_+, p_-, p_\perp)^\mu, \quad (5.3)$$

where both ways of writing the momentum are used interchangeably in the literature (and by us). The Minkowski inner product may be expanded with respect to these coordinates as

$$p \cdot q = p^+ \cdot q^- + p^- \cdot q^+ + p_\perp \cdot q_\perp = \frac{p^+ q^-}{2} + \frac{p^- q^+}{2} + p_\perp \cdot q_\perp, \quad (5.4)$$

such that in particular,

$$p^2 = 2p^+ \cdot p^- + p_\perp^2 = p^+ p^- + p_\perp^2. \quad (5.5)$$

Note the subtle difference in factors of two between using the components p_\pm from Eq.(5.3) and the vectors p_\pm^μ as defined in Eq.(5.1) to write the inner product.

A particular confusion that may arise when using lightcone coordinates is that due to the structure of the Minkowski inner product a momentum that points in the spatial n^μ direction close to the lightcone will have a small “projection” $p^+ = n \cdot p$ and a correspondingly large component $p^- = \bar{n} \cdot p$ which runs counter to the intuition one might have from Euclidean space.

With this notation in place we are now in a good position to start talking about momentum scaling, a crucial aspect in constructing the correct SCET for the process at hand.

⁹Another convenient choice is to take n, \bar{n} such that the orthogonal component p_\perp of a given fixed momentum vanishes.

5.2 Momentum regions for $e^+e^- \rightarrow$ di-jets

A SCET and the corresponding factorisation formula are always specifically constructed for the particular process under consideration [9]. Since in this thesis we want to examine the thrust distribution in the peak region ($\tau \rightarrow 0$), which is the region where all particles in the process cluster into two highly collimated jets, we have to figure out the momentum regions occupied by these physical modes. To do this we bisect momentum space into two hemispheres H, \bar{H} with respect to the plane perpendicular to the thrust axis as defined by the thrust observable Eq.(2.54) and associated with the n, \bar{n} -collinear directions each. This allows us to define the hemisphere masses

$$m_H^2 = \left(\sum_{i \in H} p_{i,H}^\mu \right)^2 = p_H^2, \quad m_{\bar{H}}^2 = \left(\sum_{i \in \bar{H}} p_{i,\bar{H}}^\mu \right)^2 = p_{\bar{H}}^2, \quad (5.6)$$

which are therefore the invariant masses of the sum of all the momenta $\{p_{i,H}^\mu\}$ and $\{p_{i,\bar{H}}^\mu\}$ pointing into hemispheres H and \bar{H} respectively. It can now be shown that the maximum in the definition Eq.(2.54) of T , attained at the thrust axis \mathbf{n}_T , can be written as (see [30], Eq.(36) for a proper derivation)

$$\tau = 1 - T = 1 - \frac{Q}{\sum_i |\mathbf{p}_i|} \sqrt{1 - 2 \frac{m_H^2 + m_{\bar{H}}^2}{Q^2} + \left(\frac{m_H^2 - m_{\bar{H}}^2}{Q^2} \right)^2}, \quad (5.7)$$

with no restriction on the number or type of final state particles involved. As in the previous sections, Q denotes the invariant momentum transfer $Q^2 = (e_+ + e_-)^2 = (\sum_i p_i^\mu)^2$. One can check that in the center of mass frame $Q = \sum_i \sqrt{\mathbf{p}_i^2 + m_i^2}$, which in limit of all massless particles leads to a unit prefactor in front of the square root in Eq.(5.7). If we allowed for masses we could write

$$\frac{Q}{\sum_i |\mathbf{p}_i|} = \frac{\sum_i \sqrt{\frac{\mathbf{p}_i^2}{Q^2} + \frac{m_i^2}{Q^2}}}{\sum_i \sqrt{\frac{\mathbf{p}_i^2}{Q^2}}}, \quad (5.8)$$

for the prefactor, which, for large Q^2 will lead to power corrections $\sim (m_i/Q)^2$ compared to the massless case we will now consider in more detail. In the region $\tau \sim 0$ of interest, we see that the parameters

$$\frac{m_H^2}{Q^2} \sim \frac{m_{\bar{H}}^2}{Q^2} \sim \lambda^2, \quad (5.9)$$

must become small as well and we can expand Eq.(5.7) to leading order in the above parameter, yielding

$$\tau = \frac{m_H^2 + m_{\bar{H}}^2}{Q^2} + \mathcal{O}(\lambda^4) \sim \mathcal{O}(\lambda^2), \quad (5.10)$$

which holds irrespective of the final state particle masses. Using the lightcone decomposition introduced earlier we then find for the hemisphere H mass,

$$Q^2 \lambda^2 \sim m_H^2 = p_H^+ p_H^- + p_{H\perp}^2 \sim Q^2 (\lambda^{H+} \lambda^{H-} + \lambda^{2H\perp}). \quad (5.11)$$

Since the largest lightcone component of the total hemisphere H momentum should be in the n -direction (i.e. p_H^-) we can infer that the only physically feasible choice of exponents in Eq.(5.11) is $H^+ = 2, H^- = 0, H^\perp = 1$, leading to the n -collinear momentum scaling

$$p_H \sim Q(\lambda^2, 1, \lambda). \quad (5.12)$$

By a similar argument using the hemisphere \bar{H} mass we obtain the \bar{n} -collinear momentum scaling $p_{\bar{H}} \sim Q(1, \lambda^2, \lambda)$. Note that if all the individual momenta in the sums Eq.(5.6) have the respective scalings shown then this is consistent with the scaling we just found for the total hemisphere momenta, since e.g. the sum of two momenta $p_{i,H}$ and $p_{j,H}$ scaling like Eq.(5.12) again scales as $p_{i,H} + p_{j,H} \sim Q(\lambda^2, 1, \lambda)$.

However, the collinear scalings are not the only ones relevant to the problem. Phenomenologically we know that in between the highly collimated jets there can be found an isotropic haze of low-energy particles being radiated at large angles from the collinear particles. For these (ultra-)soft modes we therefore expect a uniform scaling $p_{\text{us}} \sim Q(\lambda^a, \lambda^a, \lambda^a)$. To have this momentum scaling be consistent with the scaling Eq.(5.9) imposed by the thrust measurement when one or more such momenta are present in the sums Eq.(5.6), we need that for some n -collinear $p_{H,i}$ (or \bar{n} -collinear $p_{\bar{H},j}$ equivalently)

$$Q^2 \lambda^2 \sim (p_{H,i} + p_{\text{us}})^2 = p_{H,i}^+ p_{\text{us}}^- + p_{H,i}^- p_{\text{us}}^+ + p_{H,i}^\perp \cdot p_{\text{us}}^\perp \sim Q^2 (\lambda^{2+a} + \lambda^a + \lambda^{1+a}). \quad (5.13)$$

For this to not violate the power counting, we see that we need at least $a \geq 2$ to only produce terms of $\mathcal{O}(\lambda^2)$ and higher. However, if we now where to choose $a > 2$ strictly (say $a = 3$) then the right-hand side of Eq.(5.13) would be what is called power-suppressed compared to the left-hand side, that is, the measurement would be insensitive to the momentum regions pertaining to such a scaling. We therefore conclude that the only scaling which does not lead to a scaling violation when combined with collinear momenta and still has a relevant effect on the observable is $a = 2$. The corresponding momenta are called ultrasoft,

$$p_{\text{us}} \sim Q(\lambda^2, \lambda^2, \lambda^2). \quad (5.14)$$

The name ultrasoft (usoft) stems from the fact that they correspond to even lower energy particles than those conventionally called soft, scaling as $p_s \sim Q(\lambda, \lambda, \lambda)$ which are commonly encountered in other processes.

Lastly, the underlying high energy momentum transfer is (somewhat obviously) assigned the hard scaling $Q \sim Q(1, 1, 1)$. Any momentum p_h that carries this scaling is off-shell by a large amount $p_h^2 \sim Q^2 \lambda^0$ and the corresponding field modes will be integrated out in the subsequent construction of SCET.

To conclude we give a list of the relevant momentum modes for $e^+e^- \rightarrow \text{di-jets}$,

$$\begin{array}{ll} \text{hard} & p_h \sim Q(1, 1, 1), \\ n\text{-collinear} & p_n \sim Q(\lambda^2, 1, \lambda), \\ \bar{n}\text{-collinear} & p_{\bar{n}} \sim Q(1, \lambda^2, \lambda), \\ \text{usoft} & p_{\text{us}} \sim Q(\lambda^2, \lambda^2, \lambda^2), \end{array} \quad (5.15)$$

where the dynamics of the **collinear** and **usoft** modes will be kept in the effective theory, while the **hard** modes will be integrated out and moved into a so-called Wilson coefficient (c.f. Eq.(6.4)). Processes which incorporate the momentum regions Eq.(5.15) are called SCET_I-type problems in the literature.

5.3 SCET Lagrangian for $e^+e^- \rightarrow \text{di-jets}$

Let us now derive the effective Lagrangian appropriate for the process $e^+e^- \rightarrow \text{di-jets}$ we are considering. Our starting point is the full QCD Lagrangian for a quark field Ψ with mass m ,

$$\mathcal{L}_{\text{QCD}} = \mathcal{L}_A + \mathcal{L}_q \equiv -\frac{1}{4} \text{Tr}[G_{\mu\nu} G^{\mu\nu}] + \bar{\Psi} (i \not{D} - m) \Psi, \quad (5.16)$$

where the covariant derivative and the non-abelian field strength tensor read

$$iD_\mu = i\partial_\mu + g_s A_\mu, \quad G_{\mu\nu} = \frac{i}{g_s} [D_\mu, D_\nu]. \quad (5.17)$$

We will not concern ourselves with gauge-fixing and possible ghost terms, since we will not need to consider them at the level of our calculations. However, SCET does exhibit a rich gauge structure on which more can be found in [9, 31]. In SCET we expect the Lagrangian Eq.(5.16) to split into two collinear (n, \bar{n}) , and one ultrasoft sector for the quarks and gluons, with separate fields defined for each sector, that is

$$\mathcal{L}_{\text{QCD}} = \mathcal{L}_A + \mathcal{L}_q \longmapsto \mathcal{L}_{\text{SCET}} = \mathcal{L}_{A,n} + \mathcal{L}_{A,\bar{n}} + \mathcal{L}_{A,\text{us}} + \mathcal{L}_{q,n} + \mathcal{L}_{q,\bar{n}} + \mathcal{L}_{q,\text{us}} \quad (5.18)$$

In the following we will give an in-depth derivation of the n -collinear quark Lagrangian $\mathcal{L}_{q,n}$, which will introduce the general concepts and language needed to similarly derive Lagrangians for the other sectors, or indeed other processes.

5.4 n -collinear quark Lagrangian

We will now derive the SCET effective Lagrangian for a n -collinear quark with momentum scaling given as in Eq.(5.15) at leading power in λ . To begin with, we focus on the derivation of the effective theory field for the n -collinear quark. By introducing the (n, \bar{n}) -collinear projection operators

$$P_n = \frac{\not{n}\not{\bar{n}}}{4}, \quad P_{\bar{n}} = \frac{\not{\bar{n}}\not{n}}{4}, \quad P_n + P_{\bar{n}} = \mathbf{1}, \quad (5.19)$$

which project the spinor degrees of freedom of the original quark field onto the respective lightcone directions, we can define the projected fields

$$\Psi(x) = (P_n + P_{\bar{n}})\Psi(x) \equiv \Psi_n(x) + \Psi_{\bar{n}}(x). \quad (5.20)$$

These fields satisfy the projection relations $P_n\Psi_n = \Psi_n$, $\not{n}\Psi_n = 0$, $\bar{\Psi}_n P_{\bar{n}} = \bar{\Psi}_n$ and similar for $\Psi_{\bar{n}}$. The physical content of this particular definition is that the field Ψ_n encodes the so-called large spinor components that will be of primary relevance for an n -collinear particle [9]. Note that up to this point the fields defined by Eq.(5.20) still encode momentum modes of arbitrary wavelength and direction and are thus equivalent to full QCD. Indeed, only considering the quark part of the QCD Lagrangian in Eq.(5.16) we simply have

$$\mathcal{L}_q = \bar{\Psi}(i\not{D} - m)\Psi = (\bar{\Psi}_n + \bar{\Psi}_{\bar{n}})(i\not{D} - m)(\Psi_n + \Psi_{\bar{n}}). \quad (5.21)$$

To derive the collinear fields of the effective theory we may take inspiration from the free theory expansion of the projected fields

$$\Psi_n(x) = \int d^4p \delta(p^2 - m^2) \theta(p^0) \left[u_n(p) b(p) e^{-ip \cdot x} + v_n(p) d^\dagger(p) e^{+ip \cdot x} \right], \quad (5.22)$$

in terms of the projected spinors $u_n(p) = P_n u(p)$, $v_n(p) = P_n v(p)$, where we have omitted any spin sums on the spinors to avoid notational clutter. In the following we will focus only on the field in Eq.(5.22), with all of the derived relations for Ψ_n understood to hold analogously for the field $\Psi_{\bar{n}}$.

For a consistent treatment of particles and anti-particles in the effective theory [9] it will be convenient to take $p \rightarrow -p$ in the second term of Eq.(5.22) leading us to

$$\begin{aligned} \Psi_n(x) &= \int d^4p \delta(p^2 - m^2) e^{-ip \cdot x} \left[\theta(p^0) u_n(p) b(p) + \theta(-p^0) v_n(-p) d^\dagger(-p) \right] \\ &\equiv \int d^4p \delta(p^2 - m^2) e^{-ip \cdot x} \left[\theta(p^0) \Psi_n^+(p) + \theta(-p^0) \Psi_n^-(-p) \right], \end{aligned} \quad (5.23)$$

essentially interpreting the anti-particle as a negative energy particle with reversed spatial momentum. The transition to the collinear field of the effective theory is made by restricting the quark field to contain only n -collinear momentum modes. This is done by introducing the notion of label- and residual momenta p_l, p_r , that allow us to decompose a given n -collinear momentum

$$(\lambda^2, 1, \lambda)Q \sim p^\mu = p_l^\mu + p_r^\mu, \quad \text{with} \quad p_l^\mu \sim (0, 1, \lambda)Q, \quad p_r^\mu \sim (\lambda^2, \lambda^2, \lambda^2)Q, \quad (5.24)$$

such that the label momentum carries the large momentum components, while the residual momentum describes small fluctuations around a given label. The idea is now to expand the full theory around the n -collinear direction by replacing the fields $\Psi_n^\pm(p)$ in Eq.(5.23) with a set of fields $\{\xi_{n,p_l}^\pm(p_r)\}_{p_l \neq 0}$, each being identified with a fixed label momentum p_l . The thus introduced notation suggests that we think of p_l as a discrete index, labeling a set of fields, while the residual p_r remains continuous. However, both p_l and p_r will be dynamic variables of the effective theory. We have also explicitly excluded the case $p_l = 0$ which would correspond to ultrasoft scaling for p and hence violate the scaling assumed in Eq.(5.24).

The n -collinear quark field $\hat{\xi}_n(x)$ is thus defined in analogy to Eq.(5.23) as

$$\hat{\xi}_n(x) = \sum_{p_l \neq 0} e^{-ip_l \cdot x} \int d^4 p_r e^{-ip_r \cdot x_r} [\theta(\bar{n} \cdot p_l) \xi_{n,p_l}^+(p_r) + \theta(-\bar{n} \cdot p_l) \xi_{n,-p_l}^-(-p_r)], \quad (5.25)$$

and is hence arranged in such a way that for $\bar{n} \cdot p_l > 0$ the fields $\hat{\xi}_n$ and $\bar{\hat{\xi}}_n$ annihilate and create particles, while for $\bar{n} \cdot p_l < 0$ they create and annihilate anti-particles respectively. Note the sign convention for the label momentum which is always aligned with the fermion number flow, i.e. anti-particles carry negative label momentum. In the free theory we may write

$$\xi_{n,p_l}^+(p_r) = u_{n,p_l}(p_r) b_{n,p_l}(p_r), \quad \xi_{n,p_l}^-(p_r) = v_{n,p_l}(p_r) d_{n,p_l}^\dagger(p_r), \quad (5.26)$$

thus associating the field $\hat{\xi}_n(x)$ with either an incoming particle or an outgoing anti-particle in the n -collinear direction.

The power counting for the n -collinear momentum p in Eq.(5.24) has lead to the argument $p^0 = \frac{1}{2}(p^- + p^+) = \frac{1}{2}p_l^- + \mathcal{O}(\lambda)$ for the step function in Eq.(5.25). Carrying out the Fourier transform over the residual momenta we bring the field to the more compact form

$$\hat{\xi}_n(x) = \sum_{p_l \neq 0} e^{-ip_l \cdot x} [\theta(p_l^-) \xi_{n,p_l}^+(x_r) + \theta(-p_l^-) \xi_{n,-p_l}^-(x_r)] \equiv \sum_{p_l \neq 0} e^{-ip_l \cdot x} \xi_{n,p_l}(x_r) \quad (5.27)$$

We interpret the above as a (discrete) Fourier transform over label momenta p_l of the fields $\xi_{n,p_l}^+, \xi_{n,p_l}^-$ depending on $x_r \sim (\lambda^{-2}, \lambda^{-2}, \lambda^{-2})Q^{-1}$, which inherits its scaling from p_r by requiring $x_r \cdot p_r \sim (1, 1, 1)$ and thus corresponds to the long-distance modes we wish to describe with the effective theory.

In the following we will refer to expressions like Eq.(5.27), where the dependence on the label momentum of the operators is explicit, but the residual component has been transformed back to configuration space, as the label momentum representation of the respective EFT operators. It is in this representation that the collinear quark Lagrangian will eventually be formulated.

Note the hybrid nature of the field $\xi_{n,p_l}(x_r)$ in Eq.(5.27) in that it carries definite label momentum p_l but is a general superpositions of plane waves with respect to residual momenta. Correspondingly, it makes sense to introduce two kinds of derivatives, the label operator \mathcal{P}^μ and the residual derivative $i\partial_r^\mu$, acting on these fields and exhibiting the different scalings

$$\mathcal{P}^\mu \xi_{n,p_l}(x_r) \equiv p_l^\mu \xi_{n,p_l}(x_r) \sim (0, 1, \lambda)Q, \quad i\partial_r^\mu \xi_{n,p_l}(x_r) \sim (\lambda^2, \lambda^2, \lambda^2)Q. \quad (5.28)$$

Employing the label operator we can bring the n -collinear quark field to the simple form

$$\widehat{\xi}_n(x) = \sum_{p_l \neq 0} e^{-i\mathcal{P} \cdot x} \xi_{n,p_l}(x_r) \equiv e^{-i\mathcal{P} \cdot x} \xi_n(x_r), \quad \text{where} \quad \xi_n(x_r) \equiv \sum_{p_l \neq 0} \xi_{n,p_l}(x_r), \quad (5.29)$$

and we were allowed to pull the operator through the label sum which is subsequently carried out to obtain the residual space field $\xi_n(x_r)$. For later convenience we note that acting with a regular derivative on one of the fields in Eq.(5.29) we get

$$\begin{aligned} i\partial^\mu \widehat{\xi}_n(x) &= i\partial^\mu e^{-i\mathcal{P} \cdot x} \xi_n(x_r) = i\partial^\mu \sum_{p_l \neq 0} e^{-ip_l \cdot x} \xi_{n,p_l}(x_r) \\ &= \sum_{p_l \neq 0} e^{-ip_l \cdot x} (p_l^\mu + i\partial_r^\mu) \xi_{n,p_l}(x_r) = e^{-i\mathcal{P} \cdot x} (\mathcal{P}^\mu + i\partial_r^\mu) \xi_n(x_r), \end{aligned} \quad (5.30)$$

which makes manifest the decomposition of momenta Eq.(5.24) at the level of fields. Let us now go through a few general results and definitions regarding the label operator that will prove useful later. Note that the definition of the label operator in Eq.(5.28) implies the relations,

$$\begin{aligned} (\mathcal{P}^\mu \xi_{n,p_l})^\dagger &= \xi_{n,p_l}^\dagger (\mathcal{P}^\mu)^\dagger = p_l^\mu \xi_{n,p_l}^\dagger \\ (e^{-i\mathcal{P} \cdot x} \xi_{n,p_l})^\dagger &= \xi_{n,p_l}^\dagger e^{i\mathcal{P}^\dagger \cdot x} = \xi_{n,p_l}^\dagger e^{ip_l \cdot x} = e^{-i(-p_l) \cdot x} \xi_{n,p_l}^\dagger, \end{aligned} \quad (5.31)$$

which in turn suggest to expand the domain of action of the label operator to conjugate fields as

$$\mathcal{P}^\mu \xi_{n,p_l}^\dagger \equiv -p_l^\mu \xi_{n,p_l}^\dagger. \quad (5.32)$$

This convenient choice allows us to write

$$(e^{-i\mathcal{P} \cdot x} \xi_{n,p_l})^\dagger = e^{-i\mathcal{P} \cdot x} \xi_{n,p_l}^\dagger, \quad (5.33)$$

with the label momentum operator always acting from the left. Another convention we adopt is that the label operator always acts on all fields to the right of it that carry a momentum label, e.g.

$$\mathcal{P}^\mu \xi_{n,p_l}^\dagger \xi_{n,q_l} \equiv (-p_l^\mu + q_l^\mu) \xi_{n,p_l}^\dagger \xi_{n,q_l}, \quad \xi_{n,p_l}^\dagger \xi_{n,q_l} (\mathcal{P}^\dagger)^\mu \equiv (p_l^\mu - q_l^\mu) \xi_{n,p_l}^\dagger \xi_{n,q_l}, \quad (5.34)$$

and similar for products of any number of label fields. The second identity in Eq.(5.34) corresponds to the analogous relation for the adjoint label operator $(\mathcal{P}^\dagger)^\mu$ of Eq.(5.31) which by definition always acts on all fields to the left of it with opposite signs relative to \mathcal{P}^μ . Finally we demand that the label operator satisfies a product rule when acting on products of operators, i.e. as an operator equation we have

$$\mathcal{P}^\mu \mathcal{O} = [\mathcal{P}^\mu \mathcal{O}] + \mathcal{O} \mathcal{P}^\mu, \quad (5.35)$$

where the square brackets allow \mathcal{P}^μ to only act on \mathcal{O} .

We conclude the discussion of the collinear gluon field by noting that the full theory field $\Psi_{\bar{n}}$ of Eq.(5.20) encoding the small spinor components, which, as we will see, become irrelevant at leading power for n -collinear particles, is assigned to the field $\widehat{\varphi}_{\bar{n}}$ in the effective theory. Physically this field represents the remaining modes with larger off-shellness, those corresponding to other collinear directions or (ultra-)soft momenta, all of which we did not include in $\widehat{\xi}_n(x)$. With this we can finally combine the two spin projected fields as in Eq.(5.20) and write

$$\widehat{\Xi}_n(x) \equiv \widehat{\xi}_n(x) + \widehat{\varphi}_{\bar{n}}(x) = [e^{-i\mathcal{P} \cdot x} (\xi_n(x_r) + \varphi_{\bar{n}}(x_r))]. \quad (5.36)$$

Before we move on to the derivation of the collinear quark Lagrangian we have to perform a similar analysis for the gluon field $A_\mu(x)$ of the full theory which we split into a n -collinear and an ultrasoft part according to

$$A_\mu(x) = \hat{A}_\mu^n(x) + \hat{A}_\mu^{\text{us}}(x) + \mathcal{O}(\lambda^3). \quad (5.37)$$

The components of each field scale like the momentum modes they encode, i.e. $\hat{A}^n \sim (\lambda^2, 1, \lambda)Q$, $\hat{A}^{\text{us}} \sim (\lambda^2, \lambda^2, \lambda^2)Q$, and we have neglected contributions of $\mathcal{O}(\lambda^3)$ and higher which will not enter the leading power Lagrangian. For the collinear gluon field we make an analogous ansatz to Eq.(5.27) by writing

$$\begin{aligned} \hat{A}_\mu^n(x) &= \sum_{k_l \neq 0} e^{-ik_l \cdot x} \left[\theta(k_l^-) A_{\mu, k_l}^{n,+}(x_r) + \theta(-k_l^-) A_{\mu, -k_l}^{n,-}(x_r) \right] \\ &\equiv \sum_{k_l \neq 0} e^{-ik_l \cdot x} A_{\mu, k_l}^n(x_r) \equiv e^{-i\mathcal{P} \cdot x} A_\mu^n(x_r), \quad \text{where} \quad A_\mu^n(x_r) \equiv \sum_{k_l \neq 0} A_{\mu, k_l}^n(x_r). \end{aligned} \quad (5.38)$$

Just as with the quark field in Eq.(5.25), the component $A_{\mu, -k_l}^{n,-}$ of the gluon field associated with outgoing particles carries negative label momentum. The hermiticity property $(\hat{A}_\mu^n)^\dagger(x) = \hat{A}_\mu^n(x)$ of the n -collinear gluon field in configuration space leads to the condition

$$(A_{\mu, k_l}^n)^\dagger(x_r) = A_{\mu, -k_l}^n(x_r), \quad (5.39)$$

on the label fields. However, in the sum over all labels of Eq.(5.38) we find that the label momentum representation $(A_\mu^n)^\dagger(x_r) = A_\mu^n(x_r)$ of the gluon field is also hermitean.

We have now developed the formalism necessary to derive the collinear quark Lagrangian at leading power in λ . We start by simply taking Eq.(5.21) and replacing $\Psi(x) \xrightarrow{\text{SCET}} \hat{\Xi}_n(x)$, i.e.

$$\begin{aligned} \mathcal{L}_{q,n} &\equiv \bar{\hat{\Xi}}_n [i\not{D} - m] \hat{\Xi}_n = \left(\bar{\hat{\xi}}_n + \bar{\hat{\varphi}}_{\bar{n}} \right) \left[\frac{\not{n}}{2} i n \cdot D + \frac{\not{\bar{n}}}{2} i \bar{n} \cdot D + i\not{D}_\perp - m \right] \left(\hat{\xi}_n + \hat{\varphi}_{\bar{n}} \right) \\ &= \bar{\hat{\xi}}_n \frac{\not{n}}{2} i n \cdot D \hat{\xi}_n + \bar{\hat{\varphi}}_{\bar{n}} \frac{\not{\bar{n}}}{2} i \bar{n} \cdot D \hat{\varphi}_{\bar{n}} + \bar{\hat{\xi}}_n [i\not{D}_\perp - m] \hat{\varphi}_{\bar{n}} + \bar{\hat{\varphi}}_{\bar{n}} [i\not{D}_\perp - m] \hat{\xi}_n, \end{aligned} \quad (5.40)$$

where we have decomposed the covariant derivative into its lightcone components¹⁰. In the second line we made use of the spinor projection properties (see below Eq.(5.20)) of the collinear fields. However, up to this point the power counting of the effective theory was not used and so the Lagrangian still contains information to all orders in λ .

We now use the scaling properties of the effective theory gluon fields (see below Eq.(5.37)) as well as the label operator and the residual derivative in Eq.(5.28) to keep only the leading power contributions to each term in Eq.(5.40). Since we are considering all particles to be near their mass shell, i.e. $p^2 - m^2 \sim \mathcal{O}(\lambda^2)$ and $p^2 \sim \mathcal{O}(\lambda^2)$ for collinear particles, we see that $m \sim \mathcal{O}(\lambda)$ is the only consistent power counting to impose if we want to keep information about the mass in the collinear Lagrangian. Another possible scaling would be obtained by choosing $m \sim \mathcal{O}(\lambda^2)$ which would move the mass out of the collinear and into the usoft Lagrangian. Which mass scaling should be chosen ultimately depends on the phenomenology of the process at hand. Since we will eventually be studying jets initiated by energetic massive quarks $m \sim \mathcal{O}(\lambda)$ is the right scaling for our purposes. With this in mind we may write

$$\begin{aligned} i n \cdot D e^{-i\mathcal{P} \cdot x} \xi_n &= e^{-i\mathcal{P} \cdot x} [n \cdot \mathcal{P} + i n \cdot \partial_r + g_s n \cdot A^n + g_s n \cdot A^{\text{us}}] \xi_n, \\ i \bar{n} \cdot D e^{-i\mathcal{P} \cdot x} \xi_n &= e^{-i\mathcal{P} \cdot x} [\bar{n} \cdot \mathcal{P} + g_s \bar{n} \cdot A^n + \mathcal{O}(\lambda^2)] \xi_n \equiv e^{-i\mathcal{P} \cdot x} i \bar{n} \cdot D^n \xi_n + \mathcal{O}(\lambda^2) \\ (i\not{D}_\perp - m) \xi_n &= e^{-i\mathcal{P} \cdot x} [\not{\mathcal{P}}_\perp + g_s \not{A}_\perp^n - m + \mathcal{O}(\lambda^2)] \xi_n \equiv e^{-i\mathcal{P} \cdot x} (i\not{D}_\perp^n - m) \xi_n + \mathcal{O}(\lambda^2), \end{aligned} \quad (5.41)$$

¹⁰Here we make use of the lightcone decomposition of the Dirac matrices, writing $\gamma^\mu = \frac{n^\mu}{2} \not{n} + \frac{\bar{n}^\mu}{2} \not{\bar{n}} + \gamma_\perp^\mu$, where γ_\perp^μ is defined by the previous equation.

where all the fields are now in the label momentum representation and we have suppressed the dependence on the residual x_r . With this power counting in place the leading power collinear quark Lagrangian takes the form

$$\begin{aligned} \mathcal{L}_{q,n}^{(0)} = e^{-i\mathcal{P}\cdot x} & \left[\bar{\xi}_n \frac{\not{p}}{2} (n\cdot\mathcal{P} + g_s n\cdot A^n + g_s n\cdot A^{\text{us}} + in\cdot\partial_r) \xi_n + \bar{\varphi}_{\bar{n}} \frac{\not{p}}{2} (\bar{n}\cdot\mathcal{P} + g_s \bar{n}\cdot A^n) \varphi_{\bar{n}} \right. \\ & \left. + \bar{\xi}_n (\not{\mathcal{P}}_{\perp} + g_s \not{A}_{\perp}^n - m) \varphi_{\bar{n}} + \bar{\varphi}_{\bar{n}} (\not{\mathcal{P}}_{\perp} + g_s \not{A}_{\perp}^n - m) \xi_n \right]. \end{aligned} \quad (5.42)$$

Note that at leading power the field $\varphi_{\bar{n}}(x_r)$ is not dynamical since no residual derivatives act on it. We therefore integrate it out by replacing it with its classical equation of motion [32]

$$\frac{\partial \mathcal{L}_{q,n}^{(0)}}{\partial \bar{\varphi}_{\bar{n}}} = 0 \quad \Rightarrow \quad \varphi_{\bar{n}} = \frac{1}{\bar{n}\cdot\mathcal{P} + g_s \bar{n}\cdot A^n} (\not{\mathcal{P}}_{\perp} + g_s \not{A}_{\perp}^n + m) \frac{\not{p}}{2} \xi_n. \quad (5.43)$$

Plugging this back into Eq.(5.42) yields the final n -collinear quark Lagrangian

$$\mathcal{L}_{q,n}^{(0)} = e^{-i\mathcal{P}\cdot x} \bar{\xi}_n \left[in\cdot D + (i\not{D}_{\perp}^n - m) \frac{1}{i\bar{n}\cdot D^n} (i\not{D}_{\perp}^n + m) \right] \frac{\not{p}}{2} \xi_n, \quad (5.44)$$

at leading power in λ . Since all terms in Eq.(5.44) scale homogeneously we can derive the power counting for the n -collinear quark field itself by requiring that the action be of order $\mathcal{O}(\lambda^0)$, i.e.,

$$S_{q,n}^{(0)} = \int d^4x \mathcal{L}_{q,n}^{(0)} \stackrel{!}{\sim} \mathcal{O}(\lambda^0), \quad \text{where} \quad d^4x \sim \frac{1}{p^4} \sim \mathcal{O}(\lambda^{-4}), \quad (5.45)$$

for collinear momenta, such that we must have $\mathcal{L}_{q,n} \sim \mathcal{O}(\lambda^4)$ and consequently $\xi_n \sim \mathcal{O}(\lambda)$.

It should be mentioned that the leading power Lagrangian is local at the scales $\mathcal{O}(\lambda^2)$ and $\mathcal{O}(\lambda)$ since all fields in Eq.(5.44) depend on the same spacetime point (x_r in residual space) and the derivative operators with the respective scaling (c.f. Eq.(5.41)) feature in the numerator. However it is non-local at the scale $\mathcal{O}(\lambda^0)$ due to the inverse derivative operator $(i\bar{n}\cdot D^n)^{-1}$, which appeared after integrating out the field $\varphi_{\bar{n}}$. We call operators such as $(i\bar{n}\cdot\partial - i0)^{-1}$ non-local since for any field ϕ one can show that

$$\frac{1}{i\bar{n}\cdot\partial - i0} \phi(x) \equiv \int d^4p \frac{e^{-ip\cdot x}}{\bar{n}\cdot p - i0} \tilde{\phi}(p) = \int_0^\infty ds \phi(x + s\bar{n}), \quad (5.46)$$

where the choice of $i0$ -prescription was crucial in determining the path along which the field is integrated. Additionally we may heuristically expand the inverse operator in Eq.(5.44) in powers of g_s as

$$\frac{1}{\bar{n}\cdot\mathcal{P} + g_s \bar{n}\cdot A^n} = \frac{1}{\bar{n}\cdot\mathcal{P}} - \frac{1}{\bar{n}\cdot\mathcal{P}} g_s \bar{n}\cdot A^n \frac{1}{\bar{n}\cdot\mathcal{P}} + \frac{1}{\bar{n}\cdot\mathcal{P}} g_s \bar{n}\cdot A^n \frac{1}{\bar{n}\cdot\mathcal{P}} g_s \bar{n}\cdot A^n \frac{1}{\bar{n}\cdot\mathcal{P}} + \dots, \quad (5.47)$$

with each term in the above sum having identical scaling $\mathcal{O}(\lambda^0)$. Thus at leading power n -collinear quarks appear to couple to an arbitrary number of n -collinear gluons without any power suppression. We will see that this feature also leads to the emergence of so-called collinear Wilson lines.

5.5 Collinear Wilson lines

When discussing the QCD process $e^+e^- \rightarrow$ di-jets in previous sections, the final state particles were not restricted to any particular kinematic regime, and so the emissions of n/\bar{n} -collinear gluons from n/\bar{n} -collinear (anti-)quarks could all be treated on equal footing.

In SCET the story is more subtle. Let us consider the processes pictured in Fig. 5.48 where the initial and final state particles are now restricted to definite collinear sectors. Additionally we will

assume the quarks to be produced by a colour-singlet current with trivial colour structure and carrying some generic Dirac structure Γ^μ , e.g. $\Gamma^\mu = \gamma^\mu$ for the vector production current in Eq.(2.50).

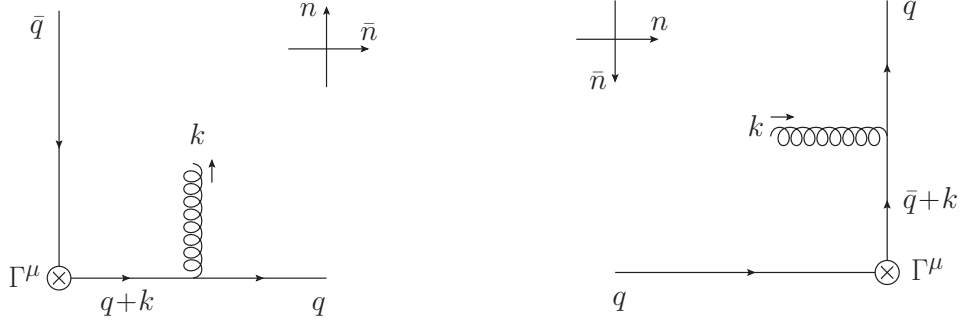


Fig. (5.48): (le.) Emission of an n -collinear gluon by an outgoing quark line pointed in the \bar{n} -collinear direction. (ri.) Absorption of an n -collinear gluon by an incoming \bar{n} -collinear anti-quark. Applying the appropriate SCET power counting to these QCD processes will show that the intermediate quark propagators are pushed far off-shell yielding the respective first order term of collinear Wilson lines.

For the detailed derivation let us focus on the emission process depicted in Fig. 5.48(1e.), which will lead us to the conclusion that the emission of n -collinear gluons from \bar{n} -collinear quarks knocks the intermediate quark propagator off-shell by a hard amount $\mathcal{O}(\lambda^0)$. The corresponding Lagrangian interaction of QCD will therefore be integrated out and replaced by an effective operator in SCET in the form of the n -collinear Wilson line. To see all of this in detail, we write down the full QCD amplitude corresponding to this process which is given by

$$i\mathcal{M}_{n,+}^{1\mu} \sim \bar{u}(q)(ig_s\tilde{\mu}^\epsilon T^{A_1}\gamma^{\mu_1})\epsilon_{\mu_1,A_1}^*(k)\frac{i(\not{q} + \not{k} + m)}{(q+k)^2 - m^2 + i0}\Gamma^\mu v(\bar{q}). \quad (5.49)$$

We are now interested in finding the operator that will generate this amplitude in the kinematic limit mentioned above, where $q \sim (1, \lambda^2, \lambda)$ and $k \sim (\lambda^2, 1, \lambda)$. Imposing this power counting, we replace the external state wave functions by the appropriate label momentum space fields Eqs.(5.29) and (5.38) in SCET. For the outgoing anti-quark we can for instance identify the spinor $v(\bar{q}) \leftrightarrow v_{n,\bar{q}_l}(\bar{q}_r)$ as being obtained from the contraction of the label field $\xi_{n,-\bar{q}_l}(x_r)$ with the final state, and similarly for the other wave functions in Eq.(5.49). Keeping only the leading terms in λ we obtain the operator

$$\mathcal{O}_{n,+}^{1\mu} \sim \bar{\xi}_{\bar{n},q_l}(x_r)A_{\mu_1,-k_l}(x_r)\gamma^{\mu_1}\left[-g_s\tilde{\mu}^\epsilon\frac{\not{q}_l^+\not{\bar{n}} + \frac{\not{k}_l^-}{2} + \mathcal{O}(\lambda)}{q_l^+k_l^- + i0 + \mathcal{O}(\lambda^2)}\right]\Gamma^\mu\xi_{n,-\bar{q}_l}(x_r), \quad (5.50)$$

where we indeed find $q_l^+k_l^- \sim \mathcal{O}(\lambda^0)$ such that the propagator is hard off-shell. In the next step we push the Dirac structure in the numerator through to the left to let it act on the \bar{n} -collinear field $\bar{\xi}_{\bar{n},q_l}$. Using $\bar{\xi}_{\bar{n}}\not{\bar{n}} = 0$ and $\bar{\xi}_{\bar{n}}P_n = \bar{\xi}_{\bar{n}}$ finally yields

$$\begin{aligned} \mathcal{O}_{n,+}^{1\mu} &\sim \bar{\xi}_{\bar{n},q_l}(x_r)\left[-g_s\tilde{\mu}^\epsilon\frac{q_l^+\bar{n}\cdot A_{-k_l}^n(x_r) + \frac{\not{k}_l^-}{2}A_{-k_l,\perp}^n(x_r)}{q_l^+k_l^- + i0}\right]\Gamma^\mu\xi_{n,-\bar{q}_l}(x_r) \\ &\sim \bar{\xi}_{\bar{n},q_l}(x_r)\left[-g_s\tilde{\mu}^\epsilon\frac{\bar{n}\cdot A_{-k_l}^n(x_r) + \mathcal{O}(\lambda)}{k_l^- + i0}\right]\Gamma^\mu\xi_{n,-\bar{q}_l}(x_r), \end{aligned} \quad (5.51)$$

in which we see that the dependence on the momentum q of the outgoing quark has dropped out of the propagator. Summing over all gluon momenta and using the label operator we can identify the

term in square brackets as coming from the first-order Wilson line in label momentum representation

$$W_{n,+}^{\dagger 1}(x_r) \equiv \sum_{k_l \neq 0} \left[-\frac{g_s \tilde{\mu}^\epsilon}{k_l^- + i0} \bar{n} \cdot A_{-k_l}^n(x_r) \right] = \left[\bar{n} \cdot A^n(x_r) \frac{(-g_s \tilde{\mu}^\epsilon)}{\bar{n} \cdot \mathcal{P}^\dagger + i0} \right], \quad (5.52)$$

which should be reminiscent of the first term in our naive expansion Eq.(5.47). Furthermore the Feynman rules have lead to the consistent inclusion of the $i0$ -prescription and the mass scale $\tilde{\mu}$ of dimensional regularisation. The subscript $n, +$ captures the fact that the gluon is n -collinear and that it is associated to a quark line (+). In using the condensed notation on the right-hand side of Eq.(5.52) we have to remember that the gluon was outgoing and so the sum $A_\mu^n(x_r) = \sum_{k_l \neq 0} A_{\mu, -k_l}^n$ needs to be performed over negative label momentum fields.

We now wish to take the label momentum Fourier transform of Eq.(5.52) to obtain a full configuration space expression. This is achieved using the definition Eq.(5.38) of the collinear gluon field, now written explicitly in terms of lightcone coordinates

$$\hat{A}_\mu^n(x) \equiv \hat{A}_\mu^n\left(\frac{x^-}{2}, \frac{x^+}{2}, x_\perp\right) = e^{-i\mathcal{P} \cdot x} A_\mu^n(x_r) = \sum_{k_l \neq 0} e^{-i(k_l^- x^+ / 2 + k_{l,\perp} \cdot x_\perp)} A_{\mu, k_l}^n(x_r). \quad (5.53)$$

Recall that by Eq.(5.24) we have $n \cdot k_l = 0$ and so the large coordinate $x^- \sim Q^{-1} \lambda^{-2}$, being the Fourier conjugate of the small momentum component $k^+ = k_r^+$, is determined by the residual momentum dependence of the field, i.e. we may identify $x^- \equiv x_r^-$, while the small coordinates $x^+ \sim Q^{-1}$, and $x_\perp \sim Q^{-1} \lambda^{-1}$ pertain to the large label momentum components. Employing the Schwinger parametrisation for the eikonal propagator in Eq.(5.52)

$$\frac{1}{k_l^- - i0} = i \int_0^\infty ds e^{-is(k_l^- - i0)}, \quad (5.54)$$

and using the definition Eq.(5.53) we may write the Fourier transform of Eq.(5.52) as

$$\begin{aligned} e^{-i\mathcal{P} \cdot x} W_{n,+}^{\dagger 1}(x_r) &= -g_s \tilde{\mu}^\epsilon \sum_{k_l \neq 0} e^{+i(k_l^- x^+ / 2 + k_{l,\perp} \cdot x_\perp)} \frac{\bar{n} \cdot A_{-k_l}^n(x_r)}{k_l^- + i0} \\ &= ig_s \tilde{\mu}^\epsilon \int_0^\infty ds \sum_{k_l \neq 0} e^{-i(k_l^- (x^+ / 2 + s) + k_{l,\perp} \cdot x_\perp)} \bar{n} \cdot A_{k_l}^n(x_r) \\ &= ig_s \tilde{\mu}^\epsilon \int_0^\infty ds \bar{n} \cdot \hat{A}^n\left(\frac{x^-}{2}, \frac{x^+}{2} + s, x_\perp\right) \equiv ig_s \tilde{\mu}^\epsilon \int_0^\infty ds \bar{n} \cdot \hat{A}^n(x + \bar{n}s) \\ &\equiv W_{n,+}^{\dagger 1}(\infty, x). \end{aligned} \quad (5.55)$$

To obtain the second line we have taken $k_l \rightarrow -k_l$ and dropped the $i0$ -prescription in the exponential which was necessary to make the integral Eq.(5.54) converge. This omission is unproblematic since the correct sign of the $i0$ -term can be uniquely determined by the contour of integration. In the second to last line we have introduced the shorthand $\left(\frac{x^-}{2}, \frac{x^+}{2} + s, x_\perp\right) \equiv x + \bar{n}s$ which is ubiquitous in the literature, and allows us to write the first-order Wilson line in a visually similar way to the expression we anticipated in Eq.(5.46).

So far we have only considered processes involving the emission and absorption of a single gluon. The full extent of the simplification of full theory amplitudes in the soft-collinear limit can be seen when we choose, as is depicted in Fig. 5.56, to attach any number m of n -collinear gluons to the \bar{n} -collinear quark in the process of Fig. 5.48(1e.) and sum over diagrams where all permutations of

external gluon lines are taken into account.

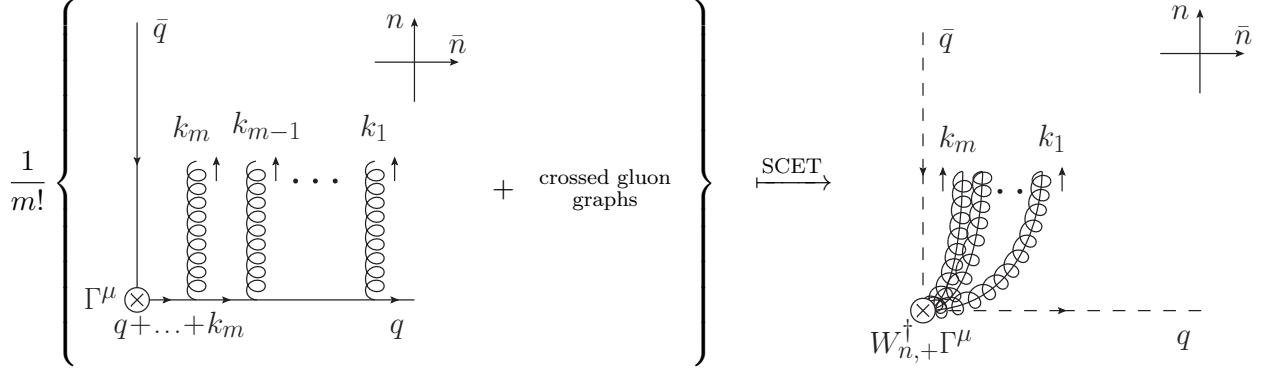


Fig. (5.56): Emission of m different n -collinear gluons, including all their permutations, by an incoming quark line pointed in the \bar{n} -collinear direction. Applying the appropriate SCET power counting to this amplitude will yield an effective vertex $W_{n,+}^\dagger \Gamma^\mu$ which we draw as a local interaction in residual space. On the right, collinear (anti-)quarks are indicated by dashed lines, while collinear gluons are represented by curly lines with a solid line through the center.

Going through analogous steps as before, and writing $k_{i,l} \equiv k_i$, $i = 1, \dots, m$, we now find the label momentum space expression

$$\mathcal{O}_{n,+}^{\dagger \mathbf{m} \mu} \sim \bar{\xi}_{\bar{n}, q_l}(x_r) \left[\frac{(-g_s \tilde{\mu}^\epsilon)^m}{m!} \sum_{\text{perms.} \{k_1, \dots, k_m\}} \frac{\bar{n} \cdot A_{-k_1}^n(x_r) \dots \bar{n} \cdot A_{-k_m}^n(x_r)}{[\bar{n} \cdot k_1 + i0] \dots [\bar{n} \cdot \sum_{i=1}^m k_i + i0]} \right] \Gamma^\mu \xi_{n, -\bar{q}_l}(x_r) + \dots, \quad (5.57)$$

where the ellipses denote power suppressed terms as before. The operator associated with the emission of m collinear gluons is obtained by summing over all possible gluon momenta and therefore reads

$$\begin{aligned} W_{n,+}^{\dagger \mathbf{m}}(x_r) &= \frac{(-g_s \tilde{\mu}^\epsilon)^m}{m!} \sum_{k_1, \dots, k_m \neq 0} \sum_{\text{perms.} \{k_1, \dots, k_m\}} \frac{\bar{n} \cdot A_{-k_1}^n(x_r) \dots \bar{n} \cdot A_{-k_m}^n(x_r)}{[\bar{n} \cdot k_1 + i0] \dots [\bar{n} \cdot \sum_{i=1}^m k_i + i0]} \\ &= \frac{1}{m!} \sum_{\text{perms.} \{m\}} \left[(-g_s \tilde{\mu}^\epsilon) \frac{\bar{n} \cdot A^n(x_r)}{\bar{n} \cdot \mathcal{P}^\dagger + i0} \dots (-g_s \tilde{\mu}^\epsilon) \frac{\bar{n} \cdot A^n(x_r)}{\bar{n} \cdot \mathcal{P}^\dagger + i0} \right], \end{aligned} \quad (5.58)$$

conveniently having made use of the property Eq.(5.34) of the label operators which are understood to always act from the right on the fields inside the square brackets. The sum is over all permutations of the m gluon fields. Fourier transforming this back to configuration space yields

$$W_{n,+}^{\dagger \mathbf{m}}(\infty, x) \equiv e^{-i\mathcal{P} \cdot x} W_{n,+}^{\dagger \mathbf{m}}(x_r) = \frac{(ig_s \tilde{\mu}^\epsilon)^m}{m!} \int_0^\infty ds_1 \dots \int_0^\infty ds_m \mathbf{P} \{ \bar{n} \cdot \hat{A}^n(x + \bar{n}s_1) \dots \bar{n} \cdot \hat{A}^n(x + \bar{n}s_m) \}, \quad (5.59)$$

where \mathbf{P} denotes path-ordering which was enforced by the $i0$ -prescription[33] in Eq.(5.58) and is defined by

$$\mathbf{P} \{ \hat{A}_{\mu_1}^n(\bar{n}s_1) \hat{A}_{\mu_2}^n(\bar{n}s_2) \} = \theta(s_1 - s_2) \hat{A}_{\mu_1}^n(\bar{n}s_1) \hat{A}_{\mu_2}^n(\bar{n}s_2) + \theta(s_2 - s_1) \hat{A}_{\mu_2}^n(\bar{n}s_2) \hat{A}_{\mu_1}^n(\bar{n}s_1), \quad (5.60)$$

and similar for higher products of fields. That is, fields with higher values of the curve parameter are placed to the left of fields with lower curve parameter. Physically, the fact that \mathbf{P} occurred is related to the gluons originally interacting with a quark line. Taking the sum over all possible gluon numbers the contributions in Eq.(5.59) conveniently arrange themselves into an exponential

$$W_{n,+}^{\dagger}(\infty, x) = \mathbf{1} + \sum_{m=1}^{\infty} W_{n,+}^{\dagger \mathbf{m}}(\infty, x) = \mathbf{P} \exp \left\{ ig_s \tilde{\mu}^\epsilon \int_0^\infty ds \bar{n} \cdot \hat{A}^n(x + \bar{n}s) \right\}, \quad (5.61)$$

which we will refer to as the configuration space n -collinear Wilson line associated with the process pictured in Fig. 5.56. In label momentum space we correspondingly find the local operator

$$\begin{aligned} W_{n,+}^\dagger(x_r) &= \mathbf{1} + \sum_{m=1}^{\infty} W_{n,+}^{\dagger \mathbf{m}}(x_r) \equiv \sum_{m=0} \frac{1}{m!} \sum_{\substack{\text{perms.} \\ \{m\}}} \left[(-g_s \tilde{\mu}^\epsilon) \frac{\bar{n} \cdot A^n(x_r)}{\bar{n} \cdot \mathcal{P}^\dagger + i0} \cdots (-g_s \tilde{\mu}^\epsilon) \frac{\bar{n} \cdot A^n(x_r)}{\bar{n} \cdot \mathcal{P}^\dagger + i0} \right] \\ &\equiv \sum_{\text{perms.}} \left[\exp \left\{ -g_s \tilde{\mu}^\epsilon \frac{\bar{n} \cdot A^n(x_r)}{\bar{n} \cdot \mathcal{P}^\dagger + i0} \right\} \right], \end{aligned} \quad (5.62)$$

where we have introduced convenient short-hand in the last line which is usually adopted in the literature.

Since the Wilson line carries a trivial Dirac structure (i.e. it is proportional to the identity) and the current in turn has trivial colour structure, we may pull $W_{n,+}^\dagger(x_r)$ through the Dirac and colour structure of the production current in Eq.(5.57) to obtain the operator

$$\mathcal{O}_{n,+}^{\dagger \mu} \sim \bar{\xi}_{\bar{n}}(x_r) \Gamma^\mu W_{n,+}^\dagger(x_r) \xi_n(x_r) \equiv \bar{\xi}_{\bar{n}}(x_r) \Gamma^\mu \chi_n(x_r), \quad (5.63)$$

where we were naturally lead to define the n -collinear jet field $\chi_n \equiv W_{n,+}^\dagger \xi_n$ that will play an important role in the discussion of the factorisation theorem in the sections to come.

Using the expressions Eq.(5.61) and Eq.(5.62) we can directly show the crucial property

$$W_{n,+}^\dagger (W_{n,+}^\dagger)^\dagger = (W_{n,+}^\dagger)^\dagger W_{n,+}^\dagger = \mathbf{1}, \quad (5.64)$$

which similarly holds for the other Wilson lines we will consider presently. The awkward notation in Eq.(5.64) suggests that $(W_{n,+}^\dagger)^\dagger \neq W_{n,+}$ as we can immediately see when we study collinear Wilson lines obtained from other processes.

For instance, analogous considerations to those outlined above for the absorption of an arbitrary number of gluons by an incoming \bar{n} -collinear anti-quark in the process Fig. 5.48(ri.) lead to the Wilson line

$$W_{n,-}^\dagger = \sum_{\text{perms.}} \left[\exp \left\{ -g_s \tilde{\mu}^\epsilon \frac{\bar{n} \cdot A^n}{\bar{n} \cdot \mathcal{P}^\dagger - i0} \right\} \right], \quad W_{n,-}^\dagger(x, -\infty) = \bar{\mathbf{P}} \exp \left\{ -ig_s \tilde{\mu}^\epsilon \int_{-\infty}^0 ds \bar{n} \cdot \hat{A}^n(x + \bar{n}s) \right\}, \quad (5.65)$$

in label momentum and configuration space respectively, where the subscript $n,-$ indicates the association of the n -collinear gluons with the anti-quark line $(-)$. Since the gluons are now incoming we have a sum $A_\mu^n(x_r) = \sum_{k_l \neq 0} A_{\mu,k_l}^n(x_r)$ over positive label fields in Eq.(5.65). Note that the absorption by an anti-quark has lead to the Wilson line being anti-path ordered $\bar{\mathbf{P}}$ such that fields at larger curve parameter are ordered to the right (effectively swapping the step functions in the definition Eq.(5.60)). We also observe that the path now runs from $-\infty$ to x along the \bar{n} -collinear direction indicating gluon absorption by an incoming particle.

The remaining Wilson lines can be obtained by exchanging the roles of the quark and anti-quark in the processes of Fig. 5.48 and considering emission (absorption) of any number of gluons. Concretely we obtain

$$W_{n,+} = \sum_{\text{perms.}} \left[\exp \left\{ -g_s \tilde{\mu}^\epsilon \frac{\bar{n} \cdot A^n}{\bar{n} \cdot \mathcal{P} + i0} \right\} \right], \quad W_{n,+}(x, -\infty) = \mathbf{P} \exp \left\{ ig_s \tilde{\mu}^\epsilon \int_{-\infty}^0 ds \bar{n} \cdot \hat{A}^n(x + \bar{n}s) \right\}, \quad (5.66)$$

for the absorption of n -collinear gluons by an incoming \bar{n} -collinear quark as well as

$$W_{n,-} = \sum_{\text{perms.}} \left[\exp \left\{ -g_s \tilde{\mu}^\epsilon \frac{\bar{n} \cdot A^n}{\bar{n} \cdot \mathcal{P} - i0} \right\} \right], \quad W_{n,-}(\infty, x) = \bar{\mathbf{P}} \exp \left\{ -ig_s \tilde{\mu}^\epsilon \int_0^\infty ds \bar{n} \cdot \hat{A}^n(x + \bar{n}s) \right\}, \quad (5.67)$$

for the emission of n -collinear gluons by an outgoing \bar{n} -collinear anti-quark. The label operator in the Wilson lines Eqs.(5.66) and (5.67) is understood to act on the fields from the left. We observe that the thus defined Wilson lines satisfy the relations $(W_{n,\pm})^\dagger = W_{n,\mp}^\dagger$ in both label momentum and configuration space. When we study the factorisation theorem for thrust we will also encounter \bar{n} -collinear Wilson lines, denoted $W_{\bar{n},\pm}^{(\dagger)}$, which will be defined analogously.

To conclude this section we want to come back and highlight the connection of the Wilson line Eq.(5.66) with the collinear quark Lagrangian Eq.(5.44) we anticipated earlier. From the definitions of the Wilson lines in Eqs.(5.61) and (5.62) it is not complicated to show the respective relations

$$\begin{aligned} i\bar{n}\cdot D_x W_{n,+}(x, -\infty) &\equiv \left(i\partial_{x^+} + g_s \tilde{\mu}^\epsilon \bar{n}\cdot \hat{A}^n(x) \right) W_{n,+}(\infty, x) = 0, \\ [i\bar{n}\cdot D^n W_{n,+}(x_r)] &= [(\bar{n}\cdot \mathcal{P} + i0 + g_s \tilde{\mu}^\epsilon \bar{n}\cdot A^n(x_r)) W_{n,+}(x_r)] = 0, \end{aligned} \quad (5.68)$$

that is, the covariant derivative (now enhanced by the proper $i0$ -prescription) of the Wilson line along its path vanishes. Using Eq.(5.35) we obtain the label momentum space operator equation

$$i\bar{n}\cdot D^n W_{n,+} = [i\bar{n}\cdot D^n W_{n,+}] + W_{n,+}(\bar{n}\cdot \mathcal{P} + i0) = W_{n,+}(\bar{n}\cdot \mathcal{P} + i0). \quad (5.69)$$

In combination with Eq.(5.64) one can then show that the inverse differential operator featuring in the collinear quark Lagrangian Eq.(5.44) can be written in terms of this Wilson line as

$$\frac{1}{i\bar{n}\cdot D^n} = W_{n,+} \frac{1}{\bar{n}\cdot \mathcal{P} + i0} (W_{n,+})^\dagger = W_{n,+} \frac{1}{\bar{n}\cdot \mathcal{P} + i0} W_{n,-}^\dagger. \quad (5.70)$$

In the next section we will combine the above result with the collinear quark Lagrangian and add the remaining sectors necessary for our discussion of the process $e^+e^- \rightarrow \text{di-jets}$.

5.6 Other sectors and final Lagrangian for $e^+e^- \rightarrow \text{di-jets}$

In addition to the collinear quark Lagrangian we derived in Eq.(5.44), we have to consider additional sectors for collinear and usoft gluons. The collinear gluon Lagrangian can be obtained by making use of the power counted derivatives in Eq.(5.41), defining

$$i\mathcal{D}_\mu^n = \frac{n_\mu}{2} (\bar{n}\cdot \mathcal{P} + g_s \bar{n}\cdot A^n) + \frac{\bar{n}_\mu}{2} (in\cdot \partial + g_s n\cdot A^n + g_s n\cdot A^{\text{us}}) + (\mathcal{P}_\mu^\perp + g_s A_\mu^{n,\perp}), \quad (5.71)$$

and then replacing $iD_\mu \mapsto i\mathcal{D}_\mu^n$ in the full QCD Lagrangian. Thus for the n -collinear gluon sector we have

$$\mathcal{L}_{A,n}^{(0)} = -\frac{1}{4} \text{Tr}[\mathcal{G}^{n\mu\nu} \mathcal{G}_{\mu\nu}^n], \quad \text{with} \quad \mathcal{G}_{\mu\nu}^n = \frac{i}{g_s} [\mathcal{D}_\mu^n, \mathcal{D}_\nu^n]. \quad (5.72)$$

The ultrasoft gluons can be treated analogously by substituting $iD_\mu \mapsto i\mathcal{D}_\mu^{\text{us}}$, where $i\mathcal{D}_\mu^{\text{us}} = i\partial_\mu + g_s A_\mu^{\text{us}}$, and the corresponding field strength is denoted $\mathcal{G}_{\mu\nu}^{\text{us}}$.

For massless quarks we would have to additionally include a kinetic term for ultrasoft modes,

$$\mathcal{L}_{q,\text{us}} = \bar{\xi}_{\text{us}} i \not{D}^{\text{us}} \xi_{\text{us}}, \quad (5.73)$$

which has power counting $i\not{D}^{\text{us}} \sim \mathcal{O}(\lambda^2)$ and, by considerations similar to Eq.(5.45), $\xi_{\text{us}} \sim \mathcal{O}(\lambda^3)$ for the ultrasoft quark field. However, when a mass term is present, the derivative in Eq.(5.73) is power suppressed compared to $m \sim \mathcal{O}(\lambda)$, and so the field is not dynamical at leading power. Just as we did for $\varphi_{\bar{n}}$, we can integrate it out by replacing it with its equation of motion $\xi_{\text{us}} = 0$, thus eliminating the term from the Lagrangian altogether.

Having described all relevant momentum regions and particles for the di-jet process under consideration we combine the previously obtained results into the final leading power SCET Lagrangian for massive quarks,

$$\mathcal{L}_{\text{SCET}}^{(0)} = -\frac{1}{4}\text{Tr}[\mathcal{G}^{n\mu\nu}\mathcal{G}_{\mu\nu}^n] - \frac{1}{4}\text{Tr}[\mathcal{G}^{\text{us}\mu\nu}\mathcal{G}_{\mu\nu}^{\text{us}}] \quad (5.74)$$

$$+ e^{-i\mathcal{P}\cdot x}\bar{\xi}_n\left[in\cdot D + (i\not{D}_\perp - m)W_{n,+}\frac{1}{\bar{n}\cdot\mathcal{P} + i0}W_{n,-}^\dagger(i\not{D}_\perp + m)\right]\frac{\not{n}}{2}\xi_n + (\bar{n}\text{-collinear}),$$

with the label momentum space collinear Wilson line given as in Eq.(5.62) and the covariant derivatives Eq.(5.41). The Wilson line can be thought of as the remnant of the ability of the full QCD Lagrangian to emit n -collinear gluons off \bar{n} -collinear (anti-)quarks, which were integrated out in SCET. The emission of n -collinear by n -collinear (anti-)quarks on the other hand remains a regular interaction in the effective theory Lagrangian, and is contained in the $\bar{\xi}_n in\cdot D \frac{\not{n}}{2}\xi_n$ term. Incidentally, this is also the only term that couples the usoft gluon to the collinear quark. We will argue in the next section that this interaction can in fact be removed from the Lagrangian by the introduction of additional, ultrasoft Wilson lines.

The \bar{n} -collinear part of the Lagrangian is given by copies of the collinear quark and gluon contributions for the fields $A^{\bar{n}}$, $\xi_{\bar{n}}$ with $n \leftrightarrow \bar{n}$. We can therefore easily accommodate any number of collinear directions by adding the appropriate terms to Eq.(5.74). This demonstrates the modularity but also the process-dependence of the SCET framework.

5.7 Ultrasoft Wilson lines

As we have alluded to at the end of the previous section, the Lagrangian Eq.(5.74) couples ultrasoft gluons and collinear quarks only through a single interaction term. We now aim to illustrate that this interaction can be cast into the form of another, now ultrasoft, Wilson line operator. An appropriate field redefinition of the collinear quark fields using this Wilson line will enable us to effectively pull the usoft interactions out of the fields, leading to a manifest decoupling of usoft and collinear degrees of freedom in the leadingpower collinear quark Lagrangian.

We proceed similarly to the analysis we carried out for the collinear Wilson line by asking what happens for diagrams of the form shown in Fig. 5.75 where an outgoing \bar{n} -collinear anti-quark emits m ultrasoft gluons whose momenta scale as $k_{i,r} \equiv k_i \sim Q(\lambda^2, \lambda^2, \lambda^2)$, $i = 1, \dots, m$.

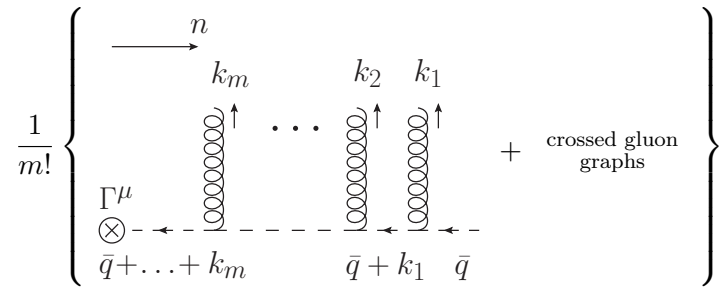


Fig. (5.75): Emission of m ultrasoft gluons by an outgoing anti-quark line pointed in the n -collinear direction, including all allowed permutations of the external gluon lines. The ultrasoft gluons are depicted as regular curly lines. This process contributes to the usoft Wilson line $Y_{n,-}^{\text{m}}$.

This process corresponds to an operator analogous to Eq.(5.58), although now in residual momentum space, which reads

$$Y_{n,-}^{\text{m}}(k_1, k_2, \dots, k_m) = \frac{(g_s \tilde{\mu}^\epsilon)^m}{m!} \sum_{\substack{\text{perms.} \\ \{k_1, \dots, k_m\}}} \left[\frac{n \cdot A^{\text{us}}(-k_m) \dots n \cdot A^{\text{us}}(-k_1)}{[n \cdot \sum_{i=1}^m k_i + i0] \dots [n \cdot k_1 + i0]} \right], \quad (5.76)$$

where the negative residual momenta appear due to the outgoing usoft gluons and the fact that $(A_\mu^{\text{us}})^\dagger(k) = A_\mu^{\text{us}}(-k)$. Note that unlike for the collinear Wilson line, the subscript n now refers to the collinear direction of the quark rather than the absorbed gluons since there is no preferred direction associated with the latter. Note that the expression Eq.(5.76) cannot be rewritten as in Eq.(5.58) using the label operator, since the usoft gluon field does not carry a label momentum. This implies that the usoft Wilson line and the label operator commute.

The configuration space Wilson line is now obtained by performing a continuous Fourier transform in the residual momenta $k_{i,r}$ rather than the discrete transformation over labels we encountered for the collinear Wilson line in Eq.(5.55). Summing over all numbers of gluon emissions we obtain the fundamental representation usoft Wilson line

$$Y_{n,-}(\infty, x_r) = \overline{\mathbf{P}} \exp \left\{ -ig_s \tilde{\mu}^\epsilon \int_0^\infty ds \, n \cdot A^{\text{us}}(x_r + ns) \right\}, \quad (5.77)$$

in residual configuration space which is structurally identical to Eq.(5.65). However, unlike the collinear Wilson line, the usoft Wilson line is a genuine residual space operator. It is further non-local in residual space, while we recall that the residual space collinear Wilson Eq.(5.62) was in fact a local operator at this scale. The non-locality of the collinear Wilson line only emerged in configuration space Eq.(5.61) through the dependence on the large label momenta in the small components x^-, x_\perp (c.f. the discussion below Eq.(5.53)). The relations between Eq.(5.77) and the remaining usoft Wilson lines $Y_{n,\pm}^{(\dagger)}$ are identical to those of the collinear Wilson lines, still satisfying $(Y_{n,\pm})^\dagger = Y_{n,\mp}^\dagger$.

It should also be mentioned that the usoft Wilson line was not obtained by imposing the effective theory power counting on a full QCD process, as was the case for the collinear Wilson line. Instead, it naturally arose out of the structure of the effective theory. This is also apparent from the structure of the diagrams in Fig. 5.75 where all fields and interactions are described by the Lagrangian Eq.(5.44) of a single collinear sector. Compare this to the process in Fig. 5.56 where the presence of more than one collinear direction was essential to the derivation of the collinear Wilson line.

Physically the usoft Wilson line reflects the fact that usoft radiation cannot change the trajectory of an energetic, collinear (anti-)quark and thus only couples to its colour degrees of freedom along the corresponding direction. The collinear and usoft Wilson lines can be thought of as dual in the following sense [34]. If we boost to a frame where the previously n -collinear particles are usoft, the previously \bar{n} -collinear and usoft particles now appear to recoil against one another. In this boosted frame the now usoft particles have to couple to \bar{n} -collinear particles through a usoft Wilson line, while the previously usoft particles, which are now n -collinear in the boosted frame, couple to the \bar{n} -collinear sector via a collinear Wilson line. Thus the role of collinear and usoft Wilson lines is interchanged through an appropriate boost.

The simplification in the Lagrangian we alluded to before can now be achieved by using the usoft Wilson line Eq.(5.77) to redefine the collinear quark and gluon fields [35],

$$\xi_{n,p} = Y_{n,-} \xi_{n,p}^{(0)}, \quad A_{n,p} = Y_{n,-} A_{n,p}^{(0)} (Y_{n,-})^\dagger = Y_{n,-} A_{n,p}^{(0)} Y_{n,+}^\dagger, \quad (5.78)$$

where we have used the Wilson line $Y_{n,-}(\infty, x_r)$ in the field redefinition to conform with the choice of [12] in later calculations. This choice is effectively due to the fact that the field ξ_n is associated with an outgoing anti-particle. With the above relations one can show that the collinear Wilson line transforms as

$$W_{n,+} = \sum_{\text{perms.}} \left[\exp \left\{ \frac{-g_s \tilde{\mu}^\epsilon}{\bar{n} \cdot \mathcal{P} + i0} Y_{n,-} \bar{n} \cdot A_n^{(0)} Y_{n,+}^\dagger \right\} \right] = Y_{n,-} W_{n,+}^{(0)} Y_{n,+}^\dagger, \quad (5.79)$$

where we can pull the usoft Wilson lines through the label operator since the two commute. Note however, that the Wilson lines themselves do not commute since the fields contained in them are always causally connected (lightlike separated) in residual space so that the transformation in Eq.(5.79) is non-trivial. Similar to the collinear Wilson line, the usoft Wilson line satisfies

$$\begin{aligned} in \cdot D_r^{\text{us}} Y_{n,-}(\infty, x_r) &\equiv (in \cdot \partial_r + g_s \tilde{\mu}^\epsilon n \cdot A^{\text{us}}(x_r)) Y_{n,-}(\infty, x_r) = 0, \\ Y_{n,+}^\dagger Y_{n,-} &= Y_{n,-} Y_{n,+}^\dagger = \mathbf{1}. \end{aligned} \quad (5.80)$$

With this in mind we can substitute the redefined fields Eq.(5.78) into the collinear quark Lagrangian to get

$$\mathcal{L}_{q,n}^{(0)} = e^{-i\mathcal{P} \cdot x} \bar{\xi}_n^{(0)} \left[in \cdot \partial + g_s n \cdot A_n^{(0)} + \left(i\not{D}_\perp^{(0)} - m \right) W_{n,+}^{(0)} \frac{1}{\bar{n} \cdot \mathcal{P} + i0} W_{n,-}^{\dagger(0)} \left(i\not{D}_\perp^{(0)} + m \right) \right] \frac{\not{n}}{2} \xi_n^{(0)}, \quad (5.81)$$

in which the usoft gluons have completely decoupled from the collinear degrees of freedom. A similar decoupling can be observed in the collinear gluon Lagrangian Eq.(5.72), thus implementing usoft-collinear factorisation. However, the usoft interactions have not been completely removed from the theory, as we will see in the next section, where they resurface in the effective theory currents whose matrix elements we wish to compute. Another aspect that should be stressed is that this decoupling can only be achieved in the leading power Lagrangian $\mathcal{L}_{q,n}^{(0)}$ [35], power suppressed terms in the action that are $\mathcal{O}(\lambda)$ and higher will still contain usoft interactions even when formulated in terms of the fields Eq.(5.78).

6 SCET factorisation theorem for thrust

In the following we want to exploit the manifest decoupling of usoft and collinear degrees of freedom in the effective theory Lagrangian to derive a factorisation theorem for the process $e^+e^- \rightarrow \gamma^* \rightarrow$ di-jets in SCET. This will allow us to write experimentally accessible quantities (such as the thrust distribution in the peak region) as a convolution of so-called factorisation functions each pertaining to a hard, collinear or usoft sector in the theory. An additional advantage of such a factorised approach lies in the transparent separation of perturbative and non-perturbative contributions to the observable at hand. In the effective theory framework the factorisation will further allow for the resummation of large logarithms encountered in Eq.(4.15) and similar observables via renormalisation group methods. The derivation will closely follow [12, 13].

6.1 Factorisation of the total cross section in the di-jet limit

Our starting point is the contribution of final states which consist entirely of two collinear quark jets and ultrasoft radiation to the total cross section in QCD. Schematically we have seen in Eq.(2.53) that at $\mathcal{O}(\alpha_{\text{em}})$ this can be written in $d = 4$ dimensions as

$$\sigma = \sum_X^{\text{res.}} \int d\Pi_X (2\pi)^4 \delta^{(4)}(Q - \sum_{i \in X} p_i) \langle \hat{L}_{\mu\nu}^{\epsilon=0} \rangle \langle 0 | \mathcal{J}_v^{\dagger\mu}(0) | X \rangle \langle X | \mathcal{J}_v^\nu(0) | 0 \rangle, \quad (6.1)$$

with the modification that X now denotes all final states which are restricted to only contain collinear and ultrasoft particles. Since the states $|X\rangle$ produced by the vector current \mathcal{J}^μ (c.f. below Eq.(2.50)) will always contain a $q\bar{q}$ -pair we can associate the quark with the n -collinear and the anti-quark with the \bar{n} -collinear direction without loss of generality. The sum in Eq.(6.1) also includes any necessary colour and spin sums. The incoming momentum of the electron-positron pair is $Q^\mu = p_{e^+}^\mu + p_{e^-}^\mu$, and we have used a modified leptonic tensor

$$\langle \hat{L}_{\mu\nu}^{\epsilon=0} \rangle = \frac{1}{2s} e_q^2 e^2 \langle L_{\mu\nu}^{\epsilon=0} \rangle \frac{1}{s^2}, \quad (6.2)$$

compared to Eq.(2.7) to comply with the notation of [13]. Note that when the restriction on the final state sum is lifted, Eq.(6.1) simply represents the total cross section for the process in QCD.

The restriction in the final state sum can be written more explicitly by separating it into a sum over jet directions \vec{n} and a sum over collinear states $X_n, X_{\bar{n}}$ along these directions as well as ultrasoft states X_{us} ,

$$\sum_X^{\text{res.}} \int d\Pi_X \equiv \sum_{\vec{n}} \sum_{X_n, X_{\bar{n}}, X_{\text{us}}}^{\text{res.}} \int d\Pi_{X_n} d\Pi_{X_{\bar{n}}} d\Pi_{X_{\text{us}}}, \quad \text{with} \quad |X\rangle \equiv |X_n X_{\bar{n}} X_{\text{us}}\rangle. \quad (6.3)$$

Our goal will now be to implement this restriction in SCET at the level of operators and matrix elements, so that the explicit restriction in the above sum can eventually be lifted. From considerations of gauge invariance (see [36]) and our calculations in Eq.(6.5), the QCD current will get matched onto the effective theory current

$$\begin{aligned} \mathcal{J}_v^\mu &= \bar{\Psi} \gamma^\mu \Psi \xrightarrow{\text{SCET}} C(\bar{n} \cdot \mathcal{P}, n \cdot \mathcal{P}, \mu) [\bar{\xi}_n W_{n,-}] \gamma^\mu [W_{\bar{n},+}^\dagger \xi_{\bar{n}}] \\ &= \int d\omega d\bar{\omega} C(\omega, \bar{\omega}, \mu) [\bar{\xi}_n W_{n,-} \delta(\omega - \bar{n} \cdot \mathcal{P}^\dagger)] \gamma^\mu [\delta(\bar{\omega} - n \cdot \mathcal{P}) W_{\bar{n},+}^\dagger \xi_{\bar{n}}] \\ &\equiv \int d\omega d\bar{\omega} C(\omega, \bar{\omega}, \mu) J_v^\mu(\omega, \bar{\omega}, \mu), \end{aligned} \quad (6.4)$$

where the Wilson coefficient $C(\bar{n}\cdot\mathcal{P}, n\cdot\mathcal{P}, \mu)$ can be restricted by gauge invariance[31] to only be a function of the large label momentum components of the fields. In the second line of Eq.(6.4) we have made explicit the label momentum of the jet fields

$$\begin{aligned}\chi_{n,\omega} &= \delta(\omega - \bar{n}\cdot\mathcal{P})W_{n,+}^\dagger\xi_n, & \chi_{\bar{n},\bar{\omega}} &= \delta(\bar{\omega} - n\cdot\mathcal{P})W_{\bar{n},+}^\dagger\xi_{\bar{n}}, \\ \bar{\chi}_{n,\omega} &= \bar{\xi}_n W_{n,-}\delta(\omega - \bar{n}\cdot\mathcal{P}^\dagger), & \bar{\chi}_{\bar{n},\bar{\omega}} &= \bar{\xi}_{\bar{n}} W_{\bar{n},-}\delta(\bar{\omega} - n\cdot\mathcal{P}^\dagger),\end{aligned}\quad (6.5)$$

for later convenience by trivially integrating over the delta functions. In Eq.(6.5) we have kept the \pm subscripts on the Wilson lines which we will from now on drop for notational brevity. With Eq.(6.4) we have implemented hard-collinear factorisation in the sense that all of the information about the hard scale which was integrated out in the construction of SCET is contained in the Wilson coefficient while low energy degrees of freedom that are still dynamic within the effective theory are encoded by matrix elements of the effective current.

In the next step we consider soft-collinear factorisation by redefining the fields according to Eq.(5.78). This leads to the according transformation of the jet fields and the effective current

$$\bar{\chi}_{n,\omega} \rightarrow \bar{\chi}_{n,\omega}^{(0)} Y_{n,+}^\dagger, \quad \chi_{\bar{n},\bar{\omega}} \rightarrow Y_{\bar{n},-} \chi_{\bar{n},\bar{\omega}}^{(0)} \Rightarrow J_v^\mu \rightarrow J_v^{(0)\mu} = \bar{\chi}_{n,\omega}^{(0)} Y_{n,+}^\dagger \gamma^\mu Y_{\bar{n},-} \chi_{\bar{n},\bar{\omega}}^{(0)}, \quad (6.6)$$

with all operators now built from the thus redefined fields. From now on we are going to drop the explicit superscript (0) and only consider quantities in terms of the usoft decoupled fields. Recall that we showed that usoft gluons completely decouple from collinear quarks in the Lagrangian Eq.(5.81). However, we have now discovered that this interaction resurfaces in the current whose matrix elements we wish to compute. For completeness we mention that for calculations involving massive quarks at two loops and higher, the effective current in Eq.(6.6) must be supplemented by additional mass mode Wilson lines S_n [12], which for the purposes of this thesis we can ignore.

Having taken care of the operators, we turn to the kinematics of Eq.(6.1), which, in the di-jet limit where all particles are either collinear to the thrust axis or usoft, allows us to decompose the final state momenta into

$$\sum_{i \in X} p_i^\mu = P_{X_n}^\mu + P_{X_{\bar{n}}}^\mu + P_{X_{\text{us}}}^\mu, \quad (6.7)$$

with the P_{X_i} denoting the sum of momenta in the n/\bar{n} -collinear and usoft sectors respectively. Substituting the SCET current into the cross section Eq.(6.1) we get

$$\begin{aligned}\sigma &= \sum_{\vec{n}} \sum_{X_n, X_{\bar{n}}, X_{\text{us}}}^{\text{res.}} \int d\Pi_{X_n} d\Pi_{X_{\bar{n}}} d\Pi_{X_{\text{us}}} \int d\omega d\bar{\omega} d\omega' d\bar{\omega}' (2\pi)^4 \delta^{(4)}(Q - P_{X_n} - P_{X_{\bar{n}}} - P_{X_{\text{us}}}) \langle \hat{L}_{\mu\nu}^{\epsilon=0} \rangle \\ &\times C(\omega, \bar{\omega}) C^*(\omega', \bar{\omega}') \langle 0 | \bar{\mathbf{T}} \left\{ \bar{\chi}_{\bar{n},\bar{\omega}'} Y_{\bar{n},+}^\dagger \gamma^\mu Y_{n,-} \chi_{n,\omega'} \right\} | X_n X_{\bar{n}} X_{\text{us}} \rangle \langle X_n X_{\bar{n}} X_{\text{us}} | \mathbf{T} \left\{ \bar{\chi}_{n,\omega} Y_{n,+}^\dagger \gamma^\nu Y_{\bar{n},-} \chi_{\bar{n},\bar{\omega}} \right\} | 0 \rangle, \end{aligned}\quad (6.8)$$

with the jet fields evaluated at $x_r = 0$ as before. Note that we had to introduce (anti-)time ordering in the effective theory matrix elements since the usoft Wilson lines are non-local functions of the gauge fields in residual space. However, we can absorb the time ordering into the Wilson lines by observing that

$$\mathbf{T} Y_{n,+}^\dagger = Y_{n,+}^\dagger, \quad \bar{\mathbf{T}} Y_{n,-} = Y_{n,-}, \quad \mathbf{T} Y_{\bar{n},-} \equiv (\bar{Y}_{\bar{n},+}^\dagger)^T, \quad \bar{\mathbf{T}} Y_{\bar{n},+}^\dagger \equiv (\bar{Y}_{\bar{n},-})^T, \quad (6.9)$$

where the superscript T denotes the colour transpose. We see that it suffices to rewrite the Wilson lines where the path ordering does not already agree with time ordering. The newly defined Wilson lines in Eq.(6.9) read

$$\bar{Y}_{\bar{n},+}^\dagger = \mathbf{P} \exp \left\{ i g_s \tilde{\mu}^\epsilon \int_0^\infty ds \bar{n} \cdot \bar{A}^{\text{us}}(x + \bar{n}s) \right\}, \quad \bar{Y}_{\bar{n},-} = \bar{\mathbf{P}} \exp \left\{ -i g_s \tilde{\mu}^\epsilon \int_0^\infty ds \bar{n} \cdot \bar{A}^{\text{us}}(x + \bar{n}s) \right\}, \quad (6.10)$$

with the barred gluon field in the $\bar{\mathbf{3}}$ representation, $\bar{A}^{\text{us}} = A_a^{\text{us}} \bar{T}^a$ and $\bar{T}^a \equiv -(T^a)^T$. In the following we will use these barred Wilson lines, allowing us to drop explicit (anti-)time ordering in the matrix elements. In addition we drop the subscripts \pm for readability.

Since the SCET Lagrangian decouples at leading power, we expect the corresponding Hilbert space of the theory to factorise so that

$$|X_n X_{\bar{n}} X_{\text{us}}\rangle = |X_n\rangle |X_{\bar{n}}\rangle |X_{\text{us}}\rangle, \quad (6.11)$$

which will allow us to dissect the matrix elements in Eq.(6.8) into three distinct pieces

$$\begin{aligned} \langle 0 | J_v^{\dagger\mu}(0) | X_n X_{\bar{n}} X_{\text{us}} \rangle \langle X_n X_{\bar{n}} X_{\text{us}} | J_v^\nu(0) | 0 \rangle &= \langle 0 | (\bar{Y}_{\bar{n}} Y_n)_{lm}(0) | X_{\text{us}} \rangle \langle X_{\text{us}} | (Y_n^\dagger \bar{Y}_{\bar{n}}^\dagger)_{ij}(0) | 0 \rangle \\ &\times \langle 0 | (\chi_{n,\omega'}^\sigma)_m(0) | X_n \rangle \langle X_n | (\bar{\chi}_{n,\omega})_i^\alpha(0) | 0 \rangle \gamma_{\alpha\beta}^\mu \\ &\times \langle 0 | (\bar{\chi}_{\bar{n},\bar{\omega}'}^\rho)_l(0) | X_{\bar{n}} \rangle \langle X_{\bar{n}} | (\chi_{\bar{n},\bar{\omega}})^\beta_j(0) | 0 \rangle \gamma_{\rho\sigma}^\nu. \end{aligned} \quad (6.12)$$

In the above expression all spinor (greek $\neq \mu, \nu$) and colour (roman) indices have been made explicit. To proceed we note that the collinear matrix elements in Eq.(6.12) are colour diagonal. Denoting by $|X_n, 1\rangle$ a n -collinear quark state with colour $a = 1$ we have e.g.

$$\langle 0 | (\chi_n)^\sigma_1(0) | X_n, 1 \rangle \langle X_n, 1 | (\bar{\chi}_n)^\alpha_j(0) | 0 \rangle \sim \delta_{1j}. \quad (6.13)$$

This allows us to take an average over colours in the collinear matrix elements by substituting

$$\langle 0 | (\chi_n)^\sigma_m(0) | X_n \rangle \langle X_n | (\bar{\chi}_n)^\alpha_i(0) | 0 \rangle \mapsto \frac{\delta_{mi}}{N_C} \langle 0 | (\chi_n)^\sigma_a(0) | X_n \rangle \langle X_n | (\bar{\chi}_n)^\alpha_a(0) | 0 \rangle, \quad (6.14)$$

and similar for the \bar{n} -collinear sector. Making the replacements in Eq.(6.12) we have already completely factorised the matrix elements pertaining to the usoft Wilson lines,

$$\begin{aligned} \langle 0 | J_v^{\dagger\mu}(0) | X \rangle \langle X | J_v^\nu(0) | 0 \rangle &= \text{Tr} \left[\langle 0 | (\bar{Y}_{\bar{n}} Y_n)(0) | X_{\text{us}} \rangle \langle X_{\text{us}} | (Y_n^\dagger \bar{Y}_{\bar{n}}^\dagger)(0) | 0 \rangle \right] \\ &\times \frac{1}{N_C} \text{Tr} \left[\langle 0 | (\chi_{n,\omega'}^\sigma)(0) | X_n \rangle \langle X_n | (\bar{\chi}_{n,\omega})^\alpha(0) | 0 \rangle \right] \gamma_{\alpha\beta}^\mu \\ &\times \frac{1}{N_C} \text{Tr} \left[\langle 0 | (\bar{\chi}_{\bar{n},\bar{\omega}'}^\rho)(0) | X_{\bar{n}} \rangle \langle X_{\bar{n}} | (\chi_{\bar{n},\bar{\omega}})^\beta(0) | 0 \rangle \right] \gamma_{\rho\sigma}^\nu, \end{aligned} \quad (6.15)$$

with the capital $\text{Tr}[\dots]$ denoting a colour trace. In Eq.(6.15) we can see that the n/\bar{n} -collinear sectors can still communicate with each other through the Dirac structure. To remedy this we employ the SCET Fierz identity, which for n -collinear jet fields reads[37],

$$\bar{\chi}_n^\alpha \chi_n^\beta = \frac{1}{2} \left[\frac{\not{n}^{\beta\alpha}}{2} \bar{\chi}_n \frac{\not{n}}{2} \chi_n - \frac{(\gamma_5 \not{n})^{\beta\alpha}}{2} \bar{\chi}_n \gamma_5 \frac{\not{n}}{2} \chi_n - \frac{(\gamma_\perp^\mu \not{n})^{\beta\alpha}}{2} \bar{\chi}_n \gamma_{\perp\mu} \frac{\not{n}}{2} \chi_n \right], \quad (6.16)$$

with an analogous relation for the \bar{n} -collinear jet field with $n \leftrightarrow \bar{n}$. Inserting the identity next to each of the jet fields and carrying out the above replacement one can check that only the first term in Eq.(6.16) survives in each collinear sector. This finally gives us a fully factorised matrix element

$$\begin{aligned} \langle 0 | J_v^{\dagger\mu}(0) | X \rangle \langle X | J_v^\nu(0) | 0 \rangle &= \text{tr} \left[\gamma^\mu \frac{\not{n}}{4} \gamma^\nu \frac{\not{n}}{4} \right] \times \text{Tr} \left[\langle 0 | (\bar{Y}_{\bar{n}} Y_n)(0) | X_{\text{us}} \rangle \langle X_{\text{us}} | (Y_n^\dagger \bar{Y}_{\bar{n}}^\dagger)(0) | 0 \rangle \right] \\ &\times \frac{1}{N_C} \text{tr} \left[\langle 0 | \frac{\not{n}}{2} \chi_{n,\omega'}(0) | X_n \rangle \langle X_n | \bar{\chi}_{n,\omega}(0) | 0 \rangle \right] \\ &\times \frac{1}{N_C} \text{tr} \left[\langle 0 | \bar{\chi}_{\bar{n},\bar{\omega}'}(0) | X_{\bar{n}} \rangle \langle X_{\bar{n}} | \frac{\not{n}}{2} \chi_{\bar{n},\bar{\omega}}(0) | 0 \rangle \right], \end{aligned} \quad (6.17)$$

where the lower case $\text{tr}[\dots]$ now denotes a Dirac trace and the colour trace on the collinear matrix elements has been made implicit. Finally, since we have isolated each jet field into its own matrix element we can pull the large label momenta out by using Eq.(6.7) so that

$$\langle 0 | \frac{\not{p}}{2} \chi_{n,\omega'}(0) | X_n \rangle = \delta(\omega' - \bar{n} \cdot P_{X_n}) \langle 0 | \frac{\not{p}}{2} \chi_n(0) | X_n \rangle, \quad \langle 0 | \bar{\chi}_{\bar{n},\bar{\omega}'}(0) | X_{\bar{n}} \rangle = \delta(\bar{\omega}' + n \cdot P_{X_{\bar{n}}}) \langle 0 | \bar{\chi}_{\bar{n}}(0) | X_{\bar{n}} \rangle, \quad (6.18)$$

with the jet fields now implicitly carrying label momenta $\omega' = \bar{n} \cdot P_{X_n}$ and $\bar{\omega}' = -n \cdot P_{X_{\bar{n}}}$ respectively. Note the negative label momentum of the \bar{n} -collinear field which is due to our choice of associating this particular direction with the jet initiated by the anti-quark (c.f. discussion below Eq.(5.25)). Integrating over the label momenta $\omega', \bar{\omega}'$ the cross section Eq.(6.8) takes the form

$$\begin{aligned} \sigma = K_0 \sum_{\bar{n}} \sum_{X_n, X_{\bar{n}}, X_{\text{us}}}^{\text{res.}} \int d\Pi_{X_n} d\Pi_{X_{\bar{n}}} d\Pi_{X_{\text{us}}} \int d\omega d\bar{\omega} (2\pi)^4 \delta^{(4)}(Q - P_{X_n} - P_{X_{\bar{n}}} - P_{X_{\text{us}}}) |C(\omega, \bar{\omega})|^2 \\ \times \text{Tr} \left[\langle 0 | \bar{Y}_{\bar{n}} Y_n | X_{\text{us}} \rangle \langle X_{\text{us}} | Y_n^\dagger \bar{Y}_{\bar{n}}^\dagger | 0 \rangle \right] \frac{1}{N_C} \text{tr} \left[\langle 0 | \frac{\not{p}}{2} \chi_n | X_n \rangle \langle X_n | \bar{\chi}_{n,\omega} | 0 \rangle \right] \frac{1}{N_C} \text{tr} \left[\langle 0 | \bar{\chi}_{\bar{n}} | X_{\bar{n}} \rangle \langle X_{\bar{n}} | \frac{\not{p}}{2} \chi_{\bar{n},\bar{\omega}} | 0 \rangle \right], \end{aligned} \quad (6.19)$$

where the (residual) spacetime dependence $x_r = 0$ is now implicit and the prefactor is given by

$$K_0 = \langle \hat{L}_{\mu\nu}^{\epsilon=0} \rangle \text{tr} \left[\gamma^\mu \frac{\not{p}}{4} \gamma^\nu \frac{\not{p}}{4} \right] = \frac{8\pi^2 e_q^2 \alpha_{\text{em}}^2}{3s^2} = \frac{2\pi}{N_C} \frac{\sigma_{\mathbf{2},\epsilon=0}^{\mathbf{LO}}}{s}, \quad (6.20)$$

with the total leading order cross section $\sigma_{\mathbf{2}}^{\mathbf{LO}}$ as in Eq.(2.10).

From the decomposition Eq.(6.7) of the final state momentum and overall momentum conservation in Eq.(6.19) we can also infer that in the center of mass frame, where $Q^\mu = (Q, \mathbf{0})^\mu$, we must have $\mathbf{P}_{X_n,\perp} + \mathbf{P}_{X_{\bar{n}},\perp} = 0 + \mathcal{O}(\lambda^2)$. Since the momentum conserving delta function in Eq.(6.8) may be written in terms of lightcone coordinates as

$$\delta^{(4)}(Q - P_{X_n} - P_{X_{\bar{n}}} - P_{X_{\text{us}}}) = 2 \delta(Q - \bar{n} \cdot P_{X_n}) \delta(Q - n \cdot P_{X_{\bar{n}}}) \delta^{(2)}(\mathbf{P}_{X_n,\perp} + \mathbf{P}_{X_{\bar{n}},\perp}), \quad (6.21)$$

this enables us to simplify the convolution over label momenta between the collinear matrix elements and the Wilson coefficient to an ordinary multiplication

$$\begin{aligned} \int d\omega d\bar{\omega} |C(\omega, \bar{\omega})|^2 \delta(Q - \bar{n} \cdot P_{X_n}) \delta(Q - n \cdot P_{X_{\bar{n}}}) \langle X_n | \bar{\chi}_{n,\omega} | 0 \rangle \langle X_{\bar{n}} | \frac{\not{p}}{2} \chi_{\bar{n},\bar{\omega}} | 0 \rangle \\ = H(Q) \delta(Q - \bar{n} \cdot P_{X_n}) \delta(Q - n \cdot P_{X_{\bar{n}}}) \langle X_n | \bar{\chi}_{n,Q} | 0 \rangle \langle X_{\bar{n}} | \frac{\not{p}}{2} \chi_{\bar{n},-Q} | 0 \rangle, \end{aligned} \quad (6.22)$$

where we used analogous relations to Eq.(6.18) for the matrix elements and defined the hard function $H(Q) = |C(Q, -Q)|^2$. In the next step we insert the identity

$$1 = \int d^4 p_n d^4 p_{\bar{n}} d^4 p_{\text{us}} \delta^{(4)}(p_n - P_{X_n}) \delta^{(4)}(p_{\bar{n}} - P_{X_{\bar{n}}}) \delta^{(4)}(p_{\text{us}} - P_{X_{\text{us}}}), \quad (6.23)$$

into Eq.(6.19) which allows us to individually manipulate the overall momenta associated with each sector. In the following we decompose the above dummy momenta into label and residual components as

$$p_i^\mu = p_{i,l} + k_i, \quad i \in \{n, \bar{n}, \text{us}\}. \quad (6.24)$$

After some rather involved manipulations[12] and together with the relations Eqs.(6.20) and (6.22), the total cross section can be brought to the form

$$\begin{aligned} \sigma = \sigma_{2,\epsilon=0}^{\text{LO}} H(Q) \int dk_n^+ dk_{\bar{n}}^- dk_{\text{us}}^+ dk_{\text{us}}^- & \left[\sum_{X_n}^{\text{res.}} \int \frac{d\Pi_{X_n}}{4\pi N_C} \int d^4x e^{ik_n^+ x^-/2} \text{tr} \left[\langle 0 | \frac{\not{n}}{2} \chi_{n,Q}(x) | X_n \rangle \langle X_n | \bar{\chi}_{n,Q} | 0 \rangle \right] \right] \\ & \times \left[\sum_{X_{\bar{n}}}^{\text{res.}} \int \frac{d\Pi_{X_{\bar{n}}}}{4\pi N_C} \int d^4y e^{ik_{\bar{n}}^- y^+/2} \text{tr} \left[\langle 0 | \bar{\chi}_{\bar{n},-Q}(y) | X_{\bar{n}} \rangle \langle X_{\bar{n}} | \frac{\not{\bar{n}}}{2} \chi_{\bar{n},-Q} | 0 \rangle \right] \right] \\ & \times \left[\sum_{X_{\text{us}}}^{\text{res.}} \int \frac{d\Pi_{X_{\text{us}}}}{4N_C(2\pi)^2} \int dz^+ dz^- e^{\frac{i}{2}(k_{\text{us}}^+ z^- + k_{\text{us}}^- z^+)} \text{Tr} \left[\langle 0 | (\bar{Y}_{\bar{n}} Y_n)(z^+, z^-) | X_{\text{us}} \rangle \langle X_{\text{us}} | Y_n^\dagger \bar{Y}_{\bar{n}}^\dagger | 0 \rangle \right] \right], \end{aligned} \quad (6.25)$$

where only integrations over residual momenta remain, label momentum conservation is exactly implemented, and all fields are to be evaluated at $x_r = 0$ unless explicitly stated otherwise. In deriving the result in Eq.(6.25) the fact that $\mathbf{P}_{X_n,\perp} = \mathbf{0}$ when the n -collinear direction is chosen to align with the thrust axis was used. In addition, the collinear matrix elements are proportional to $\delta(x^+)\delta^{(2)}(\mathbf{x}_\perp)$ and $\delta(y^-)\delta^{(2)}(\mathbf{y}_\perp)$ for the n - and \bar{n} -collinear sector respectively which reflects the fact that all short-distance modes were removed from the jet fields. The cross section thus factorises entirely into two collinear and a single usoft sector, with a universal prefactor $H(Q)$ that depends only on the hard scale and is independent of the details of the final state.

Note that in Eq.(6.25) we still have to manually impose a restriction on the final state momenta to ensure that we are considering only the kinematic di-jet limit so that all our previous approximations are valid. However, this renders a direct evaluation of the matrix elements impossible since we do not generically know the explicit states $\{|X_n\rangle|X_{\bar{n}}\rangle|X_{\text{us}}\rangle\}$ relevant to the process. In the next section we will thus introduce a measurement function (e.g. thrust) that makes sure we are only allowing regions of phase space that pertain to di-jet kinematics. This will then allow us to lift the restriction on the final state sum and make concrete computations in this factorised picture.

6.2 Hemisphere mass distribution and thrust

Recall that a thrust measurement determines a thrust axis which we use to distinguish two hemispheres H, \bar{H} . In Eq.(5.10) we have seen that thrust Eq.(2.54) and the hemisphere masses Eq.(5.6) are related in the kinematic di-jet limit. In this section we will first derive the factorised form of the doubly differential cross section in the hemisphere masses $m_H^2, m_{\bar{H}}^2$, from which the thrust distribution then easily follows.

From the way we have set up the sectors of the effective theory, the final state momenta contribute to the hemisphere momenta as

$$p_H^\mu = \sum_{i \in H} p_{i,H}^\mu = P_{X_n}^\mu + P_{X_{\text{us}},H}^\mu, \quad p_{\bar{H}}^\mu = \sum_{i \in \bar{H}} p_{i,\bar{H}}^\mu = P_{X_{\bar{n}}}^\mu + P_{X_{\text{us}},\bar{H}}^\mu, \quad P_{X_{\text{us}}}^\mu = P_{X_{\text{us}},H}^\mu + P_{X_{\text{us}},\bar{H}}^\mu, \quad (6.26)$$

where the collinear sectors are associated with a definite hemisphere, while the usoft momenta are allowed to contribute to either. Invoking SCET power counting we find

$$\begin{aligned} p_H^2 &= P_{X_n}^-(P_{X_n}^+ + P_{X_{\text{us}},H}^+) = Q(k_n^+ + k_{\text{us},H}^+), \\ p_{\bar{H}}^2 &= P_{X_{\bar{n}}}^+(P_{X_{\bar{n}}}^- + P_{X_{\text{us}},\bar{H}}^-) = Q(k_{\bar{n}}^- + k_{\text{us},\bar{H}}^-), \end{aligned} \quad (6.27)$$

where we have dropped terms of $\mathcal{O}(\lambda^3)$ and higher and used the assignment Eq.(6.23) together with the decomposition Eq.(6.24) into label and residual momenta. We can now introduce a hemisphere

mass measurement into the cross section Eq.(6.25) through the identity

$$\begin{aligned}
1 &= \int dm_H^2 dm_{\bar{H}}^2 \delta(p_H^2 - m_H^2) \delta(p_{\bar{H}}^2 - m_{\bar{H}}^2) \\
&= \frac{1}{Q^2} \int dm_H^2 dm_{\bar{H}}^2 \delta\left(k_n^+ + k_{\text{us},H}^+ - \frac{m_H^2}{Q}\right) \delta\left(k_{\bar{n}}^- + k_{\text{us},\bar{H}}^- - \frac{m_{\bar{H}}^2}{Q}\right),
\end{aligned} \tag{6.28}$$

where, with the power counting of Eq.(6.27) applied, the second equality makes sure that the observable restricts the final state phase space to the di-jet limit. This will allow us to drop the restriction on the sum over final states, since now any state that does not correspond to a di-jet configuration will have vanishing contribution to the cross section due to the observable Eq.(6.28) having no support there.

We proceed to also factorise the measurement by introducing another dummy integration

$$1 = \int dl^+ dl^- \delta(l^+ - k_{\text{us},H}^+) \delta(l^- - k_{\text{us},\bar{H}}^-), \tag{6.29}$$

which allows us to carry out all of the remaining residual momentum integrations in Eq.(6.25) leaving us with the differential cross section

$$\begin{aligned}
\frac{d^2\sigma}{dm_H^2 dm_{\bar{H}}^2} &= \sigma_{\mathbf{2}}^{\text{LO}} H(Q) \int dl^+ dl^- \left[\sum_{X_n} \int \frac{d\Pi_{X_n}}{4\pi Q N_C} \int d^4x e^{\frac{i}{2}(m_H^2/Q - l^+)x^-} \text{tr} \left[\langle 0 | \not{n} \chi_{n,Q}(x) | X_n \rangle \langle X_n | \bar{\chi}_{n,Q} | 0 \rangle \right] \right] \\
&\quad \times \left[\sum_{X_{\bar{n}}} \int \frac{d\Pi_{X_{\bar{n}}}}{4\pi Q N_C} \int d^4y e^{\frac{i}{2}(m_{\bar{H}}^2/Q - l^-)y^+} \text{tr} \left[\langle 0 | \bar{\chi}_{\bar{n},-Q}(y) | X_{\bar{n}} \rangle \langle X_{\bar{n}} | \not{\bar{n}} \chi_{\bar{n},-Q} | 0 \rangle \right] \right] \\
&\quad \times \left[\sum_{X_{\text{us}}} \int \frac{d\Pi_{X_{\text{us}}}}{N_C} \delta(l^+ - P_{X_{\text{us},H}}^+) \delta(l^- - P_{X_{\text{us},\bar{H}}}^-) \text{Tr} \left[\langle 0 | \bar{Y}_{\bar{n}} Y_n | X_{\text{us}} \rangle \langle X_{\text{us}} | Y_n^\dagger \bar{Y}_{\bar{n}}^\dagger | 0 \rangle \right] \right] \\
&\equiv \sigma_{\mathbf{2},\epsilon=0}^{\text{LO}} H(Q, \mu) \int dl^+ dl^- J_n^{\mathbf{m}}(m_H^2 - m^2 - Ql^+, \mu) J_{\bar{n}}^{\mathbf{m}}(m_{\bar{H}}^2 - m^2 - Ql^-, \mu) S_{\text{hemi}}(l^+, l^-, \mu)
\end{aligned} \tag{6.30}$$

In the first line we can see that all of the dependence on the measurement (l^+, l^-) is now contained in the soft sector and the Fourier exponent of the collinear sectors. This in turn implies that the collinear matrix elements are universal so that they can be computed independently of the observable under consideration. In the second line we have introduced convenient notation for each sector. The jet functions $J_n^{\mathbf{m}}(m_H^2 - m^2 - Ql^+, \mu), J_{\bar{n}}^{\mathbf{m}}(m_{\bar{H}}^2 - m^2 - Ql^-, \mu)$ for primary quarks of mass m capture the dynamics of n, \bar{n} -collinear particles inside the jets and can be calculated perturbatively. The hemisphere soft function $S_{\text{hemi}}(l^+, l^-, \mu)$ represents the cross talk between the collinear sectors through usoft radiation. From its definition we see that it is independent of the primary quark masses. The arguments and normalisations are chosen such that

$$\begin{aligned}
H(Q, \mu) &= 1, & S_{\text{hemi}}(l^+, l^-) &= \delta(l^+) \delta(l^-), \\
J_n^{\mathbf{m}}(m_H^2 - m^2 - Ql^+) &= \delta(m_H^2 - m^2 - Ql^+), & J_{\bar{n}}^{\mathbf{m}}(m_{\bar{H}}^2 - m^2 - Ql^-) &= \delta(m_{\bar{H}}^2 - m^2 - Ql^-),
\end{aligned} \tag{6.31}$$

at tree level since there is no additional usoft radiation ($l^+ = l^- = 0$) possible and the hemisphere momenta are simply given by the primary (anti-)quark momenta.

The fact that the sums over final states in Eq.(6.30) are now unrestricted enables us to use the generalised optical theorem (see chapter 24 in [23]) to bring the jet functions into a form suitable for direct evaluation. Concretely we can relate the sum over collinear matrix elements to the imaginary part of the corresponding forward scattering amplitude, which in our case is just a vacuum matrix

element, and therefore

$$\begin{aligned} J_n^{\mathbf{m}}(Qk_n^+ - m^2, \mu) &= \frac{-1}{4\pi N_C Q} \text{Disc} \left\{ \int d^4x e^{\frac{i}{2}k_n^+ x^-} \text{tr} \left[\langle 0 | \mathbf{T} \left\{ \bar{\chi}_{n,Q}(0) \frac{\not{x}}{2} \chi_{n,Q}(x) \right\} | 0 \rangle \right] \right\}, \\ J_{\bar{n}}^{\mathbf{m}}(Qk_{\bar{n}}^- - m^2, \mu) &= \frac{1}{4\pi N_C Q} \text{Disc} \left\{ \int d^4y e^{\frac{i}{2}k_{\bar{n}}^- y^+} \text{tr} \left[\langle 0 | \mathbf{T} \left\{ \bar{\chi}_{\bar{n},-Q}(y) \frac{\not{y}}{2} \chi_{\bar{n},-Q}(0) \right\} | 0 \rangle \right] \right\}, \end{aligned} \quad (6.32)$$

where \mathbf{T} denotes time-ordering and the different signs between sectors arise from anti-commuting the jet fields into the same order. For the hemisphere mass distributions the momenta $k_n^+ = \frac{m_H^2}{Q} - l^+$, $k_{\bar{n}}^- = \frac{m_{\bar{H}}^2}{Q} - l^-$ are dictated by the observable and physically correspond to the residual momenta of each collinear sector. Finally, the discontinuity of the amplitude is related to its imaginary part via $\text{Disc} \{ \mathcal{M} \} = 2\text{Im} \{ i\mathcal{M} \}$ (see discussion below Eq.(7.14)).

With the main result Eq.(6.30) of this section in hand, it is now straightforward to specify to thrust, which in the di-jet region is related to the hemisphere masses via Eq.(5.10). We thus insert the thrust measurement using the identity

$$1 = \int d\tau \delta\left(\tau - \frac{m_H^2 + m_{\bar{H}}^2}{Q^2}\right), \quad (6.33)$$

into Eq.(6.30) and integrate over the hemisphere masses to obtain

$$\begin{aligned} \frac{d\sigma}{d\tau} &= \sigma_{2,\epsilon=0}^{\mathbf{LO}} H(Q, \mu) \int dk_n^+ dk_{\bar{n}}^- dl^+ dl^- dm_H^2 dm_{\bar{H}}^2 \delta\left(\tau - \frac{m_H^2 + m_{\bar{H}}^2}{Q^2}\right) \\ &\times \delta\left(k_n^+ + l^+ - \frac{m_H^2}{Q}\right) \delta\left(k_{\bar{n}}^- + l^- - \frac{m_{\bar{H}}^2}{Q}\right) J_n^{\mathbf{m}}(Qk_n^+ - m^2, \mu) J_{\bar{n}}^{\mathbf{m}}(Qk_{\bar{n}}^- - m^2, \mu) S_{\text{hemi}}(l^+, l^-, \mu), \end{aligned} \quad (6.34)$$

where we have also made the hemisphere mass measurement explicit by reinstating the integrations over $k_n^+, k_{\bar{n}}^-$ from Eq.(6.25). We introduce one more dummy variable

$$1 = \int dl \delta(l - l^+ - l^-), \quad (6.35)$$

which can be interpreted as the total momentum of the usoft radiation emitted into either hemisphere and carry out the integral over the hemisphere masses which gives

$$\begin{aligned} \frac{d\sigma}{d\tau} &= \sigma_{2,\epsilon=0}^{\mathbf{LO}} H(Q, \mu) \int dl \left[\int dk_n^+ dk_{\bar{n}}^- \delta\left(\tau - \frac{k_{\bar{n}}^-}{Q} - \frac{k_n^+}{Q} - \frac{l}{Q}\right) J_n^{\mathbf{m}}(Qk_n^+ - m^2, \mu) J_{\bar{n}}^{\mathbf{m}}(Qk_{\bar{n}}^- - m^2, \mu) \right] \\ &\times \left[\int dl^+ dl^- \delta(l - l^+ - l^-) S_{\text{hemi}}(l^+, l^-, \mu) \right] \equiv \sigma_{2,\epsilon=0}^{\mathbf{LO}} H(Q, \mu) \int dl J_{\tau}^{\mathbf{m}}\left(\tau - \frac{2m^2}{Q^2} - \frac{l}{Q}, \mu\right) S_{\tau}(l, \mu), \end{aligned} \quad (6.36)$$

thus establishing the factorisation theorem for thrust. The jet and soft functions for thrust are obtained by taking symmetric convolutions of the corresponding hemisphere quantities as shown in Eq.(6.36) and at tree level give

$$S_{\tau}(l, \mu) = \delta(l), \quad J_{\tau}^{\mathbf{m}}\left(\tau - \frac{2m^2}{Q^2} - \frac{l}{Q}, \mu\right) = \delta\left(\tau - \frac{2m^2}{Q^2} - \frac{l}{Q}\right), \quad (6.37)$$

which immediately follows from Eq.(6.31) and Eq.(6.33).

Let us briefly discuss the physical interpretation of the factorisation theorem. Explicitly implementing the delta functions in Eq.(6.36) allows us to better see how the **hard**, ***n*-collinear**, ***n̄*-collinear**,

and **usoft** degrees of freedom enter into the various factorisation functions,

$$\begin{aligned} \frac{d\sigma}{d\tau} &= \sigma_2^{\text{LO}} H(Q, \mu) \int dl \, dl^+ dl^- dk_n^+ dk_{\bar{n}}^- \delta\left(\tau - \frac{k_{\bar{n}}^-}{Q} - \frac{k_n^+}{Q} - \frac{l}{Q}\right) \delta(l - l^+ - l^-) \\ &\times J_n^{\text{m}}(Q^2\tau - m^2 - Qk_{\bar{n}}^- - Ql, \mu) J_{\bar{n}}^{\text{m}}(Q^2\tau - m^2 - Qk_n^+ - Ql, \mu) \\ &\times S_{\text{hemi}}(Q\tau - k_{\bar{n}}^- - k_n^+ - l^-, Q\tau - k_{\bar{n}}^- - k_n^+ - l^+, \mu). \end{aligned} \quad (6.38)$$

To start with we consider the argument of the n -collinear jet function $J_n^{\text{m}}(Q^2\tau_n)$ which reads

$$Q^2\tau_n = Q^2\tau - m^2 - Qk_{\bar{n}}^- - Ql. \quad (6.39)$$

In the context of an event which has total thrust τ , we can interpret Eq.(6.39) as roughly the invariant mass (squared) of an n -collinear jet that was initiated by a quark of mass m . The contribution $Q^2\tau_n$ due to this jet must then be the total thrust of the event $Q^2\tau$ from which any contributions to the n -collinear direction coming from other sectors ($Qk_{\bar{n}}^-$, Ql) are removed. Conventionally we also subtract the primary quark mass m since we want to think of $Q^2\tau_n$ as the invariant mass solely due to n -collinear radiation off said quark. Similar interpretations can be applied to the arguments of the \bar{n} -collinear jet function $J_{\bar{n}}^{\text{m}}(Q^2\tau_{\bar{n}})$ and the hemisphere soft function $S_{\text{hemi}}(Q\tau_{\text{us}}^+, Q\tau_{\text{us}}^-)$ featuring in Eq.(6.38). Putting all of this together, the physical content of the factorisation theorem is that the probability of observing an event with thrust $\tau \ll 1$ is obtained as the product of

- (i), the probability density to find an n -collinear jet with invariant mass $Q^2\tau_n$ given by J_n^{m} times
- (ii), the probability density to find an \bar{n} -collinear jet with invariant mass $Q^2\tau_{\bar{n}}$ given by $J_{\bar{n}}^{\text{m}}$ times
- (iii), the probability density of having usoft radiation with invariant mass $Q\tau_{\text{us}}^-(Q\tau_{\text{us}}^+)$ emitted into hemisphere $H(\overline{H})$ given by S_{hemi} , integrated over all values of k_n^+ , $k_{\bar{n}}^-$, l^+ , l^- consistent with the measured value of τ imposed by the delta function in Eq.(6.38). All of this is multiplied by the universal function $H(Q)$ which specifies how the original $q\bar{q}$ -pair was produced in the hard QCD interaction. This recipe holds to all orders in α_s up to power corrections of $\mathcal{O}(\mu_s/\mu_j)$, $\mathcal{O}(\Lambda_{\text{QCD}}/\mu_h)$, which involve the characteristic scales of each sector whose significance we will outline in the next section.

With the factorisation theorem firmly established, we will now proceed to compute the hemisphere jet functions for massive and massless primary quarks at NLO and state results for the hemisphere soft- as well as the hard function.

7 NLO ingredients for the factorisation theorem

Having derived the factorisation theorems for hemisphere masses Eq.(6.30) and thrust Eq.(6.36) we want to focus now on calculating the various factorisation functions appearing in them at NLO.

From the results we will see that each factorisation function should be evaluated at a characteristic scale to avoid the appearance of large logarithms. These scales will turn out to be

$$\begin{aligned} H(Q, \mu_h) &\leftrightarrow \mu_h \simeq Q, \\ J_n^{\mathbf{m}}(Qk_n^+ - m^2, \mu_j), J_n^{\mathbf{m}}(Qk_n^- - m^2, \mu_j) &\leftrightarrow \mu_j \simeq m \simeq \sqrt{\tau}Q, \\ S_{\text{hemi}}(l^+, l^-, \mu_s) &\leftrightarrow \mu_s \simeq m^2/Q \simeq \tau Q, \end{aligned} \quad (7.1)$$

which could have been estimated on general grounds from the arguments the individual factorisation functions are assigned by the factorisation theorem in Eq.(6.38).

In a resummed calculation (see [28, 29]) these different scales would be evolved to a common one using the renormalisation group equation (RGE) associated with each factorisation function. This leads to the resummation of logarithmically enhanced terms and a qualitative agreement with experiment as discussed in Sec. 4.2, up to the inclusion of non-perturbative hadronisation effects. These can in fact also be accommodated by the factorisation theorem by splitting the soft function

$$S_{\text{hemi}}(l^+, l^-, \mu) = \int d\tilde{l}^+ d\tilde{l}^- S_{\text{hemi}}^{\text{pert}}(l^+ - \tilde{l}^+, l^- - \tilde{l}^-, \mu) S_{\text{hemi}}^{\text{mod}}(\tilde{l}^+, \tilde{l}^-), \quad (7.2)$$

into a perturbatively calculable part $S_{\text{hemi}}^{\text{pert}}$ (assuming $\mu_s \gg \Lambda_{\text{QCD}}$) and a model soft function $S_{\text{hemi}}^{\text{mod}}$ (see [13]) encoding the dynamics at the non-perturbative scale, which for the purposes of this thesis we can ignore.

Lastly we want to remark on the dependence of the factorisation theorem on the primary quark mass m , which is entirely contained in the jet function Eq.(6.32). In particular we see that the threshold, i.e. where the argument of the function vanishes, of the massless jet function $J_n^{\mathbf{m}=0}(Qk_n^+)$ is shifted by m^2 compared to the massive jet function $J_n^{\mathbf{m}}(Qk_n^+ - m^2)$. This is physically sound, since, as we have seen, the jet function should be interpreted as proportional to the probability density of producing a n -collinear jet with invariant mass given by its argument. For a primary quark of mass m we therefore need at least $k_n^+ = m^2/Q$ to produce the leading order configuration where the jet is formed only by that quark, whereas for a massless quark the jet can have arbitrarily low invariant mass. Indeed, the final results will show that the jet functions will only have support above their respective thresholds. This is nicely consistent with the factorisation theorem Eq.(6.38) in that having both jet functions above threshold implies

$$\tau \geq \frac{2m^2}{Q^2}, \quad (7.3)$$

and the inequality is saturated precisely at threshold where only the leading order $q\bar{q}$ -pair and no additional radiation is produced.

7.1 Hard and hemisphere soft functions

The hard function featuring in the factorisation theorem Eq.(6.30) is obtained by squaring the Wilson coefficient of the effective current Eq.(6.6) which in turn is computed by matching QCD onto SCET, i.e. requiring that the effective theory reproduces the full theory matrix element at leading power,

$$\langle q\bar{q} | \mathcal{J}_v^\mu(0) | 0 \rangle_{\text{QCD}} = C^{(0)}(Q, \mu) \langle q\bar{q} | J_v^\mu(0) | 0 \rangle_{\text{SCET}} \stackrel{!}{=} 0 + \mathcal{O}(\lambda^2). \quad (7.4)$$

At next-to-leading order in α_s this determines the bare Wilson coefficient

$$C^{(0)}(Q, \mu) = 1 + \frac{\alpha_s C_F}{4\pi} \left(\frac{\mu^2}{-Q^2 - i0} \right)^\epsilon \left\{ -\frac{2}{\epsilon^2} - \frac{3}{\epsilon} - 8 + \frac{\pi^2}{6} \right\}, \quad (7.5)$$

which still needs to be renormalised, using e.g. the $\overline{\text{MS}}$ -scheme for which the renormalisation condition and factor read

$$\text{fin} \left\{ C^{(0)}(Q, \mu) - Z_C^{\overline{\text{MS}}} C(Q, \mu) \right\} \stackrel{!}{=} 0 \Rightarrow Z_C^{\overline{\text{MS}}} = 1 + \frac{\alpha_s C_F}{4\pi} \left\{ -\frac{2}{\epsilon^2} - \frac{3}{\epsilon} - \frac{2}{\epsilon} \log \left(\frac{\mu^2}{-Q^2 - i0} \right) \right\}, \quad (7.6)$$

The renormalisation condition should be read as to state that the finite parts of the bare and renormalised quantity must coincide. Finally the hard function is obtained from the renormalised Wilson coefficient,

$$H(Q, \mu) = |C(Q, \mu)|^2 = 1 + \frac{\alpha_s C_F}{4\pi} \left[-16 + \frac{7\pi^2}{3} + 6 \log \left(\frac{Q^2}{\mu^2} \right) - 2 \log^2 \left(\frac{Q^2}{\mu^2} \right) \right]. \quad (7.7)$$

See [28, 29] for a detailed calculation of the above quantities.

Moving on to the hemisphere soft function, at next-to-leading order the diagrams in Fig. 7.8 contribute.

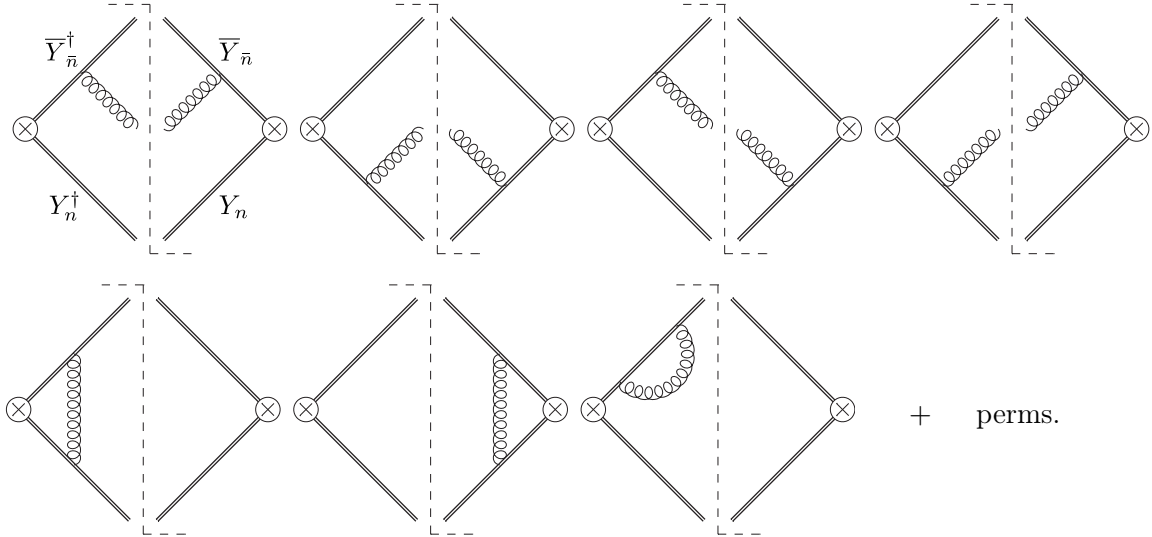


Fig. (7.8): Diagrams contributing to the SCET hemisphere soft function at $\mathcal{O}(\alpha_s)$. The usoft gluons are denoted by regular curly lines. The permutations indicate the self-energy corrections for the remaining lines.

In fact most of the above diagrams can be shown to vanish. The non-trivial contributions only involve the interference between Wilson lines associated with different collinear sectors, as we might have expected from our observation in Eq.(2.39). Computing them using the Cutkosky cutting rules gives a bare soft function

$$S_{\text{hemi}}^{(0)}(l^+, l^-) = \delta(l^+) \delta(l^-) + \frac{\alpha_s C_F}{\pi} \left\{ \left[-\frac{1}{\epsilon^2} + \frac{\pi^2}{12} \right] \delta(l^+) \delta(l^-) + \frac{1}{\epsilon} \left[\delta(l^-) \left[\frac{\theta(l^+) \mu}{l^+} \right]_+ + \delta(l^+) \left[\frac{\theta(l^-) \mu}{l^-} \right]_+ \right] \right. \\ \left. + 2 \left[\delta(l^-) \left[\frac{\theta(l^+) \log(l^+/\mu) \mu}{l^+} \right]_+ + \delta(l^+) \left[\frac{\theta(l^-) \log(l^-/\mu) \mu}{l^-} \right]_+ \right] \right\}, \quad (7.9)$$

which, since we are dealing with a distribution, now needs to be renormalised through an appropriate convolution

$$\text{fin} \left\{ S_{\text{hemi}}^{(0)}(l^+, l^-) - \int d\tilde{l}^+ d\tilde{l}^- Z_S^{\overline{\text{MS}}}(l^+ - \tilde{l}^+, l^- - \tilde{l}^-) S_{\text{hemi}}(\tilde{l}^+, \tilde{l}^-) \right\} \stackrel{!}{=} 0, \quad (7.10)$$

leading to an $\overline{\text{MS}}$ renormalisation factor

$$Z_S^{\overline{\text{MS}}}(l^+, l^-) = \delta(l^+) \delta(l^-) + \frac{\alpha_s C_F}{\pi} \left\{ -\frac{1}{\epsilon^2} \delta(l^+) \delta(l^-) + \frac{1}{\epsilon} \left[\delta(l^-) \left[\frac{\theta(l^+) \mu}{l^+} \right]_+ + \delta(l^+) \left[\frac{\theta(l^-) \mu}{l^-} \right]_+ \right] \right\}. \quad (7.11)$$

Together with the hemisphere jet functions which we will compute in the next section in more detail, the result Eq.(7.7) and the renormalised version of Eq.(7.9) can be used inside the factorisation theorem to recover the fixed order thrust distribution in the region $\tau \sim 0$.

7.2 Massive next-to-leading order SCET jet function

As derived in Eq.(6.32) the (n -collinear) SCET jet function is given as the discontinuity of a time-ordered product involving the quark jet fields $\chi_{n,\alpha}^a = W_n^\dagger \xi_{n,\alpha}^a$, with the collinear Wilson line given as the adjoint of Eq.(5.61) and the collinear quark field Eq.(5.78) after the usoft decoupling transformation. In terms of these quantities the jet function for a n -collinear primary quark of mass m takes the form

$$\begin{aligned} J_n^{\mathbf{m}}(s) &\equiv J_n^{\mathbf{m}}(Qp^+ - m^2) \equiv \frac{1}{4\pi N_C(\bar{n} \cdot p)} \text{Disc} \{ \mathcal{M}_n^{\mathbf{m}}(s) \} \\ &= \frac{1}{4\pi N_C(\bar{n} \cdot p)} \text{Disc} \left\{ \frac{\not{n}^{\alpha\beta}}{2} \delta^{ab} \int d^4x e^{\frac{i}{2} p^+ x^-} \langle 0 | \mathbf{T} \left\{ \chi_{n,\beta}^b(x) \bar{\chi}_{n,\alpha}^a(0) \right\} | 0 \rangle \right\}, \end{aligned} \quad (7.12)$$

where compared to Eq.(6.32) we have made all colour and spinor indices explicit and assume the quark to carry momentum p^μ such that $p^- = \bar{n} \cdot p = Q$. In Eq.(7.12) we have also introduced the convenient short-hand $\mathcal{M}_n^{\mathbf{m}}(s)$ for the jet matrix element and the off-shellness variable $s = p^2 - m^2$. We also recall that in deriving the factorisation theorem we have aligned the collinear momentum along the thrust axis so that $p^2 = p^+ p^- = Qp^+$ and $\mathbf{p}_\perp = \mathbf{0}$. Subsequently we will use the various notations for the argument of the jet function $J_n^{\mathbf{m}}(p^\mu, m) \equiv J_n^{\mathbf{m}}(Qp^+ - m^2) \equiv J_n^{\mathbf{m}}(p^2 - m^2) \equiv J_n^{\mathbf{m}}(s)$ where appropriate for the current purpose. At next-to-leading order the diagrams shown in Fig. 7.13 contribute to the jet function matrix element $\mathcal{M}_n^{\mathbf{m}}(s)$.

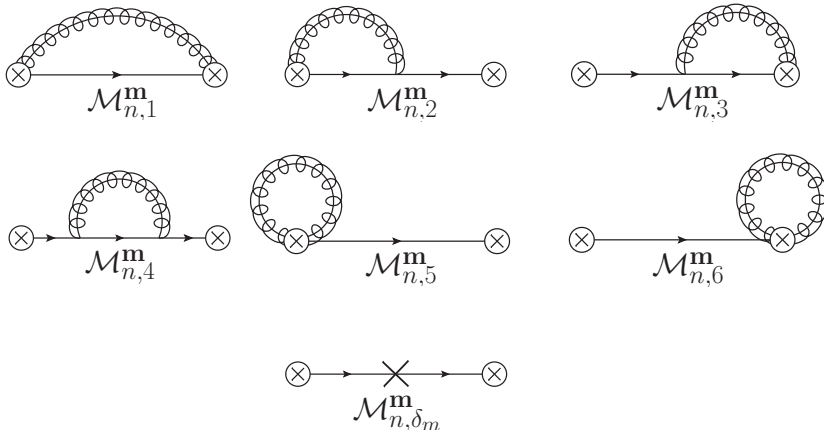


Fig. (7.13): Diagrams contributing to the SCET jet function at $\mathcal{O}(\alpha_s)$. Apart from the mass counter term $J_{\delta m}$ the same diagrams need to be considered for massive and massless primary quarks. n -collinear gluons are depicted as curly lines with a straight central line.

We would like to compute the contribution of each diagram to the jet function separately, hence we write Eq.(7.12) as

$$J_n^{\mathbf{m}}(s) = \sum_i J_{n,i}^{\mathbf{m}}(s) = \frac{1}{4\pi N_C (\bar{n} \cdot p)} \sum_i \text{Disc} \{ \mathcal{M}_{n,i}^{\mathbf{m}}(s) \}, \quad (7.14)$$

with the sum over all diagrammatic contributions i starting at leading order. Since the jet matrix element satisfies $\mathcal{M}_n^{\mathbf{m}}(s+i0) = \mathcal{M}_n^{\mathbf{m}}(s-i0)^*$ (a property satisfied by any analytic function that takes real values along the real axis) its discontinuity is related to the imaginary part by

$$\text{Disc} \{ \mathcal{M}_n^{\mathbf{m}}(s) \} = 2\text{Im}\{i\mathcal{M}_n^{\mathbf{m}}(s)\}, \quad (7.15)$$

hence we may use the equivalent expansion for the jet function

$$J_n^{\mathbf{m}}(s) = \sum_i J_{n,i}^{\mathbf{m}}(s) = \frac{1}{2\pi N_C (\bar{n} \cdot p)} \sum_i \text{Im}\{i\mathcal{M}_{n,i}^{\mathbf{m}}(s)\} \equiv \sum_i \text{Im}\{\tilde{J}_{n,i}^{\mathbf{m}}(s)\}. \quad (7.16)$$

In the discussion to follow we will call the quantities on the left-hand side of Eq.(7.16) (the $J_{n,i}^{\mathbf{m}}$'s) contributions to the jet function and the quantities on the right-hand side (the $\tilde{J}_{n,i}^{\mathbf{m}}$'s) contributions to the jet correlator. The former are simply given as the imaginary part of the latter.

7.3 Evaluation of diagrams using cutting rules

The computation of the diagrams Fig. 7.13 contributing to the jet function is carried out using the conventional QCD Feynman rules supplemented by the additional Wilson line vertices arising in SCET. This can be shown to reproduce the results following from the SCET Feynman rules derived directly from the Lagrangian Eq.(5.81)[38]. The dimensional regularisation prescriptions employed are outlined in App. B. For computational convenience all calculations are carried out in Feynman gauge ($\xi = 1$ in Eq.(H.3)). Since, by Eq.(7.14), the jet function asks us to compute the discontinuity of each matrix element $\mathcal{M}_{n,i}^{\mathbf{m}}$ it makes sense to employ the Cutkosky cutting rules (see [39, 40] or chapter 24 in [23]).

Double Wilson line contribution $J_{n,1}^{\mathbf{m}}$

The (double) Wilson line matrix element $\mathcal{M}_{n,1}^{\mathbf{m}}$ vanishes exactly in Feynman gauge, since it is proportional to $\bar{n}^2 = 0$. For the purposes of this calculation we do not have to further concern ourselves with it.

Single Wilson line contribution $J_{n,2}^{\mathbf{m}}$

The first non-trivial contribution comes from the (single) Wilson line diagram $\mathcal{M}_{n,2}^{\mathbf{m}}$. Using the Feynman rules as indicated above we can write down the jet matrix element,

$$\begin{aligned} \mathcal{M}_{n,2}^{\mathbf{m}} &= \text{Tr} \left[\frac{i(\not{p} + m)}{p^2 - m^2 + i0} (ig_s \tilde{\mu}^\epsilon T^A \gamma^\mu) \int d^d k \frac{i(\not{p} - \not{k} + m)}{(p-k)^2 - m^2 + i0} \frac{\not{\bar{n}}}{2} \right] \left(\frac{-ig_{\mu\nu} \delta^{AB}}{k^2 + i0} \right) (g_s \tilde{\mu}^\epsilon T^B) \frac{\bar{n}^\nu}{\bar{n} \cdot k + i0} \\ &= -4g_s^2 C_F N_C \tilde{\mu}^{2\epsilon} \frac{\bar{n} \cdot p}{p^2 - m^2 + i0} \int d^d k \frac{\bar{n} \cdot (p-k)}{[(p-k)^2 - m^2 + i0][k^2 + i0][\bar{n} \cdot k + i0]}. \end{aligned} \quad (7.17)$$

According to the Cutkosky cutting rules the discontinuity of the above amplitude splits into a real ($\mathcal{M}_{n,2}^{\mathbf{m},\mathbf{r}}$) and virtual ($\mathcal{M}_{n,2}^{\mathbf{m},\mathbf{v}}$) part. Correspondingly we get two contributions to the jet function

$$\text{Disc} \{ \mathcal{M}_{n,2}^{\mathbf{m}} \} \equiv \mathcal{M}_{n,2}^{\mathbf{m},\mathbf{r}} + \mathcal{M}_{n,2}^{\mathbf{m},\mathbf{v}} \quad \Rightarrow \quad J_{n,2}^{\mathbf{m}} = J_{n,2}^{\mathbf{m},\mathbf{r}} + J_{n,2}^{\mathbf{m},\mathbf{v}}, \quad (7.18)$$

which can also be interpreted diagrammatically by cutting the propagators as shown in Eq.(7.19),

$$\text{Disc} \left\{ \begin{array}{c} \text{Diagram with a loop and a cut} \\ \mathcal{M}_{n,2}^{\mathbf{m}} \end{array} \right\} = \begin{array}{c} \text{Diagram with a cut on the left} \\ \mathcal{M}_{n,2}^{\mathbf{m},\mathbf{r}} \end{array} \otimes \begin{array}{c} \text{Diagram with a cut on the right} \\ \mathcal{M}_{n,2}^{\mathbf{m},\mathbf{v}} \end{array}. \quad (7.19)$$

We proceed by computing the two contributions individually.

$J_{n,2}^{\mathbf{m},\mathbf{r}}$ (real emission)

The real emission cut of the amplitude is obtained by taking the quark and gluon in the loop on-shell, effectively replacing

$$\begin{aligned} \frac{1}{k^2 + i0} &\longrightarrow -2\pi i \theta(k^0) \delta(k^2), \\ \frac{1}{(p-k)^2 - m^2 + i0} &\longrightarrow -2\pi i \theta(p^0 - k^0) \delta((p-k)^2 - m^2), \end{aligned} \quad (7.20)$$

in the full amplitude $\mathcal{M}_{n,2}^{\mathbf{m}}$ of Eq.(7.17). The cut amplitude $\mathcal{M}_{n,2}^{\mathbf{m},\mathbf{r}}$ now takes the form

$$\mathcal{M}_{n,2}^{\mathbf{m},\mathbf{r}} = 16\pi^2 g_s^2 C_F N_C \frac{\bar{n} \cdot p}{p^2 - m^2 + i0} I_{n,2}^{\mathbf{m},\mathbf{r}}, \quad (7.21)$$

where the integral $I_{n,2}^{\mathbf{m},\mathbf{r}}$ we have to compute reads

$$I_{n,2}^{\mathbf{m},\mathbf{r}} = \tilde{\mu}^{2\epsilon} \int d^d k \theta(k^0) \theta(p^0 - k^0) \delta(k^2) \delta((p-k)^2 - m^2) \frac{\bar{n} \cdot (p-k)}{\bar{n} \cdot k + i0}. \quad (7.22)$$

The evaluation of the integral above will be carried out in detail here. Later integrals of a similar sort are then understood to be calculated analogously. We start by inserting the identity $1 = \int d^d l \delta^{(d)}(l - p + k)$ into the expression Eq.(7.22),

$$I_{n,2}^{\mathbf{m},\mathbf{r}} = \frac{\tilde{\mu}^{2\epsilon}}{(2\pi)^{4-2\epsilon}} \int d^d k \int d^d l \tilde{\delta}(k) \tilde{\delta}(l, m) \delta^{(d)}(l - p + k) \frac{\bar{n} \cdot l}{\bar{n} \cdot k + i0}, \quad (7.23)$$

where we have introduced the notation $\tilde{\delta}(k, m) = \theta(k^0) \delta(k^2 - m^2)$ to force the momenta onto the positive energy mass shell, and use the short-hand $\tilde{\delta}(k) = \tilde{\delta}(k, 0)$ for lightlike momenta.

This formally reduces Eq.(7.23) to an integration over the two-body phase space of the on-shell outgoing momenta k^μ and l^μ with an incoming momentum p^μ , which becomes particularly apparent when the identity $d^d l \tilde{\delta}(l, m) = \frac{d^{d-1} l}{2l^0}$ is used in which case we get

$$I_{n,2}^{\mathbf{m},\mathbf{r}} = \frac{\tilde{\mu}^{2\epsilon}}{(2\pi)^{4-2\epsilon}} \int \frac{d^{d-1} k}{2k^0} \frac{d^{d-1} l}{2l^0} \delta^{(d)}(l - p + k) \frac{\bar{n} \cdot l}{\bar{n} \cdot k + i0}. \quad (7.24)$$

However the above integral is not represented in the most useful coordinates for our purposes. Our integrand is naturally a function of the lightcone coordinates of the momenta involved, hence it makes sense to decompose the momentum conserving delta function in Eq.(7.24) as

$$\delta^{(d)}(l - p + k) = 2 \delta(l^- - p^- + k^-) \delta(l^+ - p^+ + k^+) \delta^{(d-2)}(\mathbf{l}_\perp + \mathbf{k}_\perp). \quad (7.25)$$

Here the assumption $\mathbf{p}_\perp = 0$ such that $p^2 = p^+ p^-$ was used again. We proceed by first carrying out the integration over l and eliminating delta functions¹¹,

$$\int d^d l \tilde{\delta}(l, m) \delta(l^- - p^- + k^-) \delta^{(d-2)}(\mathbf{l}_\perp + \mathbf{k}_\perp) = \frac{1}{2} \frac{\theta(p^- - k^-)}{p^- - k^-}. \quad (7.26)$$

¹¹For a derivation see App. B.

Note that this relation holds irrespective of the mass shell m^2 on which the momentum sits. As a consequence of implementing the delta functions in Eq.(7.26) the l^+ -component is fixed to

$$l^+ = \frac{\mathbf{l}_\perp^2 + m^2}{l^-} = \frac{\mathbf{k}_\perp^2 + m^2}{p^- - k^-}. \quad (7.27)$$

Applied to the integral Eq.(7.24) at hand this leaves us with a remaining integration over the gluon momentum of the form

$$I_{n,2}^{\mathbf{m},\mathbf{r}} = \frac{\tilde{\mu}^{2\epsilon}}{(2\pi)^{4-2\epsilon}} \int \frac{d^{d-1}k}{2k^0} \theta(p^- - k^-) \delta\left(\frac{\mathbf{k}_\perp^2 + m^2}{p^- - k^-} - p^+ + k^+\right) \frac{1}{k^- + i0}. \quad (7.28)$$

Using the fact that $k^2 = k^+k^- - \mathbf{k}_\perp^2 = 0$ the delta function in Eq.(7.28) can be explicitly written in terms of k^+ which gives

$$\delta\left(\frac{k^+k^- + m^2}{p^- - k^-} - p^+ + k^+\right) = \frac{p^- - k^-}{p^-} \delta\left(k^+ - \frac{p^+}{p^-}(p^- - k^-) + \frac{m^2}{p^-}\right). \quad (7.29)$$

Together with the lightcone decomposition of the phase space integration measure in Eq.(A.7) the integral Eq.(7.28) can be written as

$$\begin{aligned} I_{n,2}^{\mathbf{m},\mathbf{r}} &= \frac{\tilde{\mu}^{2\epsilon}}{(2\pi)^{4-2\epsilon}} \frac{\pi^{1-\epsilon}}{2\Gamma(1-\epsilon)} \frac{1}{p^-} \int dk^+ dk^- \frac{\theta(k^+)\theta(k^-)\theta(p^- - k^-)}{(k^+k^-)^\epsilon} \delta\left(k^+ - \frac{p^+}{p^-}(p^- - k^-) + \frac{m^2}{p^-}\right) \frac{p^- - k^-}{k^-} \\ &= \frac{\tilde{\mu}^{2\epsilon}}{(2\pi)^{4-2\epsilon}} \frac{\pi^{1-\epsilon}}{2\Gamma(1-\epsilon)} \frac{1}{p^-} \int dk^- \frac{\theta(p^2 - m^2 - p^+k^-)\theta(k^-)\theta(p^- - k^-)}{\left((p^2 - m^2 - p^+k^-)\frac{k^-}{p^-}\right)^\epsilon} \frac{p^- - k^-}{k^-}. \end{aligned} \quad (7.30)$$

Note that the $i0$ prescription can be dropped at this point since the lightcone propagator $(k^- + i0)^{-1}$ is dimensionally regulated by the phase space measure. Rewriting the expression in terms of the off-shellness variable $s = p^2 - m^2$ and changing variables to $k^- = \frac{s}{p^+}a^-$, where a^- is now a dimensionless parameter, the step functions in Eq.(7.30) imply

$$\theta(s - p^+k^-)\theta(k^-)\theta(p^- - k^-) = \theta(1 - a^-)\theta(a^-)\theta(p^-)\theta(s), \quad (7.31)$$

leaving us with a single, straightforward final integral

$$\begin{aligned} I_{n,2}^{\mathbf{m},\mathbf{r}} &= \frac{\tilde{\mu}^{2\epsilon}}{(2\pi)^{4-2\epsilon}} \frac{\pi^{1-\epsilon}}{2\Gamma(1-\epsilon)} \frac{\theta(p^-)\theta(s)}{s + m^2} \left(\frac{s + m^2}{s^2}\right)^\epsilon \int_0^1 da^- \frac{(1 - a^-)s + m^2}{(a^-)^{1+\epsilon}(1 - a^-)^\epsilon} \\ &= \frac{\tilde{\mu}^{2\epsilon}}{(2\pi)^{4-2\epsilon}} \frac{\pi^{1-\epsilon}}{2} \left(\frac{s + m^2}{s^2}\right)^\epsilon \frac{\Gamma(-\epsilon)}{\Gamma(2 - 2\epsilon)} \theta(p^-)\theta(s) \left[(1 - 2\epsilon) + \frac{s}{s + m^2} \epsilon\right], \end{aligned} \quad (7.32)$$

which is best carried out using **Mathematica**. Plugging this back into Eq.(7.21) yields the final result for the real emission contribution

$$\mathcal{M}_{n,2}^{\mathbf{m},\mathbf{r}} = 2\alpha_s C_F N_C p^- \theta(p^-) \left[\frac{e^{\gamma_E}(s + m^2)}{\mu^2} \right]^\epsilon \frac{\Gamma(-\epsilon)}{\Gamma(2 - 2\epsilon)} \left[\frac{\theta(s)\mu^{4\epsilon}}{s^{1+2\epsilon}}(1 - 2\epsilon) + \frac{\theta(s)\mu^{4\epsilon}}{s^{2\epsilon}} \frac{1}{s + m^2} \epsilon \right]. \quad (7.33)$$

For ϵ close to zero ($|\epsilon| < \frac{1}{2}$) we see that there is an additional singularity in Eq.(7.33) for $s \rightarrow 0$. Since the limit $\epsilon \rightarrow 0$ has to be taken eventually, we regularise this singularity by replacing the offending factor $\frac{1}{s^{1+2\epsilon}}$ with an ϵ -expansion in plus-distributions¹²,

$$\frac{\theta(s)\mu^{2a\epsilon}}{s^{1+a\epsilon}} = -\frac{1}{a\epsilon}\delta(s) + \frac{1}{\mu^2} \left[\frac{\mu^2\theta(s)}{s} \right]_+ - \frac{a\epsilon}{\mu^2} \left[\frac{\mu^2\theta(s)\log(s/\mu^2)}{s} \right]_+ + \mathcal{O}(\epsilon^2). \quad (7.34)$$

¹²For a detailed definition of plus-distributions see App. I.

Adding to Eq.(7.33) the prefactor from our definition of the jet function Eq.(7.14) and expanding to constant order in ϵ we obtain

$$J_{n,2}^{\mathbf{m},\mathbf{r}} = \frac{\alpha_s C_F}{4\pi} \theta(p^-) \left\{ \left[\frac{1}{\epsilon^2} - \frac{1}{\epsilon} \log\left(\frac{\mu^2}{m^2}\right) - \frac{\pi^2}{4} + \frac{1}{2} \log^2\left(\frac{\mu^2}{m^2}\right) \right] \delta(s) - \left[\frac{1}{\epsilon} - \log\left(\frac{\mu^2}{m^2}\right) \right] \frac{2}{\mu^2} \left[\frac{\mu^2 \theta(s)}{s} \right]_+ \right. \\ \left. + \frac{4}{\mu^2} \left[\frac{\mu^2 \theta(s) \log(s/\mu^2)}{s} \right]_+ - 2\theta(s) \left[\frac{1}{s+m^2} + \frac{1}{s} \log\left(1 + \frac{s}{m^2}\right) \right] \right\}, \quad (7.35)$$

giving the final result for the real emission contribution to the jet function coming from $\mathcal{M}_{n,2}^{\mathbf{m}}$. In arriving at the result in Eq.(7.35) we made use of the distributional identity

$$\log\left(1 + \frac{s}{m^2}\right) \frac{1}{\mu^2} \left[\frac{\mu^2 \theta(s)}{s} \right]_+ = \frac{\theta(s)}{s} \log\left(1 + \frac{s}{m^2}\right), \quad (7.36)$$

which therefore corresponds to a finite contribution to the jet function as $s \rightarrow 0$.

$J_{n,2}^{\mathbf{m},\mathbf{v}}$ (virtual contribution)

The virtual cut contribution is obtained by cutting the single collinear quark propagator as indicated in Eq.(7.19). This amounts to making the replacement

$$\frac{1}{s+i0} \longrightarrow -2\pi i \theta(p^0) \delta(s), \quad (7.37)$$

in the original amplitude Eq.(7.17), which leads to a virtual contribution of the form

$$\mathcal{M}_{n,2}^{\mathbf{m},\mathbf{v}} = 8\pi i g_s^2 C_F N_C \theta(p^0) \delta(s) p^- I_{n,2}^{\mathbf{m},\mathbf{v}}, \quad (7.38)$$

with the on-shell ($p^2 = m^2$) loop integral to be evaluated given by

$$I_{n,2}^{\mathbf{m},\mathbf{v}} = \tilde{\mu}^{2\epsilon} \int d^d k \frac{p^- - k^-}{[k^2 - 2p \cdot k + i0] [k^2 + i0] [k^- + i0]}. \quad (7.39)$$

Note that since we assume n -collinear scaling of the external quark momentum we have $p^0 = \frac{p^-}{2} + \mathcal{O}(\lambda^2)$, and can thus consistently set $\theta(p^0) = \theta(p^-)$.

We begin the evaluation of Eq.(7.39) by rewriting it in terms of lightcone coordinates using the decomposition Eq.(A.6). This gives us

$$I_{n,2}^{\mathbf{m},\mathbf{v}} = \frac{\tilde{\mu}^{2\epsilon}}{(2\pi)^{4-2\epsilon}} \frac{\pi^{1-\epsilon}}{2\Gamma(1-\epsilon)} \int \frac{dk^+ dk^- d(\mathbf{k}_\perp^2) \theta(\mathbf{k}_\perp^2) (\mathbf{k}_\perp^2)^{-\epsilon} (p^- - k^-)}{[k^+(k^- - p^-) - p^+ k^- - \mathbf{k}_\perp^2 + i0] [k^+ k^- - \mathbf{k}_\perp^2 + i0] [k^- + i0]}, \quad (7.40)$$

where the solid angle integration was already performed according to Eq.(B.1). The integration over k^+ will now be carried out by application of the residue theorem.

Let us take a closer look at the pole structure of the integrand in the complex k^+ -plane. We find two simple poles at the locations

$$\begin{aligned} \text{(i)} \quad k^+ &= \frac{\mathbf{k}_\perp^2}{k^-} - \frac{i0}{k^-}, \\ \text{(ii)} \quad k^+ &= -\frac{\mathbf{k}_\perp^2 + p^+ k^-}{p^- - k^-} + \frac{i0}{p^- - k^-}. \end{aligned} \quad (7.41)$$

We see that the two poles lie on the same half plane unless we have $0 < k^- < p^-$, which implies that the integral will vanish by Cauchy's integral theorem if we do not impose the previous condition. Since

we are looking for a non-trivial result we apply the restriction to k^- , close the contour in the upper half k^+ -plane, thereby picking up the pole corresponding to (ii) in Eq.(7.41), and find the residue

$$R_{n,2}^{\mathbf{m},\mathbf{v}}(p^\mu, k^-, \mathbf{k}_\perp^2) = \text{Res}\left(k^+ = -\frac{\mathbf{k}_\perp^2 + p^+ k^-}{p^- - k^-} + i0\right) = -\frac{\theta(\mathbf{k}_\perp^2)\theta(k^-)\theta(p^- - k^-)(\mathbf{k}_\perp^2)^{-\epsilon}(p^- - k^-)}{[-\mathbf{k}_\perp^2 p^- - (k^-)^2 p^+ + i0][k^- + i0]}. \quad (7.42)$$

With the k^+ integration carried out, the integral in Eq.(7.40) becomes

$$I_{n,2}^{\mathbf{m},\mathbf{v}} = \frac{\tilde{\mu}^{2\epsilon}}{(2\pi)^{4-2\epsilon}} \frac{\pi^{1-\epsilon}}{2\Gamma(1-\epsilon)} \int dk^- d(\mathbf{k}_\perp^2) (2\pi i) R_{n,2}^{\mathbf{m},\mathbf{v}}(k^-, \mathbf{k}_\perp^2). \quad (7.43)$$

Noting that the $i0$ prescription in the propagator involving \mathbf{k}_\perp^2 can be dropped since the denominator is manifestly non-vanishing, we proceed by carrying out the \mathbf{k}_\perp^2 integration which yields

$$\int_0^\infty d(\mathbf{k}_\perp^2) \frac{(\mathbf{k}_\perp^2)^{-\epsilon}}{\mathbf{k}_\perp^2 p^- + (k^-)^2 p^+} = \frac{1}{p^-} \left(\frac{p^-}{p^+}\right)^\epsilon (k^-)^{-2\epsilon} \Gamma(\epsilon) \Gamma(1-\epsilon). \quad (7.44)$$

Leaving the k^- integral for last, we make the convenient change of variables $k^- = p^- a^-$ to obtain

$$\int_0^1 da^- \frac{1 - a^-}{(a^-)^{1+2\epsilon}} = -\frac{1}{2\epsilon(1-2\epsilon)}. \quad (7.45)$$

Plugging expressions Eq.(7.44), Eq.(7.45) back into Eq.(7.43) the overall result for the integral reads

$$I_{n,2}^{\mathbf{m},\mathbf{v}} = \frac{-i}{16\pi^2} \left(\frac{4\pi\tilde{\mu}^2}{m^2}\right)^\epsilon \frac{\Gamma(\epsilon)}{2\epsilon(1-2\epsilon)}. \quad (7.46)$$

Reinstating all the necessary prefactors from Eq.(7.38) to get the full result for the virtual cut we arrive at

$$\mathcal{M}_{n,2}^{\mathbf{m},\mathbf{v}} = \alpha_s C_F N_C p^- \theta(p^-) \delta(s) \left(\frac{4\pi\tilde{\mu}^2}{m^2}\right)^\epsilon \frac{\Gamma(\epsilon)}{\epsilon(1-2\epsilon)}. \quad (7.47)$$

Relating the above to the jet function as in Eq.(7.14) the result we are thus left with reads

$$J_{n,2}^{\mathbf{m},\mathbf{v}} = \frac{\alpha_s C_F}{4\pi} \theta(p^-) \left[\frac{1}{\epsilon^2} + \frac{2}{\epsilon} + \frac{1}{\epsilon} \log\left(\frac{\mu^2}{m^2}\right) + 4 + \frac{\pi^2}{12} + 2\log\left(\frac{\mu^2}{m^2}\right) + \frac{1}{2} \log^2\left(\frac{\mu^2}{m^2}\right) \right] \delta(s). \quad (7.48)$$

Final result for $J_{n,2}^{\mathbf{m}}$

Finally we combine the real emission and virtual contributions Eqs.(7.35) and (7.48) to obtain

$$J_{n,2}^{\mathbf{m}} = J_{n,2}^{\mathbf{m},\mathbf{r}} + J_{n,2}^{\mathbf{m},\mathbf{v}} = \frac{\alpha_s C_F}{4\pi} \theta(p^-) \left\{ \left[\frac{2}{\epsilon^2} + \frac{2}{\epsilon} + 4 - \frac{\pi^2}{6} + 2\log\left(\frac{\mu^2}{m^2}\right) + \log^2\left(\frac{\mu^2}{m^2}\right) \right] \delta(s) \right. \\ \left. - \left[\frac{1}{\epsilon} - \log\left(\frac{\mu^2}{m^2}\right) \right] \frac{2}{\mu^2} \left[\frac{\mu^2 \theta(s)}{s} \right]_+ + \frac{4}{\mu^2} \left[\frac{\mu^2 \theta(s) \log(s/\mu^2)}{s} \right]_+ - 2\theta(s) \left[\frac{1}{s+m^2} + \frac{1}{s} \log\left(1 + \frac{s}{m^2}\right) \right] \right\}. \quad (7.49)$$

It should be noted that this result is in principle not infrared finite, and thus zero-bin subtractions[41] should be taken into account to avoid double counting with the soft function. However, in the particular case of the diagram J_2 the zero-bin can be shown to formally vanish in dimensional regularisation, i.e. it is of the form $\frac{1}{\epsilon_{\text{UV}}} - \frac{1}{\epsilon_{\text{IR}}}$ which vanishes when $\epsilon_{\text{UV}} \equiv \epsilon_{\text{IR}} \equiv \epsilon$ are identified. Thus, in what is sometimes referred to as the pull-up mechanism, the zero-bin exchanges any IR poles occurring in Eq.(7.49) with UV ones. This implies that no harm is done in pretending that all ϵ -poles in the above result correspond to UV divergences to begin with.

The other single Wilson line diagram contribution $J_{n,3}^{\mathbf{m}}$ can be shown to give an identical contribution to $J_{n,2}^{\mathbf{m}}$.

Self energy contribution $J_{n,4}^{\mathbf{m}}$

As before we start by writing down the full jet matrix element $\mathcal{M}_{n,4}^{\mathbf{m}}$ for the collinear quark self-energy diagram as shown in Fig. 7.13,

$$\begin{aligned}\mathcal{M}_{n,4}^{\mathbf{m}} &= \text{Tr} \left[\frac{i(\not{p} + m)}{p^2 - m^2 + i0} (ig_s \tilde{\mu}^\epsilon T^A \gamma^\mu) \int \bar{d}^d k \frac{i(\not{p} - \not{k} + m)}{(p-k)^2 - m^2 + i0} (ig_s \tilde{\mu}^\epsilon T^B \gamma^\nu) \frac{i(\not{p} + m)}{p^2 - m^2 + i0} \frac{\not{p}}{2} \right] \left(\frac{-i\delta^{AB} g_{\mu\nu}}{k^2 + i0} \right) \\ &= g_s^2 \tilde{\mu}^{2\epsilon} C_F N_C \frac{1}{[p^2 - m^2 + i0]^2} \int \bar{d}^d k \frac{\text{Tr} \left[(\not{p} + m) \gamma^\mu (\not{p} - \not{k} + m) \gamma_\mu (\not{p} + m) \frac{\not{p}}{2} \right]}{[k^2 + i0] [(p-k)^2 - m^2 + i0]}.\end{aligned}\quad (7.50)$$

We evaluate the trace (e.g. with `FeynCalc`[42]) and bring it to a convenient form for integration,

$$\mathcal{M}_{n,4}^{\mathbf{m}} = 4g_s^2 \tilde{\mu}^{2\epsilon} C_F N_C \frac{1}{[s + i0]^2} \int \bar{d}^d k \frac{[(1-\epsilon)[2p^- p \cdot k - s(p^- + k^-)] + 2p^- m^2}{[k^2 + i0] [(p-k)^2 - m^2 + i0]}, \quad (7.51)$$

allowing for an immediate comparison with the corresponding amplitude for a massless quark, which will become useful later.

Just as before we split the contribution of the collinear quark self-energy into a real emission ($\mathcal{M}_{n,4}^{\mathbf{m},\mathbf{r}}$) and a virtual ($\mathcal{M}_{n,4}^{\mathbf{m},\mathbf{v}}$) part by means of the Cutkosky cutting rules, such that

$$\text{Disc} \{ \mathcal{M}_{n,4}^{\mathbf{m}} \} \equiv \mathcal{M}_{n,4}^{\mathbf{m},\mathbf{r}} + \mathcal{M}_{n,4}^{\mathbf{m},\mathbf{v}} \quad \Rightarrow \quad J_{n,4}^{\mathbf{m}} = J_{n,4}^{\mathbf{m},\mathbf{r}} + J_{n,4}^{\mathbf{m},\mathbf{v}}, \quad (7.52)$$

In the case of the collinear quark self-energy we have to be a bit more careful about employing the regular cutting rules. In particular we choose to write Eq.(7.52) diagrammatically in a peculiar way,

$$\text{Disc} \left\{ \left(\otimes \rightarrow \text{loop} \rightarrow \otimes \right) \right\} = \left(\otimes \rightarrow \text{cut loop} \rightarrow \otimes \right) + \left(\otimes \rightarrow \text{cut loop} \rightarrow \otimes \right), \quad (7.53)$$

$\mathcal{M}_{n,4}^{\mathbf{m}}$ $\mathcal{M}_{n,4}^{\mathbf{m},\mathbf{r}}$ $\mathcal{M}_{n,4}^{\mathbf{m},\mathbf{v}}$

where in the last diagram both of the outer quark propagators are cut. In which sense this double-cut is to be understood will be clarified soon (c.f. Eq.(7.61)).

$J_{n,4}^{\mathbf{m},\mathbf{r}}$ (real emission)

To compute the real emission contribution from the matrix element $\mathcal{M}_{n,4}^{\mathbf{m}}$ we perform the same cuts as we did for $\mathcal{M}_{n,2}^{\mathbf{m}}$ (see Eq.(7.20)). This leads to the amplitude

$$\mathcal{M}_{n,4}^{\mathbf{m},\mathbf{r}} = -16\pi^2 g_s^2 C_F N_C \frac{p^-}{[s + i0]^2} I_{n,4}^{\mathbf{m},\mathbf{r}}, \quad (7.54)$$

with the integral over the loop momentum given by

$$I_{n,4}^{\mathbf{m},\mathbf{r}} = \tilde{\mu}^{2\epsilon} \int \bar{d}^d k \delta(k^2) \delta((p-k)^2 - m^2) \theta(k^0) \theta(p^0 - k^0) \left\{ (1-\epsilon) \left[2k \cdot p - s \left(1 + \frac{k^-}{p^-} \right) \right] + 2m^2 \right\}. \quad (7.55)$$

Performing steps identical to what we described in detail for the real emission part $\mathcal{M}_{n,2}^{\mathbf{m},\mathbf{r}}$, we arrive at the analogous expression to Eq.(7.32), which now reads

$$I_{n,4}^{\mathbf{m},\mathbf{r}} = -\frac{\tilde{\mu}^{2\epsilon}}{(2\pi)^{4-2\epsilon}} \frac{\pi^{1-\epsilon}}{2\Gamma(1-\epsilon)} \frac{\theta(p^-) \theta(s) s^{1-2\epsilon}}{(s+m^2)^{1-\epsilon}} \int_0^1 da^- \frac{(1-\epsilon) \frac{s^2}{s+m^2} a^- - 2m^2}{[a^-(1-a^-)]^\epsilon}, \quad (7.56)$$

where we have $k^- = \frac{s}{p^+} a^-$. The remaining integral over a^- can be computed using **Mathematica** and proceeding to reinstate prefactors according to Eq.(7.54) we obtain

$$\mathcal{M}_{n,4}^{\mathbf{m},\mathbf{r}} = -\alpha_s C_F N_C \frac{\theta(p^-) p^-}{s + m^2} \left[\frac{e^{\gamma_E} (s + m^2)}{\mu^2} \right]^\epsilon \frac{\Gamma(1 - \epsilon)}{\Gamma(2 - 2\epsilon)} \left[4m^2 \frac{\theta(s) \mu^{4\epsilon}}{s^{1+2\epsilon}} - (1 - \epsilon) \frac{\theta(s) \mu^{4\epsilon}}{s^{2\epsilon}} \frac{s}{s + m^2} \right]. \quad (7.57)$$

Next we expand the first term into plus distributions using Eq.(7.34) producing the singular part of the contribution, while the second term yields only finite contributions in the limit $s \rightarrow 0$. In summary the result for the real emission contribution to the jet function Eq.(7.14) from the collinear quark self energy diagram reads

$$J_{n,4}^{\mathbf{m},\mathbf{r}} = \frac{\alpha_s C_F}{4\pi} \theta(p^-) \left\{ \left[\frac{2}{\epsilon} + 4 - 2 \log \left(\frac{\mu^2}{m^2} \right) \right] \delta(s) - \frac{4}{\mu^2} \left[\frac{\mu^2 \theta(s)}{s} \right]_+ + \theta(s) \frac{5s + 4m^2}{(s + m^2)^2} \right\}. \quad (7.58)$$

To arrive at the above result the distributional identity

$$\frac{1}{\mu^2} \frac{m^2}{s + m^2} \left[\frac{\mu^2 \theta(s)}{s} \right]_+ = \frac{1}{\mu^2} \left[\frac{\mu^2 \theta(s)}{s} \right]_+ - \theta(s) \frac{1}{s + m^2}, \quad (7.59)$$

was used, which allowed us to cleanly separate singular and non-singular parts of the amplitude in the limit $s \rightarrow 0$.

$J_{n,4}^{\mathbf{m},\mathbf{v}}$ (virtual contribution)

Note that since the amplitude in Eq.(7.51) is quadratic in the collinear quark propagator we cannot cut a single line and set the quark on-shell in the usual way without the other propagator blowing up.

This calls for an alternative cutting prescription when higher powers of identical propagators are present in an amplitude. Now recall that the traditional Cutkosky cutting rule prompts us to replace

$$\frac{1}{p^2 + i0} \longrightarrow 2i\theta(p^0) \text{Im} \left\{ \frac{1}{p^2 + i0} \right\} = -2\pi i \theta(p^0) \delta(p^2), \quad (7.60)$$

where the last equality follows from the famous Sokhotski-Plemelj theorem. We propose by analogy the natural (admittedly ad-hoc) generalisation to higher powers of propagators

$$\frac{1}{[p^2 + i0]^n} \longrightarrow 2i\theta(p^0) \text{Im} \left\{ \frac{1}{[p^2 + i0]^n} \right\} = 2\pi i \theta(p^0) \frac{(-1)^n}{(n-1)!} \frac{\partial^{n-1}}{\partial (p^2)^{n-1}} \delta(p^2), \quad (7.61)$$

which can be derived by differentiating Eq.(7.60) n times with respect to p^2 and which for $n = 1$ correctly reduces to the familiar prescription.

It is in this sense that the double-cut in Eq.(7.53) is to be understood. Hence, to obtain the virtual contribution coming from the jet matrix element $\mathcal{M}_{n,4}^{\mathbf{m}}$ we have to make the replacement

$$\frac{1}{[s + i0]^2} \longrightarrow 2\pi i \theta(p^0) \delta'(s), \quad (7.62)$$

in the amplitude Eq.(7.51) which leads us to

$$\mathcal{M}_{n,4}^{\mathbf{m},\mathbf{v}} = 8\pi i g_s^2 C_F N_C p^- \theta(p^-) I_{n,4}^{\mathbf{m},\mathbf{v}}(s, m) \delta'(s), \quad (7.63)$$

where we explicitly display the (s, m) -dependence of the loop integral given by

$$I_{n,4}^{\mathbf{m},\mathbf{v}}(s, m) = \tilde{\mu}^{2\epsilon} \int d^d k \frac{(1 - \epsilon) \left[2k \cdot p - s \left(1 + \frac{k^-}{p^-} \right) \right] + 2m^2}{[k^2 + i0] [(p - k)^2 - m^2 + i0]}. \quad (7.64)$$

At this point we note that by the product rule for differentiation (in s) of distributions we can write

$$I_{n,4}^{\mathbf{m},\mathbf{v}}(s, m)\delta'(s) = I_{n,4}^{\mathbf{m},\mathbf{v}}(0, m)\delta'(s) - (I_{n,4}^{\mathbf{m},\mathbf{v}})'(0, m)\delta(s), \quad (7.65)$$

where the symbol $'$ always indicates differentiation with respect to the off-shellness s . This allows us to compute all contributions to Eq.(7.63) in terms of loop integrals where the collinear quark is manifestly on-shell. While the integral in the first term of Eq.(7.65) reads

$$I_{n,4}^{\mathbf{m},\mathbf{v}}(0, m) = \tilde{\mu}^{2\epsilon} \int d^d k \frac{2[(1-\epsilon)k \cdot p + m^2]}{[k^2 + i0][k^2 - 2k \cdot p + i0]}, \quad (7.66)$$

the derivative on the loop integral in the second term can be formally interpreted in the sense of dimensional regularisation as

$$\begin{aligned} (I_{n,4}^{\mathbf{m},\mathbf{v}})'(0, m) &= \left. \frac{\partial I_{n,4}^{\mathbf{m},\mathbf{v}}}{\partial s} \right|_{s=0} \equiv \left. \frac{p^\mu}{2p^2} \frac{\partial I_{n,4}^{\mathbf{m},\mathbf{v}}}{\partial p^\mu} \right|_{s=0} \\ &= \tilde{\mu}^{2\epsilon} \int d^d k \frac{(1-\epsilon) \left[\frac{k \cdot p}{m^2} - \left(1 + \frac{k^-}{p^-} \right) \right]}{[k^2 + i0][k^2 - 2k \cdot p + i0]} + \tilde{\mu}^{2\epsilon} \int d^d k \frac{2 \left[\epsilon k \cdot p + (1-\epsilon) \frac{(k \cdot p)^2}{m^2} - m^2 \right]}{[k^2 + i0][k^2 - 2k \cdot p + i0]^2}, \end{aligned} \quad (7.67)$$

noting that $\frac{\partial}{\partial s}$ is just as good as $\frac{\partial}{\partial p^2}$ when deriving $I_{n,4}^{\mathbf{m},\mathbf{v}}$ for constant m .

Let us first turn to evaluate Eq.(7.66). By completing the square in the numerator we can bring the integral to the form

$$I_{n,4}^{\mathbf{m},\mathbf{v}}(0, m) \equiv I_{n,4,1}^{\mathbf{m},\mathbf{v}} + I_{n,4,2}^{\mathbf{m},\mathbf{v}} = \tilde{\mu}^{2\epsilon} \int d^d k \frac{1-\epsilon}{[k^2 - 2p \cdot k + i0]} + \tilde{\mu}^{2\epsilon} \int d^d k \frac{2m^2}{[k^2 + i0][k^2 - 2p \cdot k + i0]}. \quad (7.68)$$

Note that in arriving at this decomposition we have neglected a scaleless integral of the form $\int_k k^{-2}$.

At this point it is crucial to realise that the integral $I_{n,4,1}^{\mathbf{m},\mathbf{v}}$ cannot be evaluated by our standard method of contours. Indeed, shifting the momentum $q^\mu = k^\mu - p^\mu$ and using lightcone coordinates we obtain

$$I_{n,4,1}^{\mathbf{m},\mathbf{v}} \simeq \int dq^- dq^+ d(\mathbf{q}_\perp^2) \frac{(\mathbf{q}_\perp^2)^{-\epsilon} (1-\epsilon)}{q^+ q^- - \mathbf{q}_\perp^2 - m^2 + i0}, \quad (7.69)$$

which only falls like $(q^\pm)^{-1}$ for large q^\pm and thus does not vanish fast enough for contributions from the contour off the real axis. We therefore have to evaluate the integral by more conventional means, like using the 1-loop master formula in Eq.(B.6), which applied to our case yields

$$I_{n,4,1}^{\mathbf{m},\mathbf{v}} = \frac{i\pi^{2-\epsilon} \tilde{\mu}^{2\epsilon}}{(2\pi)^{4-2\epsilon}} \Gamma(\epsilon) (m^2)^{1-\epsilon}. \quad (7.70)$$

The second integral in Eq.(7.68) can again be treated by contour integration in the usual way. In terms of lightcone coordinates we get

$$I_{n,4,2}^{\mathbf{m},\mathbf{v}} = \frac{\tilde{\mu}^{2\epsilon}}{(2\pi)^{4-2\epsilon}} \frac{\pi^{1-\epsilon}}{2\Gamma(1-\epsilon)} \int \frac{dk^- dk^+ d(\mathbf{k}_\perp^2) \theta(\mathbf{k}_\perp^2) 2m^2 (\mathbf{k}_\perp^2)^{-\epsilon}}{[k^+ k^- - \mathbf{k}_\perp^2 + i0][k^+ k^- - \mathbf{k}_\perp^2 - p^- k^+ - p^+ k^- + i0]}. \quad (7.71)$$

Analogous to how we proceeded for the virtual contribution $\mathcal{M}_{n,2}^{\mathbf{m},\mathbf{v}}$ we identify the two poles in the complex k^+ -plane which we find at

$$\begin{aligned} \text{(i)} \quad k^+ &= \frac{\mathbf{k}_\perp^2}{k^-} - \frac{i0}{k^-}, \\ \text{(ii)} \quad k^+ &= -\frac{\mathbf{k}_\perp^2 + p^+ k^-}{p^- - k^-} + \frac{i0}{p^- - k^-}, \end{aligned} \quad (7.72)$$

which forces us to impose $0 < k^- < p^-$ to get a non-vanishing result. Choosing the contour to enclose (ii) we pick up the residue

$$R_{n,4,2}^{\mathbf{m},\mathbf{v}}(p^\mu, k^-, \mathbf{k}_\perp^2) = \text{Res}\left(k^+ = -\frac{\mathbf{k}_\perp^2 + p^+ k^-}{p^- - k^-} + i0\right) = \frac{\theta(k^-)\theta(p^- - k^-)\theta(\mathbf{k}_\perp^2)(\mathbf{k}_\perp^2)^{-\epsilon}}{p^- \mathbf{k}_\perp^2 + p^+(k^-)^2 - i0}. \quad (7.73)$$

Thus, after the residue theorem has been applied we can write Eq.(7.71) as

$$I_{n,4,2}^{\mathbf{m},\mathbf{v}} = \frac{\tilde{\mu}^{2\epsilon}}{(2\pi)^{4-2\epsilon}} \frac{\pi^{1-\epsilon}(2\pi i)}{2\Gamma(1-\epsilon)} \int_0^{p^-} dk^- \int_0^\infty d(\mathbf{k}_\perp^2) \frac{(\mathbf{k}_\perp^2)^{-\epsilon}}{p^- \mathbf{k}_\perp^2 + p^+(k^-)^2 - i0}, \quad (7.74)$$

in which the remaining integrations can be performed by the use of **Mathematica**. The final results for $I_{n,4,2}^{\mathbf{m},\mathbf{v}}$ and the total integral $I_{n,4}^{\mathbf{m},\mathbf{v}}(0, m)$ read

$$\begin{aligned} I_{n,4,2}^{\mathbf{m},\mathbf{v}} &= \frac{i\pi^{2-\epsilon}\tilde{\mu}^{2\epsilon}}{(2\pi)^{4-2\epsilon}} \frac{2\Gamma(\epsilon)}{1-2\epsilon} (m^2)^{1-\epsilon}, \\ I_{n,4}^{\mathbf{m},\mathbf{v}}(0, m) &= I_{n,4,1}^{\mathbf{m},\mathbf{v}} + I_{n,4,2}^{\mathbf{m},\mathbf{v}} = \frac{i}{16\pi^2} \left(\frac{4\pi\tilde{\mu}^2}{m^2}\right)^\epsilon \Gamma(\epsilon) \frac{3-2\epsilon}{1-2\epsilon} m^2. \end{aligned} \quad (7.75)$$

Let us consider the contribution of this integral to the jet function right away, without worrying about the second term in Eq.(7.65) for the moment. Reinstating all necessary prefactors from Eq.(7.63) and Eq.(7.14), and expanding in ϵ we arrive at

$$\begin{aligned} J_{n,4}^{\mathbf{m},\mathbf{v}} &\supset \frac{\alpha_s C_F}{4\pi} \theta(p^-) \delta'(s) \left(\frac{4\pi\tilde{\mu}^2}{m^2}\right)^\epsilon (-2\Gamma(\epsilon)) \frac{3-2\epsilon}{1-2\epsilon} m^2 \\ &= \frac{\alpha_s C_F}{4\pi} \theta(p^-) \delta'(s) 2m^2 \left[-\frac{3}{\epsilon} - 4 - 3\log\left(\frac{\mu^2}{m^2}\right)\right] = \theta(p^-) \delta'(s) 2m^2 \delta Z_m^{\text{OS}}, \end{aligned} \quad (7.76)$$

which we recognise from QCD as the one-loop mass renormalisation factor in the on-shell scheme,

$$\delta Z_m^{\text{OS}} = \frac{\alpha_s C_F}{4\pi} \left[-\frac{3}{\epsilon} - 4 - 3\log\left(\frac{\mu^2}{m^2}\right)\right]. \quad (7.77)$$

The symbol \supset in Eq.(7.76) denotes the fact that we are only showing a subset of all the terms in $J_{n,4}^{\mathbf{m},\mathbf{v}}$ on the right-hand side.

With this result in mind we now turn to computing the second contribution to $J_{n,4}^{\mathbf{m},\mathbf{v}}$ which comes from Eq.(7.67). We will see that this integral is in fact related to the other renormalisation factor relevant for the diagram.

In principle we could proceed with a (PV¹³) decomposition of Eq.(7.67) analogous to what we did for $I_{n,4}^{\mathbf{m},\mathbf{v}}(0, m)$ in Eq.(7.68), again identifying integrals that can be evaluated by contour integration and those that cannot. This procedure would allow us to arrive at an analytic expression for $(I_{n,4}^{\mathbf{m},\mathbf{v}})'(0, m)$ similar to Eq.(7.75). Since we have discussed all necessary techniques to perform this calculation, we do not mention any further details at this point and state the result in its already expanded form which can be obtained directly using software like **PackageX** [45],

$$(I_{n,4}^{\mathbf{m},\mathbf{v}})'(0, m) = \frac{i}{16\pi^2} \left[-\frac{1}{\epsilon_{\text{IR}}} - \frac{1}{2\epsilon_{\text{UV}}} - 2 - \frac{3}{2}\log\left(\frac{\mu^2}{m^2}\right)\right]. \quad (7.78)$$

Note that we have left an explicit distinction between IR and UV poles. This leads to a jet function contribution

$$J_{n,4}^{\mathbf{m},\mathbf{v}} \supset \frac{\alpha_s C_F}{4\pi} \theta(p^-) \delta(s) \left[-\frac{2}{\epsilon_{\text{IR}}} - \frac{1}{\epsilon_{\text{UV}}} - 4 - 3\log\left(\frac{\mu^2}{m^2}\right)\right] = \theta(p^-) \delta(s) \delta Z_\psi^{\text{OS}}, \quad (7.79)$$

¹³Passarino-Veltman[43, 44]

which exactly reproduces the on-shell wavefunction renormalisation factor $\delta Z_\psi^{\text{OS}}$ of a massive quark in QCD. When we add the virtual contribution above to the real emission result Eq.(7.58), it is in fact the ϵ_{IR} divergence from Eq.(7.79) that cancels between them, leaving the pure ϵ_{UV} pole from Eq.(7.76) in the final result.

From our equations Eq.(7.76) and Eq.(7.79) now follows the beautifully simple result for the “double-cut” virtual contribution from the collinear quark self energy in Eq.(7.53),

$$\begin{aligned} J_{n,4}^{\mathbf{m},\mathbf{v}} &= \theta(p^-) \{ \delta Z_\psi^{\text{OS}} \delta(s) + 2m^2 \delta Z_m^{\text{OS}} \delta'(s) \} \\ &= \frac{\alpha_s C_F}{4\pi} \theta(p^-) \left\{ - \left[\frac{3}{\epsilon} + 4 + 3 \log \left(\frac{\mu^2}{m^2} \right) \right] (\delta(s) + 2m^2 \delta'(s)) \right\}, \end{aligned} \quad (7.80)$$

where we have now neglected to distinguish between UV and IR divergences. While in the following we will explicitly introduce a mass counter term to absorb the UV divergences coming from δZ_m^{OS} , no such term needs to be considered for the wavefunction renormalisation $\delta Z_\psi^{\text{OS}}$. Recall that this was also the case in full QCD where the UV divergences associated with the self energy correction of the external legs simply canceled in the sum of all virtual contributions (c.f. App. C).

Final result for $J_{n,4}^{\mathbf{m}}$

It is now time to collect the results for the real emission and virtual parts Eqs.(7.58) and (7.80) to obtain the full discontinuity of the collinear quark self-energy,

$$\begin{aligned} J_{n,4}^{\mathbf{m}} &= J_{n,4}^{\mathbf{m},\mathbf{r}} + J_{n,4}^{\mathbf{m},\mathbf{v}} = \frac{\alpha_s C_F}{4\pi} \theta(p^-) \left\{ - \left[\frac{1}{\epsilon} + 5 \log \left(\frac{\mu^2}{m^2} \right) \right] \delta(s) - \frac{4}{\mu^2} \left[\frac{\mu^2 \theta(s)}{s} \right]_+ \right. \\ &\quad \left. - 2m^2 \left[\frac{3}{\epsilon} + 4 + 3 \log \left(\frac{\mu^2}{m^2} \right) \right] \delta'(s) + \theta(s) \frac{5s + 4m^2}{(s + m^2)^2} \right\}. \end{aligned} \quad (7.81)$$

Note that unlike the result we obtained for $J_{n,2}^{\mathbf{m}}$ in Eq.(7.49) this is infrared finite since the cancellation of IR-divergences has occurred between the real and virtual contribution within the diagram. Therefore even in principle no zero-bin subtractions need to be considered.

Wilson line tadpole contributions $J_{n,5}^{\mathbf{m}}$ and $J_{n,6}^{\mathbf{m}}$

The Wilson line tadpole matrix elements $\mathcal{M}_{n,5}^{\mathbf{m}}$ and $\mathcal{M}_{n,6}^{\mathbf{m}}$ are both proportional to $\bar{n}^2 = 0$ as long as we are in Feynman gauge. Thus there is nothing for us to do.

Mass counter term $J_{n,\delta m}^{\mathbf{m}}$

The mass counter term will be calculated in an arbitrary mass scheme which is related to the on-shell scheme by the finite difference of renormalisation factors

$$\delta_m = \delta Z_m - \delta Z_m^{\text{OS}}. \quad (7.82)$$

The full jet matrix element pertaining to the counter term is then given by

$$\mathcal{M}_{n,\delta m}^{\mathbf{m}} = \text{Tr} \left[\frac{i(\not{p} + m)}{p^2 - m^2 + i0} (-im \delta Z_m) \frac{i(\not{p} + m)}{p^2 - m^2 + i0} \frac{\not{n}}{2} \right] = \frac{4ip^- N_C}{[s + i0]^2} m^2 \delta Z_m, \quad (7.83)$$

where we recall that the factor of N_C comes from the implicit trace over colours in Eq.(7.12). Employing the generalised cutting rule Eq.(7.61) and collecting prefactors from Eq.(7.14) we obtain

$$J_{n,\delta m}^{\mathbf{m}} = -2m^2 \delta Z_m \theta(p^-) \delta'(s) = -2m^2 (\delta Z_m^{\text{OS}} + \delta_m) \theta(p^-) \delta'(s). \quad (7.84)$$

By construction the first term on the right-hand side of Eq.(7.84) precisely cancels the UV-divergent part of $J_{n,4}^{\mathbf{m}}$ (c.f. Eq.(7.81)) which is proportional to m^2 .

7.4 Massive jet function and jet correlator results

Collecting the results for each contributing diagram (c.f. Eqs.(7.49), (7.81) and (7.84)), and adding the leading order result Eq.(6.31), we give the final expression for the massive SCET jet function Eq.(7.12) up to next-to-leading order,

$$\begin{aligned}
J_n^{\mathbf{m}} &= J_{n,\text{LO}}^{\mathbf{m}} + J_{n,\text{NLO}}^{\mathbf{m}} = J_{n,\text{LO}}^{\mathbf{m}} + 2J_{n,2}^{\mathbf{m}} + J_{n,4}^{\mathbf{m}} + J_{n,\delta m}^{\mathbf{m}} \\
&= \delta(s) - 2m^2\delta_m\theta(p^-)\delta'(s) + \frac{\alpha_s C_F}{4\pi}\theta(p^-)\left\{\left[\frac{4}{\epsilon^2} + \frac{3}{\epsilon} + 8 - \frac{\pi^2}{3} - \log\left(\frac{\mu^2}{m^2}\right) + 2\log^2\left(\frac{\mu^2}{m^2}\right)\right]\delta(s) \right. \\
&\quad - \left[\frac{1}{\epsilon} + 1 - \log\left(\frac{\mu^2}{m^2}\right)\right]\frac{4}{\mu^2}\left[\frac{\mu^2\theta(s)}{s}\right]_+ + \frac{8}{\mu^2}\left[\frac{\mu^2\theta(s)\log(s/\mu^2)}{s}\right]_+ \\
&\quad \left. + \theta(s)\left[\frac{s}{(s+m^2)^2} - \frac{4}{s}\log\left(1 + \frac{s}{m^2}\right)\right]\right\}. \tag{7.85}
\end{aligned}$$

This agrees with the expression found in the literature[13], which was obtained not by the use of cutting rules but by explicitly taking the imaginary part of the amplitude after evaluation of the jet correlators, thus providing a good consistency check for our calculation.

For later use we also state the results for the corresponding jet correlators as defined in Eq.(7.16) which can be obtained by straightforward computation of the amplitudes Eq.(7.17) and Eq.(7.50) without employing the Cutkosky rules, and read

$$\begin{aligned}
\tilde{J}_n^{\mathbf{m}} &= \tilde{J}_{n,\text{LO}}^{\mathbf{m}} + \tilde{J}_{n,\text{NLO}}^{\mathbf{m}} = \tilde{J}_{n,\text{LO}}^{\mathbf{m}} + 2\tilde{J}_{n,2}^{\mathbf{m}} + \tilde{J}_{n,4}^{\mathbf{m}} + \tilde{J}_{\delta m}^{\mathbf{m}}, \\
\tilde{J}_{n,\text{LO}}^{\mathbf{m}}(s) &= -\frac{1}{\pi}\frac{1}{s+i0}, \\
\tilde{J}_{n,2}^{\mathbf{m}}(s) &= \frac{\alpha_s C_F}{4\pi}\frac{1}{\pi}\frac{1}{s+i0}\left\{-\frac{2}{\epsilon^2} - \frac{2}{\epsilon} - \frac{\pi^2}{2} - 4 - 2\left[\frac{1}{\epsilon} + 1 - \log\left(\frac{\mu^2}{m^2}\right)\right]\log\left(\frac{\mu^2}{-s-i0}\right) \right. \\
&\quad - \log^2\left(\frac{\mu^2}{m^2}\right) - 2\log^2\left(\frac{\mu^2}{-s-i0}\right) + \frac{2m^2}{s+m^2+i0}\log\left(\frac{m^2}{-s-i0}\right) \\
&\quad \left. - 2\log\left(\frac{m^2}{-s-i0}\right)\log\left(1 + \frac{s+i0}{m^2}\right) + 2\text{Li}_2\left(\frac{-s-i0}{m^2}\right)\right\}, \\
\tilde{J}_{n,4}^{\mathbf{m}}(s) + \tilde{J}_{n,\delta m}^{\mathbf{m}}(s) &= -\frac{1}{\pi}\frac{2m^2\delta_m}{[s+i0]^2} + \frac{\alpha_s C_F}{4\pi}\frac{1}{\pi}\frac{1}{s+i0}\left\{\frac{1}{\epsilon} + \log\left(\frac{\mu^2}{m^2}\right) + \log\left(\frac{m^2}{-s-i0}\right) \right. \\
&\quad \left. + \frac{s}{s+m^2+i0} - m^2\frac{5m^2+6s}{[s+m^2+i0]^2}\log\left(\frac{m^2}{-s-i0}\right)\right\}. \tag{7.86}
\end{aligned}$$

The above expressions can be shown to correspond to the jet function contributions we computed above by making use of the imaginary parts identities listed in Eq.(I.5).

7.5 Massless jet function and jet correlator results

For the purposes of this thesis we will need the jet function contributions for the case of massless primary quarks as well. The computation of the relevant quantities proceeds in complete analogy to what was shown above for massive quarks, whence only the final results are stated. We start by quoting the full massless next-to-leading order SCET jet function,

$$\begin{aligned}
J_n^{\mathbf{m}=0} &= J_{n,\text{LO}}^{\mathbf{m}=0} + J_{n,\text{NLO}}^{\mathbf{m}=0} = J_{n,\text{LO}}^{\mathbf{m}=0} + 2J_{n,2}^{\mathbf{m}=0} + J_{n,4}^{\mathbf{m}=0} \\
&= \delta(p^2) + \frac{\alpha_s C_F}{4\pi}\left\{\left[\frac{4}{\epsilon^2} + \frac{3}{\epsilon} + 7 - \pi^2\right]\delta(p^2) - \left[\frac{4}{\epsilon} + 3\right]\frac{1}{\mu^2}\left[\frac{\mu^2\theta(p^2)}{p^2}\right]_+ + \frac{4}{\mu^2}\left[\frac{\mu^2\theta(p^2)\log(p^2/\mu^2)}{p^2}\right]_+ \right\} \tag{7.87}
\end{aligned}$$

with the off-shellness now given by $s = p^2$, and where the individual contributions (each corresponding to its respective diagram in Fig. 7.13) yield

$$\begin{aligned} J_{n,\text{LO}}^{\mathbf{m}=0}(p^2) &= \delta(p^2), \\ J_{n,2}^{\mathbf{m}=0}(p^2) &= \frac{\alpha_s C_F}{4\pi} \left\{ \left[\frac{2}{\epsilon^2} + \frac{2}{\epsilon} + 4 - \frac{\pi^2}{2} \right] \delta(p^2) - \left[\frac{1}{\epsilon} + 1 \right] \frac{2}{\mu^2} \left[\frac{\mu^2 \theta(p^2)}{p^2} \right]_+ + \frac{2}{\mu^2} \left[\frac{\mu^2 \theta(p^2) \log(p^2/\mu^2)}{p^2} \right]_+ \right\}, \\ J_{n,4}^{\mathbf{m}=0}(p^2) &= \frac{\alpha_s C_F}{4\pi} \left\{ - \left[\frac{1}{\epsilon} + 1 \right] \delta(p^2) + \frac{1}{\mu^2} \left[\frac{\mu^2 \theta(p^2)}{p^2} \right]_+ \right\}. \end{aligned} \quad (7.88)$$

Just as before, the Cutkosky cutting rules allow us to split the next-to-leading order contributions in Eq.(7.88) into a real emission ($J_{n,\text{LO}}^{\mathbf{m}=0,\text{r}}$) and a virtual ($J_{n,\text{LO}}^{\mathbf{m}=0,\text{v}}$) part,

$$J_{n,2}^{\mathbf{m}=0,\text{r}} = J_{n,2}^{\mathbf{m}=0}, \quad J_{n,2}^{\mathbf{m}=0,\text{v}} = 0, \quad J_{n,4}^{\mathbf{m}=0,\text{r}} = J_{n,4}^{\mathbf{m}=0}, \quad J_{n,4}^{\mathbf{m}=0,\text{v}} = 0. \quad (7.89)$$

We note that the virtual contributions to both diagrams are formally zero in dimensional regularisation (scaleless). Thus the full amplitudes are determined entirely by the real emission part.

For reference we also state the explicit expressions for the jet correlators, which are related to the jet function as in Eq.(7.16),

$$\begin{aligned} \tilde{J}_n^{\mathbf{m}=0} &= \tilde{J}_{n,\text{LO}}^{\mathbf{m}=0} + \tilde{J}_{n,\text{NLO}}^{\mathbf{m}=0} = \tilde{J}_{n,\text{LO}}^{\mathbf{m}=0} + 2\tilde{J}_{n,2}^{\mathbf{m}=0} + \tilde{J}_{n,4}^{\mathbf{m}=0}, \\ \tilde{J}_{n,\text{LO}}^{\mathbf{m}=0}(p^2) &= -\frac{1}{\pi} \frac{1}{p^2 + i0}, \\ \tilde{J}_{n,2}^{\mathbf{m}=0}(p^2) &= \frac{\alpha_s C_F}{4\pi} \frac{1}{\pi} \frac{1}{p^2 + i0} \left\{ -\frac{2}{\epsilon^2} - \frac{2}{\epsilon} - 2 \left[\frac{1}{\epsilon} + 1 \right] \log \left(\frac{\mu^2}{-p^2 - i0} \right) - \log^2 \left(\frac{\mu^2}{-p^2 - i0} \right) - 4 + \frac{\pi^2}{6} \right\}, \\ \tilde{J}_{n,4}^{\mathbf{m}=0}(p^2) &= \frac{\alpha_s C_F}{4\pi} \frac{1}{\pi} \frac{1}{p^2 + i0} \left\{ \frac{1}{\epsilon} + 1 + \log \left(\frac{\mu^2}{-p^2 - i0} \right) \right\}. \end{aligned} \quad (7.90)$$

7.6 Jet function renormalisation

Since the pole structure of the massive jet function coincides with that of the massless one (c.f. Eqs.(7.85) and (7.87)), the renormalisation factor required to render these quantities finite can be chosen identically for both. We conventionally take the renormalised ($J_{n,\text{ren}}$) and bare ($J_n^{(0)}$) jet function to be related by

$$J_{n,\text{ren}}(s) = \int ds' Z_J^{-1}(s-s') J_n^{(0)}(s'), \quad (7.91)$$

where s, s' stand for the off-shellness in both the massive and massless case. In the $\overline{\text{MS}}$ -scheme the renormalisation factor is given by

$$Z_J^{\overline{\text{MS}}}(s) = \delta(s) + \frac{\alpha_s C_F}{4\pi} \left\{ \left[\frac{4}{\epsilon^2} + \frac{3}{\epsilon} \right] \delta(s) - \frac{4}{\epsilon} \frac{1}{\mu^2} \left[\frac{\mu^2 \theta(s)}{s} \right]_+ \right\}. \quad (7.92)$$

In fact the above renormalisation factor even cancels the divergences appearing in the jet correlators in Eq.(7.90) and Eq.(7.86) when appropriately convolved with them. We will explicitly check this claim by renormalising the massless correlator

$$\begin{aligned} \tilde{J}_{n,\text{ren}}^{\mathbf{m}=0}(s) &= \int ds' \left(Z_J^{\overline{\text{MS}}} \right)^{-1}(s-s') \tilde{J}_n^{\mathbf{m}=0(0)}(s') \\ &= -\frac{1}{\pi} \frac{1}{s + i0} \left\{ 1 + \frac{\alpha_s C_F}{4\pi} \left[7 - \frac{\pi^2}{3} + 3 \log \left(\frac{\mu^2}{-s - i0} \right) + 2 \log^2 \left(\frac{\mu^2}{-s - i0} \right) \right] \right\}, \end{aligned} \quad (7.93)$$

where, crucially, the convolution properties of the plus distributions in Eq.(I.6) were used. As claimed, the result does no longer contain any divergences. We proceed by taking the imaginary part of Eq.(7.93), employing the identities listed in Eq.(I.5) to arrive at

$$\text{Im}\left\{\tilde{J}_{n,\text{ren}}^{\mathbf{m}=\mathbf{0}}(s)\right\} = \delta(s) + \frac{\alpha_s C_F}{4\pi} \left\{ \left[7 - \pi^2\right] \delta(s) - \frac{3}{\mu^2} \left[\frac{\mu^2 \theta(s)}{s} \right]_+ + \frac{4}{\mu^2} \left[\frac{\mu^2 \theta(s) \log(s/\mu^2)}{s} \right]_+ \right\}, \quad (7.94)$$

which is the exact result we would get by directly performing the convolution in Eq.(7.91). This establishes the consistency condition $\text{Im}\{\tilde{J}_{n,\text{ren}}^{\mathbf{m}=\mathbf{0}}\} = J_{n,\text{ren}}^{\mathbf{m}=\mathbf{0}}$, in essence telling us that renormalising and taking the imaginary part of the jet matrix elements commute. The massive jet function (and matrix elements) can be treated analogously.

7.7 Discussion of results and non-local singularity

Comparing the results for the massive Eq.(7.85) and massless Eq.(7.87) jet function we see that the divergences between the two naively agree, apart from the threshold shift discussed at the beginning of this section. As we have remarked before, some of the divergences, i.e. those from the diagram J_2 in Eq.(7.49), in fact correspond to IR divergences and are only converted to proper UV divergences through the scaleless zero-bin contributions, which can be shown to be identical for the massive and massless jet function.

This implies that when the massless jet function is appropriately subtracted (in a sense we will outline shortly) from the massive jet function all poles in ϵ must cancel and the result should be finite in $d = 4$ dimensions, regardless of whether zero-bin cancellations are explicitly considered or not.

Moreover, we were able to split the jet functions into real emission and virtual parts Eqs.(7.19) and (7.53), which should be regarded as analogues to the respective contributions Eqs.(2.69) and (2.70) in the full QCD computation of thrust, since they are directly related through the factorisation theorem Eq.(6.36). Note however, that in the effective theory calculation new kinds of divergences compared to QCD (c.f. Eq.(3.52)) have occurred. In particular the real emission graph of the Wilson line diagram contains a singularity of the type

$$J_{n,2}^{\mathbf{m},\mathbf{r}} \supset -\theta(p^-) \frac{\alpha_s C_F}{4\pi} \frac{1}{\epsilon} \frac{4}{\mu^2} \left[\frac{\mu^2 \theta(s)}{s} \right]_+, \quad (7.95)$$

with $s = p^2 - m^2$ and an analogous contribution in the massless jet function with $s = p^2$. Since the ϵ -pole multiplies a plus distribution, and not simply a delta function $\delta(s)$ the divergence as $\epsilon \rightarrow 0$ persists for any finite value of s , whence we will call this a non-local divergence. This contrasts with the real and virtual contributions to the thrust distribution in QCD or indeed with all other jet function diagrams for which the limit $\epsilon \rightarrow 0$ can be safely taken as long as $s \neq 0$ since all ϵ -poles arise as local threshold singularities, i.e. they are proportional to $\delta(\tau)$ or $\delta(s)$ respectively. In particular this implies that we cannot use conventional subtraction terms, like the ones we derived in Eq.(3.48), to cancel this non-local divergence. This provides the motivation for the introduction of the so-called “subtracted jet function” in the next section.

The origin of the non-local divergence is the eikonal structure of the Wilson line propagator $(n \cdot k + i0)^{-1}$ (c.f. Eq.(7.17)). In a conventional SCET calculation the IR divergence of the naive result in Eq.(7.95) would be pulled up to the UV by the zero-bin contribution and then removed using an appropriate renormalisation factor (see Eq.(7.92)).

7.8 Subtracted massive jet function: a first look

We have already hinted that the non-local divergence can be canceled between the massive and massless jet function. To facilitate the subtraction we compute the ratio of the two which may be

schematically written as

$$J_{n,\text{sub}}^{\mathbf{m}} = (J_n^{\mathbf{m}=0})^{-1} * J_n^{\mathbf{m}}, \quad (7.96)$$

where the symbol $*$ on the right-hand side is short-hand for a convolution (c.f. Eq.(7.100)) in the off-shellness of the jet functions involved. We will refer to the object on the left-hand side as the “subtracted massive jet function”. The claim is that in the ratio Eq.(7.96) the divergences cancel diagram by diagram and that the dependence on the renormalisation scale μ drops out in their sum. To conclude, we add up all contributions and present the final, subtracted jet function.

The inverse massive(massless) jet function is defined by the equation

$$(J_n^{\mathbf{m}=0})^{-1} * J_n^{\mathbf{m}=0} \stackrel{!}{=} \delta \quad \Rightarrow \quad (J_n^{\mathbf{m}=0})^{-1} = J_{n,\text{LO}}^{\mathbf{m}=0} - J_{n,\text{NLO}}^{\mathbf{m}=0} + \mathcal{O}(\alpha_s^2), \quad (7.97)$$

which at NLO leads us to the expression on the right. Compare this to the jet functions Eqs.(7.85) and (7.87) where the sign between LO and NLO contributions is exactly opposite. The δ on the left-hand side of Eq.(7.97) denotes a delta function with threshold appropriate to the mass m associated with the primary quark, i.e. $\delta(p^2 - m^2)$ in the massive, and $\delta(p^2)$ in the massless case.

Both jet functions are written in terms of their expansion into LO and NLO contributions (c.f. Eqs.(7.85) and (7.88)), which means that the ratio in Eq.(7.96) can be expressed more explicitly as

$$\begin{aligned} J_{n,\text{sub}}^{\mathbf{m}} &\equiv J_{n,\text{LO}}^{\mathbf{m}=0} * J_{n,\text{LO}}^{\mathbf{m}} + J_{n,\text{LO}}^{\mathbf{m}=0} * J_{n,\text{NLO}}^{\mathbf{m}} - J_{n,\text{NLO}}^{\mathbf{m}=0} * J_{n,\text{LO}}^{\mathbf{m}} + \mathcal{O}(\alpha_s^2) \\ &= J_{n,\text{LO}}^{\mathbf{m}=0} * J_{n,\text{LO}}^{\mathbf{m}} + J_{n,\text{LO}}^{\mathbf{m}=0} * (2J_{n,2}^{\mathbf{m}} + J_{n,4}^{\mathbf{m}} + J_{n,\delta_m}^{\mathbf{m}}) - (2J_{n,2}^{\mathbf{m}=0} + J_{n,4}^{\mathbf{m}=0}) * J_{n,\text{LO}}^{\mathbf{m}} + \mathcal{O}(\alpha_s^2) \\ &\equiv J_{n,\text{LO},\text{sub}}^{\mathbf{m}} + 2J_{n,2,\text{sub}}^{\mathbf{m}} + J_{n,4,\text{sub}}^{\mathbf{m}} + \mathcal{O}(\alpha_s^2), \end{aligned} \quad (7.98)$$

The individual subtracted diagram-by-diagram contributions in the second line of Eq.(7.98) read

$$\begin{aligned} J_{n,\text{LO},\text{sub}}^{\mathbf{m}} &= J_{n,\text{LO}}^{\mathbf{m}=0} * J_{n,\text{LO}}^{\mathbf{m}}, \\ J_{n,2,\text{sub}}^{\mathbf{m}} &= J_{n,\text{LO}}^{\mathbf{m}=0} * J_{n,2}^{\mathbf{m}} - J_{n,2}^{\mathbf{m}=0} * J_{n,\text{LO}}^{\mathbf{m}}, \\ J_{n,4,\text{sub}}^{\mathbf{m}} &= J_{n,\text{LO}}^{\mathbf{m}=0} * (J_{n,4}^{\mathbf{m}} + J_{n,\delta_m}^{\mathbf{m}}) - J_{n,4}^{\mathbf{m}=0} * J_{n,\text{LO}}^{\mathbf{m}}, \end{aligned} \quad (7.99)$$

where we have chosen to add the mass counter term to the definition of the subtracted diagram $J_{4,\text{sub}}^{\mathbf{m}}$, in order to have only manifestly finite quantities on the left-hand side.

To make transparent the notation we use to calculate the ratios shown in Eq.(7.99) we write out the convolution in detail at the level of the sum of diagrams

$$\begin{aligned} J_{n,\text{sub}}^{\mathbf{m}}(p^\mu, m) &\equiv J_{n,\text{sub}}^{\mathbf{m}}(p^2 - m^2) = \int d^4q \, (J_n^{\mathbf{m}=0})^{-1}(p^2 - q^2) J_n^{\mathbf{m}}(q^2 - m^2) \\ &= \int d^4q \, J_{n,\text{LO}}^{\mathbf{m}=0}(p^2 - q^2) J_{n,\text{LO}}^{\mathbf{m}}(q^2 - m^2) \\ &\quad + \int d^4q \, \left[J_{n,\text{LO}}^{\mathbf{m}=0}(p^2 - q^2) J_{n,\text{NLO}}^{\mathbf{m}}(q^2 - m^2) - J_{n,\text{NLO}}^{\mathbf{m}=0}(p^2 - q^2) J_{n,\text{LO}}^{\mathbf{m}}(q^2 - m^2) \right] + \mathcal{O}(\alpha_s^2) \\ &= \delta(p^2 - m^2) + [J_{n,\text{NLO}}^{\mathbf{m}}(p^2 - m^2) - J_{n,\text{NLO}}^{\mathbf{m}=0}(p^2 - m^2)] + \mathcal{O}(\alpha_s^2). \end{aligned} \quad (7.100)$$

Here the convolution acts as a shift in the threshold of the massless jet function such that the subtracted result has a threshold consistent with a massive jet function. Computing the NLO contributions to Eq.(7.100) diagram by diagram we start with

$$\begin{aligned} J_{n,2,\text{sub}}^{\mathbf{m}}(s) &= \frac{\alpha_s C_F}{4\pi} \left\{ \left[\frac{\pi^2}{3} + 2\log\left(\frac{\mu^2}{m^2}\right) + \log^2\left(\frac{\mu^2}{m^2}\right) \right] \delta(s) + \left[1 + \log\left(\frac{\mu^2}{m^2}\right) \right] \frac{2}{\mu^2} \left[\frac{\mu^2 \theta(s)}{s} \right]_+ \right. \\ &\quad \left. + \frac{2}{\mu^2} \left[\frac{\mu^2 \theta(s) \log(s/\mu^2)}{s} \right]_+ - 2\theta(s) \left[\frac{1}{s+m^2} + \frac{1}{s} \log\left(1 + \frac{s}{m^2}\right) \right] \right\}, \end{aligned} \quad (7.101)$$

which shows that indeed the divergences cancel between the massive and the massless jet function. To make the μ -independence of the result, which is not readily visible in Eq.(7.101), explicit, we perform the substitution $s = \kappa^2 x$ for some dummy scale κ . This allows us to use the recursion relation for plus distributions in Eq.(I.4), thereby effectively replacing any occurrence of μ with κ in the above result for $J_{n,2,\text{sub}}^{\mathbf{m}}$. Since we are free to choose κ independently of the renormalisation scale μ , the claim follows.

We proceed by giving the result for the subtracted contribution of $J_{n,4,\text{sub}}^{\mathbf{m}}$ in its already manifestly μ -independent form,

$$J_{n,4,\text{sub}}^{\mathbf{m}}(s) = -2m^2 \delta_m \delta'(s) + \frac{\alpha_s C_F}{4\pi} \left\{ \left[1 - 5 \log \left(\frac{\kappa^2}{m^2} \right) \right] \delta(s) - \frac{5}{\kappa^2} \left[\frac{\kappa^2 \theta(s)}{s} \right]_+ + \theta(s) \frac{5s + 4m^2}{(s + m^2)^2} \right\}. \quad (7.102)$$

Finally adding all the results as indicated in Eq.(7.98), we obtain the full subtracted jet function

$$\begin{aligned} J_{n,\text{sub}}^{\mathbf{m}}(s) = & \delta(s) - 2m^2 \delta_m \delta'(s) + \frac{\alpha_s C_F}{4\pi} \left\{ \left[1 + \frac{2\pi^2}{3} - \log \left(\frac{\kappa^2}{m^2} \right) + 2 \log^2 \left(\frac{\kappa^2}{m^2} \right) \right] \delta(s) \right. \\ & - \left[1 - 4 \log \left(\frac{\kappa^2}{m^2} \right) \right] \frac{1}{\kappa^2} \left[\frac{\kappa^2 \theta(s)}{s} \right]_+ + \frac{4}{\kappa^2} \left[\frac{\kappa^2 \theta(s) \log(s/\kappa^2)}{s} \right]_+ \\ & \left. + \theta(s) \left[\frac{s}{(s + m^2)^2} - \frac{4}{s} \log \left(1 + \frac{s}{m^2} \right) \right] \right\}. \end{aligned} \quad (7.103)$$

To avoid large logarithms we evaluate the jet function at its natural scale (c.f. Eq.(7.1)) by setting $\kappa = m = \mu_j$ and get

$$\begin{aligned} J_{n,\text{sub}}^{\mathbf{m}}(s) = & \delta(s) - 2m^2 \delta_m \delta'(s) + \frac{\alpha_s C_F}{4\pi} \left\{ \left[1 + \frac{2\pi^2}{3} \right] \delta(s) - \frac{1}{m^2} \left[\frac{m^2 \theta(s)}{s} \right]_+ \right. \\ & \left. + \frac{4}{m^2} \left[\frac{m^2 \theta(s) \log(s/m^2)}{s} \right]_+ + \theta(s) \left[\frac{s}{(s + m^2)^2} - \frac{4}{s} \log \left(1 + \frac{s}{m^2} \right) \right] \right\}, \end{aligned} \quad (7.104)$$

which is a particularly simple form of the subtracted jet function in Eq.(7.103).

For completeness we also give the analogous results for the subtracted massive jet correlator, which is again defined as a convolution with the massless jet function

$$\tilde{J}_{n,\text{sub}}^{\mathbf{m}} = (J_n^{\mathbf{m}=0})^{-1} * \tilde{J}_n^{\mathbf{m}}. \quad (7.105)$$

The expansion of $\tilde{J}_{n,\text{sub}}^{\mathbf{m}}$ in terms of individual, subtracted diagrams is given precisely as in Eq.(7.98) and Eq.(7.99), only putting tildes on the appropriate factors.

The leading order contribution is given simply by

$$\begin{aligned} \tilde{J}_{n,\text{LO},\text{sub}}^{\mathbf{m}}(p^\mu, m) = & (J_{n,\text{LO}}^{\mathbf{m}=0} * \tilde{J}_{n,\text{LO}}^{\mathbf{m}})(p^2 - m^2) \\ = & \int dq^2 \delta(p^2 - q^2) \left(-\frac{1}{\pi} \frac{1}{q^2 - m^2 + i0} \right) = -\frac{1}{\pi} \frac{1}{p^2 - m^2 + i0}. \end{aligned} \quad (7.106)$$

Using the convolution properties in Eq.(I.6) we arrive at the following result for the next-to-leading order contributions

$$\begin{aligned} \tilde{J}_{n,2,\text{sub}}^{\mathbf{m}} = & \frac{\alpha_s C_F}{4\pi} \frac{1}{\pi} \frac{1}{s + i0} \left\{ -\frac{2\pi^2}{3} - \log^2 \left(\frac{m^2}{-s - i0} \right) + \frac{2m^2}{s + m^2 + i0} \log \left(\frac{m^2}{-s - i0} \right) \right. \\ & \left. - 2 \log \left(\frac{m^2}{-s - i0} \right) \log \left(1 + \frac{s + i0}{m^2} \right) + 2 \text{Li}_2 \left(\frac{-s - i0}{m^2} \right) \right\}, \\ \tilde{J}_{n,4,\text{sub}}^{\mathbf{m}} = & -\frac{1}{\pi} \frac{2m^2 \delta_m}{[s + i0]^2} + \frac{\alpha_s C_F}{4\pi} \frac{1}{\pi} \frac{1}{s + i0} \left\{ -1 + \frac{s}{s + m^2 + i0} - m^2 \frac{5m^2 + 6s}{[s + m^2 + i0]^2} \log \left(\frac{m^2}{-s - i0} \right) \right\}, \end{aligned} \quad (7.107)$$

which are again manifestly finite and independent of the renormalisation scale μ . Note that as a consistency check we can take the imaginary part of the results in Eq.(7.107) to recover the expressions found in Eq.(7.101) and Eq.(7.102) respectively.

Adding all of the above contributions we are left with the full, subtracted massive jet correlator

$$\begin{aligned}\tilde{J}_{n,\text{sub}}^{\mathbf{m}} &= \tilde{J}_{n,\text{LO},\text{sub}}^{\mathbf{m}} + 2\tilde{J}_{n,2,\text{sub}}^{\mathbf{m}} + \tilde{J}_{n,4,\text{sub}}^{\mathbf{m}} \\ &= -\frac{1}{\pi} \frac{1}{s+i0} \left\{ -\frac{2m^2\delta_m}{s+i0} + \frac{\alpha_s C_F}{4\pi} \left[1 + \frac{4\pi^2}{3} + \frac{s}{s+m^2+i0} + 2\log^2\left(\frac{m^2}{-s-i0}\right) \right. \right. \\ &\quad \left. \left. + m^2 \frac{2s+m^2}{[s+m^2+i0]^2} \log\left(\frac{m^2}{-s-i0}\right) + 4\log\left(\frac{m^2}{-s-i0}\right) \log\left(1 + \frac{s+i0}{m^2}\right) + 4\text{Li}_2\left(\frac{-s-i0}{m^2}\right) \right] \right\},\end{aligned}\tag{7.108}$$

which is consistent with our previous result Eq.(7.104) upon taking the imaginary part.

Having now demonstrated that the divergences do indeed cancel in the ratio of the massive and massless jet function as well as the correlator, we turn to the more subtle problem of considering the cancellations for the real and virtual parts (which can only be defined for the jet function, not the correlator) of each diagram separately. To subtract the jet functions as we did above, we relied on exact analytic results which had been calculated beforehand.

In the next section we will therefore seek a different approach that will allow us to perform the subtraction for the jet function at the level of the integrand, thereby setting up the problem of canceling divergences between real emission and virtual contributions in an analogous way to what we encountered earlier in the full QCD calculation of thrust. In particular this will enable a numerical treatment of the subtraction in the EFT even in the presence of non-local divergences such as the one discussed in Eq.(7.95).

8 Integrand-level subtraction of real emission and virtual contributions

Recalling the definition of the subtracted jet function contributions in Eq.(7.99) we split them up further into real emission and virtual parts by introducing the quantities

$$J_{n,2/4,\text{sub}}^{\mathbf{m},\text{r/v}} = J_{n,2/4}^{\mathbf{m},\text{r/v}} * J_{n,\text{LO}}^{\mathbf{m}=0} - J_{n,\text{LO}}^{\mathbf{m}} * J_{n,2/4}^{\mathbf{m}=0,\text{r/v}}, \quad (8.1)$$

such that $J_{n,2/4,\text{sub}}^{\mathbf{m}} = J_{n,2/4,\text{sub}}^{\mathbf{m},\text{r}} + J_{n,2/4,\text{sub}}^{\mathbf{m},\text{v}}$. In this section we proceed to calculate these quantities explicitly only for the real emission contributions (real-real, RR) by implementing the subtraction not at the level of the final jet function as was done in the previous section, but already at the level of the integrand. Note that this means we need to refine the definition of the subtracted jet function given in Eq.(7.100) since at amplitude level the jet functions are not manifest functions of the invariants $p^2 - m^2, p^2$ yet and the integrands Eq.(7.17) and Eq.(7.50) in principle depend on all components of the external momentum p^μ . To achieve the shift necessary for aligning the threshold of the massless jet function with its massive counterpart we introduce an auxiliary vector

$$a_n^\mu(p^\mu, q^2) = a_n^- \frac{n^\mu}{2} + a_n^+ \frac{\bar{n}^\mu}{2} \equiv p^- \frac{n^\mu}{2} + \frac{q^2}{p^-} \frac{\bar{n}^\mu}{2}, \quad (8.2)$$

which is a function of the original external momentum p^μ and the shift parameter q^2 that allows to vary the off-shellness, since $a_n^2 = q^2$. As the notation suggests the auxiliary vector is specific to the collinear direction associated with the jet function. Essentially this is because the factorisation theorem ensures that the argument of the jet function is determined entirely by the small component of the collinear momentum that is fed into it (c.f. Eq.(6.32)). For the n -collinear jet function we have been concerned with so far this means that using the auxiliary momentum Eq.(8.2) we get

$$\begin{aligned} J_n^{\mathbf{m}}(a_n^\mu(p^\mu, q^2), m) &= J_n^{\mathbf{m}}(Qa_n^+ - m^2) = J_n^{\mathbf{m}}(q^2 - m^2), \\ J_n^{\mathbf{m}=0}(a_n^\mu(p^\mu, q^2)) &= J_n^{\mathbf{m}=0}(Qa_n^+) = J_n^{\mathbf{m}=0}(q^2), \end{aligned} \quad (8.3)$$

where we recall that we assume $p^- = Q$ for the original external momentum. Therefore, replacing p^μ with $a_n^\mu(p^\mu, q^2)$ at the level of the integrand will produce a jet function result with off-shellness given by the right-hand side of Eq.(8.3) after integration.

With this notation in place we can give a more general definition of the subtracted jet function, also valid at the integrand-level,

$$\begin{aligned} J_{n,\text{sub}}^{\mathbf{m}}(p^\mu, m) &\equiv J_{n,\text{sub}}^{\mathbf{m}}(p^2 - m^2) = \int dq^2 (J_n^{\mathbf{m}=0})^{-1}(a_n^\mu(p^\mu, p^2 - q^2)) J_n^{\mathbf{m}}(a_n^\mu(p^\mu, q^2), m) \\ &= \int dq^2 J_{n,\text{LO}}^{\mathbf{m}=0}(a_n^\mu(p^\mu, p^2 - q^2)) J_{n,\text{LO}}^{\mathbf{m}}(a_n^\mu(p^\mu, q^2), m) \\ &+ \int dq^2 \left[J_{n,\text{LO}}^{\mathbf{m}=0}(a_n^\mu(p^\mu, p^2 - q^2)) J_{n,\text{NLO}}^{\mathbf{m}}(a_n^\mu(p^\mu, q^2), m) \right. \\ &\quad \left. - J_{n,\text{NLO}}^{\mathbf{m}=0}(a_n^\mu(p^\mu, p^2 - q^2)) J_{n,\text{LO}}^{\mathbf{m}}(a_n^\mu(p^\mu, q^2), m) \right] + \mathcal{O}(\alpha_s^2) \\ &= \delta(p^2 - m^2) + [J_{n,\text{NLO}}^{\mathbf{m}}(a_n^\mu(p^\mu, p^2), m) - J_{n,\text{NLO}}^{\mathbf{m}=0}(a_n^\mu(p^\mu, p^2 - m^2))] + \mathcal{O}(\alpha_s^2), \end{aligned} \quad (8.4)$$

which correctly reduces to Eq.(7.100) when the relations Eq.(8.3) are used. Similarly we can define the subtracted jet function for the \bar{n} -collinear sector by using the auxiliary vector

$$a_{\bar{n}}^\mu(\bar{p}^\mu, \bar{q}^2) = a_{\bar{n}}^- \frac{\bar{n}^\mu}{2} + a_{\bar{n}}^+ \frac{\bar{p}^\mu}{2} \equiv \bar{p}^+ \frac{\bar{n}^\mu}{2} + \frac{\bar{q}^2}{\bar{p}^+} \frac{\bar{n}^\mu}{2}. \quad (8.5)$$

However, we will continue to focus only on the n -collinear sector here and proceed by evaluating each diagram, split into its real emission and virtual part, contributing to the subtracted jet function defined in Eq.(8.4).

8.1 $J_{n,2}$ RR-subtraction

From Eq.(7.21) we know that the massive and massless real emission contributions to the jet function are given respectively by

$$J_{n,2}^{\mathbf{m}(=0),\mathbf{r}}(p^\mu, m(=0)) = 16\pi^2 \alpha_s C_F \frac{1}{s} I_{n,2}^{\mathbf{m}(=0),\mathbf{r}}(p^\mu, m(=0)). \quad (8.6)$$

Using the notation $\tilde{\delta}(k, m) = \theta(k^0) \delta(k^2 - m^2)$ and in particular $\tilde{\delta}(k) = \tilde{\delta}(k, 0)$, we can cast the integrals $I_{n,2}^{\mathbf{m}(=0),\mathbf{r}}$ appearing in Eq.(8.6) into the form of physical phase space integrals,

$$\begin{aligned} I_{n,2}^{\mathbf{m},\mathbf{r}}(p^\mu, m) &= \frac{\tilde{\mu}^{2\epsilon}}{(2\pi)^{4-2\epsilon}} \int d^d k d^d l \tilde{\delta}(k) \tilde{\delta}(l, m) \delta^{(d)}(l - p + k) \frac{p^- - k^-}{k^-}, \\ I_{n,2}^{\mathbf{m}=0,\mathbf{r}}(p^\mu) &= \frac{\tilde{\mu}^{2\epsilon}}{(2\pi)^{4-2\epsilon}} \int d^d k d^d l \tilde{\delta}(k) \tilde{\delta}(l) \delta^{(d)}(l - p + k) \frac{p^- - k^-}{k^-}. \end{aligned} \quad (8.7)$$

With the notation of the previous section in place we define the subtracted real emission contribution to the Wilson line diagram by the convolution

$$\begin{aligned} J_{n,2,\text{sub}}^{\mathbf{m},\mathbf{r}}(p^\mu, m) &= \int d^d q^2 \left[\delta(p^2 - q^2) J_{n,2}^{\mathbf{m},\mathbf{r}}(a_n^\mu(p^\mu, q^2), m) - J_{n,2}^{\mathbf{m}=0,\mathbf{r}}(a_n^\mu(p^\mu, p^2 - q^2)) \delta(q^2 - m^2) \right] \\ &= 16\pi^2 \alpha_s C_F \frac{1}{s} \left[I_{n,2}^{\mathbf{m},\mathbf{r}}(a_n^\mu(p^\mu, p^2), m) - I_{n,2}^{\mathbf{m}=0,\mathbf{r}}(a_n^\mu(p^\mu, p^2 - m^2)) \right] \\ &\equiv 16\pi^2 \alpha_s C_F \frac{1}{s} I_{n,2,\text{sub}}^{\mathbf{m},\mathbf{r}}(p^\mu, m). \end{aligned} \quad (8.8)$$

Writing out the subtracted integral in detail gives us

$$\begin{aligned} I_{n,2,\text{sub}}^{\mathbf{m},\mathbf{r}}(p^\mu, m) &= \frac{\tilde{\mu}^{2\epsilon}}{(2\pi)^{4-2\epsilon}} \int d^d k d^d l \tilde{\delta}(k) \left\{ \frac{a_n^-(p^\mu, p^2) - k^-}{k^-} \tilde{\delta}(l, m) \delta^{(d)}(l - a_n(p^\mu, p^2) + k) \right. \\ &\quad \left. - \frac{a_n^-(p^\mu, p^2 - m^2) - k^-}{k^-} \tilde{\delta}(l) \delta^{(d)}(l - a_n(p^\mu, p^2 - m^2) + k) \right\} \\ &= \frac{2\tilde{\mu}^{2\epsilon}}{(2\pi)^{4-2\epsilon}} \int d^d k d^d l \tilde{\delta}(k) \delta(l^- - p^- + k^-) \delta^{(d-2)}(\mathbf{l}_\perp + \mathbf{k}_\perp) \frac{p^- - k^-}{k^-} \\ &\quad \times \left\{ \tilde{\delta}(l, m) \delta(l^+ - p^+ + k^+) - \tilde{\delta}(l) \delta\left(l^+ - \frac{p^2 - m^2}{p^-} + k^+\right) \right\}, \end{aligned} \quad (8.9)$$

where in the second line we have split up the momentum conserving delta functions into lightcone components. In Eq.(8.9) we can explicitly see how the subtraction takes place at the integrand-level. While the concrete amplitude we are considering is naturally a function of lightcone components and thus lends itself particularly well to the decomposition Eq.(8.2), we could in principle satisfy any dependence of the integrand on a given component of a_n^μ .

We proceed by using Eq.(7.26) to eliminate the integral over $d^d l$ with the delta functions for the $(-, \perp)$ -components and implementing the respective mass-shell conditions $\tilde{\delta}(l, m(=0))$,

$$\begin{aligned} I_{n,2,\text{sub}}^{\mathbf{m},\mathbf{r}}(p^\mu, m) &= \frac{\tilde{\mu}^{2\epsilon}}{(2\pi)^{4-2\epsilon}} \frac{1}{p^-} \int d^d k \tilde{\delta}(k) \theta(p^- - k^-) \frac{p^- - k^-}{k^-} \\ &\quad \times \left\{ \delta\left(k^+ - \frac{s}{p^-} \left(1 - \frac{p^+ k^-}{s}\right)\right) - \delta\left(k^+ - \frac{s}{p^-} \left(1 - \frac{k^-}{p^-}\right)\right) \right\}, \end{aligned} \quad (8.10)$$

where $s = p^2 - m^2$ now denotes the off-shellness of the massive external momentum. Decomposing $d^d k$ into lightcone components as in Eq.(A.7), and carrying out the k^+ integration yields

$$\begin{aligned} I_{n,2,\text{sub}}^{\mathbf{m},\mathbf{r}}(p^\mu, m) &= \frac{\tilde{\mu}^{2\epsilon}}{(2\pi)^{4-2\epsilon}} \frac{\pi^{1-\epsilon}}{2\Gamma(1-\epsilon)} \frac{\theta(p^-)}{p^-} \theta(s) \int dk^- \theta(k^-) \frac{p^- - k^-}{(k^-)^{1+\epsilon}} \left(\frac{p^-}{s}\right)^\epsilon \\ &\quad \times \left\{ \theta\left(1 - \frac{p^+ k^-}{s}\right) \left(1 - \frac{p^+ k^-}{s}\right)^{-\epsilon} - \theta\left(1 - \frac{k^-}{p^-}\right) \left(1 - \frac{k^-}{p^-}\right)^{-\epsilon} \right\}, \end{aligned} \quad (8.11)$$

where the above step functions were simplified according to

$$\theta\left(\frac{s}{p^-}\left(1 - \frac{p^+ k^-}{s}\right)\right) = \theta(s)\theta\left(1 - \frac{p^+ k^-}{s}\right), \quad \theta\left(\frac{s}{p^-}\left(1 - \frac{k^-}{p^-}\right)\right) = \theta(s)\theta\left(1 - \frac{k^-}{p^-}\right). \quad (8.12)$$

Note that each of the equalities in Eq.(8.12) only holds modulo all other step functions in Eq.(8.11). In particular the first identity prompts us to define $a^- = \frac{p^+}{s}k^-$ as a convenient variable for integration. To be able to safely take the limit $\epsilon \rightarrow 0$ in the subtraction we rearrange Eq.(8.11) according to the regions of overlapping ($0 \leq a^- \leq 1$) and non-overlapping ($1 < a^- \leq 1/\Delta$) support of the step functions restricting the upper limit on a^- . Here we introduced the dimensionless parameter $\Delta = \frac{s}{s+m^2}$ satisfying $0 \leq \Delta < 1$. Thus, recollecting all prefactors from Eq.(8.8) allows us to write

$$J_{n,2,\text{sub}}^{\mathbf{m},\mathbf{r}}(p^\mu, m) = \frac{\alpha_s C_F}{4\pi} \frac{2}{\Gamma(1-\epsilon)} \left[\frac{e^{\gamma_E}(s+m^2)}{\mu^2} \right]^\epsilon \frac{\theta(s)\mu^{4\epsilon}}{s^{1+2\epsilon}} \theta(p^-) \\ \times \left\{ \int_0^1 da^- \frac{1-\Delta a^-}{(a^-)^{1+\epsilon}} \left[\frac{1}{(1-a^-)^\epsilon} - \frac{1}{(1-\Delta a^-)^\epsilon} \right] - \int_1^{\frac{1}{\Delta}} da^- \frac{(1-\Delta a^-)^{1-\epsilon}}{(a^-)^{1+\epsilon}} \right\}. \quad (8.13)$$

Carrying out the integrals in Eq.(8.13) we find

$$I_{n,2,\text{sub}}^{\mathbf{m},\mathbf{r},1} \equiv \frac{\theta(s)\mu^{4\epsilon}}{s^{1+2\epsilon}} \int_0^1 da^- \frac{1-\Delta a^-}{(a^-)^{1+\epsilon}} \left[\frac{1}{(1-a^-)^\epsilon} - \frac{1}{(1-\Delta a^-)^\epsilon} \right] = -\frac{\pi^2}{12}\delta(s) + \mathcal{O}(\epsilon), \\ I_{n,2,\text{sub}}^{\mathbf{m},\mathbf{r},2} \equiv \frac{\theta(s)\mu^{4\epsilon}}{s^{1+2\epsilon}} \int_1^{\frac{1}{\Delta}} da^- \frac{(1-\Delta a^-)^{1-\epsilon}}{(a^-)^{1+\epsilon}} = \left\{ \left[\frac{1}{2\epsilon^2} + \frac{1}{\epsilon} + \frac{1}{\epsilon} \log\left(\frac{\mu^2}{m^2}\right) + 2 - \frac{\pi^2}{6} + \log\left(\frac{\mu^2}{m^2}\right) \right. \right. \\ \left. \left. + \frac{1}{2} \log^2\left(\frac{\mu^2}{m^2}\right) \right] \delta(s) - \left[1 + \log\left(\frac{\mu^2}{m^2}\right) \right] \frac{1}{\mu^2} \left[\frac{\mu^2 \theta(s)}{s} \right]_+ - \frac{1}{\mu^2} \left[\frac{\mu^2 \theta(s) \log(s/\mu^2)}{s} \right]_+ \right. \\ \left. + \theta(s) \left[\frac{1}{s+m^2} + \frac{1}{s} \log\left(1 + \frac{s}{m^2}\right) \right] + \mathcal{O}(\epsilon) \right\}. \quad (8.14)$$

In particular we see that if we are only interested in the region where $s > 0$ strictly, we can safely take the limit $\epsilon \rightarrow 0$ even before performing the integration without running into divergent integrals. As we discussed earlier this would not have been possible with the initial jet function contributions in Eq.(7.88) and Eq.(7.85) since there the terms proportional to $\frac{1}{\epsilon} \left[\frac{\mu^2 \theta(s)}{s} \right]_+$ would have rendered this limit ill-defined, even at finite s .

Assuming $s > 0$ and $\epsilon = 0$ the integrals in Eq.(8.14) can be directly (and in principle also numerically) evaluated to give

$$I_{n,2,\text{sub}}^{\mathbf{m},\mathbf{r},1}|_{\epsilon=0}^{s>0} = 0, \\ I_{n,2,\text{sub}}^{\mathbf{m},\mathbf{r},2}|_{\epsilon=0}^{s>0} = \frac{\theta(s)}{s} \left[-1 + \frac{s}{s+m^2} + \log\left(1 + \frac{s}{m^2}\right) - \log\left(\frac{s}{m^2}\right) \right]. \quad (8.15)$$

With the above results we can now give the finite part of the RR-subtracted jet function Eq.(8.13),

$$J_{n,2,\text{sub}}^{\mathbf{m},\mathbf{r}}|_{\epsilon=0}^{s>0}(p^\mu, m) = \frac{\alpha_s C_F}{2\pi} \theta(p^-) \left\{ I_{n,2,\text{sub}}^{\mathbf{m},\mathbf{r},1}|_{\epsilon=0}^{s>0} - I_{n,2,\text{sub}}^{\mathbf{m},\mathbf{r},2}|_{\epsilon=0}^{s>0} \right\} \\ = \frac{\alpha_s C_F}{4\pi} \theta(s) \theta(p^-) \left[\frac{2}{s} - \frac{2}{s+m^2} - \frac{2}{s} \log\left(1 + \frac{s}{m^2}\right) + \frac{2}{s} \log\left(\frac{s}{m^2}\right) \right], \quad (8.16)$$

which is now also independent of the renormalisation scale μ . As the results obtained in Eq.(8.14) already indicate, this is not going to be the case for the full, analytic result including singular terms.

For completeness we also state the full analytic result for Eq.(8.13) valid for $s = 0$ and $\varepsilon \neq 0$. Collecting terms according to inverse powers of the off-shellness $s = p^2 - m^2$ it reads

$$J_{n,2,\text{sub}}^{\mathbf{m},\mathbf{r}}(p^\mu, m) = \frac{\alpha_s C_F}{4\pi} \theta(p^-) \left[\frac{e^{\gamma_E}(s+m^2)}{\mu^2} \right]^\epsilon \frac{2\Gamma(-\epsilon)}{\Gamma(2-2\epsilon)} \left[\frac{\theta(s)\mu^{4\epsilon}}{s^{1+2\epsilon}}(1-2\epsilon) + \frac{\theta(s)\mu^{4\epsilon}}{s^{2\epsilon}} \frac{1}{s+m^2} \epsilon \right. \\ \left. - \frac{\theta(s)\mu^{2\epsilon}}{s^{1+\epsilon}} \left(\frac{\mu^2}{s+m^2} \right)^\epsilon (1-\epsilon) \right] = J_{n,2}^{\mathbf{m},\mathbf{r}}(p^2 - m^2) - J_{n,2}^{\mathbf{m}=0,\mathbf{r}}(p^2 - m^2), \quad (8.17)$$

where we recognise the blue terms as $J_{n,2}^{\mathbf{m},\mathbf{r}}$ before it was expanded into plus distributions (c.f. Eq.(7.33)) and identify the remaining red terms as corresponding to $J_{n,2}^{\mathbf{m}=0,\mathbf{r}}$ with appropriately shifted threshold. Expanding Eq.(8.17) to constant order in ϵ yields the RR-subtracted contribution

$$J_{n,2,\text{sub}}^{\mathbf{m},\mathbf{r}}(p^\mu, m) = \frac{\alpha_s C_F}{4\pi} \theta(p^-) \left\{ \left[-\frac{1}{\epsilon^2} - \frac{2}{\epsilon} - \frac{1}{\epsilon} \log\left(\frac{\mu^2}{m^2}\right) + \frac{\pi^2}{4} - 4 + \frac{1}{2} \log^2\left(\frac{\mu^2}{m^2}\right) \right] \delta(s) \right. \\ \left. + \left[1 + \log\left(\frac{\mu^2}{m^2}\right) \right] \frac{2}{\mu^2} \left[\frac{\mu^2 \theta(s)}{s} \right]_+ + \frac{2}{\mu^2} \left[\frac{\mu^2 \theta(s) \log(s/\mu^2)}{s} \right]_+ \right. \\ \left. - 2\theta(s) \left[\frac{1}{s+m^2} + \frac{1}{s} \log\left(1 + \frac{s}{m^2}\right) \right] \right\}, \quad (8.18)$$

which we could have also obtained by directly combining the results in Eq.(8.14). As a consistency check Eq.(8.18) yields the correct finite part Eq.(8.16) when we take $s > 0$ and $\epsilon = 0$. Note that since the zero-bin, which normally facilitates the pull up from IR to UV, cancels between massive and massless jet functions all the divergences remaining in the above result are of IR origin.

We further see that the subtracted real emission jet function contains a term proportional to $\frac{1}{\epsilon} \log(\mu^2/m^2)$, and whence, unlike the full subtracted result in Eq.(7.101) and the finite part for $s > 0$, cannot be brought to a μ -independent form. Independence of the renormalisation scale is therefore only established once the virtual part (the VV-subtraction, see Eq.(8.32)) is added, or $s > 0$ is strictly imposed.

8.2 $J_{n,4}$ RR-subtraction

We proceed in complete analogy to the treatment of the RR subtraction for $J_{n,2,\text{sub}}^{\mathbf{m},\mathbf{r}}$. The massless and massive real emission jet function contributions $J_{n,4}^{\mathbf{m}(=0),\mathbf{r}}$ are given by (c.f. Eq.(7.54))

$$J_{n,4}^{\mathbf{m}(=0),\mathbf{r}}(p^\mu, m(=0)) = -16\pi^2 \alpha_s C_F \frac{1}{s^2} I_{n,4}^{\mathbf{m}(=0),\mathbf{r}}(p^\mu, m(=0)), \quad (8.19)$$

where the integrals to be calculated read

$$I_{n,4}^{\mathbf{m},\mathbf{r}}(p^\mu, m) = \frac{\tilde{\mu}^{2\epsilon}}{(2\pi)^{4-2\epsilon}} \int d^d k d^d l \tilde{\delta}(k) \tilde{\delta}(l, m) \delta^{(d)}(l - p + k) \\ \times \left\{ (1-\epsilon) \left[k^- p^+ + k^+ p^- - s \left(1 + \frac{k^-}{p^-} \right) \right] + 2m^2 \right\}, \quad (8.20)$$

$$I_{n,4}^{\mathbf{m}=0,\mathbf{r}}(p^\mu, m) = \frac{\tilde{\mu}^{2\epsilon}}{(2\pi)^{4-2\epsilon}} \int d^d k d^d l \tilde{\delta}(k) \tilde{\delta}(l) \delta^{(d)}(l - p + k) (1-\epsilon) \left[k^- p^+ + k^+ p^- - p^2 \left(1 + \frac{k^-}{p^-} \right) \right].$$

Just as in Eq.(8.8) we use the n -collinear auxiliary momentum Eq.(8.2) to define the RR subtracted contribution

$$J_{n,4,\text{sub}}^{\mathbf{m},\mathbf{r}}(p^\mu, m) = \int dq^2 \left[\delta(p^2 - q^2) J_{n,4}^{\mathbf{m},\mathbf{r}}(a_n^\mu(p^\mu, q^2), m) - J_{n,4}^{\mathbf{m}=0,\mathbf{r}}(a_n^\mu(p^\mu, p^2 - q^2)) \delta(q^2 - m^2) \right] \\ = -16\pi^2 \alpha_s C_F \frac{1}{s^2} \left[I_{n,4}^{\mathbf{m},\mathbf{r}}(a_n^\mu(p^\mu, p^2), m) - I_{n,4}^{\mathbf{m}=0,\mathbf{r}}(a_n^\mu(p^\mu, p^2 - m^2)) \right] \\ \equiv -16\pi^2 \alpha_s C_F \frac{1}{s^2} I_{n,4,\text{sub}}^{\mathbf{m},\mathbf{r}}(p^\mu, m). \quad (8.21)$$

Writing out the above integral in detail we get

$$\begin{aligned}
I_{n,4,\text{sub}}^{\mathbf{m},\mathbf{r}}(p^\mu, m) &= \frac{2\mu^{2\epsilon}}{(2\pi)^{4-2\epsilon}} \int d^d k d^d l \tilde{\delta}(k) \delta(l^- - p^- + k^-) \delta^{(d-2)}(\mathbf{l}_\perp + \mathbf{k}_\perp) \\
&\times \left\{ \left[(1-\epsilon) \left[k^+ p^- + k^- p^+ - s \left(1 + \frac{k^-}{p^-} \right) \right] + 2m^2 \right] \tilde{\delta}(l, m) \delta(l^+ - p^+ + k^+) \right. \\
&\left. - (1-\epsilon) \left[k^+ p^- + k^- \frac{s}{p^-} - s \left(1 + \frac{k^-}{p^-} \right) \right] \tilde{\delta}(l, m) \delta \left(l^+ - \frac{p^2 - m^2}{p^-} + k^+ \right) \right\}.
\end{aligned} \tag{8.22}$$

Following steps essentially identical to what we did for $I_{n,2,\text{sub}}^{\mathbf{m},\mathbf{r}}$ to eliminate all delta functions in Eq.(8.22) we arrive at an expression analogous to Eq.(8.11), which now reads

$$\begin{aligned}
I_{n,4,\text{sub}}^{\mathbf{m},\mathbf{r}}(p^\mu, m) &= -\frac{\mu^{2\epsilon}}{(2\pi)^{4-2\epsilon}} \frac{\pi^{1-\epsilon}}{2\Gamma(1-\epsilon)} \frac{\theta(p^-)\theta(s)}{p^-} \int dk^- \theta(k^-) \left(\frac{p^-}{sk^-} \right)^\epsilon \\
&\times \left\{ \theta \left(1 - \frac{p^+ k^-}{s} \right) \left(1 - \frac{p^+ k^-}{s} \right)^{-\epsilon} \left[(1-\epsilon) s \frac{k^-}{p^-} - 2m^2 \right] \right. \\
&\left. - \theta \left(1 - \frac{k^-}{p^-} \right) \left(1 - \frac{k^-}{p^-} \right)^{-\epsilon} (1-\epsilon) s \frac{k^-}{p^-} \right\}.
\end{aligned} \tag{8.23}$$

The remaining integration is now convenient to carry out using the variable $a^- = \frac{p^+}{s} k^-$. Reinstating the prefactors from Eq.(8.19) and arranging the contributions according to overlapping ($0 \leq a^- \leq 1$) and non-overlapping ($1 < a^- \leq 1/\Delta$) regions of a^- as well as powers of m^2 yields

$$\begin{aligned}
J_{n,4,\text{sub}}^{\mathbf{m},\mathbf{r}}(p^\mu, m) &= \frac{\alpha_s C_F}{4\pi} \frac{2}{\Gamma(1-\epsilon)} \left[\frac{e^{\gamma_E}(s+m^2)}{\mu^2} \right]^\epsilon \theta(p^-) \frac{\theta(s)\mu^{4\epsilon}}{s^{1+2\epsilon}} \\
&\times \left\{ (1-\epsilon) \Delta^2 \int_0^1 da^- (a^-)^{1-\epsilon} \left[\frac{1}{(1-a^-)^\epsilon} - \frac{1}{(1-\Delta a^-)^\epsilon} \right] \right. \\
&\left. - (1-\epsilon) \Delta^2 \int_1^{\frac{1}{\Delta}} da^- \frac{(a^-)^{1-\epsilon}}{(1-\Delta a^-)^\epsilon} - \frac{2m^2}{s+m^2} \int_0^1 da^- \frac{1}{[(1-a^-)a^-]^\epsilon} \right\}.
\end{aligned} \tag{8.24}$$

As a reminder, the above result is given in terms of the dimensionless parameter $\Delta = \frac{s}{s+m^2}$. Carrying out the integrals in Eq.(8.24) and expanding in ϵ we get

$$I_{n,4,\text{sub}}^{\mathbf{m},\mathbf{r},\mathbf{1}} = (1-\epsilon) \Delta^2 \frac{\theta(s)\mu^{4\epsilon}}{s^{1+2\epsilon}} \int_0^1 da^- (a^-)^{1-\epsilon} \left[\frac{1}{(1-a^-)^\epsilon} - \frac{1}{(1-\Delta a^-)^\epsilon} \right] = 0 + \mathcal{O}(\epsilon), \tag{8.25}$$

$$\begin{aligned}
I_{n,4,\text{sub}}^{\mathbf{m},\mathbf{r},\mathbf{2}} &= (1-\epsilon) \Delta^2 \frac{\theta(s)\mu^{4\epsilon}}{s^{1+2\epsilon}} \int_1^{\frac{1}{\Delta}} da^- \frac{(a^-)^{1-\epsilon}}{(1-\Delta a^-)^\epsilon} = -\frac{1}{2} \left[\frac{1}{\epsilon} + 1 + \log \left(\frac{\mu^2}{m^2} \right) \right] \delta(s) + \frac{1}{2} \frac{1}{\mu^2} \left[\frac{\mu^2 \theta(s)}{s} \right]_+ \\
&- \theta(s) \frac{1}{2} \frac{s}{(s+m^2)^2} + \mathcal{O}(\epsilon),
\end{aligned}$$

$$I_{n,4,\text{sub}}^{\mathbf{m},\mathbf{r},\mathbf{m}} = \frac{2m^2}{s+m^2} \frac{\theta(s)\mu^{4\epsilon}}{s^{1+2\epsilon}} \int_0^1 da^- \frac{1}{[(1-a^-)a^-]^\epsilon} = -\left[\frac{1}{\epsilon} + 2 \right] \delta(s) + \frac{2}{\mu^2} \left[\frac{\mu^2 \theta(s)}{s} \right]_+ - \theta(s) \frac{2}{s+m^2} + \mathcal{O}(\epsilon),$$

all of which are perfectly finite when we take $s > 0$ strictly and $\epsilon \rightarrow 0$, just as we discussed below Eq.(8.14). Assuming a finite s and directly performing the integrals in Eq.(8.25) with $\epsilon = 0$ thus yields

$$\begin{aligned}
I_{n,4,\text{sub}}^{\mathbf{m},\mathbf{r},\mathbf{1}}|_{\epsilon=0}^{s>0} &= 0, \\
I_{n,4,\text{sub}}^{\mathbf{m},\mathbf{r},\mathbf{2}}|_{\epsilon=0}^{s>0} &= \frac{\theta(s)}{2} \left[\frac{1}{s} - \frac{s}{(s+m^2)^2} \right], \\
I_{n,4,\text{sub}}^{\mathbf{m},\mathbf{r},\mathbf{m}}|_{\epsilon=0}^{s>0} &= \theta(s) \frac{2m^2}{s(s+m^2)}.
\end{aligned} \tag{8.26}$$

Combining the above results gives the finite part of the RR-subtracted jet function contribution

$$\begin{aligned} J_{n,4,\text{sub}}^{\mathbf{m},\mathbf{r}}|_{\epsilon=0}^{s>0}(p^\mu, m) &= \frac{\alpha_s C_F}{2\pi} \theta(p^-) \left\{ I_{n,4,\text{sub}}^{\mathbf{m},\mathbf{r},\mathbf{1}}|_{\epsilon=0}^{s>0} - I_{n,4,\text{sub}}^{\mathbf{m},\mathbf{r},\mathbf{2}}|_{\epsilon=0}^{s>0} - I_{n,4,\text{sub}}^{\mathbf{m},\mathbf{r},\mathbf{m}}|_{\epsilon=0}^{s>0} \right\} \\ &= \frac{\alpha_s C_F}{4\pi} \theta(s) \theta(p^-) \left\{ -\frac{5}{s} + \frac{5s + 4m^2}{(s + m^2)^2} \right\}. \end{aligned} \quad (8.27)$$

Additionally, the full, analytic result can be arranged by inverse powers of $s = p^2 - m^2$ and thus be brought to a similarly suggestive form as in Eq.(8.17),

$$\begin{aligned} J_{n,4,\text{sub}}^{\mathbf{m},\mathbf{r}}(p^\mu, m) &= \frac{\alpha_s C_F}{4\pi} \frac{\Gamma(1-\epsilon)}{\Gamma(2-2\epsilon)} \theta(p^-) \left\{ \frac{1}{s + m^2} \left[\frac{e^{\gamma_E}(s + m^2)}{\mu^2} \right]^\epsilon \left[4m^2 \frac{\theta(s) \mu^{4\epsilon}}{s^{1+2\epsilon}} - \frac{\theta(s) \mu^{4\epsilon}}{s^{2\epsilon}} \frac{s(1-\epsilon)}{s + m^2} \right] \right. \\ &\quad \left. - \frac{\theta(s) \mu^{2\epsilon}}{s^{1+\epsilon}} (e^{\gamma_E})^\epsilon (1-\epsilon) \right\} = J_{n,4}^{\mathbf{m},\mathbf{r}}(p^\mu, m) - J_{n,4}^{\mathbf{m}=0,\mathbf{r}}(p^\mu, m). \end{aligned} \quad (8.28)$$

Expanded into distributional form the above result reads

$$J_{n,4,\text{sub}}^{\mathbf{m},\mathbf{r}}(p^\mu, m) = \frac{\alpha_s C_F}{4\pi} \theta(p^-) \left\{ \left[\frac{3}{\epsilon} + 5 - 2\log\left(\frac{\mu^2}{m^2}\right) \right] \delta(s) - \frac{5}{\mu^2} \left[\frac{\mu^2 \theta(s)}{s} \right]_+ + \theta(s) \frac{5s + 4m^2}{(s + m^2)^2} \right\}, \quad (8.29)$$

which could have also been obtained by subtracting the two distributional expressions for $J_{n,4}^{\mathbf{m},\mathbf{r}}$ in Eq.(7.58) and $J_{n,4}^{\mathbf{m}=0,\mathbf{r}}$ in Eq.(7.89) as indicated in Eq.(8.1), or by combining the results in Eq.(8.25) directly. Note that the finite part of Eq.(8.29) correctly reproduces Eq.(8.27).

8.3 Subtracted real emission and virtual jet function (final results)

Combining the analytic results Eq.(8.18) and Eq.(8.29) yields the full real emission part of the subtracted massive jet function

$$\begin{aligned} J_{n,\text{NLO},\text{sub}}^{\mathbf{m},\mathbf{r}}(p^\mu, m) &= 2J_{n,2,\text{sub}}^{\mathbf{m},\mathbf{r}} + J_{n,4,\text{sub}}^{\mathbf{m},\mathbf{r}} \\ &= \frac{\alpha_s C_F}{4\pi} \left\{ \left[-\frac{2}{\epsilon^2} - \frac{1}{\epsilon} - \frac{2}{\epsilon} \log\left(\frac{\mu^2}{m^2}\right) + \frac{\pi^2}{2} - 3 - 2\log\left(\frac{\mu^2}{m^2}\right) + \log^2\left(\frac{\mu^2}{m^2}\right) \right] \delta(s) \right. \\ &\quad - \left[1 - 4\log\left(\frac{\mu^2}{m^2}\right) \right] \frac{1}{\mu^2} \left[\frac{\mu^2 \theta(s)}{s} \right]_+ + \frac{4}{\mu^2} \left[\frac{\mu^2 \theta(s) \log(s/\mu^2)}{s} \right]_+ \\ &\quad \left. + \theta(s) \left[\frac{s}{(s + m^2)^2} - \frac{4}{s} \log\left(1 + \frac{s}{m^2}\right) \right] \right\}. \end{aligned} \quad (8.30)$$

Note that the above result fulfills the important consistency condition that the terms contributing to $s > 0$ are identical to those of the full subtracted jet function in Eq.(7.103). This is expected since the virtual contributions can only contribute as terms proportional to $\delta(s)$ and should eventually cancel the remaining ϵ -poles. Taking $s > 0$ and $\epsilon = 0$ in Eq.(8.30) we obtain

$$J_{n,\text{NLO},\text{sub}}^{\mathbf{m},\mathbf{r}}(p^\mu, m)|_{\epsilon=0}^{s>0} = \frac{\alpha_s C_F}{4\pi} \theta(p^-) \theta(s) \left\{ -\frac{1}{s} + \frac{s}{(s + m^2)^2} + \frac{4}{s} \log\left(\frac{s}{m^2}\right) - \frac{4}{s} \log\left(1 + \frac{s}{m^2}\right) \right\}, \quad (8.31)$$

which could have equivalently been obtained by adding the individual contributions Eq.(8.16) and Eq.(8.27). This implies that the above result can in principle be obtained by numerical methods, directly evaluating the integrals Eq.(8.14) and Eq.(8.25) in $d = 4$.

The quantity in Eq.(8.31) should be thought of as analogous to the non-singular part of the real emission thrust distribution Eq.(2.77), which we showed to be calculable without any regularisation. However, to correctly reproduce the contributions coming from $\tau = 0$ in a numerical calculation we had to rely on techniques such as the dipole subtraction method. A similar implementation would

be needed here to rearrange the remaining local IR divergences between the real emission and virtual part of the subtracted jet function.

For completeness we now turn, without giving the specifics of the calculation, to quoting the results for the virtual contributions (VV-subtraction, c.f. Eq.(8.1)) to the subtracted jet function,


$$\begin{aligned}
J_{n,\text{NLO,sub}}^{\mathbf{m},\mathbf{v}}(p^\mu, m) &= 2J_{n,2,\text{sub}}^{\mathbf{m},\mathbf{v}} + J_{n,4,\text{sub}}^{\mathbf{m},\mathbf{v}} + J_{n,\delta_m}^{\mathbf{m}} \\
&= -2m^2 \delta_m \theta(p^-) \delta'(s) + \frac{\alpha_s C_F}{4\pi} \theta(p^-) \left\{ \frac{2}{\epsilon^2} + \frac{1}{\epsilon} + \frac{2}{\epsilon} \log\left(\frac{\mu^2}{m^2}\right) + 4 + \frac{\pi^2}{6} \right. \\
&\quad \left. + \log\left(\frac{\mu^2}{m^2}\right) + \log^2\left(\frac{\mu^2}{m^2}\right) \right\} \delta(s), \\
J_{n,2,\text{sub}}^{\mathbf{m},\mathbf{v}}(p^\mu, m) &= \frac{\alpha_s C_F}{4\pi} \theta(p^-) \left\{ \frac{1}{\epsilon^2} + \frac{2}{\epsilon} + \frac{1}{\epsilon} \log\left(\frac{\mu^2}{m^2}\right) + 4 + \frac{\pi^2}{12} + 2\log\left(\frac{\mu^2}{m^2}\right) + \frac{1}{2} \log^2\left(\frac{\mu^2}{m^2}\right) \right\} \delta(s), \\
J_{n,4,\text{sub}}^{\mathbf{m},\mathbf{v}}(p^\mu, m) &= 2m^2 \delta Z_m^{\text{OS}} \theta(p^-) \delta'(s) + \frac{\alpha_s C_F}{4\pi} \theta(p^-) \left\{ -\frac{3}{\epsilon} - 4 - 3\log\left(\frac{\mu^2}{m^2}\right) \right\} \delta(s).
\end{aligned} \tag{8.32}$$

It should be noted that just like the subtracted real emission contributions all of the above quantities are UV finite (i.e. all remaining poles are in ϵ_{IR}) since the zero-bin cancels between them. In particular we observe that the coefficient proportional to $\delta(s)$ in $J_{n,4,\text{sub}}^{\mathbf{m},\mathbf{v}}$ in the last line of Eq.(8.32) arises as

$$-\frac{3}{\epsilon_{\text{IR}}} - 4 - 3\log\left(\frac{\mu^2}{m^2}\right) = \delta Z_\psi^{\mathbf{m},\text{OS}} - \delta Z_\psi^{\mathbf{m}=0,\text{OS}}, \tag{8.33}$$

with the renormalisation factor $\delta Z_\psi^{\mathbf{m},\text{OS}}$ for a massive quark given as in Eq.(7.79) and the massless wave function renormalisation factor $\delta Z_\psi^{\mathbf{m}=0,\text{OS}}$ as in Eq.(C.3). The latter appears as the scaleless virtual contribution (c.f. Eq.(7.89)) $J_{n,4}^{\mathbf{m}=0,\mathbf{v}}$ in the subtraction. The real emission and virtual subtracted jet functions in Eq.(8.31) and Eq.(8.32) are consistent in that when added they give the correct full result we computed in Eq.(7.103).

To summarise the calculations of the previous sections we want to explicitly compare the structure of quantities arising in our treatment of the SCET jet function with the thrust distribution of full QCD discussed in Sec. 2.6. We hope that this comparison is facilitated by the following “dictionary”:

SCET (jet function)	eq.	QCD (thrust)	eq.
$J_{n,2}^{\mathbf{m},\mathbf{r}} \simeq \frac{1}{\epsilon} \delta(s), \frac{1}{\epsilon} \left[\frac{\theta(s)}{s} \right]_+$	(7.35)		-
$J_{n,2,\text{sub}}^{\mathbf{m},\mathbf{r}}, J_{n,2,\text{sub}}^{\mathbf{m},\mathbf{v}} \simeq \frac{1}{\epsilon} \delta(s)$	(8.18), (8.32)	$\frac{d\sigma^{\mathbf{r}}}{d\tau}, \frac{d\sigma^{\mathbf{v}}}{d\tau}$	(2.68), (2.70)
$J_{n,2,\text{sub}}^{\mathbf{m},\mathbf{r}} _{\epsilon=0}, J_{n,2,\text{sub}}^{\mathbf{m},\mathbf{v}} _{\epsilon=0} \simeq \frac{\theta(s)}{s} \times \text{fin.}$	(8.16)	$\frac{d\sigma^{\mathbf{r}}}{d\tau} _{\tau>0}, \frac{d\sigma^{\mathbf{v}}}{d\tau} _{\tau>0}$	(2.77)
$J_{n,2,\text{sub}}^{\mathbf{m}} \simeq \left[\frac{\theta(s)}{s} \right]_+ \times \text{fin.}$	(7.101)	$\frac{d\sigma}{d\tau}$	(2.71)

Tab.(8.3): Outline of structural similarities between the SCET jet function and full QCD thrust.

We can see that the conventional jet function exhibiting the non-local divergence has no structural analogue in the full theory. By introducing the subtracted jet function as in Eq.(8.4) we are able to separate the information contained in the jet function in a way that is similar to the real emission and virtual parts encountered in the QCD thrust distribution, containing only local divergences at $s = 0$, $\tau = 0$. Moreover, we have shown that the finite parts away from the threshold and given in line three of Tab.8.3 can be numerically calculated. Consistently incorporating the remaining contributions from the threshold $s = 0$, $\tau = 0$ in a numerical routine will now only require a subtraction procedure similar to the dipole method of QCD, as opposed to having to introduce new counter term prescriptions to treat the non-local divergence. This presents a distinct advantage of the subtracted jet function.

8.4 Subtracted jet function in the factorisation theorem

In this section we explain how the subtracted massive jet function calculated in the previous section can be useful in implementing resummed calculations in a semi-analytic way via the factorisation theorem. Concretely we consider the inverse of Eq.(8.4), i.e. we want to write the regular massive jet function in terms of a convolution of the massless jet function with the subtracted massive jet function

$$\begin{aligned}
J_n^{\mathbf{m}}(p^\mu, m, \mu) &\equiv \int dq^2 J_n^{\mathbf{m}=0}(a_n^\mu(p^\mu, p^2 - q^2), \mu) J_{n,\text{sub}}^{\mathbf{m}}(a_n^\mu(p^\mu, q^2), m) \\
&= \int dq^2 J_{n,\text{LO}}^{\mathbf{m}=0}(a_n^\mu(p^\mu, p^2 - q^2)) J_{n,\text{LO},\text{sub}}^{\mathbf{m}}(a_n^\mu(p^\mu, q^2), m) \\
&+ \int dq^2 \left[J_{n,\text{LO}}^{\mathbf{m}=0}(a_n^\mu(p^\mu, p^2 - q^2)) J_{n,\text{NLO},\text{sub}}^{\mathbf{m}}(a_n^\mu(p^\mu, q^2), m) \right. \\
&\quad \left. + J_{n,\text{NLO}}^{\mathbf{m}=0}(a_n^\mu(p^\mu, p^2 - q^2), \mu) J_{n,\text{LO},\text{sub}}^{\mathbf{m}}(a_n^\mu(p^\mu, q^2), m) \right] + \mathcal{O}(\alpha_s^2) \\
&= \delta(p^2 - m^2) + [J_{n,\text{NLO},\text{sub}}^{\mathbf{m}}(a_n^\mu(p^\mu, p^2), m) + J_{n,\text{NLO}}^{\mathbf{m}=0}(a_n^\mu(p^\mu, p^2 - m^2), \mu)] + \mathcal{O}(\alpha_s^2).
\end{aligned} \tag{8.35}$$

Note that we have made explicit the dependence on the renormalisation scale μ which is entirely contained in the massless jet function. This is crucial since it allows us to separate the information unique to the massive jet function in the finite, numerically calculable, subtracted factor, while the UV-divergent, hence μ -dependent, behaviour necessary for the resummation of large logarithms is still analytically accessible.

Let us now look at the factorisation theorem Eq.(6.36) for thrust in the light of Eq.(8.35). Focusing on the jet functions in particular we get

$$\begin{aligned}
\frac{d\sigma}{d\tau} &= \sigma_2^{\text{LO}} H(Q, \mu) \int dq^2 d\bar{q}^2 \int dl dk_n^+ dk_{\bar{n}}^- \delta\left(\tau - \frac{k_{\bar{n}}^-}{Q} - \frac{k_n^+}{Q} - \frac{l}{Q}\right) S_\tau(l, \mu) \\
&\times J_n^{\mathbf{m}=0}(a_n^\mu(k_n^\mu, k_n^2 - q^2), \mu) J_{n,\text{sub}}^{\mathbf{m}}(a_n^\mu(k_n^\mu, q^2), m) J_{\bar{n}}^{\mathbf{m}=0}(a_{\bar{n}}^\mu(k_{\bar{n}}^\mu, k_{\bar{n}}^2 - \bar{q}^2), \mu) J_{\bar{n},\text{sub}}^{\mathbf{m}}(a_{\bar{n}}^\mu(k_{\bar{n}}^\mu, \bar{q}^2), m),
\end{aligned} \tag{8.36}$$

with the auxiliary vectors $a_n^\mu, a_{\bar{n}}^\mu$ defined as in Eqs.(8.2) and (8.5). Assuming we are able to calculate the subtracted jet function numerically, which, for now, we have shown to be possible for the finite part $s > 0$, we can proceed as follows. Just as in a conventional calculation within the framework of the factorisation theorem the massless jet function needs to be renormalised (see Eq.(7.91)) which induces its RGE and associated running leading to the resummation of large logarithms in the peak region (see Eq.(4.19) and discussion below). However, it is only the massless jet function that is affected by this running which is carried out analytically. We can then include mass effects by carrying out the convolutions over q^2, \bar{q}^2 numerically, in a sense bootstrapping the massive result from the massless one without any further need for analytic calculation.

9 Conclusion and outlook

The main conceptional emphasis of this thesis was put on the introduction of the subtracted SCET jet function in Eq.(7.100), which in the context of the well-established SCET factorisation theorem Eq.(8.36) promises to allow for a numerical incorporation of quark mass effects on top of the analytically controlled resummation of large logarithms.

Regarding the subtracted jet function itself, we showed that non-local divergences, as well as any zero-bin ambiguities particular to the conventional SCET jet function are absent in the thus modified version. The local IR divergences ($s = 0$) of the subtracted jet function were found to resemble the structures found in the full QCD calculation of thrust ($\tau = 0$). We explicitly showed that away from the threshold region (i.e. for $s > 0$) the finite subtracted jet function can be numerically computed without any need for further regularisation.

To consistently take into account contributions to the subtracted jet function at the threshold $s = 0$, which by Eq.(7.3) are necessary to correctly reproduce the behaviour of the thrust distribution at $\tau = 0$, future work may see the implementation of a subtraction prescription analogous to the dipole method discussed in Sec. 3. This would allow for a numerical cancellation of threshold singularities, between the real emission and virtual parts Eqs.(8.30) and (8.32) of the subtracted jet function. Alternatively the Feynman tree theorem[46, 47] may be used to facilitate a direct cancellation of these divergences at the integrand level, without the need for constructing additional counter terms.

In addition to numerically taking into account mass effects as discussed in Sec. 8.4, future investigations may include the incorporation of lifetime effects, e.g. the decay of a primary top quark pair through electroweak interactions[48], into a framework similar to the one proposed in this work.

A Phase space in d spacetime dimensions

The Lorentz-invariant definition of the cross section for $2 \rightarrow n$ particle scattering is given by

$$d\sigma_{2 \rightarrow n} = \frac{1}{F(p_1, p_2)} |\mathcal{M}|^2 d\Phi_n(q_1, \dots, q_n), \quad (\text{A.1})$$

where the flux factor $F(p_1, p_2) = 4\sqrt{(p_1 \cdot p_2)^2 - (m_1 m_2)^2}$ is determined by the incoming particles with momenta p_i and masses m_i . Note the particular case $m_1 = m_2 = 0$, then $F = 2s$, with $s = (p_1 + p_2)^2$ the center of mass energy of the two particles. The other objects featuring in Eq.(A.1) are the squared matrix element $|\mathcal{M}|^2$ and the n -particle phase space element $d\Phi_n$. The generalisation of $d\Phi_n$ to $d = 4 - 2\epsilon$ dimensions of spacetime reads

$$d\Phi_n = (2\pi)^d \delta^{(d)}\left(p_1 + p_2 - \sum_{i=1}^n q_i\right) \prod_{i=1}^n \left\{ \frac{d^d q_i}{(2\pi)^{d-1}} \tilde{\delta}(q_i^2 - m_i^2) \right. \\ \left. \frac{d^{d-1} q_i}{(2\pi)^{d-1} 2E_i} \right\} \quad (\text{A.2})$$

where the on-shell condition $\tilde{\delta}(q^2 - m^2) = \theta(q^0) \delta(q^2 - m^2)$ was explicitly implemented in the second expression. The Lorentz-invariant phase space measure for two particles, where the integrand is assumed to be independent of the final state momenta, reads

$$\int d\Phi_2 = \frac{1}{4\pi} \frac{\hat{p}}{\sqrt{s}} \left(\frac{\pi}{\hat{p}^2} \right)^\epsilon \frac{\Gamma(1 - \epsilon)}{\Gamma(2 - 2\epsilon)}, \quad (\text{A.3})$$

with the center of mass momentum given by $\hat{p} = \frac{\sqrt{s}}{2} \lambda\left(1, m_q^2/s, m_{\bar{q}}^2/s\right)$. Here we use the Källén function $\lambda(x, y, z) = x^2 + y^2 + z^2 - 2xy - 2yz - 2xz$, which in the massless limit leads to $\hat{p} = \frac{\sqrt{s}}{2} \lambda(1, 0, 0) = \frac{\sqrt{s}}{2}$. To evaluate the necessary angular integrals in d -dimensions the identity Eq.(B.1) was used. The three particle Lorentz-invariant phase space measure in d spacetime dimensions, written in terms of the momentum fractions Eq.(2.35) takes the form

$$\int d\Phi_3 = \frac{s}{2(4\pi)^3} \left(\frac{4\pi}{Q^2} \right)^{2\epsilon} \frac{1}{\Gamma(2 - 2\epsilon)} \int_0^1 dx_q \int_0^1 dx_{\bar{q}} \frac{\theta(x_q + x_{\bar{q}} - 1)}{[(1 - x_q)(1 - x_{\bar{q}})(x_q + x_{\bar{q}} - 1)]^\epsilon}, \quad (\text{A.4})$$

where, again, the integrand was assumed to be independent of any angular variables and the corresponding integrations were already carried out.

The decomposition of the loop integral measure over the momentum

$$k^\mu = k^- \frac{n^\mu}{2} + k^+ \frac{\bar{n}^\mu}{2} + k_\perp^\mu, \quad k^- = \bar{n} \cdot k, \quad k^+ = n \cdot k, \quad (\text{A.5})$$

of an internal line in terms of lightcone coordinates reads

$$d^d k = \frac{1}{4(2\pi)^{4-2\epsilon}} d^{d-2} \Omega dk^+ dk^- d(\mathbf{k}_\perp^2) (\mathbf{k}_\perp^2)^{-\epsilon} \theta(\mathbf{k}_\perp^2), \quad (\text{A.6})$$

where $\mathbf{k}_\perp^2 \equiv |\vec{k}_\perp|^2 = -\eta_{\mu\nu} k_\perp^\mu k_\perp^\nu > 0$ denotes the square of the Euclidean perpendicular momentum \mathbf{k}_\perp such that $k^2 = k^+ k^- - \mathbf{k}_\perp^2$.

The decomposition of the d -dimensional Lorentz-invariant phase space measure associated with a positive-energy, on-shell particle into lightcone coordinates Eq.(5.3) yields

$$\frac{d^{d-1} k}{2k^0} = \frac{1}{4} \Omega_{\text{tot}}^{d-2} dk^+ dk^- \frac{\theta(k^+) \theta(k^-)}{(k^+ k^-)^\epsilon}, \quad (\text{A.7})$$

where we have used $k^0 = \frac{1}{2}(k^+ + k^-)$ and the integrand was assumed not to depend on angular variables, or the perpendicular momentum component \mathbf{k}_\perp .

B Integral identities and conventions for Dimensional Regularisation

Throughout this thesis the (almost) standard parametrisation $d = 4 - 2\epsilon$ is used. When performing integrals in d euclidean dimensions, we often separate the integration measure into an angular and a radial part

$$\int d^d x = \int d^{d-1} \Omega \int dx x^{d-1}, \quad \int d^{d-1} \Omega = \frac{2\pi^{\frac{d}{2}}}{\Gamma(\frac{d}{2})} = \frac{2\pi^{1-\epsilon}}{\Gamma(1-\epsilon)}, \quad (\text{B.1})$$

where we have explicitly evaluated the angular integration for integrands that are independent of these variables. This simply gives the volume of the d -dimensional unit sphere.

Loop integrals over Feynman propagators are only well-defined when the “ $i0$ -prescription” is consistently adhered to. Here we give a couple of examples for manipulations involving the “ $i0$ -prescription” that are commonly used when evaluating loop amplitudes.

$$\begin{aligned} (\Delta - i0)^\alpha &= (-1 - i0)^\alpha (-\Delta + i0)^\alpha, & \Delta < 1 \\ (-1 + i0)^\alpha &= (-1 - i0)^{-\alpha} = \exp(i\alpha\pi) \\ \log(\Delta \pm i0) &= \log(|\Delta|) \pm i\pi & \Delta < 0. \end{aligned} \quad (\text{B.2})$$

For momentum integrals we adopt the convention that the measure of each component comes supplemented with a factor of $\frac{1}{2\pi}$ and use the convenient notation

$$\frac{d^d q}{(2\pi)^d} \equiv \mathbb{d}^d q, \quad (\text{B.3})$$

being reminiscent of the reduced Planck constant $\hbar = \frac{h}{2\pi}$.

Conventionally we choose the dimensionful scale introduced by dimensional regularisation to be

$$\tilde{\mu}^2 \equiv \mu^2 e^{\gamma_E - \log(4\pi)}, \quad (\text{B.4})$$

which is used in the context of calculations in the $\overline{\text{MS}}$ scheme and conveniently removes universal finite terms of the form $-\gamma_E + \log(4\pi)$ (where $\gamma_E \simeq 0.577216$ is the Euler-Mascheroni constant) associated with divergences from loop integrals, leaving only poles in ϵ and the scale μ in the final result.

For $\alpha, \beta \in \mathbb{N}$ the basic scalar 1-loop master integral in dimensional regularisation evaluates to

$$\int \mathbb{d}^d q \frac{(q^2)^\beta}{[q^2 - \Delta + i0]^\alpha} = \frac{i(-1)^\beta}{(4\pi)^{\frac{d}{2}}} \frac{\Gamma(\frac{d}{2} - \beta)}{\Gamma(\alpha) \Gamma(\frac{d}{2})} \Gamma(\alpha - \beta - \frac{d}{2}) (-1 + i0)^{-\frac{d}{2} - \beta} (-\Delta + i0)^{\frac{d}{2} + \beta - \alpha}. \quad (\text{B.5})$$

This integral will cover all our needs when it comes to full QCD amplitudes. However, for convenience we also give the integral

$$\int \mathbb{d}^d q \frac{1}{[q^2 + 2Q \cdot q - \Delta + i0]^\alpha} = \frac{i\pi^{2-\epsilon}}{(2\pi)^{4-2\epsilon}} \frac{\Gamma(\alpha + \epsilon - 2)}{\Gamma(\alpha)} \frac{(-1)^\alpha}{[Q^2 + \Delta - i0]^{\alpha + \epsilon - 2}}. \quad (\text{B.6})$$

where the square in the propagator is not complete.

Real emission phase space integral in lightcone coordinates

In the derivation of the real emission contributions $J_{n,2}^{\mathbf{m},\mathbf{r}}, J_{n,4}^{\mathbf{m},\mathbf{r}}$ we had to perform an integration of the form Eq.(7.26). Here we want to give some intermediate steps to make the calculation more tractable. We begin by decomposing the measure into lightcone components

$$\begin{aligned} I(p^- - k^-) &= \int d^d l \theta(l^0) \delta(l^2 - m^2) \delta(l^- - p^- + k^-) \delta^{(d-2)}(\mathbf{l}_\perp + \mathbf{k}_\perp) \\ &= \frac{1}{2} \int dl^+ dl^- \theta(l^+ + l^-) \int d^{d-2} \mathbf{l}_\perp \delta(l^+ l^- - \mathbf{l}_\perp^2 - m^2) \delta(l^- - p^- + k^-) \delta^{(d-2)}(\mathbf{l}_\perp + \mathbf{k}_\perp), \end{aligned} \quad (\text{B.7})$$

where the relation $l^0 = \frac{1}{2}(l^- + l^+)$ was used in the step function. Integrating over the $d-2$ perpendicular components and rearranging the on-shell delta function explicitly in terms of l^+ we obtain

$$\begin{aligned} I(p^- - k^-) &= \frac{1}{2} \int dl^+ dl^- \theta(l^+ + l^-) \frac{1}{l^-} \delta\left(l^+ - \frac{\mathbf{k}_\perp^2 + m^2}{l^-}\right) \delta(l^- - p^- + k^-) \\ &= \frac{1}{2} \frac{1}{p^- - k^-} \theta\left(\frac{\mathbf{k}_\perp^2 + m^2}{p^- - k^-} + p^- - k^-\right), \end{aligned} \quad (\text{B.8})$$

where through the integration we set the variables

$$l^- = p^- - k^-, \quad l^+ = \frac{\mathbf{k}_\perp^2 + m^2}{p^- - k^-}. \quad (\text{B.9})$$

To conclude we observe that the argument of the step function in Eq.(B.8) can be written as

$$\theta\left(\frac{1}{p^- - k^-} [\mathbf{k}_\perp^2 + m^2 + (p^- - k^-)^2]\right) = \theta(p^- - k^-), \quad (\text{B.10})$$

since the expression in the numerator on the left-hand side is strictly non-negative. This leaves us with the result claimed in Eq.(7.26).

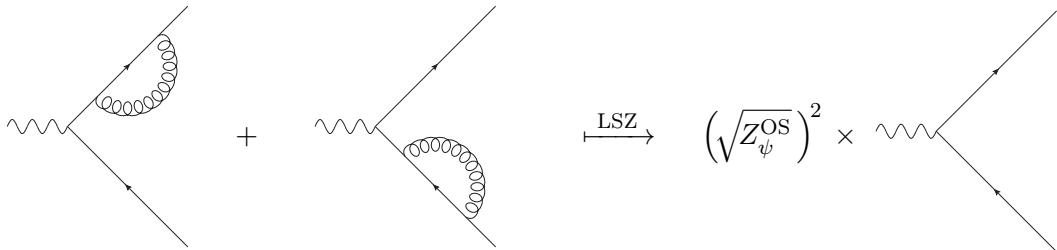
C Ultraviolet divergences in the QCD virtual correction

When we computed the loop integral for the virtual-tree interference diagram in Eq.(2.28) we could have found by naive power counting that the integral must, besides the infrared (IR) divergences we are ultimately interested in, also contain ultraviolet (UV) divergences. In fact, expanding Eq.(2.43) and being careful to distinguish IR and UV divergences we indeed find

$$\begin{aligned} \mathcal{M}_{2,\text{gi}}^{\text{v,LO}} &= -\frac{\hat{\mathcal{M}}}{(4\pi)^2} \frac{(1-\epsilon)^2}{3-2\epsilon} \left\{ \frac{1}{\epsilon_{\text{IR}}^2} + \frac{2}{\epsilon_{\text{IR}}} - \frac{1}{2\epsilon_{\text{UV}}} + \frac{1}{\epsilon_{\text{IR}}} \log\left(\frac{\mu^2}{-Q^2 - i0}\right) + 4 - \frac{\pi^2}{12} \right. \\ &\quad \left. + \frac{3}{2} \log\left(\frac{\mu^2}{-Q^2 - i0}\right) + \frac{1}{2} \log^2\left(\frac{\mu^2}{-Q^2 - i0}\right) + \mathcal{O}(\epsilon) \right\}, \end{aligned} \quad (\text{C.1})$$

where the prefactor $\hat{\mathcal{M}}$ is defined in Eq.(2.34). We see that Eq.(C.1) clearly contains an UV divergence. However, in the discussion of the main text we never needed to treat this divergence with renormalisation and even saw that the cancellation of divergences between the real emission diagrams, which do not contain any UV divergences, and the virtual contribution took place regardless. While it may look like we illegally cancelled UV against IR divergences at this stage, this is in fact not the case.

The answer to this apparent conundrum lies in the LSZ reduction formula (for a thorough treatment see [49]). Recall that true S-matrix elements are obtained by taking the corresponding amputated Green's function and equipping each of the external lines with the appropriate renormalisation factor encoding the self-energy contributions of the particle at hand. In the calculation of the main text we have therefore (purposefully) overlooked two contributions,



$$+ \quad \xrightarrow{\text{LSZ}} \quad \left(\sqrt{Z_\psi^{\text{OS}}}\right)^2 \times \quad , \quad (\text{C.2})$$

where Z_ψ^{OS} denotes the (massless) quark field renormalisation factor in the on-shell scheme. Note that the diagrams on the left-hand side of Eq.(C.2) are to be regarded as contributions to the (unamputated) Green's function and not as S-matrix elements. The right-hand side then shows the S-matrix contribution after the LSZ reduction has been applied to the Green's function.

At one loop the massless on-shell quark field renormalisation factor is given by

$$Z_\psi^{\text{OS}} = 1 + \delta Z_\psi^{\text{OS}} + \mathcal{O}(\alpha_s^2) = 1 - \frac{\alpha_s C_F}{4\pi} \left(\frac{1}{\epsilon_{\text{UV}}} - \frac{1}{\epsilon_{\text{IR}}} \right) + \mathcal{O}(\alpha_s^2). \quad (\text{C.3})$$

We can see that had we not distinguished between UV and IR divergences (and so $\epsilon_{\text{IR}} = \epsilon_{\text{UV}} \equiv \epsilon$) the $\mathcal{O}(\alpha_s)$ contribution of Eq.(C.3) would formally vanish. To consistently carry out the cross section calculation we have to consider precisely this $\mathcal{O}(\alpha_s)$ contribution coming from the interference diagram of the right-hand side of Eq.(C.2) with the leading order diagram, which takes a form analogous to Eq.(2.9) modified by the one-loop term of Z_ψ^{OS} ,

$$\mathcal{M}_{2,\text{LSZ}}^{\text{v,LO}} = 4e^4 e_q^2 \tilde{\mu}^{2\epsilon} N_C \frac{(1-\epsilon)^2}{3-2\epsilon} \delta Z_\psi^{\text{OS}} = -\frac{\hat{\mathcal{M}}}{(4\pi^2)} \frac{(1-\epsilon)^2}{3-2\epsilon} \frac{1}{2} \left(\frac{1}{\epsilon_{\text{UV}}} - \frac{1}{\epsilon_{\text{IR}}} \right). \quad (\text{C.4})$$

Adding this contribution to the original virtual-tree interference in Eq.(C.1) yields

$$\begin{aligned} \mathcal{M}_{2,\text{gi}}^{\text{v,LO}} + \mathcal{M}_{2,\text{LSZ}}^{\text{v,LO}} = & -\frac{\hat{\mathcal{M}}}{(4\pi)^2} \frac{(1-\epsilon)^2}{3-2\epsilon} \left\{ \frac{1}{\epsilon_{\text{IR}}^2} + \frac{2}{\epsilon_{\text{IR}}} - \frac{1}{2\epsilon_{\text{IR}}} + \frac{1}{\epsilon_{\text{IR}}} \log \left(\frac{\mu^2}{-Q^2 - i0} \right) + 4 - \frac{\pi^2}{12} \right. \\ & \left. + \frac{3}{2} \log \left(\frac{\mu^2}{-Q^2 - i0} \right) + \frac{1}{2} \log^2 \left(\frac{\mu^2}{-Q^2 - i0} \right) + \mathcal{O}(\epsilon) \right\}, \end{aligned} \quad (\text{C.5})$$

where we see that the UV divergence has canceled and is replaced by a corresponding IR divergence, that is, the sum of all virtual contributions is manifestly UV-finite.

If we drop the distinction between the different kinds of poles the results in Eqs.(C.1) and (C.5) are formally identical. This is the reason why we got away with ignoring the contributions from Eq.(C.2) in the main text, intentionally misinterpreting some UV divergences as IR.

D Colour/Helicity space formulation of amplitudes

In deriving the dipole counter terms it is convenient to think of the amplitude for a given $(m+1)$ -parton final state as an abstract vector in the combined colour/helicity space of these particles,

$$i\mathcal{M}_{\mathbf{m}}(p_1, \dots, p_m) = |1, \dots, m\rangle_{\mathbf{m}}, \quad (\text{D.1})$$

where $\{1, \dots, m\}$ denote the respective parton momenta. Note that the amplitude in Eq.(D.1) carries no explicit indices for the final state particle's helicities and colours. These are made explicit only after a projection to the appropriate colour/helicity basisket,

$$i\mathcal{M}_{\mathbf{m}}^{c_1 \dots c_m}_{s_1 \dots s_m} = \langle s_1, \dots, s_m; c_1, \dots, c_m | 1, \dots, m \rangle_{\mathbf{m}}, \quad (\text{D.2})$$

where the indices take values $s_i \in \{1, 2\}$, $c_i \in \{1, \dots, N_C\}$ if parton i is a(n anti-)quark and $s_j \equiv \mu_j \in \{1, \dots, d\}$, $c_j \in \{1, \dots, N_C^2 - 1\}$ if parton j is a gluon. We can therefore expand the amplitude Eq.(D.1) in terms of these basiskets as

$$|1, \dots, m\rangle_{\mathbf{m}} = i\mathcal{M}_{\mathbf{m}}^{c_1 \dots c_m}_{s_1 \dots s_m} |1, \dots, s_m; c_1, \dots, c_m\rangle, \quad (\text{D.3})$$

the sum over helicities and colours being performed implicitly. In the context of this thesis we will usually think of $|1, \dots, m\rangle_{\mathbf{m}}$ as representing the gauge-invariant sum over all diagrams for the final

state under consideration at a given order in α_s . With this in mind the squared amplitude summed over final state colours and helicities simply reads

$$|\mathcal{M}_{\mathbf{m}}|^2 = {}_{\mathbf{m}}\langle 1, \dots, m | 1, \dots, m \rangle_{\mathbf{m}} = (\mathcal{M}_{\mathbf{m} s_1 \dots s_m}^{c_1 \dots c_m})^* \mathcal{M}_{\mathbf{m} s_1 \dots s_m}^{c_1 \dots c_m}. \quad (\text{D.4})$$

To make the notation more transparent we give a concrete example. Writing

$$|q, \bar{q}, k\rangle_{\mathbf{3}} = |(q, k), \bar{q}\rangle_{\mathbf{3}} + |(\bar{q}, k), q\rangle_{\mathbf{3}}, \quad (\text{D.5})$$

for the sum of the real emission amplitudes in Eq.(2.12) where the gluon is emitted from the (anti-)quark respectively (now including the initial state), we establish a term-by-term correspondence to Eq.(2.36) via

$$\begin{aligned} |\mathcal{M}_{\mathbf{3}}^{\mathbf{r}}|^2 = \frac{1}{4} \Big\{ & {}_{\mathbf{3}}\langle (q, k), \bar{q} | (q, k), \bar{q} \rangle_{\mathbf{3}} + {}_{\mathbf{3}}\langle (\bar{q}, k), q | (\bar{q}, k), q \rangle_{\mathbf{3}} \\ & + {}_{\mathbf{3}}\langle (q, k), \bar{q} | (\bar{q}, k), q \rangle_{\mathbf{3}} + {}_{\mathbf{3}}\langle (\bar{q}, k), q | (q, k), \bar{q} \rangle_{\mathbf{3}} \Big\} = \frac{1}{4} {}_{\mathbf{3}}\langle q, \bar{q}, k | q, \bar{q}, k \rangle_{\mathbf{3}}. \end{aligned} \quad (\text{D.6})$$

Note that the factor pertaining to the average over the helicities of the incoming e^+e^- -pair appears explicitly in Eq.(D.6) since it is not taken care of by Eq.(D.4). In all our calculations we will nonetheless absorb this averaging factor into the definition of ${}_{\mathbf{3}}\langle q, \bar{q}, k | q, \bar{q}, k \rangle_{\mathbf{3}}$ for convenience.

Colour charge operators and the soft limit

We now turn to introducing the colour charge operators \mathbf{T}_i^a , whose purpose it is to mimic the emission of a gluon with colour a from a final state parton i in colour space. That is, it takes a m parton colour space basisket where said parton i carries colour c_i , to a linear combination of $m+1$ parton basiskets given by

$$\mathbf{T}_i^a |c_1, \dots, c_i, \dots, c_m\rangle = \sum_{b_i} (T_i^a)_{b_i c_i} |c_1, \dots, b_i, \dots, c_m, a\rangle, \quad (\text{D.7})$$

where the coefficients $(T_i^a)_{b_i c_i}$ relate to the $SU(N)$ generators sitting in the respective representation of the emitting parton. Explicitly, for different parton types i the generators read

$$\begin{aligned} (T_i^a)_{bc} &= T_{bc}^a & \text{for } i = q, \quad b, c = 1, \dots, N_C, \\ (T_i^a)_{bc} &= \bar{T}_{bc}^a = -(T^a)_{bc}^* & \text{for } i = \bar{q}, \quad b, c = 1, \dots, N_C, \\ (T_i^a)_{bc} &= -if_{abc} & \text{for } i = g, \quad b, c = 1, \dots, N_C^2 - 1, \end{aligned} \quad (\text{D.8})$$

where we have been careful to distinguish between indices b, c in the adjoint and fundamental representation respectively. Note that in Eq.(D.7) there is no implied sum over the colour of the emitted gluon, such that it carries definite colour a . The colour charge operators obey the algebra

$$\mathbf{T}_i \cdot \mathbf{T}_j \equiv \mathbf{T}_i^a \mathbf{T}_j^a = \mathbf{T}_i \cdot \mathbf{T}_j, \quad \mathbf{T}_i^2 = \mathbf{T}_i \cdot \mathbf{T}_i = C_i \mathbf{1}, \quad (\text{D.9})$$

where C_i denotes the Casimir factor of the representation pertaining to parton i . At amplitude level the action of a colour charge operator onto a m parton final state yields

$$\begin{aligned} \langle c_1, \dots, c_i, \dots, c_m, \tilde{a} | \mathbf{T}_i^a | 1, \dots, m \rangle_{\mathbf{m}} &= \delta_{\tilde{a}a} \sum_{b_i} T_{c_i b_i}^a \langle c_1, \dots, b_i, \dots, c_m | 1, \dots, m \rangle_{\mathbf{m}} \\ &= i\delta_{\tilde{a}a} \sum_{b_i} T_{c_i b_i}^a \mathcal{M}_{\mathbf{m}}^{c_1 \dots b_i \dots c_m} \end{aligned} \quad (\text{D.10})$$

with any helicity indices suppressed for readability. Using Eq.(D.10) we can define squared tree amplitudes which are colour-correlated through the final state partons i, j exchanging a gluon in colour space as

$$|\mathcal{M}_{\mathbf{m}}^{i,j}|^2 = {}_{\mathbf{m}}\langle 1, \dots, m | \mathbf{T}_i \cdot \mathbf{T}_j | 1, \dots, m \rangle_{\mathbf{m}} = (\mathcal{M}_{\mathbf{m} s_1 \dots s_m}^{c_1 \dots b_i \dots c_j \dots c_m})^* T_{b_i c_i}^a T_{c_j b_j}^a \mathcal{M}_{\mathbf{m} s_1 \dots s_m}^{c_1 \dots c_i \dots b_j \dots c_m}, \quad (\text{D.11})$$

where now all summations have been made implicit and $(T^a)_{c_i c_j}^* = T_{c_j c_i}^a$ was used. When we say that the gluon is exchanged “in colour space” we mean that only the colour degree of freedom is connecting the partons (i, j) , no momentum flow and spin correlations between them are implied.

The structure Eq.(D.11) naturally appears in the universal soft limit of QCD (c.f. Eq.(E.3)). The square of a given $(m+1)$ -parton tree-level matrix element in the limit where the parton j goes soft (c.f. Eq.(3.15)), that is $j^\mu = \lambda p^\mu$ for some arbitrary p^μ and $\lambda \rightarrow 0$, can be shown to almost factorise and take the form,

$$\begin{aligned} {}_{\mathbf{m}+1}\langle 1, \dots, j, \dots, m+1 | 1, \dots, j, \dots, m+1 \rangle_{\mathbf{m}+1} &\xrightarrow{\lambda \rightarrow 0} -\frac{1}{\lambda^2} 8\pi \tilde{\mu}^{2\epsilon} \alpha_s \sum_i \frac{1}{i \cdot p} \sum_{k \neq i} \frac{i \cdot k}{(i+k) \cdot p} \\ &\times {}_{\mathbf{m}}\langle 1, \dots, \not{j}, \dots, m+1 | \mathbf{T}_i \cdot \mathbf{T}_k | 1, \dots, \not{j}, \dots, m+1 \rangle_{\mathbf{m}}. \end{aligned} \quad (\text{D.12})$$

Both sums run over the momenta i, k , where $i \neq k$, in the amplitude $|1, \dots, \not{j}, \dots, m+1\rangle_{\mathbf{m}}$ with only m partons in the final state which is obtained from the original $(m+1)$ -parton amplitude by removing the parton j . It is in one part the structure of Eq.(D.12) that inspires the definition of the dipole operator Eq.(3.17). The other kinematic limit that is important to determining the dipole counter terms is the one where two final state particles become collinear and is discussed in the next section.

Before we continue, let us briefly check the validity of the above relation by comparing to what we have already calculated in Chapter 2. Recall from the discussion below Eq.(2.39) that only the interference diagrams where the gluon is exchanged between the quark/anti-quark lines contribute to the soft singularity. Indeed, setting $k^\mu = \lambda p^\mu$ in Eq.(2.33) and keeping only singular terms as $\lambda \rightarrow 0$ we can write

$$\begin{aligned} {}_3\langle q, \bar{q}, k | q, \bar{q}, k \rangle_3 &\subset \mathcal{M}_{3, \mathbf{gi}}^{\mathbf{r}, 12} + \mathcal{M}_{3, \mathbf{gi}}^{\mathbf{r}, 21} \xrightarrow{\lambda \rightarrow 0} -\frac{1}{\lambda^2} 8\pi \alpha_s \tilde{\mu}^{2\epsilon} (-C_F |\mathcal{M}_2^{\mathbf{LO}}|^2) \\ &\times \left(\frac{q \cdot \bar{q}}{q \cdot p} \frac{1}{(q + \bar{q}) \cdot p} + \frac{q \cdot \bar{q}}{\bar{q} \cdot p} \frac{1}{(q + \bar{q}) \cdot p} \right), \end{aligned} \quad (\text{D.13})$$

where we have used the tree-level amplitude from Eq.(2.9) and the partial fraction decomposition

$$\frac{q \cdot \bar{q}}{(q \cdot p)(\bar{q} \cdot p)} = \frac{q \cdot \bar{q}}{q \cdot p (q + \bar{q}) \cdot p} + \frac{q \cdot \bar{q}}{\bar{q} \cdot p (q + \bar{q}) \cdot p}, \quad (\text{D.14})$$

to isolate the overlapping collinear singularities of the soft momentum (i.e. $p \parallel q$ and $p \parallel \bar{q}$) each into its separate term. Finally using that $(-C_F |\mathcal{M}_2^{\mathbf{LO}}|^2) = {}_2\langle q, \bar{q} | -C_F | q, \bar{q} \rangle_2 = {}_2\langle q, \bar{q} | -\mathbf{T}_q^2 | q, \bar{q} \rangle_2$ and colour conservation we get

$${}_3\langle q, \bar{q}, k | q, \bar{q}, k \rangle_3 \xrightarrow{\lambda \rightarrow 0} -\frac{1}{\lambda^2} 8\pi \alpha_s \tilde{\mu}^{2\epsilon} \sum_{i=q, \bar{q}} \frac{1}{i \cdot p} \sum_{k \neq i} \frac{i \cdot k}{(i+k) \cdot p} {}_2\langle q, \bar{q} | \mathbf{T}_i \cdot \mathbf{T}_k | q, \bar{q} \rangle_2, \quad (\text{D.15})$$

which is in fact consistent with what was claimed in Eq.(D.12).

To conclude we note that if the amplitude $|1, \dots, m\rangle_{\mathbf{m}}$ refers to a gauge-invariant sum of diagrams the colour charge operators additionally fulfill the colour conservation relation

$$\sum_i \mathbf{T}_i^c |1, \dots, m\rangle_{\mathbf{m}} = 0. \quad (\text{D.16})$$

This follows directly from gauge invariance by applying a $SU(N)$ transformation to the amplitude

$$\mathbf{U}(\alpha) |1, \dots, m\rangle_{\mathbf{m}} = e^{-i\alpha_i^c \mathbf{T}_i^c} |1, \dots, m\rangle_{\mathbf{m}} \stackrel{!}{=} |1, \dots, m\rangle_{\mathbf{m}}, \quad (\text{D.17})$$

and considering $(\alpha_i^c) \equiv 1$ as a particular case. However, to elucidate the formalism involved we show Eq. (D.16) explicitly for the simple case of (colour space) gluon emission from the q, \bar{q} final state considered in the leading order process Eq. (2.4). There we find

$$\sum_{i=q, \bar{q}} \mathbf{T}_i^a |q, \bar{q}\rangle_{\mathbf{2}} = \sum_{c_1, c_2=1}^{N_C} (\mathbf{T}_q^a + \mathbf{T}_{\bar{q}}^a) |c_1, c_2\rangle_{\mathbf{2}} \langle c_1, c_2 | q, \bar{q}\rangle_{\mathbf{2}}. \quad (\text{D.18})$$

Since the q, \bar{q} pair was produced by a photon it must be in a colour singlet configuration implying $\langle c_1, c_2 | q, \bar{q}\rangle_{\mathbf{2}} = \delta_{c_1 c_2}$. Using the definition of the colour charge operator Eq. (D.7) and the explicit representations Eq. (D.8) we can further write Eq. (D.18) as

$$\begin{aligned} \sum_{i=q, \bar{q}} \mathbf{T}_i^a |q, \bar{q}\rangle_{\mathbf{2}} &= \sum_{c, b=1}^{N_C} ((T^a)_{bc} |b, c, a\rangle + (\bar{T}^a)_{bc} |c, b, a\rangle) \\ &= \sum_{c, b=1}^{N_C} ((T^a)_{bc} + (-T^a)_{cb}^*) |b, c, a\rangle = 0, \end{aligned} \quad (\text{D.19})$$

establishing the claim. In the last line a relabelling of indices $b \leftrightarrow c$ was performed for the second term and the hermiticity property of the generator was used to cancel the colour factors. Colour conservation for a colour singlet gluon state $|g_1, g_2\rangle_{\mathbf{2}}$ can be shown by analogous means where again $\langle c_1, c_2 | g_1, g_2\rangle = \delta_{c_1 c_2}$ but now $c_1, c_2 = 1, \dots, N_C^2 - 1$ are indices in the adjoint representation.

Helicity operators and the collinear limit

Apart from the colour charge operators introduced before, the dipole operator in Eq. (3.17) also contains the splitting operator $\mathbf{V}_{ij,k}$ pertaining to the dipole $\{(i, j), k\}$ (c.f. diagram in Eq. (3.22)) that takes care of helicity correlations between final state partons. In addition it will reproduce the correct kinematic singularity structure in the counter term when two final state particles go collinear. To be more precise we first perform a decomposition for the emitter momenta i, j , similar to the one in Eq. (5.3),

$$i^\mu = z p^\mu - \frac{q_\perp^2}{z(\bar{n} \cdot p)} \frac{\bar{n}^\mu}{2} + q_\perp^\mu, \quad j^\mu = (1-z) p^\mu - \frac{q_\perp^2}{(1-z)(\bar{n} \cdot p)} \frac{\bar{n}^\mu}{2} - q_\perp^\mu, \quad (\text{D.20})$$

with some arbitrary momentum p^μ specifying the direction along which the momenta become collinear and satisfying $p^2 = \bar{n}^2 = 0$ and $p \cdot q_\perp = \bar{n} \cdot q_\perp = 0$, where \bar{n}^μ is another arbitrary lightlike vector needed to uniquely perform the decomposition. The perpendicular component is given by a spacelike vector that may be parameterised as $q_\perp^\mu = |\mathbf{q}_\perp| n_\perp^\mu$ where $n_\perp^2 = -1$ and is defined by Eq. (D.20). We may further identify z as the momentum fraction of i along the combined dipole momentum, that is

$$z = \frac{2 i \cdot (i + j + k)}{(i + j + k)^2} = \frac{i \cdot (j + k)}{i \cdot j + i \cdot k + j \cdot k}. \quad (\text{D.21})$$

The collinear limit where the parton momenta align along the direction picked out by p^μ is then defined as

$$i \cdot j = -\frac{q_\perp^2}{2z(1-z)} \xrightarrow{q_\perp^2 \rightarrow 0} 0. \quad (\text{D.22})$$

In this limit, squared QCD tree-level matrix elements with $(m+1)$ partons exhibit a quasi-factorisation (see [14]) in terms of m -parton amplitudes similar to Eq.(D.12), that is

$$\begin{aligned} & \mathbf{m}+1 \langle 1, \dots, i, \dots, j, \dots, m+1 | 1, \dots, i, \dots, j, \dots, m+1 \rangle_{\mathbf{m}+1} \xrightarrow{q_\perp^2 \rightarrow 0} \frac{1}{i \cdot j} 4\pi \tilde{\mu}^{2\epsilon} \alpha_s \\ & \times \mathbf{m} \langle 1, \dots, \hat{i}, \dots, \hat{j}, \dots, \hat{j}, \dots, m+1 | \mathbf{P}_{\hat{i}\hat{j},i}(z, q_\perp, \epsilon) | 1, \dots, \hat{i}, \dots, \hat{j}, \dots, m+1 \rangle_{\mathbf{m}}, \end{aligned} \quad (\text{D.23})$$

where the reduced amplitude is obtained by removing partons i, j from the $(m+1)$ -particle amplitude and replacing them with a single parton $\hat{i}\hat{j}$ whose type is determined as in Eq.(3.21) and which carries momentum p^μ . The splitting operator $\mathbf{P}_{\hat{i}\hat{j},i}$ acts on the spin degrees of freedom of the combined parton $\hat{i}\hat{j}$, its matrix elements are proportional to the Altarelli-Parisi splitting functions [50]. For example, in the case where a(n anti-)quark and gluon (i, j) in the $(m+1)$ -parton amplitude get reduced to a(n anti-)quark $(\hat{i}\hat{j})$ (c.f. first two lines of Eq.(3.21)), the splitting operator matrix element reads

$$\langle s | \mathbf{P}_{\hat{i}\hat{j},i}(z, q_\perp, \epsilon) | s' \rangle = \delta_{ss'} C_F \left\{ \frac{1+z^2}{1-z} - \epsilon(1-z) \right\}. \quad (\text{D.24})$$

Just as the splitting operator in Eq.(D.23), the helicity operator $\mathbf{V}_{ij,k}$ featuring in the definition of the dipole counter term Eq.(3.17) only depends on the helicities of the combined (emitter) parton $\hat{i}\hat{j}$. Employing the kinematics Eq.(3.19) and the momentum invariants introduced in Eq.(3.18) the matrix elements of the helicity operator are defined as

$$\langle s | \mathbf{V}_{ij,k} | s' \rangle = 8\pi \tilde{\mu}^{2\epsilon} \alpha_s C_F \delta_{ss'} \left\{ \frac{2}{1-z_i(1-y_{ij,k})} - (1+z_i) - \epsilon(1-z_i) \right\}, \quad (\text{D.25})$$

for dipoles where a reduction $(i, j) = (q, g) \mapsto \hat{i}\hat{j} = q$ or $(i, j) = (\bar{q}, g) \mapsto \hat{i}\hat{j} = \bar{q}$ took place. Note that the explicit form of these matrix elements is particular to the subtraction procedure and as such cannot be physically motivated. It is only justified by its applicability as a valid subtraction term, as we will see in App. E. The matrix elements for the remaining reductions in Eq.(3.21) will not be needed in this thesis and can be found in [14].

E Dipole operator matrix elements in the soft and collinear limit

Let us now argue why the dipole contributions as defined by Eq.(3.16) should reproduce the singularity structure of the squared real emission matrix element. To be able to be more explicit in our derivation we will focus on (anti-)quark/gluon splitting only, with other splittings to be treated analogously. For such processes, where a dipole reduction $\{(i, j), k\}$ to $\{\hat{i}\hat{j}, \underline{k}\}$ according to Eq.(3.22) is being performed, the dipole operator matrix element in terms of the momentum invariants Eq.(3.18) reads

$$\begin{aligned} \mathcal{D}_{ij,k} = & -\frac{8\pi \tilde{\mu}^{2\epsilon} \alpha_s C_F}{2(i \cdot j)} \left\{ \frac{2}{1-z_i(1-y_{ij,k})} - (1+z_i) - \epsilon(1-z_i) \right\} \\ & \times \mathbf{m} \langle 1, \dots, \hat{i}\hat{j}, \dots, \underline{k}, \dots, m+1 | \frac{\mathbf{T}_{\hat{i}\hat{j}} \cdot \mathbf{T}_{\underline{k}}}{\mathbf{T}_{\hat{i}\hat{j}}^2} | 1, \dots, \hat{i}\hat{j}, \dots, \underline{k}, \dots, m+1 \rangle_{\mathbf{m}}, \end{aligned} \quad (\text{E.1})$$

where we have explicitly written out the helicity operator matrix element from Eq.(D.25).

Soft limit

Recalling the definition of the soft limit, that is setting $j^\mu = \lambda p^\mu$ and considering the limit $\lambda \rightarrow 0$, the kinematic variables appearing in Eq.(E.1) can be shown to approach

$$y_{ij,k} \xrightarrow{\lambda \rightarrow 0} 0, \quad z_i \xrightarrow{\lambda \rightarrow 0} 1, \quad \frac{1}{1-z_i(1-y_{ij,k})} \xrightarrow{\lambda \rightarrow 0} \frac{1}{\lambda} \frac{i \cdot k}{p \cdot (i+k)}. \quad (\text{E.2})$$

With this, the dipole momenta Eq.(3.19) reduce to $\underline{i}j^\mu \xrightarrow{\lambda \rightarrow 0} i^\mu$ and $\underline{k}^\mu \xrightarrow{\lambda \rightarrow 0} k^\mu$, such that the dipole operator matrix element becomes

$$\mathcal{D}_{ij,k} \stackrel{\text{soft}}{\simeq} -\frac{8\pi\tilde{\mu}^{2\epsilon}\alpha_s C_F}{\lambda^2(i \cdot p)} \left\{ \frac{i \cdot k}{p \cdot (i+k)} + \mathcal{O}(\lambda) \right\} \times_{\mathbf{m}} \langle 1, \dots, i, \dots, k, \dots, m+1 | \frac{\mathbf{T}_i \cdot \mathbf{T}_k}{\mathbf{T}_i^2} | 1, \dots, i, \dots, k, \dots, m+1 \rangle_{\mathbf{m}}. \quad (\text{E.3})$$

We can now use $C_F^{-1} \mathbf{m} \langle \dots, i, \dots | \dots, i, \dots \rangle_{\mathbf{m}} = \mathbf{m} \langle \dots, i, \dots | (\mathbf{T}_i^2)^{-1} | \dots, i, \dots \rangle_{\mathbf{m}}$ and that the colour/helicity space states in Eq.(E.3) are identical to those in Eq.(D.12). With this, and dropping terms less singular than λ^{-2} we obtain

$$\mathcal{D}_{ij,k} \stackrel{\text{soft, sing.}}{\simeq} -\frac{1}{\lambda^2} 8\pi\tilde{\mu}^{2\epsilon}\alpha_s \frac{1}{(i \cdot p)} \frac{i \cdot k}{p \cdot (i+k)} \mathbf{m} \langle 1, \dots, \not{j}, \dots, m+1 | \mathbf{T}_i \cdot \mathbf{T}_k | 1, \dots, \not{j}, \dots, m+1 \rangle_{\mathbf{m}}, \quad (\text{E.4})$$

correctly reproducing one of the terms in the sum of Eq.(D.12). This makes particularly clear that the soft singularity in the real emission matrix element is only correctly reproduced once the sum over all dipoles is performed as in Eq.(3.14).

Collinear limit

The collinear limit as defined by Eq.(D.20) and Eq.(D.22) implies for the kinematic variables in Eq.(E.1)

$$z_i \xrightarrow{q_\perp^2 \rightarrow 0} z, \quad y_{ij,k} \xrightarrow{q_\perp^2 \rightarrow 0} 0, \quad (\text{E.5})$$

with z defined as in Eq.(D.21). The projected dipole momenta reduce to $\underline{i}j^\mu \xrightarrow{q_\perp^2 \rightarrow 0} i^\mu + j^\mu$ and $\underline{k}^\mu \xrightarrow{q_\perp^2 \rightarrow 0} k^\mu$ respectively. Applying this to the matrix element in Eq.(E.1) yields

$$\mathcal{D}_{ij,k} \stackrel{\text{coll.}}{\simeq} -\frac{8\pi\tilde{\mu}^{2\epsilon}\alpha_s C_F}{2(i \cdot j)} \left\{ \frac{2}{1-z} - (1+z) - \epsilon(1-z) \right\} \times_{\mathbf{m}} \langle 1, \dots, i+j, \dots, m+1 | \frac{\mathbf{T}_{i+j} \cdot \mathbf{T}_k}{\mathbf{T}_{i+j}^2} | 1, \dots, i+j, \dots, m+1 \rangle_{\mathbf{m}}, \quad (\text{E.6})$$

where we have identified $\underline{i}j^\mu \equiv p^\mu$ as the collinear direction when compared with Eq.(D.23). To reproduce the correct singular limit of the real emission amplitude we have to sum over all spectators k for a fixed emitter (i, j) , c.f. Eq.(3.22), which we assumed to be a(n anti-)quark-gluon pair. Performing the sum we thus obtain

$$\sum_{k \neq (i,j)} \mathcal{D}_{ij,k} \stackrel{\text{coll.}}{\simeq} -\frac{8\pi\tilde{\mu}^{2\epsilon}\alpha_s C_F}{2(i \cdot j)} \left\{ \frac{1+z^2}{1-z} - \epsilon(1-z) \right\} \times \left\{ \mathbf{m} \langle 1, \dots, i+j, \dots, m+1 | \sum_{k \neq (i,j)} \frac{\mathbf{T}_{i+j} \cdot \mathbf{T}_k}{\mathbf{T}_{i+j}^2} | 1, \dots, i+j, \dots, m+1 \rangle_{\mathbf{m}} + \mathcal{O}(q_\perp) \right\}, \quad (\text{E.7})$$

where we can already identify the prefactor as being proportional to the appropriate Altarelli-Parisi splitting function matrix element in Eq.(D.24). The fact that we were allowed to pull the summation through this prefactor is that in the collinear limit where $i^\mu \simeq z \underline{i}j^\mu + q_\perp^\mu$ and $j^\mu \simeq (1-z) \underline{i}j^\mu - q_\perp^\mu$ (neglecting terms of order q_\perp^2 in Eq.(D.20)) we have

$$z_i \simeq \frac{z \underline{i}j \cdot k + q_\perp \cdot k}{\underline{i}j \cdot k} = z + \mathcal{O}(q_\perp), \quad (\text{E.8})$$

that is, the momentum fractions z_i and z become equal and independent of the spectator momentum k up to terms of order q_\perp . This means that the only dependence on k that is left in Eq.(E.7) at leading order in q_\perp is contained in the colour charge operator \mathbf{T}_k , which, making use of colour conservation Eq.(D.16) allows us to write

$$\sum_{k \neq (i,j)} \mathbf{T}_k |1, \dots, i+j, \dots, m+1\rangle_{\mathbf{m}} = -\mathbf{T}_{i+j} |1, \dots, i+j, k, \dots, m+1\rangle_{\mathbf{m}}. \quad (\text{E.9})$$

Plugging the above into Eq.(E.7) and keeping only the most singular terms of order $\mathcal{O}(q_\perp^{-2})$ we can write

$$\sum_{k \neq (i,j)} \mathcal{D}_{ij,k}^{\text{coll., sing.}} \simeq -\frac{1}{i \cdot j} 4\pi \tilde{\mu}^{2\epsilon} \alpha_s \times_{\mathbf{m}} \langle 1, \dots, i+j, \dots, m+1 | \mathbf{P}_{ij,i}(z, q_\perp, \epsilon) | 1, \dots, ij, \dots, m+1 \rangle_{\mathbf{m}}, \quad (\text{E.10})$$

obtaining the result claimed in Eq.(D.23). Note that unlike the soft limit, where we had to sum over all dipole contributions $\{(i, j), k\}$ to obtain the correct singular behaviour, for the limit where partons (i, j) become collinear it suffices to sum over all allowed spectators k for the given pair.

F Dipole map and factorisation of dipole phase space

Using the momentum projection proposed in Eq.(3.19), it is possible to factorise the Lorentz invariant phase space

$$d\Phi_{\mathbf{3}}(i, j, k) = \frac{d^d i}{(2\pi)^d} \tilde{\delta}(i^2) \frac{d^d j}{(2\pi)^{d-1}} \tilde{\delta}(j^2) \frac{d^d k}{(2\pi)^{d-1}} \tilde{\delta}(k^2) (2\pi)^d \delta^{(d)}(Q - i - j - k), \quad (\text{F.1})$$

of three particles with momenta i, j, k into a two particle phase space of momenta ij, \underline{k} times a modified measure corresponding to the single particle phase space for the emission of an additional parton with momentum j at NLO, which we will show to be of the form

$$d\Phi_{\mathbf{3}}(i, j, k) = d\Phi_{\mathbf{2}}(ij, \underline{k}) dj(ij, \underline{k}). \quad (\text{F.2})$$

In Eq.(F.1) we have used the notation $\tilde{\delta}(k^2) = \theta(k^0) \delta(k^2)$ to ensure that all particles are on the positive-energy mass shell. The single particle integral measure associated with the emitted parton has the form

$$dj(ij, \underline{k}) = \frac{d^d j}{(2\pi)^{d-1}} \tilde{\delta}(j^2) \mathcal{J}(ij, \underline{k}, j), \quad (\text{F.3})$$

with the Jacobian factor $\mathcal{J}(ij, \underline{k}, j)$ arising from the momentum projection map.

It is most useful to think of going from the momenta $\{(i, j), k\}$ of a given dipole (which we will also call the physical momenta) to $\{ij, \underline{k}, j\}$ (projected momenta) as related to a pseudo-process where an emitter particle with initial momentum $ij = i + j$ splits into two particles of momentum i and j with a spectator particle k running along, similar to the left-hand side of the depiction in Eq.(3.22). We now wish to find a relation between the projected momenta $\{ij, \underline{k}\}$ and the dipole momenta $\{(i, j), k\}$.

Derivation of dipole momentum map

To derive the dipole projection map Eq.(3.19), we start out by using Eq.(D.20) to decompose the emitter momenta i and j . Recall that for the decomposition to work, both reference vectors p^μ, \bar{n}^μ have to be null. The momenta available in the pseudo-process under consideration (which are not i

and j themselves) are $ij = i + j$ and k . However, we have $(ij)^2 = 2i \cdot j \neq 0$ in general, and so ij does not by itself constitute a valid reference vector. This can easily be remedied by introducing a null vector \underline{ij} that lies in the same spatial direction as ij , i.e.

$$\underline{ij}^\mu = (|\mathbf{ij}|, \mathbf{ij})^\mu, \quad \underline{ij}^2 = 0. \quad (\text{F.4})$$

In keeping with the notation of Eq.(D.20), we thus set the reference vectors $p^\mu = \underline{ij}^\mu$ and $\bar{n}^\mu = k^\mu$ which yields the decomposition

$$i^\mu = z \underline{ij}^\mu - \frac{q_\perp^2}{z} \frac{k^\mu}{2(k \cdot \underline{ij})} + q_\perp^\mu, \quad j^\mu = (1 - z) \underline{ij}^\mu - \frac{q_\perp^2}{1 - z} \frac{k^\mu}{2(k \cdot \underline{ij})} - q_\perp^\mu, \quad i \cdot j = \frac{-q_\perp^2}{2z(1 - z)}, \quad (\text{F.5})$$

In the next step we would like to invert the relations in Eq.(F.5) to obtain an expressions for the projected momentum \underline{ij} in terms of $\{(i, j), k\}$. We start by substituting the expansion of i and j into the definition of ij

$$ij^\mu = i^\mu + j^\mu = \underline{ij}^\mu - \frac{q_\perp^2}{2z(1 - z)} \frac{k^\mu}{k \cdot \underline{ij}} = \underline{ij}^\mu + \frac{i \cdot j}{k \cdot \underline{ij}} k^\mu. \quad (\text{F.6})$$

All the physical momenta are assumed to be null, hence the denominator in the last term above can be written as $k \cdot \underline{ij} = k \cdot ij$. This allows us to explicitly state the projected momentum \underline{ij} in terms of the physical momenta

$$\underline{ij}^\mu = ij^\mu - \frac{i \cdot j}{k \cdot ij} k^\mu = i^\mu + j^\mu - \frac{y_{ij,k}}{1 - y_{ij,k}} k^\mu, \quad (\text{F.7})$$

with the dimensionless momentum fraction $y_{ij,k}$ defined as in Eq.(3.18), thus establishing the first of the relations claimed in Eq.(3.19). The second projected momentum \underline{k} is determined by requiring that the projection conserve momentum, i.e.,

$$i^\mu + j^\mu + k^\mu \stackrel{!}{=} \underline{ij}^\mu + \underline{k}^\mu \quad \Rightarrow \quad \underline{k}^\mu = \frac{1}{1 - y_{ij,k}} k^\mu, \quad (\text{F.8})$$

reproducing the second relation. For completeness we also invert the relations Eqs.(F.7) and (F.8) to give the decomposition of the physical emitter momenta (i, j) in terms of the projected momenta $(\underline{ij}, \underline{k})$,

$$\begin{aligned} i^\mu &= z_i \underline{ij}^\mu + (1 - z_i) y_{ij,k} \underline{k}^\mu + \sqrt{2(\underline{ij} \cdot \underline{k}) z_i (1 - z_i) y_{ij,k}} n_\perp^\mu, \\ j^\mu &= (1 - z_i) \underline{ij}^\mu + z_i y_{ij,k} \underline{k}^\mu - \sqrt{2(\underline{ij} \cdot \underline{k}) z_i (1 - z_i) y_{ij,k}} n_\perp^\mu, \end{aligned} \quad (\text{F.9})$$

where we have rewritten $q_\perp^\mu = |\mathbf{q}_\perp| n_\perp^\mu$, with $n_\perp^2 = -1$, and have identified the momentum fraction $z \equiv z_i$ compared with Eq.(F.5). This identification is allowed since, as we showed in Eq.(E.8), the collinear limits of the decompositions using either z or z_i coincide which is all we ultimately care about. Now that we have sufficiently motivated the momentum map, we would like to show that it indeed allows for a factorisation of the three particle phase space of the dipole.

Jacobian factor and single particle phase space

In this section we turn to calculating the Jacobian factor $\mathcal{J}(\underline{ij}, \underline{k}, j)$ found in the phase space factor Eq.(F.3). We consider the part of the phase space factor pertaining only to the physical momenta i and k , and implement their mass-shell conditions explicitly, i.e.

$$d\Phi_2(i, k) = \frac{d^d i}{(2\pi)^{d-1}} \frac{d^d k}{(2\pi)^{d-1}} \tilde{\delta}(i^2) \tilde{\delta}(k^2) = \frac{d^{d-1} i}{(2\pi)^{d-1} 2i^0} \frac{d^{d-1} k}{(2\pi)^{d-1} 2k^0}. \quad (\text{F.10})$$

Performing a change of variables to the projected momenta $\underline{i}j, \underline{k}$ defined as in Eq.(3.19), we can rewrite the phase space factor as

$$d\Phi_2(i, k) = \frac{d^{d-1}\underline{i}j}{(2\pi)^{d-1}2\underline{i}j^0} \frac{d^{d-1}\underline{k}}{(2\pi)^{d-1}2\underline{k}^0} \frac{\underline{i}j^0 \underline{k}^0}{i^0 k^0} |\det J| \equiv d\Phi_2(\underline{i}j, \underline{k}) \mathcal{J}(\underline{i}j, \underline{k}, j), \quad (\text{F.11})$$

which defines the Jacobian factor $\mathcal{J}(\underline{i}j, \underline{k}, j)$, introducing a dependence on the momentum j of the additionally emitted particle through the expansion Eq.(F.7). The Jacobian J , which in d dimensions will be a $2(d-1) \times 2(d-1)$ dimensional matrix, is given by

$$J = \frac{\partial(i, k)}{\partial(\underline{i}j, \underline{k})} = \begin{pmatrix} \frac{\partial i}{\partial \underline{i}j} & \frac{\partial k}{\partial \underline{i}j} \\ \frac{\partial i}{\partial \underline{k}} & \frac{\partial k}{\partial \underline{k}} \end{pmatrix}, \quad (\text{F.12})$$

where the momenta whose derivatives we need to take are as in Eqs.(F.8) and (F.9).

If we want to explicitly calculate the entries of this Jacobian we have to be careful to take into account the on-shell constraint we explicitly implemented in Eq.(F.10). This means that we have to effectively treat the particle energies as functions of the spatial momenta, e.g. $\underline{i}j^0 = \underline{i}j^0(\underline{i}j) = |\underline{i}j|$. When calculating derivatives with respect to the a -th component of a projected momentum, this implies for instance

$$\frac{\partial}{\partial \underline{i}j^a}(\underline{i}j \cdot j) = \frac{j^0}{\underline{i}j^0} \underline{i}j_a - j_a, \quad (\text{F.13})$$

with analogous expressions for the other scalar products involved. Using these relations we can explicitly compute all the entries in the Jacobian matrix,

$$\begin{aligned} \frac{\partial i^a}{\partial \underline{i}j^b} &= \delta_b^a + \Delta \underline{k}^a \left(\left[\frac{j^0}{\underline{i}j^0} \underline{i}j_b - j_b \right] - y_{ij,k} \left[\frac{\underline{k}^0}{\underline{i}j^0} \underline{i}j_b - \underline{k}_b \right] \right), \\ \frac{\partial i^a}{\partial \underline{k}^b} &= y_{ij,k} \delta_b^a - \Delta y_{ij,k} \underline{k}^a \left(\frac{\underline{i}j^0}{\underline{k}^0} \underline{k}_b - \underline{i}j_b - \frac{j^0}{\underline{k}^0} \underline{k}_b + j_b \right), \\ \frac{\partial k^a}{\partial \underline{i}j^b} &= -\Delta \underline{k}^a \left(\left[\frac{j^0}{\underline{i}j^0} \underline{i}j_b - j_b \right] - y_{ij,k} \left[\frac{\underline{k}^0}{\underline{i}j^0} \underline{i}j_b - \underline{k}_b \right] \right), \\ \frac{\partial k^a}{\partial \underline{k}^b} &= (1 - y_{ij,k}) \delta_b^a + \Delta y_{ij,k} \underline{k}^a \left(\frac{\underline{i}j^0}{\underline{k}^0} \underline{k}_b - \underline{i}j_b - \frac{j^0}{\underline{k}^0} \underline{k}_b + j_b \right), \end{aligned} \quad (\text{F.14})$$

where we introduced the short-hand $\Delta = (\underline{k} \cdot (\underline{i}j - j))^{-1}$.

In order to compute the determinant we start by considering the simplest case of $d=2$. Using canonical Minkowski coordinates we choose the center of mass frame of the emitter $\underline{i}j$ and the spectator \underline{k} , such that

$$\underline{i}j^\mu = \frac{Q}{2} (1, -1)^\mu, \quad \underline{k}^\mu = \frac{Q}{2} (1, 1)^\mu, \quad j^\mu = (j^0, j_\parallel). \quad (\text{F.15})$$

In this frame the kinematic variables Eq.(3.18) take the form

$$\begin{aligned} y_{ij,k} &= \frac{j^0 + j_\parallel}{Q - j^0 + j_\parallel} \quad \Delta = \frac{2}{Q} (Q - j^0 + j_\parallel)^{-1}, \\ z_i &= \frac{Q - j^0 + j_\parallel}{Q} \quad 1 - z_i = \frac{j^0 - j_\parallel}{Q}. \end{aligned} \quad (\text{F.16})$$

The determinant of Eq.(F.12) in two dimensions is computed by brute force, and after some algebra can be shown to be a Lorentz invariant function of the kinematic invariants above,

$$\det J_2 = \frac{Q - 2j^0 + Q y_{ij,k}}{Q - j^0 + j_\parallel} = \frac{1 - z_i(1 - y_{ij,k})}{z_i}. \quad (\text{F.17})$$

Having done the computation for $d = 2$ the generalisation to arbitrary spacetime dimension d turns out to be not too difficult. Going again to the center of mass frame, we now have

$$\underline{j}^\mu = \frac{Q}{2} (1, \mathbf{0}_\perp, -1)^\mu \quad \underline{k}^\mu = \frac{Q}{2} (1, \mathbf{0}_\perp, 1)^\mu, \quad j^\mu = (j^0, \mathbf{j}_\perp, j_\parallel)^\mu. \quad (\text{F.18})$$

The Jacobian matrix involving d -dimensional momenta then takes the form

$$J_d = \begin{pmatrix} \begin{bmatrix} \ddots & & \ddots \\ & \mathbf{1}_{d-2} & \\ \ddots & & \ddots \end{bmatrix} & \vdots & \begin{bmatrix} \ddots & & \ddots \\ & \mathbf{0}_{d-2} & \\ \ddots & & \ddots \end{bmatrix} & \vdots \\ \dots \mathbf{f}_1(\mathbf{j}_\perp) \dots & (J_2)_{11} & \dots \mathbf{f}_2(\mathbf{j}_\perp) \dots & (J_2)_{12} \\ \begin{bmatrix} \ddots & & \ddots \\ & y_{ij,k} \mathbf{1}_{d-2} & \\ \ddots & & \ddots \end{bmatrix} & \vdots & \begin{bmatrix} \ddots & & \ddots \\ & (1 - y_{ij,k}) \mathbf{1}_{d-2} & \\ \ddots & & \ddots \end{bmatrix} & \vdots \\ \dots \mathbf{f}_3(\mathbf{j}_\perp) \dots & (J_2)_{21} & \dots \mathbf{f}_4(\mathbf{j}_\perp) \dots & (J_2)_{22} \end{pmatrix}, \quad (\text{F.19})$$

where $(J_2)_{ij}$ are the matrix elements of the Jacobian in two dimensions. When computing the determinant of Eq.(F.19) we can first expand $(d - 2)$ times in the rows of the upper-left unit matrix $\mathbf{1}_{d-2}$, thereby eliminating any dependence on the functions $\mathbf{f}_{1,3}(\mathbf{j}_\perp)$. In the next step we expand in the $(d - 2)$ rows of the lower right matrix $(1 - y_{ij,k}) \mathbf{1}_{d-2}$ to remove the dependence on $\mathbf{f}_{2,4}(\mathbf{j}_\perp)$. Note that in this way we have removed any dependence on the transverse momentum \mathbf{j}_\perp , and the row expansion of the determinant reduces to the determinant in two dimensions times a prefactor,

$$\det J_d = (1 - y_{ij,k})^{d-2} \det J_2. \quad (\text{F.20})$$

The final ingredient for the Jacobian factor is to calculate the ratio of energies appearing in Eq.(F.11). A priori it is not clear that this ratio is indeed a Lorentz scalar. However, making use of the relations Eq.(F.16) one finds

$$\frac{\underline{k}^0 \underline{j}^0}{i^0 k^0} = \frac{1}{(1 - z_i(1 - y_{ij,k}))(1 - y_{ij,k})}, \quad (\text{F.21})$$

so that we are indeed dealing with a Lorentz invariant quantity. Putting together the results from Eqs.(F.17), (F.20) and (F.21) we obtain the final result for the Jacobian factor

$$\mathcal{J}(\underline{j}, \underline{k}, j) = \frac{(1 - y_{ij,k})^{d-3}}{z_i}. \quad (\text{F.22})$$

Thus the separated one particle phase space in Eq.(F.3) may be written as

$$dj(\underline{j}, \underline{k}) = \frac{d^d j}{(2\pi)^{d-1}} \tilde{\delta}(j^2) \Theta(1 - z_i) \Theta(1 - y_{ij,k}) \frac{(1 - y_{ij,k})^{d-3}}{z_i}. \quad (\text{F.23})$$

In the last step we would like to decompose the measure Eq.(F.23) entirely in terms of the kinematic invariants $y_{ij,k}$ and z_i . To do this we note that a general lightcone decomposition of the form

$$j^\mu = \alpha \underline{j}^\mu + \beta \underline{k}^\mu - |\mathbf{q}_\perp| n_\perp^\mu, \quad (\text{F.24})$$

can be shown to lead to a decomposition of the single particle phase space measure that reads

$$\begin{aligned} \frac{d^d j}{(2\pi)^{d-1}} \tilde{\delta}(j^2) &= \frac{d\alpha d\beta d|\mathbf{q}_\perp| d^{d-3} \Omega}{(2\pi)^{d-1}} \frac{\delta(|\mathbf{q}_\perp| - \sqrt{2(\underline{j} \cdot \underline{k})\alpha\beta})}{2\sqrt{2(\underline{j} \cdot \underline{k})\alpha\beta}} (\underline{j} \cdot \underline{k}) |\mathbf{q}_\perp|^{d-3} \\ &= \frac{d\alpha d\beta d^{d-3} \Omega}{(2\pi)^{d-1}} \frac{1}{4} (2\underline{j} \cdot \underline{k})^{\frac{d}{2}-1} (\alpha\beta)^{\frac{d}{2}-2}, \end{aligned} \quad (\text{F.25})$$

where we have integrated over $|\mathbf{q}_\perp|$ in the last line, implementing the on-shell constraint. Comparing the decompositions Eqs.(F.9) and (F.24) we see that we have to identify

$$\alpha = 1 - z_i, \quad \beta = z_i y_{ij,k}, \quad (\text{F.26})$$

which, when performing the change of variables $(\alpha, \beta) \mapsto (y_{ij,k}, z_i)$ leads to an additional Jacobian factor

$$\det \tilde{J} = \det \begin{pmatrix} \frac{\partial \alpha}{\partial z_i} & \frac{\partial \beta}{\partial z_i} \\ \frac{\partial \alpha}{\partial y_{ij,k}} & \frac{\partial \beta}{\partial y_{ij,k}} \end{pmatrix} = -z_i. \quad (\text{F.27})$$

In terms of the kinematic invariants the single particle phase space pertaining to j in Eq.(F.25) now reads

$$\frac{d^d j}{(2\pi)^{d-1}} \tilde{\delta}(j^2) = \frac{dz_i dy_{ij,k} d^{d-3} \Omega}{(2\pi)^{d-1}} \frac{z_i}{4} (2\underline{j} \cdot \underline{k})^{\frac{d}{2}-1} (z_i(1 - z_i)y_{ij,k})^{\frac{d}{2}-2}, \quad (\text{F.28})$$

which, plugging the above into Eq.(F.23), gives the phase space of the separated particle as stated in Eq.(3.25).

G Alternative calculation of subtracted real emission thrust distribution

In this section we explore an alternative method for analytically determining the subtracted real emission thrust distribution Eq.(3.49) while staying closer in spirit to its original (albeit ill-defined) definition Eq.(3.45). In particular all calculations will be carried out in $d=4$ dimensions. We start out by considering the finite real emission thrust distribution (c.f. Eq.(2.77))

$$\begin{aligned} \left. \frac{d\sigma_{\mathbf{3}}}{d\tau} \right|_{\epsilon=0}^{\tau>0} &= \frac{\hat{\sigma}(\epsilon=0)}{s} \frac{\alpha_s C_F}{\pi} \left\{ \left[-\frac{3}{2} + 3\tau + \frac{9}{2}\tau^2 + \frac{2-3\tau(1-\tau)}{1-\tau} \log(1-2\tau) \right] \frac{1}{\tau} + \left[3\tau - \frac{2}{1-\tau} \right] \frac{\log(\tau)}{\tau} \right\} \\ &\equiv \frac{\hat{\sigma}(\epsilon=0)}{s} \frac{\alpha_s C_F}{\pi} \left\{ a(\tau) \frac{1}{\tau} + b(\tau) \frac{\log(\tau)}{\tau} \right\}, \end{aligned} \quad (\text{G.1})$$

which defines the functions $a(\tau), b(\tau)$ and can be obtained by direct evaluation or from the result in Eq.(2.69) by first assuming $\tau > 0$ strictly and then taking the limit $\epsilon \rightarrow 0$. Note that the result Eq.(G.1) is divergent when $\tau \rightarrow 0$, which is fine as long as we restrict ourselves to considering $\tau > 0$. However, we will be able to regain information about the singular part (at $\tau = 0$) of the subtracted thrust distribution by integrating the above result against a test function $\phi(\tau)$ in the interval $(\delta_\tau, \frac{1}{3})$ where we assume δ_τ to be a small thrust cutoff which we shall want to take to zero eventually. Concretely we want to consider the integral

$$\int_{\delta_\tau}^{\frac{1}{3}} d\tau \left. \frac{d\sigma_{\mathbf{3}}}{d\tau} \right|_{\epsilon=0}^{\tau>0} \phi(\tau) = \frac{\hat{\sigma}(\epsilon=0)}{s} \frac{\alpha_s C_F}{\pi} \int_{\delta_\tau}^{\frac{1}{3}} d\tau \left[\frac{a(\tau)}{\tau} + b(\tau) \frac{\log(\tau)}{\tau} \right] \phi(\tau). \quad (\text{G.2})$$

Focusing only on the term involving $a(\tau)$ for the moment we can write

$$\begin{aligned} \int_{\delta_\tau}^{\frac{1}{3}} d\tau \frac{a(\tau)}{\tau} \phi(\tau) &= \int_{\delta_\tau}^{\frac{1}{3}} d\tau \frac{\phi(\tau)a(\tau) - \phi(0)a(0)}{\tau} + \phi(0)a(0) \int_{\delta_\tau}^{\frac{1}{3}} \frac{d\tau}{\tau} + \phi(0)a(0) \log\left(\frac{1}{3}\right) - \phi(0)a(0) \log\left(\frac{1}{3}\right) \\ &= \int_{\delta_\tau}^{\frac{1}{3}} d\tau \frac{\phi(\tau)a(\tau) - \phi(0)a(0)}{\tau} + \phi(0)a(0) \log\left(\frac{1}{3}\right) - \phi(0)a(0) \log(\delta_\tau), \end{aligned} \quad (\text{G.3})$$

where we have done nothing but to add zero in a particular way. Note that the singular behaviour of Eq.(G.3) when $\delta_\tau \rightarrow 0$ is encapsulated in the term containing $\log(\delta_\tau)$, while the other terms are finite in this limit. Performing similar manipulations for the term involving $b(\tau)$ in Eq.(G.2) we arrive at

$$\begin{aligned} \int_{\delta_\tau}^{\frac{1}{3}} d\tau \frac{d\sigma_{\mathbf{3}}}{d\tau} \Big|_{\epsilon=0}^{\tau>0} \phi(\tau) &= \frac{\hat{\sigma}(\epsilon=0)}{s} \frac{\alpha_s C_F}{\pi} \left\{ \int_{\delta_\tau}^{\frac{1}{3}} d\tau \frac{\phi(\tau)a(\tau) - \phi(0)a(0)}{\tau} + \phi(0)a(0) \log\left(\frac{1}{3}\right) - \phi(0)a(0) \log(\delta_\tau) \right. \\ &\quad \left. + \int_{\delta_\tau}^{\frac{1}{3}} d\tau \log(\tau) \frac{\phi(\tau)b(\tau) - \phi(0)b(0)}{\tau} + \phi(0)b(0) \frac{\log^2(\frac{1}{3})}{2} - \phi(0)b(0) \frac{\log^2(\delta_\tau)}{2} \right\}. \end{aligned} \quad (\text{G.4})$$

Using the definition of plus distributions Eq.(I.2), we can thus interpret Eq.(G.4) in its entirety as a distribution in the sense that

$$\begin{aligned} \frac{d\sigma_{\mathbf{3}}}{d\tau} \Big|_{\epsilon=0}^{\tau>0} &= \frac{\hat{\sigma}(\epsilon=0)}{s} \frac{\alpha_s C_F}{\pi} \left\{ a(\tau) \left[\frac{\theta(\tau - \delta_\tau)}{\tau} \right]_+ + b(\tau) \left[\frac{\theta(\tau - \delta_\tau) \log(\tau)}{\tau} \right]_+ \right. \\ &\quad \left. + \frac{3}{2} \log(\delta_\tau) \delta(\tau) + \log^2(\delta_\tau) \delta(\tau) \right\} \end{aligned} \quad (\text{G.5})$$

where we have used $a(0) = -\frac{3}{2}$ and $b(0) = -2$. Note that Eq.(G.5) is well-defined as a distribution as long as $\delta_\tau > 0$, even for $\tau = 0$. Keeping this result in mind we turn to integrating the counter terms. As already mentioned this will necessitate an additional regularisation prescription since the integral

$$\frac{1}{2s} \int d\Phi_{\mathbf{3}} [\mathcal{D}_{qk,\bar{q}} + \mathcal{D}_{\bar{q}k,q}] \Big|_{\epsilon=0} \delta(\tau), \quad (\text{G.6})$$

corresponding to the counter-term is divergent in $d = 4$ dimensions. Now recall from the form of the integrals Eq.(2.65) and Eq.(2.66) that the thrust observable regularises the real emission thrust distribution by effectively acting as a phase space cut-off. In close analogy we therefore define the regularised integral corresponding to Eq.(G.6) using the cut-off δ_τ introduced in Eq.(G.2) as

$$\frac{1}{2s} \int_{\text{reg}} d\Phi_{\mathbf{3}} [\mathcal{D}_{qk,\bar{q}} + \mathcal{D}_{\bar{q}k,q}] \Big|_{\epsilon=0} \delta(\tau) \equiv \frac{1}{4(4\pi)^3} \int_{2\delta_\tau}^{1-\delta_\tau} dx_q \int_{1-x_q}^{1-\delta_\tau} dx_{\bar{q}} [\mathcal{D}_{qk,\bar{q}} + \mathcal{D}_{\bar{q}k,q}] (x_q, x_{\bar{q}}) \Big|_{\epsilon=0} \delta(\tau) \quad (\text{G.7})$$

where the explicit form of the three particle phase space Eq.(A.4) in $d=4$ was used and the integrand expressed in terms of momentum fractions reads (c.f. Eq.(3.30)),

$$[\mathcal{D}_{qk,\bar{q}} + \mathcal{D}_{\bar{q}k,q}] (x_q, x_{\bar{q}}) \Big|_{\epsilon=0} = \frac{\hat{\mathcal{M}}}{3s} \left\{ \frac{x_q^2 + x_{\bar{q}}^2}{(1-x_q)(1-x_{\bar{q}})} + \frac{1-x_q}{x_{\bar{q}}} + \frac{1-x_{\bar{q}}}{x_q} \right\}, \quad (\text{G.8})$$

with $\hat{\mathcal{M}}$ defined in Eq.(2.34). Integrating the above as in Eq.(G.7) we find

$$\frac{1}{2s} \int_{\text{reg}} d\Phi_{\mathbf{3}} [\mathcal{D}_{qk,\bar{q}} + \mathcal{D}_{\bar{q}k,q}] \Big|_{\epsilon=0} \delta(\tau) = \frac{\hat{\sigma}(\epsilon=0)}{s} \frac{\alpha_s C_F}{\pi} \left\{ \frac{3}{2} - \frac{\pi^2}{6} + \frac{3}{2} \log(\delta_\tau) + \log^2(\delta_\tau) + \mathcal{O}(\delta_\tau) \right\} \delta(\tau), \quad (\text{G.9})$$

which, when subtracted from Eq.(G.5), cancels the divergences proportional to $\log^n(\delta_\tau)$ therein. With these terms out of the way, nothing prevents us from taking the thrust cutoff $\delta_\tau \rightarrow 0$. Comparing with Eq.(3.49) we indeed find

$$\begin{aligned} \frac{d\sigma_{\mathbf{3}\text{sub}}^{\mathbf{r}}}{d\tau} &= \left[\frac{d\sigma_{\mathbf{3}}^{\mathbf{r}}}{d\tau} \Big|_{\epsilon=0}^{\tau>0} - \frac{1}{2s} \int_{\text{reg}} d\Phi_{\mathbf{3}} [\mathcal{D}_{qk,\bar{q}} + \mathcal{D}_{\bar{q}k,q}] \Big|_{\epsilon=0}^{\delta(\tau)} \right]_{\delta_\tau=0} \\ &= \frac{\hat{\sigma}(\epsilon=0)}{s} \frac{\alpha_s C_F}{\pi} \left\{ \left[-\frac{3}{2} + \frac{\pi^2}{6} \right] \delta(\tau) + a(\tau) \left[\frac{\theta(\tau)}{\tau} \right]_+ + b(\tau) \left[\frac{\theta(\tau) \log(\tau)}{\tau} \right]_+ \right\}. \end{aligned} \quad (\text{G.10})$$

This shows that the subtracted real emission thrust distribution, including the contribution from terms proportional to $\delta(\tau)$, can be obtained in a manifestly four dimensional calculation. In particular, no information about the d -dimensional matrix element $|\mathcal{M}_{\mathbf{3}}^{\mathbf{r}}|^2$ or dipole contributions $\mathcal{D}_{qk,\bar{q}}, \mathcal{D}_{\bar{q}k,q}$ was necessary. This ensures that a numerical implementation of the subtraction, which can only work in $d=4$, will still produce the correct result.

H Feynman rules

For the computation of QCD matrix elements we use the following Feynman rules in R_ξ gauge. Throughout our calculations we will adopt Feynman gauge, $\xi = 1$. To also accomodate later calculations in SCET we state all the expressions with masses.

$$\begin{array}{c} j, \beta \quad \xrightarrow{\quad p \quad} \quad i, \alpha \end{array} = \frac{i(\not{p} + m)_{\alpha\beta} \delta_{ij}}{p^2 - m^2 + i0}, \quad (\text{H.1})$$

$$\begin{array}{c} j, \nu \quad \text{---} \quad k \quad \text{---} \quad i, \mu \end{array} = \frac{i \left(-g_{\mu\nu} + (1 - \xi) \frac{k_\mu k_\nu}{k^2} \right)}{k^2 + i0}, \quad (\text{H.2})$$

$$\begin{array}{c} j, \nu, B \quad \text{---} \quad k \quad \text{---} \quad i, \mu, A \end{array} = \frac{i \left(-g_{\mu\nu} + (1 - \xi) \frac{k_\mu k_\nu}{k^2} \right) \delta_{AB}}{k^2 + i0}, \quad (\text{H.3})$$

$$\begin{array}{c} \mu, A \\ \text{---} \\ j \quad \text{---} \quad i \end{array} = ig_s \tilde{\mu}^\epsilon \gamma^\mu T_{ij}^A, \quad (\text{H.4})$$

We will use the above Feynman rules also for SCET computations where n, \bar{n} -collinear quarks couple to gluons in the same collinear sector. For the more complicated SCET Feynman rules that directly follow from the effective Lagrangian Eq.(5.74) see [9]. When calculating S-matrix elements we have

to attach the appropriate wave functions to incoming and outgoing particle legs, which are

$$\begin{array}{ccc}
\begin{array}{c} p_i, k_i \\ \longrightarrow \\ u_\alpha^i(p_i) \end{array} & \begin{array}{c} \alpha, i \\ \longrightarrow \bullet \end{array} & \begin{array}{c} p_f, k_f \\ \longrightarrow \\ \bullet \end{array} \\
\begin{array}{c} \bar{v}_\alpha^i(p_i) \end{array} & \begin{array}{c} \alpha, i \\ \longrightarrow \bullet \end{array} & \begin{array}{c} \bullet \end{array} \\
\begin{array}{c} \epsilon_{\mu,A}(k_i) \end{array} & \begin{array}{c} \mu, A \\ \text{---} \bullet \end{array} & \begin{array}{c} \bullet \end{array} \\
\begin{array}{c} \bar{u}_\beta^j(p_f) \end{array} & \begin{array}{c} \beta, j \\ \longrightarrow \bullet \end{array} & \begin{array}{c} \bullet \end{array} \\
\begin{array}{c} v_\beta^j(p_f) \end{array} & \begin{array}{c} \beta, j \\ \longrightarrow \bullet \end{array} & \begin{array}{c} \bullet \end{array} \\
\begin{array}{c} \epsilon_{\nu,B}^*(k_f) \end{array} & \begin{array}{c} \nu, B \\ \text{---} \bullet \end{array} & \begin{array}{c} \bullet \end{array}
\end{array} \quad (H.5)$$

The Feynman rules associated with the usoft and collinear Wilson lines that appear in the hemisphere soft and jet function respectively are presented here to first order in α_s .

$$\begin{array}{ccc}
\begin{array}{c} k, n \\ \curvearrowright \\ j \otimes W_n \end{array} & = \frac{g_s \tilde{\mu}^\epsilon \bar{n}^\mu T_{ij}^A}{\bar{n} \cdot k + i0} & \begin{array}{c} \mu, A \\ \curvearrowright \\ j \text{---} \text{---} i \end{array} \\
\begin{array}{c} \mu, A \\ \curvearrowright \\ j \text{---} \text{---} i \end{array} & = \frac{g_s \tilde{\mu}^\epsilon \bar{n}^\mu T_{ij}^A}{\bar{n} \cdot k - i0} & \begin{array}{c} k, n \\ \curvearrowright \\ j \text{---} \text{---} i \otimes W_n^\dagger \end{array}
\end{array} \quad (H.6)$$

$$\begin{array}{ccc}
\begin{array}{c} \mu, A \\ \text{---} \\ j \text{---} Y_n \text{---} i \end{array} & = & \begin{cases} \frac{g_s \tilde{\mu}^\epsilon n^\mu T_{ij}^A}{n \cdot k + i0} & \text{for } Y_n, \\ -\frac{g_s \tilde{\mu}^\epsilon n^\mu T_{ij}^A}{n \cdot k + i0} & \text{for } Y_n^\dagger, \\ \frac{g_s \tilde{\mu}^\epsilon n^\mu \bar{T}_{ij}^A}{n \cdot k + i0} & \text{for } \bar{Y}_n, \\ -\frac{g_s \tilde{\mu}^\epsilon n^\mu \bar{T}_{ij}^A}{n \cdot k + i0} & \text{for } \bar{Y}_n^\dagger. \end{cases} \quad (H.7)
\end{array}$$

Here we have shown all Wilson lines pertaining to n -collinear particles or usoft gluon emission therefrom. For \bar{n} -collinear particles the rules are completely analogous and obtained by replacing $n \leftrightarrow \bar{n}$.

I Plus distribution miscellanies

The plus distribution of n -th degree for a dimensionless variable x is defined in terms of the limit [13]

$$\begin{aligned}
\left[\frac{\theta(x) \log^n(x)}{x} \right]_+ &\equiv \lim_{\beta \rightarrow 0} \frac{d}{dx} \left[\theta(x - \beta) \int dx \frac{\log^n(x)}{x} \right] \\
&= \lim_{\beta \rightarrow 0} \left[\theta(x - \beta) \frac{\log^n(x)}{x} + \frac{1}{n+1} \log^{n+1}(\beta) \delta(x - \beta) \right].
\end{aligned} \quad (I.1)$$

Integrated against a test function $\phi(x)$ up to some upper bound x_+ we find

$$\int_0^{x_+} dx \left[\frac{\theta(x) \log^n(x)}{x} \right]_+ \phi(x) = \int_0^{x_+} dx \frac{\phi(x) - \phi(0)}{x} \log^n(x) + \phi(0) \frac{\log^{n+1}(x_+)}{n+1}, \quad (I.2)$$

which, when we integrate against the identity function gives us the convenient relation

$$\int_0^{x+} dx \left[\frac{\theta(x) \log^n(x)}{x} \right]_+ = \frac{\log^{n+1}(x_+)}{n+1}. \quad (\text{I.3})$$

The plus distributions obey a convenient recursion relation. For $n \in \mathbb{N}_0$ and some dimensionless constant $\Delta > 0$ it holds that

$$\Delta \left[\frac{\theta(x) \log^n(\Delta x)}{\Delta x} \right]_+ = \frac{\log^{n+1}(\Delta)}{n+1} \delta(x) + \sum_{k=0}^n \frac{n!}{(n-k)!k!} \log^{n-k}(\Delta) \left[\frac{\theta(x) \log^k(x)}{x} \right]_+. \quad (\text{I.4})$$

Together with the delta function the plus distributions Eq.(I.1) form “a complete set” of distributions which characterise the singular behaviour of any jet observable [25].

Imaginary part identities

For the extraction of the imaginary parts from jet correlators in Eqs.(7.86) and (7.90) the following identities can be used

$$\begin{aligned} \frac{1}{\pi} \text{Im} \left\{ \frac{1}{s+i0} \right\} &= -\delta(s), \\ \frac{1}{\pi} \text{Im} \left\{ \frac{1}{[s+i0]^2} \right\} &= \delta'(s), \\ \frac{1}{\pi} \text{Im} \left\{ \frac{1}{s+i0} \log \left(\frac{\mu^2}{-s-i0} \right) \right\} &= \frac{1}{\mu^2} \left[\frac{\mu^2 \theta(s)}{s} \right]_+, \\ \frac{1}{\pi} \text{Im} \left\{ \frac{1}{s+i0} \log \left(\frac{m^2}{-s-i0} \right) \right\} &= \frac{1}{\mu^2} \left[\frac{\mu^2 \theta(s)}{s} \right]_+ - \log \left(\frac{m^2}{\mu^2} \right) \delta(s), \\ \frac{1}{\pi} \text{Im} \left\{ \frac{1}{s+i0} \log^2 \left(\frac{\mu^2}{-s-i0} \right) \right\} &= \frac{\pi^2}{3} \delta(s) - \frac{2}{\mu^2} \left[\frac{\mu^2 \theta(s) \log(s/\mu^2)}{s} \right]_+, \\ \frac{1}{\pi} \text{Im} \left\{ \frac{1}{s+i0} \text{Li}_2 \left(\frac{-s-i0}{m^2} \right) \right\} &= \frac{\theta(-s-m^2)}{s} \log \left(\frac{m^2}{-s} \right), \\ \frac{1}{\pi} \text{Im} \left\{ \frac{1}{s+i0} \log \left(\frac{m^2}{-s-i0} \right) \log \left(1 + \frac{s+i0}{m^2} \right) \right\} &= \frac{\theta(-s-m^2)}{s} \log \left(\frac{m^2}{-s} \right) \\ &\quad + \log \left(1 + \frac{s}{m^2} \right) \frac{1}{\mu^2} \left[\frac{\mu^2 \theta(s)}{s} \right]_+, \\ &= \frac{\theta(-s-m^2)}{s} \log \left(\frac{m^2}{-s} \right) \\ &\quad + \frac{\theta(s)}{s} \log \left(1 + \frac{s}{m^2} \right) \\ \frac{1}{\pi} \text{Im} \left\{ \frac{1}{s+i0} \frac{m^2}{s+m^2+i0} \log \left(\frac{m^2}{-s-i0} \right) \right\} &= \frac{1}{\mu^2} \left[\frac{\mu^2 \theta(s)}{s} \right]_+ - \frac{\theta(s)}{s+m^2} - \log \left(\frac{m^2}{\mu^2} \right) \delta(s), \\ \frac{1}{\pi} \text{Im} \left\{ \frac{1}{[s+m^2+i0]^2} \log \left(\frac{m^2}{-s-i0} \right) \right\} &= \log \left(\frac{m^2}{-s} \right) \delta'(s+m^2) + \frac{\theta(s)}{(s+m^2)^2} \\ &= -\frac{1}{m^2} \delta(s+m^2) + \frac{\theta(s)}{(s+m^2)^2}. \end{aligned} \quad (\text{I.5})$$

Convolution properties

To perform the convolution between jet correlators and jet functions (or renormalisation factors) the following identities prove useful,

$$\begin{aligned} \int ds' \frac{1}{\mu^2} \left[\frac{\mu^2 \theta(s-s')}{s-s'} \right]_+ \frac{1}{s'+i0} &= -\frac{1}{s+i0} \log \left(\frac{\mu^2}{-s-i0} \right), \\ \int ds' \frac{1}{\mu^2} \left[\frac{\mu^2 \theta(s-s')}{s-s'} \log \left(\frac{s-s'}{\mu^2} \right) \right]_+ \frac{1}{s'+i0} &= \frac{1}{s+i0} \left[\frac{\pi^2}{6} + \frac{1}{2} \log^2 \left(\frac{\mu^2}{-s-i0} \right) \right]. \end{aligned} \tag{I.6}$$

References

- [1] G. P. Salam, in *From My Vast Repertoire...: Guido Altarelli's Legacy* (World Scientific, 2018), pp. 101–121, [arXiv:1712.05165](#).
- [2] G. Corcella, “The Top-Quark Mass: Challenges in Definition and Determination”, *Frontiers in physics* **7**, 54 (2019), [arXiv:1903.06574](#).
- [3] A. H. Hoang, “What is the Top Quark Mass?”, *Annu. Rev. Nucl. Part. Sci.* **70**, annurev (2020), [arXiv:2004.12915](#).
- [4] G. Sterman, “Partons, Factorization and Resummation”, (1996).
- [5] T. Cohen, “As Scales Become Separated: Lectures on Effective Field Theory”, (2019), [arXiv:1903.03622](#).
- [6] G. Sterman, “QCD and Jets”, in *Theoretical Advanced Study Institute in Elementary Particle Physics: Physics in $D > 4$* , Vol. 44 (2004), pp. 67–145.
- [7] C. W. Bauer, S. Fleming, and M. Luke, “Summing Sudakov logarithms in $B \rightarrow X_s \gamma$ in effective field theory”, *Phys. Rev. - Part. Fields Gravit. Cosmol.* **63**, 13 (2001).
- [8] C. W. Bauer, S. Fleming, D. Pirjol, and I. W. Stewart, “An effective field theory for collinear and soft gluons: Heavy to light decays”, *Phys. Rev. - Part. Fields Gravit. Cosmol.* **63**, 17 (2001).
- [9] I. W. Stewart and C. W. Bauer, “The Soft-Collinear Effective Theory”, Lecture Notes (2014), https://courses.edx.org/c4x/MITx/8.EFTx/asset/notes_sctnotes.pdf.
- [10] T. Becher, A. Broggio, and A. Ferroglia, “Introduction to Soft-Collinear Effective Theory”, *Lect. Notes Phys.* **896**, 1 (2015), [arXiv:1410.1892](#).
- [11] R. K. Ellis, W. J. Stirling, and B. R. Webber, *QCD and Collider Physics* (Cambridge university press, 1996), <https://doi.org/10.1017/CB09780511628788>.
- [12] S. Fleming, A. H. Hoang, S. Mantry, and I. W. Stewart, “Jets from Massive Unstable Particles: Top-Mass Determination”, *Phys. Rev. - Part. Fields Gravit. Cosmol.* **77**, 074010 (2008).
- [13] S. Fleming, A. H. Hoang, S. Mantry, and I. W. Stewart, “Top jets in the Peak Region: Factorization Analysis with next-to-leading-log Resummation”, *Phys. Rev. - Part. Fields Gravit. Cosmol.* **77**, 114003 (2008), [arXiv:0711.2079](#).
- [14] S. Catani and M. H. Seymour, “A general algorithm for calculating jet cross sections in NLO QCD”, *Nucl. Phys. B* **485**, 291 (1997).
- [15] D. Binosi and L. Theußl, “JaxoDraw: A graphical user interface for drawing Feynman diagrams”, *Comput. Phys. Commun.* **161**, 76 (2004).
- [16] L. D. Landau, “On analytic properties of vertex parts in quantum field theory”, *Nucl. Phys.* **13**, 181 (1959).
- [17] S. Coleman and R. E. Norton, “Singularities in the physical region”, *Il Nuovo Cimento Ser. 10* **38**, 438 (1965).
- [18] T. Kinoshita, “Mass singularities of Feynman Amplitudes”, *J. Math. Phys.* **3**, 650 (1962).
- [19] G. Dissertori, I. G. Knowles, and M. Schmelling, *Quantum Chromodynamics: High Energy Experiments and Theory* (Oxford University Press, 2010).
- [20] C. W. Bauer, S. Fleming, C. Lee, and G. Sterman, “Factorization of e^+e^- Event Shape Distributions with Hadronic Final States in Soft Collinear Effective Theory”, *Phys. Rev. - Part. Fields Gravit. Cosmol.* **78**, 034027 (2008), [arXiv:0801.4569](#).

- [21] Inc., Wolfram Research, “Mathematica, Version 12.1”, <https://www.wolfram.com/mathematica>.
- [22] T. Huber and D. Maître, “HypExp 2, Expanding hypergeometric functions about half-integer parameters”, *Comput. Phys. Commun.* **178**, 755 (2008), [arXiv:0708.2443](#).
- [23] M. D. Schwartz, *Quantum Field Theory and the Standard Model* (Cambridge University Press, 2014).
- [24] The OPAL Collaboration, “Measurement of event shape distributions and moments in $e^+e^- \rightarrow$ hadrons at 91-209 GeV and a determination of α_s ”, *Eur. Phys. J. C* **40**, 287 (2005).
- [25] L. G. Almeida et al., “Comparing and counting logs in direct and effective methods of QCD resummation”, *J. High Energy Phys.* **2014**, 174 (2014), [arXiv:1401.4460](#).
- [26] T. Becher and M. D. Schwartz, “A precise determination of α_s from LEP thrust data using effective field theory”, *J. High Energy Phys.* **2008**, 034 (2008), [arXiv:0803.0342](#).
- [27] A. Heister et al., “Studies of QCD at e^+e^- centre-of-mass energies between 91 and 209 GeV”, *Eur. Phys. J. C* **35**, 457 (2004).
- [28] C. Lepenik, “Heavy Jet Mass with Massive Quarks”, Master’s Thesis (University of Vienna, 2016), <http://othes.univie.ac.at/42441/>.
- [29] M. Preißer, “C-Parameter with Massive Quarks”, Master’s Thesis (University of Vienna, 2014), <http://othes.univie.ac.at/34188/>.
- [30] S. Catani, L. Trentadue, G. Turnock, and B. R. Webber, “Resummation of large logarithms in e^+e^- event shape distributions”, *Nucl. Phys. Sect. B* **407**, 3 (1993).
- [31] C. W. Bauer and I. W. Stewart, “Invariant Operators in Collinear Effective Theory”, *Phys. Lett. Sect. B Nucl. Elem. Part. High-Energy Phys.* **516**, 134 (2001).
- [32] A. K. Leibovich, Z. Ligeti, and M. B. Wise, “Comment on Quark Masses in SCET”, *Phys. Lett. Sect. B Nucl. Elem. Part. High-Energy Phys.* **564**, 231 (2003).
- [33] J. Chay, C. Kim, G. K. Yeaong, and J. P. Lee, “Soft Wilson lines in the soft-collinear effective theory”, *Phys. Rev. - Part. Fields Gravit. Cosmol.* **71**, 1 (2005).
- [34] S. M. Freedman and M. Luke, “SCET, QCD, and Wilson lines”, *Phys. Rev. - Part. Fields Gravit. Cosmol.* **85**, 014003 (2012), [arXiv:1107.5823](#).
- [35] C. W. Bauer, D. Pirjol, and I. W. Stewart, “Soft-Collinear Factorization in Effective Field Theory”, *Phys. Rev. - Part. Fields Gravit. Cosmol.* **65**, 17 (2002).
- [36] C. W. Bauer et al., “Hard Scattering Factorization from Effective Field Theory”, *Phys. Rev. - Part. Fields Gravit. Cosmol.* **66**, 3 (2002).
- [37] C. C. Nishi, “Simple derivation of general Fierz-type identities”, *Am. J. Phys.* **73**, 1160 (2005).
- [38] C. W. Bauer, O. Cata, and G. Ovanessian, “On different ways to quantize Soft-Collinear Effective Theory”, (2008), [arXiv:0809.1099](#).
- [39] R. E. Cutkosky, “Singularities and Discontinuities of Feynman Amplitudes”, *J. Math. Phys.* **1**, 429 (1960).
- [40] M. Veltman, *Diagrammatica: The Path to Feynman Diagrams* (Cambridge University Press, 1994).
- [41] A. V. Manohar and I. W. Stewart, “The Zero-Bin and Mode Factorization in Quantum Field Theory”, *Phys. Rev. - Part. Fields Gravit. Cosmol.* **76**, 074002 (2007).

- [42] V. Shtabovenko, R. Mertig, and F. Orellana, “FeynCalc 9.3: New features and improvements”, *Comput. Phys. Commun.* **256**, 107478 (2020), [arXiv:2001.04407](#), <http://arxiv.org/abs/2001.04407>.
- [43] G. Passarino and M. Veltman, “One-loop corrections for e^+e^- annihilation into $\mu^+\mu^-$ in the Weinberg model”, *Nucl. Phys. Sect. B* **160**, 151 (1979).
- [44] R. K. Ellis, Z. Kunszt, K. Melnikov, and G. Zanderighi, “One-loop calculations in quantum field theory: From Feynman diagrams to unitarity cuts”, *Phys. Rep.* **518**, 141 (2012), [arXiv:1105.4319](#), <http://arxiv.org/abs/1105.4319><http://dx.doi.org/10.1016/j.physrep.2012.01.008>.
- [45] H. H. Patel, “Package-X: A Mathematica package for the analytic calculation of one-loop integrals”, *Comput. Phys. Commun.* **197**, 276 (2015), [arXiv:1503.01469](#).
- [46] R. P. Feynman, in *Magic Without Magic: John Archibald Wheeler*, edited by L. M. E. Brown (World Scientific, Singapore 2000, 1971), pp. 355–375.
- [47] S. Catani et al., “From loops to trees by-passing Feynman’s theorem”, *J. High Energy Phys.* **2008**, 065 (2008), [arXiv:0804.3170](#).
- [48] M. Preißer, “Jet Shapes with Massive Quarks for e^+e^- Annihilation”, PhD Thesis (University of Vienna, 2018), <http://othes.univie.ac.at/56440/>.
- [49] A. Duncan, *The Conceptual Framework of Quantum Field Theory* (Oxford University Press, 2012).
- [50] G. Altarelli and G. Parisi, “Asymptotic freedom in parton language”, *Nucl. Phys. Sect. B* **126**, 298 (1977).